

https://dspace.org/

Developing a novel theory for the synthesis and design of membrane-based separations

Peters, Mark George Dominic

2009-04-01T13:11:37Z
http://hdl.handle.net/10539/6862

Downloaded from a DSpace repository. https://dspace.org/

Developing a Novel Theory for the Synthesis and Design of Membrane-based Separations

By

Mark George Dominic Peters

A thesis submitted to

The School of Chemical and Metallurgical Engineering,

Faculty of Engineering and the Built Environment

University of the Witwatersrand, Johannesburg

In fulfilment of the requirements for the degree of

Doctor of Philosophy

DECLARATION

I declare that, except where acknowledged, this thesis is my own, unaided work. It is being submitted for the degree of Doctor of Philosophy to the University of the Witwatersrand, Johannesburg. It has not been submitted before for any degree or examination in any other University.

_____

Mark Peters

_____ day of _____ year _____.

ABSTRACT

A novel approach for the design and synthesis of membrane separation systems has been developed. The theory is shown to be applicable to both batch and continuous membrane operations, and has been formulated in such a way that it is valid for any type of membrane. In this thesis, however, only vapour permeation and pervaporation membranes are incorporated for illustration purposes. The method, which employs a graphical technique, allows one to calculate and visualise the change in composition of the retentate. An integral part of the approach was the derivation of the Membrane Residue Curve Map (M-RCM), and the related differential material balance which describes it. By definition, this plot shows the change, in time, of the retentate composition in a batch still. However, it has been shown that the M-RCM is applicable to conventional continuously-operated membrane units, as well as infinite reflux membrane columns. Finite reflux columns and cascades have been examined by using column sections (CS): any column, or arrangement, no matter how complex, can be broken down into smaller units, namely CS. The development of the Difference Point Equation (DPE) for non-constant flow allowed one to generate, and interpret, profiles for individual CS's, which can ultimately be connected to form a membrane column arrangement. The profiles, which are more complex than those obtained in the M-RCM, exhibit a unique behavior. Since there is varying flow, the reflux is continually changing, orientating the profile so as to seek a stable node that is "mobile". Thus, the movement of CS profile is dictated by the location and direction of the pinch point locus. Finally, having membrane permeators examined in an analogous manner to other separation methods, allows for easy synthesis and design of combinations of different processes. Hybrid distillation-membrane systems are analyzed by incorporating CS's and the appropriate DPE's which describe each. Investigating the arrangement as a thermally-coupled column introduces a novel way of synthesizing hybrids. Regions of feasibility, which are dictated by the relevant pinch point loci of each separation method, are ultimately sought.

ACKNOWLEDGEMENTS

"If I have seen further, it is by standing on the shoulders of giants" *- Isaac Newton*

The material presented in this thesis is a result of four years of work and dedication. Although my name appears solely on the cover, there are numerous people and institutions that have influenced the outcome of this research.

Firstly, I would like to express my gratitude to my supervisors, Prof. Diane Hildebrandt, Prof. David Glasser and Dr. Shehzaad Kauchali. Their guidance and assistance in this research has been invaluable. The weekly meetings were always filled with exciting new, and sometimes crazy, ideas. A special mention also goes to Dr. Brendon Hausberger, Dr. Michaela Very and Dr. Simon Holland for their thoughts and ideas regarding my research. It has been a privilege to be able to work with a group of supervisors that instil a remarkable high standard of excellence. It has also been an honour to have two A-rated scientists involved in my work.

I am also grateful to have worked with Japie Scholtz of Sasol Technology, and Prof. Andreas Linninger and Dr. Libin Zhang at the University of Illinois at Chicago.

A big thanks to the many colleagues I have worked with throughout my time at Wits – Cameron Wilson for his "phantom" imagination, Alecia Moodley for her incredible cuisine skills, Riaan van Wyk for the many worlds' problems we have solved over a cup of coffee, and Craig Griffiths for his talented coding abilities. A special note of thanks to Dr. Tshepo Modise and Ronald Abbas.

To my friends and family – your confidence and belief in me over the years has brought me to complete this thesis. Thank you!

Finally, to Sasol and the National Research Foundation (NRF) for their financial support – it is gratefully appreciated.

CONTENTS

DECLARATION…… i

ABSTRACT…….. ii

ACKNOWLEDGEMENTS…….. iii

TABLE OF CONTENTS……..... v

LIST OF FIGURES…… xi

LIST OF TABLES…….…… xviii

NOMENCLATURE…… xix

1. INTRODUCTION…… 1

1.1 OVERALL INTRODUCTION……. 1

1.2 AIM OF THESIS…….. 2

1.3 THESIS OVERVIEW…… 2

2. CHAPTER 2: DERIVATION AND PROPERTIES OF MEMBRANE RESIDUE CURVE MAPS……..... 4

ABSTRACT……... 4

2.1 INTRODUCTION……... 5

2.2 DERIVATION OF M-RCM'S…… 9

2.2.1 A Thought Experiment……. 9

2.2.2 Mass Balances…….. 10

2.2.3 Permeation Modelling…….. 11

2.2.4 An Ideal Map…… 14

2.3 PROPERTIES OF M-RCM'S……. 15

2.3.1 Stationary Points…….. 15

2.3.2 Membrane Vector Field……... 16

2.3.3 Unidistribution Lines……... 17

2.3.4 The effect of α-values on the topology of M-RCM's……. 19

2.4 A REAL M-RCM……... 21
2.4.1 Case 1: When the permeate side is at vacuum conditions… 22
2.4.2 Case 2: When the permeate side is non-zero…… 24
2.5 CONCLUSION…….. 27

3. CHAPTER 3: APPLICATION OF MEMBRANE RESIDUE CURVE MAPS TO BATCH AND CONTINUOUS PROCESSES…… 29
ABSTRACT…….. 29
3.1 INTRODUCTION…….. 31
3.2 BATCH MEMBRANE OPERATION:
OPERATING LEAVES IN BATCH PERMEATION…… 37
3.2.1 Material Balances…… 37
3.2.2 Permeation Model……... 39
3.2.3 Operating Regions: Non-selective Membranes……... 41
3.2.4 Operating Regions: Selective Membranes…….. 43
3.3 BATCH MEMBRANE OPERATION: PERMEATION TIME…… 45
3.4 CONTINUOUS MEMBRANE OPERATION:
NON-REFLUX EQUIPMENT…… 49
3.4.1 Material Balances……... 50
3.4.2 Relevance of the Batch Experiment……... 52
3.4.3 Local permeate mixing with the bulk stream……. 52
3.4.4 Permeation Area……. 53
3.5 CONTINUOUS MEMBRANE OPERATION: REFLUX EQUIPMENT….. 54
3.5.1 Total Reflux……..... 54
3.5.2 Infinite Reflux…… 56
3.5.3 Finite Reflux……... 61
3.6 HYBRID DISTILLATION-MEMBRANE COLUMNS……..... 61
3.6.1 Synthesis of a hybrid configuration……..... 63
3.6.2 Design of a hybrid configuration……..... 65
3.7 CONCLUSION……... 77

4. CHAPTER 4: COLUMN PROFILES FOR MEMBRANE COLUMN SECTIONS…….. 79

ABSTRACT……. 79

4.1 INTRODUCTION……. 80

4.2 THEORY…… 84

4.2.1 Membrane Column Sections……... 84

4.2.2 The Difference Point Equation…… 86

4.2.3 Permeation Modelling……. 87

4.2.4 Properties of the DPE…….. 90

4.3 COLUMN SECTION PROFILES: OPERATING CONDITION 1……... 91

4.3.1 Statement……. 91

4.3.2 Mathematics…… 91

4.3.3 Membrane Residue Curve Map…….. 92

4.3.4 Stationary Points……. 94

4.3.5 Discontinuity……... 95

4.4 COLUMN SECTION PROFILES: OPERATING CONDITION 2……... 96

4.4.1 Statement……. 96

4.4.2 Mathematics…… 96

4.4.3 Column Profile…… 97

4.4.4 Analysis…….. 98

4.4.5 Pinch Point Loci……. 102

4.4.6 Further Column Profiles……. 104

4.4.7 Direction of δ_T…… 106

4.4.8 Direction of integration…….. 106

4.4.9 Crossing the MBT boundary…….. 107

4.5 COLUMN SECTION PROFILES: OPERATING CONDITIONS 3 & 4….. 108

4.5.1 Statement……. 108

4.5.2 Mathematics……..... 108

4.5.3 Column Profile……..... 110

4.5.4 Pinch Point Loci…….. 111

4.5.5 Analysis of Column Profile……. 112
4.5.6 Pinch Point……... 114
4.5.7 Further Column Profiles…….. 115
4.5.8 Variations in $\mathbf{X}_{\Delta}$ and r_{Δ}…… 116
4.6 APPLICATIONS AND CONCLUSION…….. 118

5. CHAPTER 5: NOVEL GRAPHICAL DESIGN METHODS FOR COMPLEX MEMBRANE CONFIGURATIONS AND HYBRID PROCESSES …….. 120
ABSTRACT…….. 120
5.1 INTRODUCTION…….. 121
5.2 COLUMN SECTIONS…… 124
5.2.1 Definition……. 124
5.2.2 The Difference Point Equation…… 126
5.2.3 Vapour-Liquid Equilibrium and Permeation Flux…….. 128
5.2.4 Column Profiles…….. 129
5.3 COMPLEX MEMBRANE CONFIGURATION DESIGNS: GENERAL……. 130
5.3.1 Overview……. 130
5.3.2 Petlyuk Membrane Arrangement…… 130
5.3.3 Material Balances…… 133
5.4 COMPLEX MEMBRANE CONFIGURATION DESIGNS: OPERATING CONDITION 1……. 134
5.4.1 Statement…… 134
5.4.2 Mathematics……... 134
5.4.3 Column Profiles……. 137
5.4.4 Requirements for Feasibility…….. 138
5.4.5 Analysis and Behaviour of Column Profiles…….. 139
5.4.6 Feasible Coupled Columns……. 144
5.5 COMPLEX MEMBRANE CONFIGURATION DESIGNS: OPERATING CONDITION 2……. 152
5.5.1 Statement…… 152

5.5.2 Mathematics…… 153
5.5.3 Column Profiles…….. 154
5.5.4 Feasibility…… 155
5.6 COMPARISON WITH DISTILLATION SYSTEMS……. 159
5.7 HYBRID DISTILLATION-MEMBRANE DESIGN……. 161
5.7.1 Overview……. 161
5.7.2 Material Balances…… 163
5.7.3 Feasibility…… 164
5.8 CONCLUSION……. 175

6. CHAPTER 6: RELIABLE METHODOLOGY FOR FINDING ALL STATIONARY POINTS IN MULTICOMPONENT NONIDEAL MIXTURES... 176
ABSTRACT……... 176
6.1 INTRODUCTION……... 178
6.2 THE FORMULATION OF THE FIXED POINTS IN A DISTILLATION COLUMN……. 180
6.3 DEFINITION OF A PINCH POINT……... 181
6.4 INTERVAL ANALYSIS AND HOMOTOPY CONTINUOUS METHOD….. 183
6.4.1 Interval Analysis…….. 183
6.4.2 Homotopy Continuous Method…… 183
6.5 RESULTS AND DISCUSSION……. 189
6.5.1 Ideal Mixture…… 189
6.5.2 Nonideal Mixture with Azeotrope…… 191
6.5.3 Nonideal Mixture with Tangent Pinch Point…… 193
6.6 CONCLUSION…….. 193

7. CHAPTER 7: CONCLUDING REMARKS…….. 195

REFERENCES…… 198

APPENDIX A..... 207
APPENDIX B..... 210
APPENDIX C..... 211
APPENDIX D..... 214
APPENDIX E..... 225

LIST OF FIGURES

CHAPTER 2:

Figure 2.1: Simple batch membrane separation. …… 9

Figure 2.2: Membrane Residue Curve Map (M-RCM) for an ideal A-B-C system with $\alpha_{AB}^{M} = 3$, $\alpha_{CB}^{M} = 1.5$ and $r = 10$. ……. 15

Figure 2.3: Regions created with in the M-RCM by the unidistribution line for component C. ……. 18

Figure 2.4: The effect of changing the order of the relative permeabilities: (a) A – unstable node, B – saddle point, C – stable node (b) Components A and B have equal permeabilities, while that of C is lower. …….. 20

Figure 2.5: M-RCM for methanol/MTBE/butene with $\pi_P \approx 0$. ……. 23

Figure 2.6: M-RCM for methanol/MTBE/butene. (a) π_P = 0.5 bar, (b) π_P = 1.0 bar, and (c) π_P = 1.5 bar. Unshaded region = From retentate To permeate (effective separation) Shaded region = From permeate To retentate (ineffective separation)……. 26

CHAPTER 3:

Figure 3.1: Membrane Residue Curve Map (M-RCM) for an ideal A-B-C system with $\alpha_{AB}^{M} = 3$, $\alpha_{CB}^{M} = 1.5$ and $r = 10$. (Reproduced from Peters et al. (2006a))……. 35

Figure 3.2: Simple batch membrane separation, with accumulating permeate…… 37

Figure 3.3: Initial retentate composition $x(0)$ = [0.4, 0.3].
(a) (*i*) Residue curve, (*ii*) Permeate curve, and
(*iii*) Accumulated permeated curve,
(b) Operating region or "leaf". The region is bounded
by the curves (*i*) and (*iii*), as well as mass balance
lines (*A*) and (*B*). ……. 41

Figure 3.4: Operating line in the methanol/butene/MTBE system
(a) $\pi_P = 0$, (b) $\pi_P > 0$. …….. 44

Figure 3.5: (a) Residue (solid) and Permeate (dashed) curves for example.
(b) Inverse of separation vector (g_i) versus x_B.
(c) Graph of h_i versus x_B…….. 46

Figure 3.6: Single stage non-reflux continuous membrane
operating under a co-current flow regime. …….. 49

Figure 3.7: Membrane column.
(a) Total reflux, (b) Infinite and Finite Reflux. ……... 54

Figure 3.8: Bow-tie region bounded by direct and indirect
mass balance lines. …….. 57

Figure 3.9: Sequencing of membrane columns using
(a) direct split, (b) indirect split, and (c) non-sharp split. … 59

Figure 3.10: Sequencing of cascades of membrane modules for
methanol separation at (a) $\pi_p = 0$, and (b) $\pi_p > 0$. ……... 60

Figure 3.11: D-RCM at P = 6bar. …… 62

Figure 3.12: (a) Operating leaves for distillate and bottoms
products, and membrane profile for the
(b) process configuration.
(Reproduced from Peters et al. (2006b)) ……. 64

Figure 3.13: (a) A possible hybrid configuration,
(b) The column sections for the hybrid system
(reproduced from Peters et al. (2006b)) …….. 66

Figure 3.14: Feasibility ranges for $R_{\Delta 1}$ ($0 < x_{2top} < 1$). ……... 70

Figure 3.15: Column and membrane profiles for the hybrid design in Figure 3.12 with $R_{\Delta 1} = 40$ and $n_1 = 5$. …… 71

Figure 3.16: Profile options (a) and (b) for the hybrid design in Figure 3.12 with $R_{\Delta 1} = 40$ and $n_1 = 5$. …… 72

Figure 3.17: Attainable Region for $n_1 = 4$, operating at r_{min}. Select $R_{\Delta 1}$ -values between 41.77 and 250 have been chosen. ….. 74

Figure 3.18: (a) Attainable Region for $R_{\Delta 1} = 70$, operating at r_{min}. $2 < n_1 < 7$.
(b) minimum n_1, and
(c) maximum n_1 tangent to CS 3 profile. …… 75

CHAPTER 4:

Figure 4.1: Example of a single stage non-reflux continuous membrane unit, operating under a counter-current flow regime. ……. 81

Figure 4.2: (a) A continuous membrane column.
(b) Column section breakdown. ……. 81

Figure 4.3: A generalized membrane column section. ……. 84

Figure 4.4: Strip of membrane column section. …… 88

Figure 4.5: Membrane Residue Curve Map (M-RCM) for an ideal A-B-C system with $\alpha_A = 3$, $\alpha_C = 1.5$.
(Reproduced from Peters et al. (2006a)) …… 92

Figure 4.6: Entire M-RCM.
MBT in blue, line of discontinuity in green. ……. 94

Figure 4.7: Membrane column profile for Case 2. Positive Integration.
$R_T = 100$ *mol/s*, $\boldsymbol{\delta}_T = [0.1, -0.05]$, $\mathbf{x}_T = [0.3, 0.3]$. ……. 98

Figure 4.8: Shifted M-RCMs. The blue triangle represents the MBT, the red shows the transformed triangle. (a) $\beta(A=0) = 1$, (b) $\beta(A) = 1.667$. $\boldsymbol{\delta}_\mathbf{T} = [0.1, -0.05]$, $\mathbf{x}_\mathbf{T} = [0.3\ 0.3]$. Actual membrane profile (see Figure 4.4) is tangent to bold profile at the point indicated. ……. 100

Figure 4.9: Tangency of curves to the column profile. Each curve corresponds to a different $\beta(A)$-value, and is allowed to run to its stable pinch point. ……. 102

Figure 4.10: Pinch Point Loci for $\boldsymbol{\delta}_\mathbf{T} = [+, -, -]$. …… 103

Figure 4.11: Column Profiles for selected values of (a) R_T with $\mathbf{x}_\mathbf{T} = [0.3, 0.3]$, (b) $\mathbf{x}_\mathbf{T}$ with $R_T = 100$ *mol/s*. Figure 4.5(a) has been superimposed. …… 105

Figure 4.12: Membrane column profile for Cases 3 & 4. Positive Integration. …… 110

Figure 4.13: Pinch Point Loci for $\mathbf{X}_\boldsymbol{\Delta} = [0.3, 0.3]$. …….. 111

Figure 4.14: Shifted M-RCM. The blue triangle represents the MBT, the red shows the transformed triangle. $\mathbf{X}_\boldsymbol{\Delta} = [0.3, 0.3]$, $\mathbf{x}_\mathbf{T} = [0.3, 0.2]$, $r_\Delta = 6$. Actual membrane profile (see Figure 4.12) is tangent to bold profile at the point indicated. …… 112

Figure 4.15: Tangency of curves to the column profile. Each curve corresponds to a different r_Δ-value, and is allowed to run to its stable pinch point. …… 113

Figure 4.16: Column Profiles for selected values of (a) r_Δ with $\mathbf{x}_\mathbf{T} = [0.3, 0.2]$, (b) $\mathbf{x}_\mathbf{T}$ with $r_\Delta = 6$. ……. 116

Figure 4.17: Effect of the sign of r_Δ on the trajectory of the profile. Each profile is influenced by its associated stable pinch point locus. …… 118

CHAPTER 5:

Figure 5.1: Generalized column sections (CS).
(a) Distillation, (b) Membrane. …….. 125

Figure 5.2: (a) Petlyuk-type arrangement for membranes.
(b) Column Section breakdown. …… 131

Figure 5.3: Petlyuk arrangement operating at overall infinite reflux. .. 132

Figure 5.4: Coupled membrane column sections. …… 132

Figure 5.5: Retentate (solid) and permeate (dotted) column profiles for CS 1 (red) and 2 (blue). $\mathbf{x_T} = [0.2, 0.3]$, $\mathbf{X_\Delta} = [0.3, 0.3]$, $r_{\Delta 1} = 5$, and $r_{\Delta 2} = -5$. …… 137

Figure 5.6: (a) Pinch point loci for $\mathbf{X_\Delta} = [0.3, 0.3]$.
(b) Tangency of curves to a column profile commencing at $\mathbf{x_T} = [0.3, 0.2]$. Each curve corresponds to a different r_Δ-value, and is allowed to run to its stable pinch point.
(reproduced from Peters et al. (2007)). …… 140

Figure 5.7: Effect of the sign of r_Δ on the location of **y** with respect to **x** and $\mathbf{X_\Delta}$. …… 146

Figure 5.8: (a) Example of retentate profile (solid) passing through the pinch point loci (crosses), resulting in the permeate curve (dotted) intersecting with the retentate.
(b) Zoomed in version of (a),
showing the mass balance lines (dashed). …….. 147

Figure 5.9: Region of $\mathbf{x_T}$-locations for feasibility with $\mathbf{X_\Delta} = [0.3, 0.3]$ in the membrane coupled column sections. …… 148

Figure 5.10: Feasible $\mathbf{x_T}$ regions for
(a) $\mathbf{X_\Delta} = [-,+,-]$ and (b) $\mathbf{X_\Delta} = [+,-,+]$. …… 149

Figure 5.11: Retentate (solid) and permeate (dotted) profiles for CS 1 (red) and CS 2 (blue), commencing at $\mathbf{x_T} = [0.45, 0.4]$, with $\mathbf{X_\Delta} = [0.3, 0.3]$ operating at (a) $r_{\Delta 1}\big|_T = 10 = -r_{\Delta 2}\big|_T$, (b) $r_{\Delta 1}\big|_T = 16.037 = -r_{\Delta 2}\big|_T$, and (c) $r_{\Delta 1}\big|_T = 20 = -r_{\Delta 2}\big|_T$. ……. 151

Figure 5.12: Retentate (solid) and permeate (dotted) column profiles for CS 1 (red) and CS 2 (blue). $\mathbf{x_T} = [0.3, 0.3]$, $R_{T1} = 100\ mol/s = R_{T2}$, $\boldsymbol{\delta_{T1}} = [0.04, -0.08] = -\boldsymbol{\delta_{T2}}$ are represented in green. …….. 155

Figure 5.13: Retentate (solid) and permeate (dotted) column profiles for CS 1 (red) and CS 2 (blue). $\mathbf{x_T} = [0.3, 0.3]$, $\boldsymbol{\delta_{T1}} = [0.04, -0.08] = -\boldsymbol{\delta_{T2}}$ are represented in green. (a) Fixed flowrates (i.e. $\beta(A) = 1$), (b) Varying flowrates with $R_{T1} = 100\ mol/s = R_{T2}$. …… 158

Figure 5.14: Possible variations of a membrane module thermally linked to a distillation column. ……... 162

Figure 5.15: Coupled distillation and membrane column sections. …… 162

Figure 5.16: (a) – (c) Commencing the retentate profiles at various $\mathbf{x_T}$-values. The corresponding permeate profile eventually always approximates its pinch point curve. …… 166

Figure 5.17: Some liquid profiles (solid), and their corresponding vapour profiles (dashed) relative to $\mathbf{X_\Delta}$. ……. 168

Figure 5.18: Liquid pinch point locus within the MBT. ……. 170

Figure 5.19: The permeate (purple) and liquid (green) pinch point loci defining an initial region of feasibility. …… 170

Figure 5.20: CPM for the DCS at $r_{\Delta D} = -5$ and $\mathbf{X_\Delta} = [0.3, 0.3]$. MBT in blue, shifted triangle in red. ……... 172

Figure 5.21: Region of possible $\mathbf{x_T}$ locations, for the operating conditions chosen, that would result in a feasible arrangement. …….. 172

Figure 5.22: (a) Column profiles for the membrane and distillation sections with $\mathbf{x_T}$ in the feasible region. (b) Zoomed in version of (a). 173

CHAPTER 6:

Figure 6.1: Fixed points in a ternary mixture and residual errors of equations 6.3 and 6.5. ……. 182

Figure 6.2: The homotopy continuation function. The simple function is the residue map equations with ideal mixture.
(a) Its solution is the pure component (A,B,C) at *t = 0*.
(b) Final solution is the pinch point when *t = 1*. …… 185

Figure 6.3: Solution branch on the composition triangle and bifurcation diagram for the fixed points for the ideal mixture
(a) Stable pinch point, (b) Unstable Pinch point,
(c) Saddle point. …….. 190

Figure 6.4: Solution branch on the composition triangle
(a) and bifurcation diagram (b) for the fixed points for the azeotropic mixture (Acetone, Chloroform and Benzene).
(α) Unstable Point, (β) Saddle Point, (γ) Pinch Point. …… 191

Figure 6.5: Solution branch on the composition triangle
(a) bifurcation diagram (b) for all fixed points and
(c) trajectory of pinch branch γ for the azeotropic mixture (Acetone, Chloroform and Methanol).
(α) Unstable Point, (β) Saddle Point, (γ) Pinch Point. …… 192

Figure 6.6: Composition profiles showing the presence of tangent pinch and solution branch successfully identified tangent pinch for a nonideal mixture (Acetaldhyde, Methonal and Water) by homotopy continuation method. …… 194

LIST OF TABLES

Table 3.1: Design variables in hybrid configuration (refer to Figure 3.13). $R_{\Delta 1}$ is a degree of freedom. …… 68

Table 3.2: Design parameters for the different cases displayed in Figure 3.16. ……. 73

Table 5.1: Nomenclature and symbols used in equations 5.1 and 5.2. 126

Table 5.2: (a) Signs of permeate and retentate flows for a CS with a positive r_{Δ}. …… 136

Table 5.2: (b) Signs of permeate and retentate flows for a CS with a negative r_{Δ}. ……... 136

NOMENCLATURE

- Scalar quantities represented in *italics*.
- Vector quantities represented in **bold**.

SYMBOLS

A	:	Membrane area [m^2]
A'	:	Dimensionless membrane area
B	:	Bottoms flowrate [*mol/s*]
c	:	Number of components
D	:	Distillate flowrate [*mol/s*]
F	:	Feed flowrate [*mol/s*]
J	:	Membrane flux $\left[\frac{mol}{s \cdot m^2}\right]$
$\mathbf{J}$	:	Vector of fluxes
J_i	:	Flux of component *i* through the membrane $\left[\frac{mol}{s \cdot m^2}\right]$
k_i	:	parameter value for component *i* (see Appendix B for values)
L	:	Liquid flowrate [*mol/s*]
n	:	Number of theoretical stages in a distillation column section
p_i^0	:	Saturation pressure of component *i* [*Pa*]
P	:	Permeate flowrate [*mol/s*]
P_i'	:	Permeability of component *i* $\left[\frac{mol \cdot m}{s \cdot m^2 \cdot Pa}\right]$
$\dot{P}$	:	Permeate removal rate [*mol/s*]
R	:	(continuous) Retentate flowrate [*mol/s*]
R	:	(batch) Retentate hold-up [*mol*]
r	:	Ratio of pressures (flux model)
r	:	Split ratio (hybrid design – see section 3.6.2)

R_Δ	:	Reflux ratio (used in distillation CS's in section 3.2.6)
r_Δ	:	Reflux ratio (used in Chapters 4 and 5)
$\mathbf{s}$	:	Separation vector
S	:	Side-draw flowrate [*mol/s*]
t	:	Time [*s*]
V	:	Vapour flowrate [*mol/s*]
x	:	Residual fluid molar composition
$\mathbf{x}$	:	Retentate composition
X_Δ	:	Difference point (scalar)
$\mathbf{X_\Delta}$	:	Difference point (vector)
$\mathbf{y}$	:	Permeate composition
y	:	Vapour phase molar composition

GREEK LETTERS

α_{ij}^{D}	:	Relative volatility for distillation.
α_{ij}^{M}	:	Ratio of permeabilities, or *membrane selectivity*
$\beta(A)$	:	Ratio of R_T to $R(A)$
Δ	:	Net molar flow in a column section [*mol/s*]
δ	:	Thickness of the membrane [*m*]
$\boldsymbol{\delta}$	:	Difference vector
γ_i	:	Liquid phase activity coefficient
π_P	:	Permeate (low) pressure [*Pa*]
π_R	:	Retentate (high) pressure [*Pa*]
τ	:	Dimensionless time

SUBSCRIPTS

acc	:	Referring to an accumulated amount
D	:	Referring to distillation
i	:	Referring to component *i*
j	:	Referring to component *j*
M	:	Referring to membrane separation
P	:	Referring to permeate
R	:	Referring to retentate
T	:	Referring to the top

SUPERSCRIPTS

D	:	Referring to distillation
M	:	Referring to membrane separation

ABBREVIATIONS

AR	:	Attainable Region
CPM	:	Column Profile Map
CS	:	Column Section
DCS	:	Distillation Column Section
DE	:	Differential Equation
DPE	:	Difference Point Equation
D-RCM	:	Distillation Residue Curve Map
MBT	:	Mass Balance Triangle
MCS	:	Membrane Column Section.
M-RCM	:	Membrane Residue Curve Map
MTBE	:	Methyl Tertiary-Butyl Ether
SP	:	Stationary Point
VLE	:	Vapour-Liquid Equilibrium

CHAPTER 1:

INTRODUCTION

1.1 OVERALL INTRODUCTION

Novel separation procedures have been an important focus for researchers and engineers in recent decades. Separation processes, both batch and continuously operated, are essential in the chemical industry. Distillation is the most commonly used of all separation techniques, especially for the separation of fluid mixtures. While this conventional method has proven its worth, it has unfortunately come at a price – distillation is renowned for being both capital and energy intensive.

The global drive for cleaner, more energy-efficient processes has lead to the search for alternative separation methods. Membrane permeation is one such alternative. It is different from distillation since it is not equilibrium-based, and thus does not exhibit the same limitations, such as azeotropes. Various types of membranes have been proposed and designed, each performing a unique type of separation (Rautenbach and Albrecht (1989)). Pervaporation and vapour permeation membranes, however, are the most attractive alternatives for distillation.

Although expensive, distillation still receives a great deal of attention in literature, especially with regard to the design of such systems. Membrane systems are also well researched and documented. However, the nature of the research is very different from distillation, therefore making it difficult to find any correlations between the two processes, if any. One important difference is that the design of distillation systems makes use of various graphical techniques, while it is not as prominent in membrane design. These graphical methods do not only allow one to design traditional distillation circuits (Fien and Lui (1994)), but also provide insight

into their operation and performance. Furthermore is that they also allow one to design complex configurations (Tapp et al. (2004), Holland et al. (2004a)). Such developments are not possible with the current methods proposed for membrane design.

1.2 AIM OF THESIS

The aim of this thesis is to introduce graphical methods to membrane permeation design. The techniques are then applied to both conventional batch and continuous processes. The ideas are further extended to more complex arrangements of membrane units. Finally, and most importantly, since the unit operations for both membrane and distillation are analyzed from the same perspective, the design of hybrid arrangements of the two takes on a novel approach.

1.3 THESIS OVERVIEW

The chapters in the thesis have been written in the style of journal articles. Each of the chapters has been published, submitted for publication, or prepared for submission in a reputable international engineering journal. The current status of the each paper is given at the beginning of each chapter. As the chapters were written independently of each other, repetition of the basics occurs from one chapter to the next. However, this does allow each chapter to be read independently, with each having its own abstract, introduction and conclusion. The chapters have been placed in a suggested order for reading, as one chapter builds on the work and ideas given in the chapter prior to it.

Chapter 2 introduces and derives Membrane Residue Curve Maps (M-RCM). Plots are generated for both ideal and real systems, and the properties of each are explored.

Chapter 3 follows from the preceding chapter, and displays the various direct applications of M-RCM's to both batch and continuous processes, including hybrids. Operating regions (or "leaves"), permeation time (or area), and sequencing are some of the results that emerge.

Chapter 4 adapts the M-RCM and the equations which describe it to a general membrane permeator, or column section, operating finite reflux. All possible flow and composition arrangements are explored, and the behavioral properties of the profiles are explained.

Chapter 5 employs the profiles for finite reflux into synthesizing complex arrangements of membrane units, as well as hybrids containing membrane separation and distillation. A thermally-coupled arrangement is used for demonstration purposes. Methods of locating regions of feasibility are given.

Chapter 6 presents work done together with Dr. Libin Zhang (University of Illinois at Chicago). I was involved in the preliminary fundamentals, but he is responsible for the Newton-Raphson method and Bifurcation Detection which constitute a major portion of the work. He wrote the paper, and agreed for me to place it in my thesis. Although different in nature from the previous chapters, this work is relevant in this thesis since it begins to address the need for finding reliable methods for calculating stationary points and pinch point loci. As will be shown in Chapters 4 and 5, the knowledge of these is important. This chapter is written from a distillation point of view, but its relevance will be evident from the prior chapters.

CHAPTER 2:

DERIVATION AND PROPERTIES OF MEMBRANE RESIDUE CURVE MAPS

The material in this chapter has been published in Industrial and Engineering Chemistry Research. Reference: Peters, M.; Kauchali, S.; Hildebrandt, D.; Glasser, D. Derivation and Properties of Membrane Residue Curve Maps. *Ind. Eng. Chem. Res.*, **2006**, *45*, 9080–9087.

ABSTRACT

Residue curve maps have been developed for membrane permeation systems. A "thought experiment" was conducted whereby a fluid mixture was allowed to permeate through a diffusion membrane in a batch still. The differential equations which describe any residue curve are derived from mass balances, implying that Membrane Residue Curve Maps (M-RCM's) can be used for any type of membrane, provided the appropriate permeation (flux) model is used. In this paper a simple constant relative permeability model is used for demonstration purposes, and as an example an M-RCM is plotted for the methanol/butene/MTBE using the appropriate flux data. The curves in an M-RCM trace the change in composition of the residual retentate in the batch still. At any time during batch permeation, the permeate composition is related to that of the retentate at that particular time, thus allowing a *membrane separation vector* to be defined as the vector difference between the two compositions.

2.1 INTRODUCTION

Separation processes are of fundamental importance in the chemical industry. It is inevitable that during any chemical process, be it continuous or batch, the need for effective separation will arise. There are a variety of separation options available. However, distillation has proven to be the most effective and commonly used method, especially for the separation of mixtures containing compounds with relatively low molecular weights, such as organic substances. Other separation techniques that have demonstrated efficient use are absorption as well as liquid-liquid (solvent) extraction. Membrane permeation has, only in recent years, come to the fore as a successful method of separating mixtures, both gaseous and liquid (Pressly and Ng (1998)). One would like to have available a method to select the appropriate method of separation to achieve the required product specialties. This chapter will begin to help to address the need.

Membranes have been developed for various applications (Rautenbach and Albrecht (1989)). In this paper, only diffusion membranes (e.g. gas separation and pervaporation membranes) will be considered, but the method described can be applied to the other kinds of membranes. In diffusion membranes, a high pressure fluid mixture comes into contact with a membrane which selectively permeates certain components of the mixture. The separation is achieved by maintaining a low pressure (sometimes vacuum) on the *permeate* side of the membrane. The remaining high pressure fluid is known as the *retentate*. Gas separation involves the diffusion of a gaseous mixture, whilst pervaporation is a separation process where one component in a liquid mixture is preferentially transported through the membrane, and is evaporated on the downstream side, thus leaving as a vapour.

The conventional way of analysing membrane separators is to ask what *permeate* composition can be achieved for a particular *feed*, such as was done in the experiment conducted by Van Hoof et al. (2004) , as well as the one performed by Lu et al.

(2002). Furthermore, the flux of a particular component through the membrane is also reported as a function of the feed in these and similar experiments. However, it must be remembered that the flux of any of the components may not necessarily remain the same, and may vary as permeation proceeds down the length of the membrane. Thus, the conventional information, although accurate, is insufficient, especially when it comes to designing industrial-scale membrane separators, as well as sequencing of such equipment.

When examining how the other, more established, separation processes are analysed, it can be seen that the methods used for membranes are somewhat ineffective. In distillation, as well as single stage flash separations, one never reports how either the tops or bottoms products are related to the feed, but rather how they are related to each other. A similar kind of analysis is made when designing solvent extraction circuits – one requires the equilibrium data that relates the aqueous phase to the organic phase.

Relating the two product streams to each other allows one to design multiple flash units, or cascades, as well as counter-current liquid-extraction circuits. The design of such reflux cascades would be impossible to perform if either one of the product compositions was related to the feed to any of the units within the cascade. It is necessary to analyze membrane separators in a similar manner – one needs to investigate how the permeate composition is related to that of the retentate.

The mathematical modelling of how the permeate is related to the retentate has previously been performed. Eliceche et al. (2002) model a pervaporation unit for a binary separation – the analysis was done by considering the flux of each component through the membrane, as well as solving simultaneous mass and energy balance equations. Stephan et al. (1995), on the other hand, described the permeation by a simple dual mode transport model, and made use of Henry's Law to relate the permeate composition to the composition of the retentate. A more fundamental and

thermodynamic approach is given in the article by Wijmans and Baker (1995). In this review, the concentration and pressure gradients in the membrane are described using *chemical potentials* as the fundamental starting point. By appropriately modelling the chemical potentials, and by making use of Fick's Law of diffusion, Wijmans and Baker (1995) are able to model the permeation for the various types of membranes, including gas separation and pervaporation. The details of the resulting equation for gas separation are discussed later in Section 2.2.3.

Although the information in these models is correct, it is somewhat difficult to interpret. We thus formulate a **graphical technique** that can incorporate the appropriate models in order to interpret, analyse and design membrane separators in a convenient and efficient manner.

Traditionally, it was believed that Residue Curve Maps (RCM's) were only suitable for *equilibrium-based* separations, and could not be used for the representation of kinetically-based processes (Fien and Liu (1994)). However, the differential equations which describe a residue curve are merely a combination of *mass balance equations*. Because of this, the inherent nature of RCM's is such that they can be used for equilibrium- as well as non-equilibrium-based processes. This now allows one to be able to consider kinetically-based processes, such as reactive distillation (Barbosa and Doherty (1998), Doherty and Malone (2001), and Huang et al. (2004)) as well as membrane separation processes.

In this chapter, RCM's for membrane separation (without reaction) are introduced. The origin of these plots is described, and their various properties are discussed. Huang et al. (2004) perform a somewhat similar analysis. Although the main focus of their paper is on reactive membrane separation (whereby a reaction is allowed to proceed within the liquid phase before it is vaporized and permeated), they do also look at the non-reactive case, and plot the appropriate residue curve maps. However, the investigation discussed here is different from the one given by Huang et al. (2004)

since it *isolates* the membrane separation process. This allows one to understand the fundamental operation of membrane permeation on its own before combining it with, for example, boiling and/or reaction. Furthermore, any non-idealities, such as azeotropes, that may exist within the Vapour-Liquid Equilibrium (VLE) or reaction will not be reflected in the membrane separation. When creating a system that combines more than one phenomenon (e.g. reaction, boiling and permeation, as in the paper by Huang et al. (2004)) it becomes difficult to analyze which particular separation phenomenon is responsible for the observed behavior of the system. It also becomes difficult to determine where the advantages of each of the phenomena lie. It is for this reason that, in this chapter, membrane separation is analyzed on its own.

One of the objectives of developing M-RCM's was ultimately to design and synthesize hybrid distillation-membrane processes. It was realized that the level at which membrane separations had been researched was not at the same level as distillation. Not to say that irrelevant work had been done in the field, but rather that the nature of the work was not quite the same as distillation. Now, with the development of such maps, not only is it possible to understand the fundamentals of membrane separations more easily, but it is now possible to design such hybrid systems using a novel graphical technique. And with looking at the membrane individually, one is not limited to one hybrid configuration, as presented by Huang et al. (2004), making the possibilities infinite. By decoupling the membrane map from the VLE map, one can look at all possible combinations and indeed try to find when to use one or the other or combinations of both – that is, synthesize a process, rather than analyse it. Of course, much of this work is out of the scope of this article, but will be presented in future publications (see Chapters 3 and 5).

2.2 DERIVATION OF M-RCM'S

2.2.1 A THOUGHT EXPERIMENT

Consider the following "thought experiment": If a high pressure (π_R) fluid mixture, of quantity R [mol], is enclosed in batch still by a membrane, and a low pressure (π_P) is maintained on the other side of membrane, as shown in Figure 2.1, separation may occur. If the permeate is removed as soon as it is formed, separation will continue to occur until all the high pressure fluid has permeated through the membrane. One could, in practice, perform this experiment by using a balloon made out of the material of the membrane. By simply maintaining a high pressure on the inside of the balloon, its contents would permeate through the balloon to a controlled low pressure region on the outside.

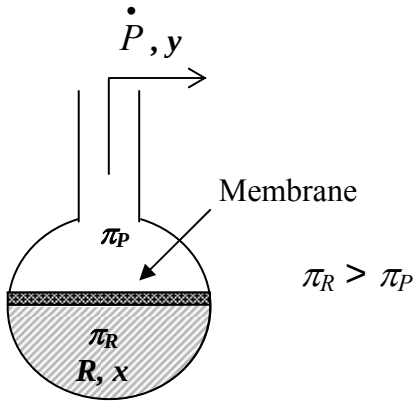

Figure 2.1: Simple batch membrane separation.

If one continuously analyses the composition of the residual fluid, or *retentate*, with time until the last trace of fluid mixture permeates through the membrane, one is then able to plot the change in retentate composition. Such a curve is known as a *membrane residue curve*. One could repeat the experiment with different initial feed compositions, and would be able to create an entire series of membrane residue

curves that populate the entire mass balance region – such a plot is called a *Membrane Residue Curve Map (M-RCM)*.

***Definition**: A Membrane Residue Curve Map (M-RCM) plots the change, over time, in composition of the retentate in a batch still.*

As mentioned before, Huang et al. (2004) perform a similar thought experiment. In their experiment, a liquid is boiled, and vaporized, in a batch still. The vapour is then allowed to permeate through a gas separation membrane. This differs from the set-up displayed here in that it does not isolate the membrane permeation on its own. As discussed in the Introduction (see Section 2.1), by analyzing batch membrane permeation as an individual process will allow one to investigate its usefulness. Furthermore, any non-idealities that may arise from the VLE or reaction kinetics will not influence the membrane permeation.

2.2.2 MASS BALANCES

One could also describe this residual plot mathematically: Since the high pressure fluid is charged to the still at time t_o, and there is no reaction taking place, the following overall and component mass balances on the batch still can respectively be written (refer to Figure 2.1):

$$0 = \dot{P} + \frac{d}{dt}(R), \tag{2.1}$$

$$0 = \dot{P} \cdot y_i + \frac{d}{dt}(R \cdot x_i) = \dot{P} \cdot y_i + R \cdot \frac{d}{dt}(x_i) + x_i \cdot \frac{d}{dt}(R) \tag{2.2}$$

where $\dot{P}$ is vapour removal rate [mol/s],

R is the amount of residual fluid remaining in the still at any time during the permeation process [mol], and

t is time [s].

x_i is the mole composition of component i in the retentate phase,

y_i is the mole composition of component i in the permeate phase,

Substituting equation 2.1 into equation 2.2, the following set of differential equations (DE's) are obtained (refer to Appendix A for proof):

$$\frac{d}{d\tau}(x_i) = (x_i - y_i) \qquad i = 1,\ 2,\ \ldots,\ c-1, \tag{2.3}$$

where c is the number of components present in the initial charge, and

τ is a dimensionless time, defined by

$$\tau(t) = \ln\left[R(0) \Big/ R(t) \right], \tag{2.4}$$

with *R(0)* and *R(t)* being the total molar retentate hold-up in the still at $t = 0$ (i.e. initially) and at time t, respectively. Thus, τ is the reciprocal of the natural logarithm of the fraction of retentate that needs to be removed (i.e. permeated) from the still to obtain a desired purity.

2.2.3 PERMEATION MODELING

In order to solve the DE's in equation 2.3 and plot a M-RCM, it is necessary to understand how y_i is related to x_i. It is important to recognize that a membrane is used for separation because of the differential rate of permeation of different species.

As discussed in the Introduction, there are numerous methods of describing how x_i is related to y_i. A fundamental thermodynamic approach is taken here, using the model described by Wijmans and Baker (1995). Thus the *flux* of component *i* through a gas separation membrane may be described as:

$$J_i = \frac{P_i^{'}(\pi_R x_i - \pi_P y_i)}{\delta} \tag{2.5}$$

where J_i is the flux of component *i* through the membrane $\left[\frac{mol}{s \cdot m^2}\right]$,

$P_i^{'}$ is the permeability of component *i* (which is equal to the product of solubility and diffusivity) $\left[\frac{mol \cdot m}{s \cdot m^2 \cdot Pa}\right]$,

π_R is the (high) retentate pressure [Pa],

π_P is the (low) permeate pressure [Pa], and

δ is the effective thickness of the membrane [m].

The reader is referred to Wijmans and Baker (1995) for the full derivation of equation 2.5. It should, however, be noted that the flux model given in equation 2.5 applies to **gas separation** only. Appropriate modeling can be performed for other types of membrane operation. *What's important to note, however, is that the method displayed here can be applied for all membrane types, provided an appropriate flux model is used*! The gas separation model is used in this chapter for demonstration purposes.

Since the flux of any component is the amount of material that permeates through the membrane per unit time per unit area, one may also write:

$$J_i = \frac{P \cdot y_i}{A_m} \tag{2.6}$$

An expression for component *i* can be written by combining equations 2.5 and 2.6. A similar expression can be written for component *j*. Dividing the two expressions yields the following general model:

$$\frac{y_i}{y_j} = \alpha_{ij}^{M} \frac{(rx_i - y_i)}{(rx_j - y_j)}, \quad \text{where} \quad \alpha_{ij}^{M} = \frac{P_i'}{P_j'} \text{ and } r = \frac{\pi_R}{\pi_P} \tag{2.7}$$

where α_{ij}^{M} is known as *membrane selectivity*, or the permeability of *i* with respect to *j*.

r is known as the ratio of pressures.

Furthermore, for an *effective* separation to occur

$$\pi_R x_i > \pi_P y_i \quad \text{or} \quad \frac{y_i}{x_i} < r \quad . \tag{2.8}$$

Often in practice, however, to ensure that permeation will occur effectively, a vacuum is maintained on the permeation side of the membrane, i.e. $\pi_P \approx 0$. Using this value in equation 2.5, and following the same method as before, the general equation under this condition is simplified to:

$$\frac{y_i}{y_j} = \alpha_{ij}^{M} \frac{x_i}{x_j} \tag{2.9}$$

One is able to use the above-described models (equation 2.7 or equation 2.9) in the membrane residue curve equation (equation 2.3) and solve the set of simultaneous equations in order to plot the M-RCM.

It is accepted that the permeabilities of the components may well depend on a number of variables, such as the retentate and/or permeate composition, and that mass transfer through the membrane can be quite complex. However, for the purposes of illustrating membrane systems with residue curve maps, a simple point of view will be taken. Thus, we will not go into the details of the mechanisms of mass transfer. For this reason, *constant relative permeabilities* will be assumed. With constant permeability ratios, the only driving force for permeation is the partial pressure difference (refer to equation 2.5), resulting in what is known as a *Knudsen-membrane* (Huang et al. (2004)).

2.2.4 AN IDEAL MAP

Using a batch still with a non-zero permeate pressure, and assuming the following values:

$$\alpha_{AB}^{M} = 3,\ \alpha_{CB}^{M} = 1.5,\ r = 10 \tag{2.10}$$

The resulting M-RCM is shown in Figure 2.2.

The relative permeability values inform us that component A has the highest rate of permeation, and thus the retentate is depleted of A. This can be seen graphically on the M-RCM – the membrane residue curves move out of pure A. Component B has the lowest permeation rate, implying that the retentate will become richer in B, hence the residue curves move towards pure B. Component C has a permeation rate that lies in between that of A and B, thus curves neither originate nor terminate at pure C, but do tend to move towards pure C, before moving to B. It is worth noting that the curves never reach pure C – some may get very close, but will never terminate there.

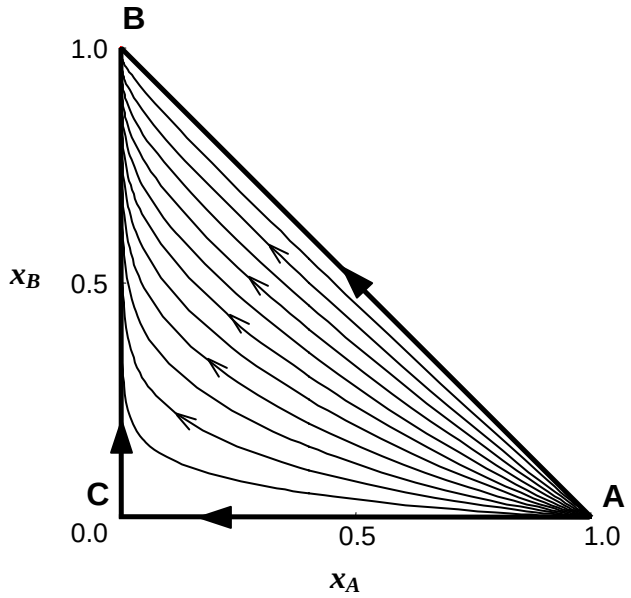

Figure 2.2: Membrane Residue Curve Map (M-RCM) for an ideal A-B-C system with $\alpha_{AB}^{M} = 3$, $\alpha_{CB}^{M} = 1.5$ and $r = 10$.

In a similar manner, one could plot the M-RCM for a batch membrane system with a vacuum on the permeation side. The resulting plot, as it turns out, is topologically very similar to the one shown in Figure 2.2.

2.3 PROPERTIES OF M-RCM'S

2.3.1 STATIONARY POINTS

Stationary points occur when $x_i = y_i$ (for all i), and are classified as either stable, unstable or saddle point (Fien and Liu (1994) and Kiva et al. (2003)). The stationary points for the M-RCM in Figure 2.2 are: pure A is the unstable node, pure B is the stable node and pure C is the saddle point.

Stationary points also occur at any point where the retentate composition is equal to the vapour composition, and is not changing with time. Such a point is known as an *arheotrope* (Huang, et al.(2004)). Figure 2.2 exhibits no arheotropes, since α_{ij}^{M}-values are constant. The M-RCM shown in Figure 2.2 is *ideal*. A membrane permeation system would only exhibit arheotropes (see Section 2.4) if the permeabilities of the substances became dependent on the retentate and/or permeate composition. That is, the membrane behaved non-ideally.

2.3.2 MEMBRANE VECTOR FIELD

If x_i and y_i are viewed as *vectors*, then one can re-write the set of DE's in equation 2.3 as a single vector DE:

$$\frac{d}{d\tau}(\mathbf{x}) = (\mathbf{x} - \mathbf{y}) \tag{2.11}$$

The degree of separation obtained at any time during permeation would be the difference between the vapour and liquid compositions at that time. Formally, one may refer to this as the *membrane separation vector*:

$$\mathbf{s} = (\mathbf{x} - \mathbf{y}) \tag{2.12}$$

As can be seen, **s** is simply the right hand side of the DE in vector form. Furthermore, it can be deduced that **s** is *tangent* to a residue curve at the retentate composition.

The separation vector is only a function of **x** at that particular point. This means that a separation vector can be defined at every point within the Mass Balance Triangle (MBT), resulting in the entire space termed the *Membrane Vector Field*.

2.3.3 UNIDISTRIBUTION LINES

At any time during batch separation, it is possible that one of the components will be distributed between the retentate and permeate in such a way that both phases will have the same composition of that particular component. Thus, unidistribution occurs when $x_i = y_i$ for component i only. This results in the residue curves going through a turning point, with respect to x_i. To locate the turning points on the residue curves one needs to identify where the gradient of the curves go to zero relative to component i. The locus of these turning points yields what is known as the *unidistribution line*. Kiva et al. (2003) give a summary of this work (for distillation processes) which was initially discussed by Serfimov (1970). Such a plot is shown in Figure 2.3. This plot shows the unidistribtion line for component C for the M-RCM given in Figure 2.2.

The unidistribution line shown in Figure 2.3 initiates at pure C, and appears to end at about $x_A = 0.4$ on the AB binary line. However, every point along the AB binary is a turning point for component C, since no C exists in such a mixture! Thus, the entire AB binary line is, in fact, the end point for the unidistribution line. Notice that, in this particular M-RCM, unidistribution lines for components A and B do not exist. This is due to the nature and curvature of the residue curves. The only point where unidistribution for these components occurs is at their pure (stationary) points.

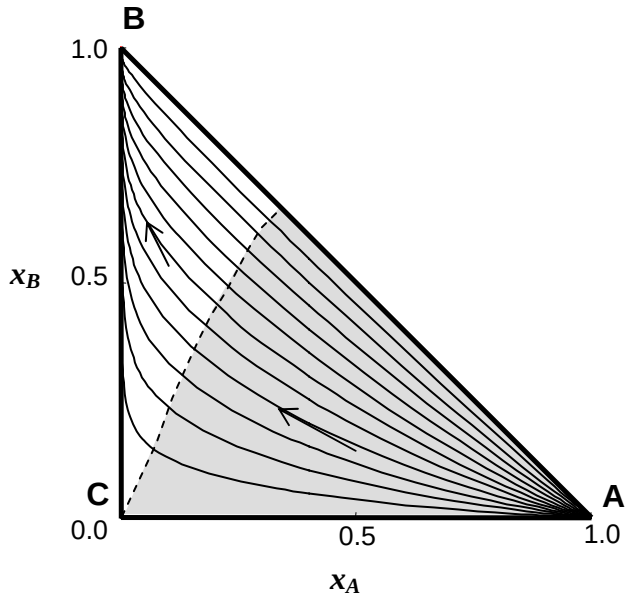

Figure 2.3: Regions created with in the M-RCM by the unidistribution line for component C.

Consider the 2 regions within the MBT created by the unidistribution line, as shown in Figure 2.3. Any separation vector in the larger (grey) region, such as the example shown, will exhibit the following properties: $x_A < y_A$, $x_B > y_B$, and $x_C > y_C$. In the smaller region: $x_A < y_A$, $x_B > y_B$, and $x_C < y_C$. It is clear that on either side of the boundary, the distribution of A and B remain the same, with the permeate being richer in A and the retentate richer in B in both regions. Component C, on the other hand, is richer in the retentate phase than the permeate in the larger region, but in the adjacent region, the opposite occurs.

Such information is useful when one needs to identify in which phase, for example, component C would ultimately report to. If one wants a permeate phase rich in A, then operating in the larger region would yield this since the retentate will be richer in components B and C. Operating in the smaller region would allow one to obtain a B-rich retentate, with most of the A and C leaving in the permeate. Furthermore, the maximum amount of C that can be obtained in either phase is indicated by the point where the appropriate residue curve (that the batch experiment follows) intersects the

unidistribution line. Such information is very difficult to extract from mathematical equations, yet is quite simple to visualize with the use of the M-RCM.

2.3.4 THE EFFECT OF α-VALUES ON THE TOPOLOGY OF M-RCM'S

The location of nodes and/or saddles as well as the curvature of the lines is collectively known as the *topology* of a residue curve map. The rate at which the various components permeate through the membrane is what will ultimately determine the topology of an M-RCM. Thus, the topology of an M-RCM is dependent on the relative permeabilities. The relative permeabilities, themselves, are dependent on the inherent properties of the membrane and the material it is made out of.

The order of permeability (from highest to lowest) of the MRCM shown in Figure 2.2 is A-C-B. If the values of the relative permeabilities are changed, whilst keeping the order the same, the location of the stationary points will not be altered. However, the curvature of the curves will be changed. The larger the difference in the values of the relative permeabilities, the easier the separation becomes, resulting in the residue curves being less curved.

If the order of the relative permeabilities is altered, the topology of the map is re-arranged. For example, if the order of permeabilities is changed from A-C-B, as in Figure 2.2, to A-B-C, the locations of the stationary points are changed. An example of such a plot is shown in Figure 2.4(a), where the pure B component point is now the saddle point, and C has now become the stable node since it now has the lowest relative permeability. There are many different scenarios which can occur, all of which depend on the order of the relative permeabilities of the involved substances. Furthermore, within each case it is also possible to analyse the curvature (whilst keeping the order the same), as was done for the A-C-B case.

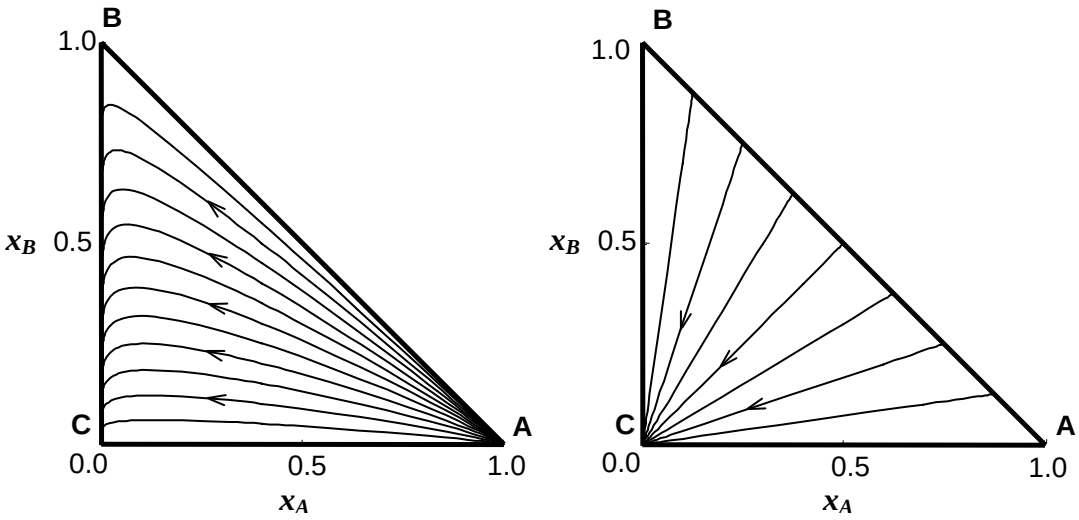

Figure 2.4: The effect of changing the order of the relative permeabilities:
(a) A – unstable node, B – saddle point, C – stable node
(b) Components A and B have equal permeabilities, while that of C is lower.

A "special case" that arises is when two of the relative permeability values are equal to each other. Physically, this means that two of the three components are permeating through the membrane at exactly the same rate. Mathematically, it results in the M-RCM consisting of curves that are essentially straight lines: These lines originate (or terminate) from the pure component node of the substance that permeates at a higher (or lower) rate than the other two which are permeating at the same rate. Figure 2.4(b) shows an example of a M-RCM when the permeation rate of A and B are equal to each other, and that of C is lower than A and B. This means that all the curves terminate at pure C, making that point the only stationary point in the entire map. In this particular case, that point is a stable node. If, however, the relative permeability of pure C is higher than that of A and B, then the stationary point would be an unstable node.

2.4 A REAL M-RCM

As discussed before, the membrane residue curve equations (equation 2.3) are *general*, and are not limited to the constant relative permeability case, and furthermore are not limited to only gas separation. Provided an appropriate and accurate method of calculating the flux of each component through the membrane is employed (the choice of which, of course, is left to the designer), one is able to generate the plot for the chosen membrane. As an example on how M-RCM's are useful, consider the following real system for separation:

Methyl tertiary butyl ether (MTBE) is a fuel additive used to enhance engine performance, as well as allow for cleaner and more complete combustion. It is produced by the reaction of methanol and *i*-butene. The reaction is equilibrium-limited, resulting in the need for efficient separation processes.

Sulzer Chemtech (Ltd) produce high performance plasma-polymerized membranes for the removal of methanol (and other alcohols). Since there is excess methanol in the reactor product, the idea of removing it efficiently is attractive. A certain pervaporation membrane, PERVAP 1137, has the following empirical formulae for calculating the flux of each component through the membrane (1 = methanol, 2 = butene, 3 = MTBE) (Bausa and Marquardt (2000)):

$$J_1 = k_1\left(\gamma_1 x_1 + \frac{\pi_P}{p_1^0}\right)\left(\gamma_1 p_1^0 x_1 - \pi_P\right) \tag{2.13}$$

$$J_2 = k_2\gamma_2 p_2^0 x_2 J_1 \tag{2.14}$$

$$J_3 = k_3\gamma_3 p_3^0 x_3 J_1 \tag{2.15}$$

where k_i is the parameter value for component i (refer to Appendix B for the values)

γ_i is the activity coefficient for component i,

p_i^0 is the saturation pressure of component i.

The membrane has a very high selectivity for methanol, resulting in the *permeate* having a mole fraction of methanol always higher than 0.98.

Although very different from the solution-diffusion model, this flux model can be used in the general equations for a M-RCM. Notice also, that previous M-RCM's were generated for gas separation membranes, and this membrane is in fact a pervaporation membrane. This, again, is fine, since the M-RCM equations are not limited to one type of membrane!

As discussed by Bausa and Marquardt (2000), the temperature of the liquid (retentate) will decrease as material permeates. This is due to the fact that the concentration of the permeating components is reducing, as well as the fact that the permeate is leaving as a vapour, thereby removing its associated heat of vaporization from the liquid phase. The manufacturers specifications for the membrane states that the maximum allowable temperature is 100°C (Bausa and Marquardt (2000)). In the examples which follow, it is assumed that the feed temperature is $T_f = 80^o C$. This would be the maximum temperature in the membrane module(s).

The system of DE's was solved for 2 cases: one where a vacuum is maintained on the permeate side, and another where the permeate pressure is non-zero. Each case is discussed in more detail.

2.4.1 CASE 1: WHEN THE PERMEATE SIDE IS AT VACUUM CONDITIONS (I.E. $\pi_P \approx 0$)

This is a very common mode of operation for membrane systems. In this case, the flux equation for methanol is reduced to:

$$J_1 = k_1 p_1^0 (\gamma_1 x_1)^2 \tag{2.16}$$

Using this flux, along with the fluxes of the other 2 components, the M-RCM is plotted as shown in Figure 2.5.

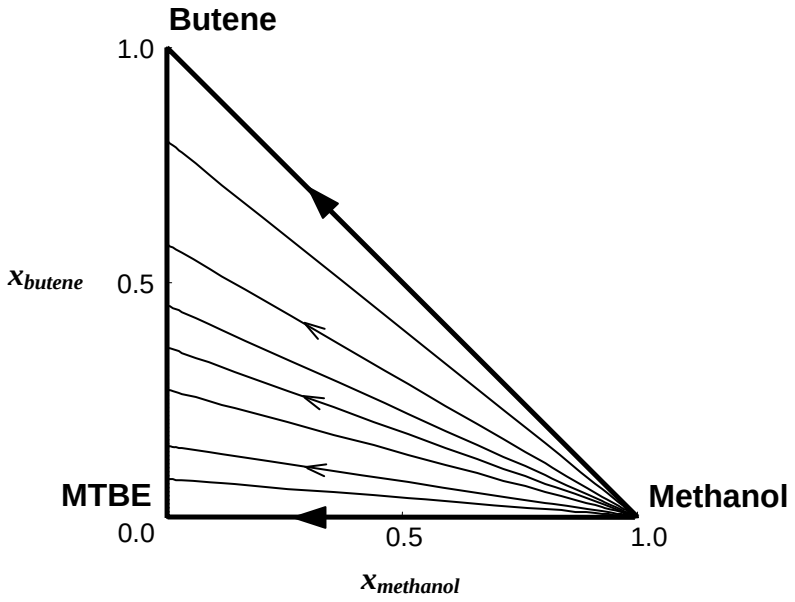

Figure 2.5: M-RCM for methanol/MTBE/butene with $\pi_P \approx 0$.

As stated before, the membrane is selective to methanol permeation, resulting in the permeate having a high concentration of methanol (this is not seen in the Figure 2.5, since the M-RCM shows the change in *retentate* composition only!). Because the retentate is rapidly depleted of its methanol, the residue curves move out of the pure methanol node, making this point the unstable node.

The flux equations for MTBE and butene (equations 2.14 and 2.15) do not depend on the pressure of the permeate, but do, however, depend on the flux of methanol. As soon as the net flux of methanol equals zero, the fluxes of the other two components go to zero. This results in the liquid (retentate) composition not changing with time, reaching an arheotrope. The arheotrope will occur when $x_1 = 0$ (refer to equation 2.16). Since this is the only condition for arheotropism in this system, the entire

MTBE/butene binary (vertical) line is a *"locus of arheotropes"*. This means that each residue curve originates from the pure methanol (unstable) node and terminates when it reaches a point on the MTBE/butene binary line. The curves do not move into either the MTBE or the butene node, but rather terminate at whatever binary composition the residual retentate is at when $x_1 = 0$. Only curves moving along the methanol/MTBE binary (horizontal) or methanol/butene binary (diagonal) will terminate at either pure MTBE or butene respectively.

This phenomenon of a "locus of arheotropes" seems to be unique to membrane systems, since the inherent properties of the membrane only allow for selective permeation. Such a phenomenon does not occur in distillation processes, for example, since boiling will continue no matter what components are present. The locus of arheotropes is, of course, dependant on the membrane used, and may or may not a occur. If the membrane is not selective to which species it allows through, then it will more than likely not occur. In this case, however, the membrane is highly selective to methanol permeation. When methanol completely permeates, separation no longer occurs, and a locus of arheotropes exists.

2.4.2 CASE 2: WHEN THE PERMEATE PRESSUE IS NON-zero (i.e. $\pi_P > 0$)

As established in case 1 above, permeation will stop when the flux of methanol goes to zero. Solving equation 2.13 for $J_1 = 0$, remembering that $x_1 > 0$:

$$x_1 = \frac{\pi_P}{p_1^0 \gamma_1} \tag{2.17}$$

Equation 2.17 tells us that there is, in fact, some value of $x_1 > 0$ that will make the flux of methanol go to zero. From this we can conclude that, at $\pi_P > 0$, it is not possible to deplete the retentate of ***all*** its methanol. Such an occurrence is due to the properties of the membrane.

Using equation 2.17, it is possible to find the locus of arheotropes for a set permeate pressure. In order to simplify the calculation, an isothermal process of 80°C was assumed. Figure 2.6(a) – (c) show the resulting M-RCM's for chosen permeate pressures of 0.5, 1.0 and 1.5 bar.

In Figure 2.6(a), it can be seen that the locus of arheotropes has moved from the MTBE/butene binary into the MBT region, as represented by the dotted line. Operation in the unshaded region to the right of the locus will result in the permeate being effectively stripped of its methanol. However, when the associated residue curve reaches the locus of arheotropes, permeation will cease. Using the diagram, it is possible for one to easily calculate how much methanol can be removed from the retentate, as well as determine the amount of methanol remaining in the retentate. Such a calculation would prove to be difficult to solve without the use of the M-RCM and its associated equations.

In the shaded region, which lies to the left of the locus of arheotropes, the methanol concentration in the retentate is such that its flux is negative. This results in the fluxes of the other 2 components being negative too. Physically, this means that permeation through the membrane has now been reversed! That is, material is moving from the low pressure vapour permeate side to the high pressure liquid retentate, and the liquid is now being enriched with methanol. Since the membrane was designed to remove methanol from the retentate, rather than enrich it, it can be said that this region represents a region of ineffective separation. But as before, when the curves in this region intersect the locus of arheotropes, there is no more permeation in either direction.

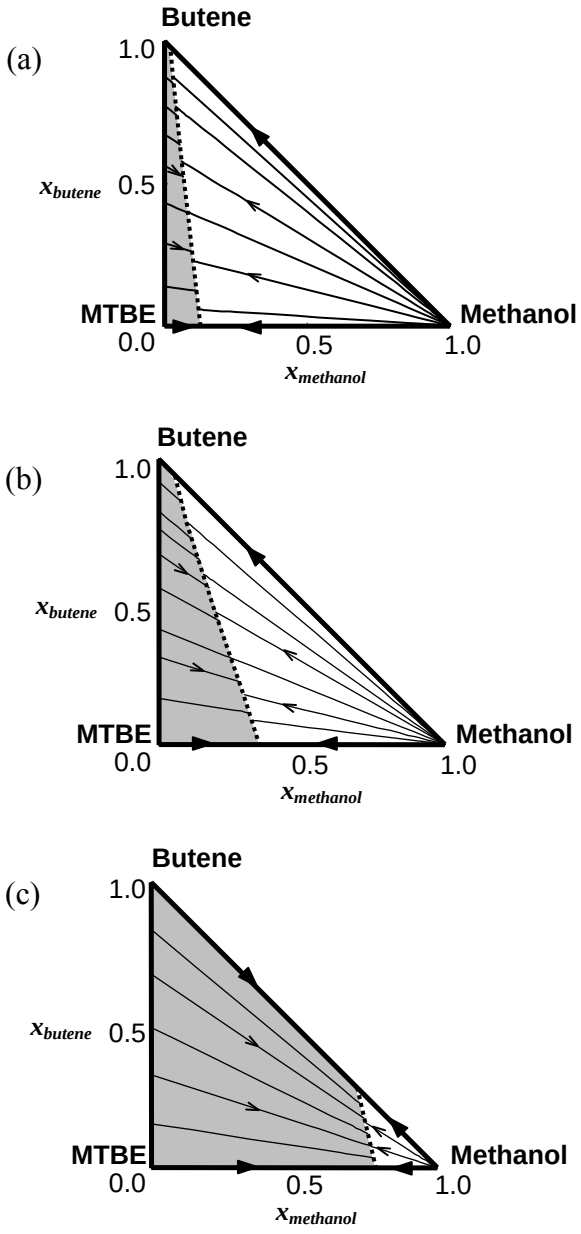

Figure 2.6: M-RCM for methanol/MTBE/butene.

(a) π_P = 0.5 bar, (b) π_P = 1.0 bar, and (c) π_P = 1.5 bar.

Unshaded region = From retentate To permeate (effective separation)

Shaded region = From permeate To retentate (ineffective separation)

Figures 2.6(b) and (c) graphically verify the fact that as the permeate pressure increases, the driving force for effective separation decreases. This results in the effective separation region reducing in size as the permeate pressure increases. Although it is agreed that it is unlikely for one to operate at such high permeate pressures, Figures 2.6(b) and (c) have been included for demonstration purposes. They serve to enlighten the reader how the permeate pressure affects the degree of separation obtainable. This phenomenon can be acquired from the flux equations themselves, but are easily visualized and understood through the M-RCM. Using the M-RCM, it is also easier for the designer to choose and appropriate permeate pressure to operate at, no matter how small.

Essentially, it is only methanol that permeates through the membrane – the other components move through in relatively small amounts, and only do so when methanol permeates. Thus, for vaporization to occur, the permeate pressure has to equal the saturation pressure of methanol. This is only possible when pure methanol is permeating. Although permeation will occur, it is not very useful, and furthermore, the composition will not change as permeation proceeds. Thus, the locus of arheotropes collapses into a single point at the pure methanol node, and the entire MBT becomes a region of ineffective separation. Such a result can be confirmed by analyzing equation 2.17. For permeate pressures greater than the saturation pressure of methanol, the phenomenon of arheotropism is no longer in the MBT, and the entire MBT is in a state of ineffective separation.

2.5 CONCLUSION

This chapter serves as the theoretical background to M-RCM's. A Residue Curve Map for membrane permeation systems has been produced. Since the equations which describe a single residue curve are merely a combination of mass balances, it can be concluded that an RCM could be used for kinetically-based process, and is not

restricted to equilibrium-based process, as was previously agreed. The curves that exist within the map trace out the composition of the retentate in a batch separation process, as discussed in Section 2.2.1. At any time during batch permeation, the permeate composition is related to that of the retentate *at that particular time*, thus allowing a membrane separation vector to be defined as the vector difference between the two compositions.

An M-RCM was produced for a real system, using flux data obtained from literature. The resulting plots gave valuable insight into the operation of the particular membrane. The qualitative understanding of how the permeate pressure influences the effective separation was confirmed, and the result can easily be seen by examining the appropriate M-RCM. Furthermore, using the M-RCM, the concentration of methanol remaining in the retentate as well as the amount of methanol removed from a particular feed can be determined with ease.

A follow-up of this chapter will show how an M-RCM can be used in the conceptual design of both batch and continuous membrane operations (see Chapter 3). In future publications (refer to Chapters 3 and 5), graphical design methods of hybrid distillation-membrane systems will be explored using RCM's.

CHAPTER 3:

APPLICATION OF MEMBRANE RESIDUE CURVE MAPS TO BATCH AND CONTINUOUS PROCESSES

The material in this chapter has been accepted by the editorial office for publication in Industrial and Engineering Chemistry Research. The paper is currently at the publishers. The current reference is: Peters, M.; Kauchali, S.; Hildebrandt, D.; Glasser, D. Application of Membrane Residue Curve Maps to Batch and Continuous Processes. *Ind. Eng. Chem. Res.*, **2008**, accepted for publication.

ABSTRACT

Membrane residue curve maps (M-RCMs) [Peters, M.; Kauchali, S.; Hildebrandt, D.; Glasser, D. *Ind. Eng. Chem. Res.* **2006**. *45*, 9080] plot the change, over time, of the retentate composition in a batch still. In this chapter, the relevance of M-RCMs to both batch and continuous processes is investigated. A constant relative permeability model is used for demonstration purposes, and the theory is then extended to a real system of methanol/butene/methyl tertiary butyl ether (MTBE). It has been shown that the differential material balances over a continuously-operated membrane unit are mathematically equivalent to those which describe the M-RCM. The time variable in the batch set-up is analogous to the spatial variable in continuous units. The retentate composition in a non-reflux continuous unit, for example, will follow the residue curve that passes through the initial feed composition. The M-RCM, in conjunction with the necessary flux equations, allows a designer to determine permeation area (or time) required in a continuous (or batch) process. Membrane columns operating at total and infinite reflux are discussed. A novel approach in

synthesizing and designing hybrid distillation-membrane processes emerges: using the M-RCM in conjunction with column profile maps (CPMs) allows one to graphically interpret hybrids in an efficient manner. The method generates the attainable region (AR) for a chosen configuration and informs the designer of parameters like membrane area and number of distillation stages required.

3.1 INTRODUCTION

Throughout the past several decades, membrane-based processes have received a substantial amount of interest as an attractive alternative to conventional separation methods. Not only are membranes an economically viable option, but they also offer unique separation behaviour. Being a kinetically-based process, it is not limited by equilibrium constraints, and allows for effective "breaking" of azeotropes (Rautenbach and Albrecht (1985a)). However, only a few membrane units, both continuous and batch, have yet to find their place in industrial practice (Clement et al. (1992)), either as stand-alone or as part of a hybrid arrangement. One of the reasons for this is the lack of high performance membranes for various applications. Another reason is that the design of membrane separators is complex, and not as well understood and formulated as traditional separation methods, such as distillation or liquid-liquid extraction.

These customary separation units, such as distillation or absorption, are *equilibrium-based* processes. Membrane separators, on the other hand, are *rate-based* operations and are conventionally analysed and assessed in the same manner as other kinetic processes. Traditionally, it was understood that the graphical technique of Residue Curve Maps (RCMs) was only appropriate for *equilibrium-based* separations (Fien and Liu (1994)). However, the equations describing any single residue curve are purely a combination of material balance equations. With this said, RCMs can be used for both equilibrium- as well as rate-based processes. This now enables one to consider kinetically-based processes, of which membrane permeation is an example, in the same manner as equilibrium-processes.

There is a broad spectrum of membranes that have been developed for various applications (Wijmans and Baker (1995), Rautenbach and Albrecht (1989)). The work displayed in this chapter is not limited to a single type of membrane, but is general and can be applied to any membrane. However, only diffusion membranes

(i.e. gas separation and pervaporation) will be considered here, so as to display and demonstrate the theory presented. The work can then further be extended and applied to other membrane types. The driving force for separation in diffusion membranes is the difference in partial pressures for each component on either side of the membrane.

A vast amount of research has been done in the development of membranes. Numerous works have focused on the modelling of permeation fluxes through various membranes, as well as the relationship between permeate and retentate phases. These have been formulated both theoretically and experimentally. Wijmans and Baker (1995) provide a review on the solution-diffusion model. They describe general flux models for a wide-range of membrane operations, making use of chemical potentials as the starting point for derivations. Stephan et al. (1995), on the other hand, employ Henry's Law for describing the permeate composition as a function of that of the retentate. Mathematical modeling of a membranes performance using the appropriate transport equations has been researched (Rautenbach and Albrecht (1985a), Rautenbach and Albrecht (1985b), Marriott et al. (2001), Marriott and Sørensen (2003a)).

A membrane can be utilised in numerous ways in order to achieve a required outcome – either production of desired products, or to provide data for modelling and scale-up design. A batch membrane operation, in the form of a bench-scale or pilot tests, is usually used to select a membrane best-suited for a required purification. Such work has been done by authors like Feng and Huang (1992), and Qiao et al. (2005), to mention a few. Similar tests are also used to determine suitable selectivity and flux models of a particular membrane (Clement et al. (1992) for example). Work by Stoica-Guzun et al. (1996) provides an example that batch membrane systems have found a substantial place in the biomedical field too. While the batch experiments are necessary for continuous process design and scale-up, operating a membrane in a batch process may have very little commercial value.

Continuously-operated membranes, in contrast, have shown their economical value, especially in the last 20 years, or so. Different modes of operation have been researched and modeled accordingly. Non-reflux membrane equipment is designed such that a particular feed mixture undergoes a single pass separation without being recycled back. Due to the area required as well as energy considerations, a series of such membranes with inter-heaters may be necessary to achieve a desired separation (Bausa and Marquardt (2000)). Ideal flow patterns of perfect mixing, cross flow, counter-current flow and co-current flow, and their associated models, have been documented (Rautenbach and Albrecht (1989)). Blaisdell and Kammermeyer (1973) discuss the Weller-Steiner and Naylor-Backer models for both co- and counter-current continuous gas permeations, while Marriot et al. (2001) aim to derive a generalised model, irrespective of flow regime and simplifying assumptions. Various methods and techniques of the modeling, design and optimization of membrane systems have been the topic of numerous works in recent years (Tessendorf et al. (1999), Marriott and Sørensen (2003b), Chang and Hou (2006)).

A wide range of reflux units have previously been researched. A membrane column was first identified by Hwang and Thorman (1980). Filled with hollow-fibre membranes, a high pressure is maintained on one side in order to allow permeation through the membrane to the low-pressure side. To allow the recycle streams to flow, a valve and compressor are needed. It is claimed that complete separation of a binary mixture into pure products is achievable in a finite area (Hwang and Thorman (1980)). Variations of the membrane column have also been mentioned and examined, such as the recycle permeator (Yoshisato and Hwang (1984)) and two-membrane column (Matson et al. (1983)).

As will be discussed later in this chapter, it is impossible to obtain all pure products with a membrane that is selective to a single species for mixtures containing 3 or more components. For this reason, the membrane needs to be used in conjunction with either a different membrane, or with a different method of separation, such as a

distillation column. Hybrid designs are assembled such that each unit present functions in the most advantageous manner. Methods of designing and optimizing hybrid distillation-membrane processes have been very topical in recent years (Stephan et al. (1995), Bausa and Marquardt (2000), Eliceche et al. (2002), Verhoef et al. (2007)). The financial savings incurred with such a process have proven to be immense (Pressly and Ng (1998), Van Hoof et al. (2004), Sommer and Melin (2004)).

Peters et al. (2006a) proposed a novel method to analyse and understand membrane permeation systems. A simple "thought" experiment was conducted whereby a high pressure fluid mixture was allowed to permeate through a membrane in a batch still to a maintained low pressure side. One could continually analyze the change in retentate composition over time, with differing initial feed compositions. Similarly, one can write the appropriate unsteady-state material balances. Peters et al. (2006a) showed that the combination of the overall and component mass balances resulted in the *membrane residue curve equation*:

$$\frac{d}{d\tau}(x_i) = (x_i - y_i), \qquad i = 1,\ 2,\ \ldots,\ c-1, \tag{3.1}$$

where x_i is the mole composition of component i in the retentate phase,
y_i is the mole composition of component i in the permeate phase,
c is the number of components present in the initial charge, and
τ is a dimensionless time, defined by

$$\tau = \ln\left[R(0) \Big/ R(t) \right]. \tag{3.2}$$

where $R(0)$ is the initial charge of material to the batch still [mol],
$R(t)$ is the amount of retentate present at time t [mol],

In order to demonstrate the graphical representation of the membrane residue curve equation, a simple gas permeation model, with constant relative permeabilities, was used to relate y_i to x_i. This model is discussed in more detail in Section 3.2.2. Figure 3.1 shows a Membrane Residue Curve Map (M-RCM) for the relative permeabilities (α_{ij}^{M}) and pressure ratio (r) as indicated.

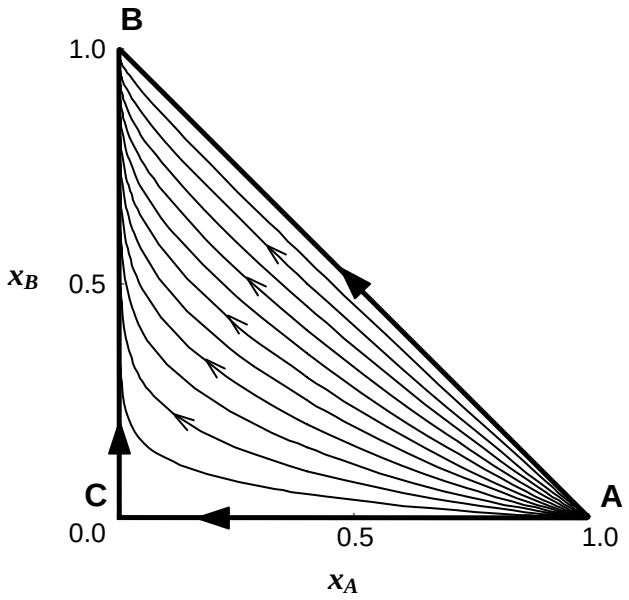

Figure 3.1: Membrane Residue Curve Map (M-RCM) for an ideal A-B-C system with $\alpha_{AB}^{M} = 3$, $\alpha_{CB}^{M} = 1.5$ and $r = 10$. (Reproduced from Peters et al. (2006a))

In this chapter, the applicability of M-RCM's to the synthesis and design of batch and continuous processes is discussed. The graphical technique allows one to understand and evaluate membrane systems in an expedient and efficient manner. The batch experiment, although somewhat straightforward, provides valuable insights into continuous operation, both reflux and non-reflux. As is shown in Section 3.4, the differential balance over a non-reflux separator is mathematically analogous to equation 3.1. Furthermore, with the developments of such maps, analysis of hybrid configurations takes on a novel approach.

Some of the results obtained and displayed in this chapter may appear to mirror that arrived at in the distillation field. *It must, however, be remembered that the techniques being shown are innovative for the understanding of membrane separations, being a kinetically-based process*. While similarities do arise, there are subtle yet distinct differences between distillation and membrane permeation. These are discussed in the chapter where necessary, and will be dealt with in more detail in a future publication (see Chapter 4).

Several authors have focussed on binary systems due to the ease of the equations that result. It is worth noting that the methods shown and discussed in this chapter are done for ternary systems, but are not limited to 3 component systems. The conclusions arrived at can be applied to both binary and higher order systems, even when graphical visualization becomes difficult.

The following section of this chapter deals extensively with the M-RCM and the batch process. Operation regions and obtainable products are discussed. An equation to calculate the time needed for permeation is also derived. In Sections 3.4 and 3.5, the applicability of the M-RCM to various modes of continuous membrane operation is detailed – both non-reflux as well as total and infinite reflux. Where pertinent, the similarities to the batch process are included. The practicality of the M-RCM is further extended in the design and synthesis of hybrid distillation-membrane processes in Section 3.6.

3.2 BATCH MEMBRANE OPERATION: OPERATING LEAVES IN BATCH PERMEATION

A "thought" experiment was conducted by Peters et al. (2006a), whereby a fluid mixture was allowed to permeate through a batch still, with the permeate being removed as soon as it was formed. Now, consider the following extension to the experiment: *The permeate is stored and accumulated in a separate container*. Figure 3.2 diagrammatically shows this addition.

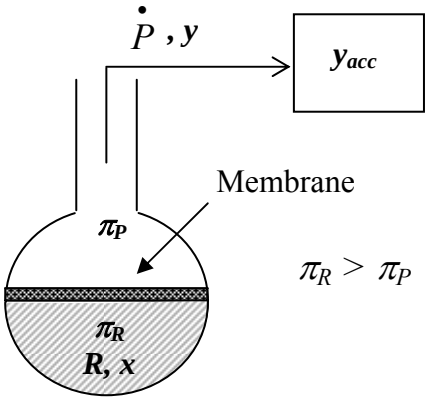

Figure 3.2: Simple batch membrane separation, with accumulating permeate.

3.2.1 MATERIAL BALANCES

One can write time-dependant overall and component mass balances across the entire still/storage container system:

$$R(0) = R(t) + \dot{P}\Delta t \tag{3.3}$$

$$R(0)x_i(0) = R(t)x_i(t) + \dot{P}\,y_{i,acc}(t)\Delta t \tag{3.4}$$

where $R(0)$ is the initial charge of material to the batch still [mol],

$x_i(0)$ is the initial retentate composition of component i,

$R(t)$ is the amount of retentate present at time t [mol],

$x_i(t)$ is the composition of component i in the retentate at time t,

$\dot{P}$ is the permeate removal rate [mol/s],

t is the time [s], and

$y_{i,acc}(t)$ is the accumulated permeate composition of component i.

A differential material balance across the still only has previously been written. As discussed in Section 3.1, equation 3.1 is known as the *membrane residue curve equation*, and a full derivation is provided by Peters et al. (2006a)

Combining equations 3.2, 3.3 and 3.4 in an appropriate manner, it can be shown that:

$$y_{i,acc}(t) = \frac{x_i(0) - e^{-\tau} x_i(t)}{1 - e^{-\tau}} \tag{3.5}$$

Notice that the expression for the accumulated permeate composition is independent of R. More important, however, is as $t \rightarrow \infty$, $y_{i,acc} \rightarrow x_i(0)$. This result is expected, and will be discussed later in this section.

Using the differential mass balance over the still (equation 3.1), for a particular value of τ, there is a corresponding x_i value – that is, the composition of the retentate left in the batch still after the experiment has been allowed to run for a dimensionless time of τ. At that particular time, the accumulated y-value can also be determined using equation 3.5.

3.2.2 PERMEATION MODEL

In order to solve the set of differential equations in equation 3.1, it is necessary to incorporate a suitable flux model that describes the permeation rate of each component through the membrane. For a gas-to-gas membrane, it has been shown that (Peters et al. (2006a)):

$$\frac{y_i}{y_j} = \alpha_{ij}^{M} \frac{\left(rx_i - y_i\right)}{\left(rx_j - y_j\right)}, \tag{3.6}$$

where α_{ij}^{M} is known as *membrane selectivity*, or the relative permeability of *i* with respect to *j*:

$$\alpha_{ij}^{M} = P_i' \Big/ P_j' \text{, and}$$

r is known as the ratio of pressures (retentate : permeate).

Equation 3.6 is for a non-zero permeate pressure. If the permeate pressure is kept sufficiently low, close to vacuum conditions, then $r >> 1$, and the model reduces to:

$$\frac{y_i}{y_j} = \alpha_{ij}^{M} \frac{x_i}{x_j} \tag{3.7}$$

As highlighted by Peters et al. (2006a), the permeabilities of the species may depend on a number of variables, and that mass transfer through the membrane can be quite complex. A simple *constant relative permeability* assumption will be incorporated for the purposes of illustrating the application of M-RCMs. In particular, a Knudsen Membrane is one which the relative permeabilities remain constant.

Broadly speaking, membranes can be classified as either non-selective or selective. Both kinds will be discussed throughout the chapter, where appropriate.

- A ***non-selective*** membrane is one which allows all species present in the initial feed (charge) to permeate, but at different rates. This implies that the relative permeabilities of each component are not equal. *In this chapter all M-RCMs and related plots for non-selective membranes will be generated for a system with* $\alpha_{AB}^{M} = 3$, $\alpha_{BB}^{M} = 1$ *and* $\alpha_{CB}^{M} = 1.5$. *A vacuum pressure on the permeate side will be maintained throughout*.

- A ***selective*** membrane, on the contrary, is designed to permeate only a single component from the mixture. However, trace amounts of the other components may appear on the downstream side of the membrane due to being chemically attached to the selective species. In other words, the other species may permeate through the membrane but at a rate that is extremely slow compared to the rate of permeation of the selective component. For example, if component *C* is the selective species then $\alpha_{AB}^{M} = \alpha_{BB}^{M} = 1$, *and* $\alpha_{CB}^{M} >> 1$. *Rather than using a Knudsen Membrane in this case, a real pervaporation membrane designed by Sulzer Chemtech (Ltd) will be used as a case study*. This is done so as to demonstrate the flexibility of M-RCMs. PERVAP 1137 has a very high selectivity to methanol and is best-suited for depleting a methanol/butene/methyl tertiary butyl ether (MTBE) of its methanol. The flux equations are provided in Appendix B, and the corresponding M-RCMs have been generated (Peters et al. (2006a)).

3.2.3 OPERATING REGIONS: NON-SELECTIVE MEMBRANES

For an initial retentate (feed) composition, the plots of

(i) the change in the retentate composition (referred to as a *membrane residue curve*),
(ii) the local (or instantaneous) permeate composition, and
(iii) the accumulated permeate composition

can be generated. These are produced by allowing permeation in the batch still to occur for a certain time period. An example is shown in Figure 3.3(a).

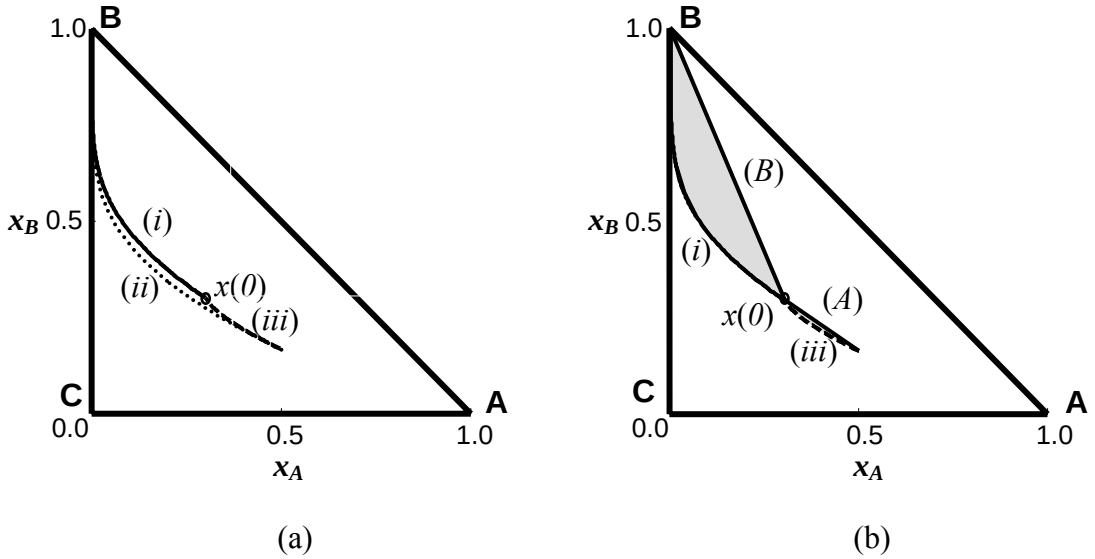

Figure 3.3: Initial retentate composition $x(0)$ = [0.4, 0.3].
(a) (*i*) Residue curve, (*ii*) Permeate curve, and (*iii*) Accumulated permeated curve,
(b) Operating region or "leaf". The region is bounded by the
curves (*i*) and (*iii*), as well as mass balance lines (*A*) and (*B*).

Equations 3.3 and 3.4 are straight line mass balances, and can be plotted for every retentate composition (and corresponding permeate fraction). The very first mass balance line that is set up during an experiment, is the one that includes the initial

permeate composition. The local permeate as well as the accumulated permeate curves begin at the same point – namely, the compositional value of the very first amount of material that diffuses through the membrane. This is also the permeate composition that will contain the highest fraction of the most permeable component (namely A in this case). The time lapse to produce the first amount is essentially zero, and by analyzing equation 3.4, it is obvious that the retentate composition has only changed ever so slightly. The straight line connecting the feed, initial permeate and retentate composition can be plotted, as shown in Figure 3.3(b) (refer to line (A)).

The other important mass balance line is the one that exists when the last drop of retentate is about to diffuse through the membrane. This would happen after allowing permeation to occur for an infinite length of dimensionless time (refer to equation 3.2). Equation 3.4 depicts that by this stage, the accumulated permeate composition is essentially equal to the initial retentate charge. This result is expected since by this stage all the material has permeated through the membrane and is being accumulated in storage. This particular mass balance is shown in Figure 3.3(b) as well (see line (B)).

The entire region(s) bounded by these 2 mass balance lines as well as the residue and accumulated permeate curves is the region of operation for the batch still. This so-called 'operation leaf' shows graphically the region of all possible products attainable in a batch membrane permeation with an initial charge (feed) of $x(0)$.

The relevance of an operating leaf is that it informs one of the all possible products obtainable from a feed of $x(0)$ using a batch membrane separation process. It yields, in a graphical manner, the retentate and accumulated permeate compositions. Furthermore, a knowledge of the initial amount of retentate charged to the still easily allows one to calculate the respective amounts of the final products obtained. Also, embedded within the calculations is the actual time it would take to achieve the desired separation (refer to Section 3.3).

In a batch still that utilizes a non-selective membrane that has different permeation rates for all three components, the operating leaf shows graphically some important results:

- It is only ever possible to obtain a purity of 1 for single component only, namely the species with the lowest permeation rate (component B, in this case).
- In order to obtain this pure component, however, the amount of remaining retentate would only be as much as a single drop (refer to the mass balance line (B) in Figure 3.3(b)).
- The composition of the most permeable component (A, in this case) would be the highest when permeation initially commences, where-after its composition tends towards that of the initial feed, as previously explained.

Although some of these results may be somewhat intuitive, the method is unique in that one can rapidly deduce such outcomes from the graph.

One can generate operating leaves for any given $x(0)$. The plot obtained will be similar to the one displayed in Figure 3.3(b), and the result is as discussed above.

3.2.4 OPERATING REGIONS: SELECTIVE MEMBRANES

The results obtained for a non-selective membrane do not hold true for membranes where one component is preferentially transported through the membrane, and/or where the composition of the permeate is essentially pure in that component. An example of this type of membrane is PERVAP 1137, discussed earlier. The membrane has a very high selectivity for methanol, resulting in the *permeate* having a mole fraction of methanol always higher than 0.98 (Bausa and Marquardt (2000)) This means both the permeate as well as the accumulated permeate compositions will

always have a value greater than 0.98. For simplifications, assume that these values represent a *pure* fraction of methanol. Analysis of equations 3.3 and 3.4 yields that $x(t)$, $x(0)$ and $y_{acc}(t)$ must all lie on the same straight line, and that the locus of $x(t)$ is the same straight line. Hence, the operating leaf collapses into a single straight line, as shown in Figures 3.4(a) and (b). Furthermore the "operating line" happens to be the residue curve passing through $x(0)$. The reader is referred to Peters et al. (2006a) for a full discussion on the properties of this particular map.

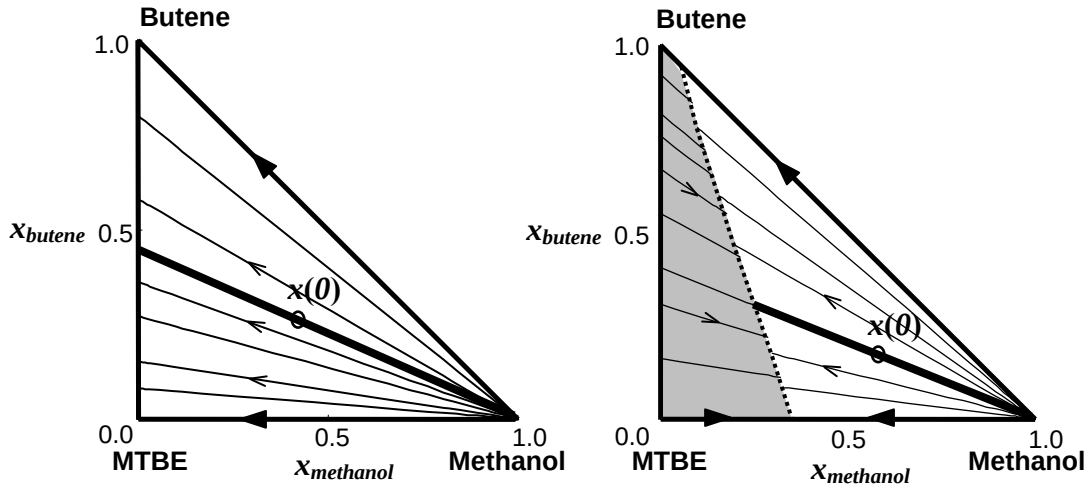

(a) (b)

Figure 3.4: Operating line in the methanol/butene/MTBE system

(a) $\pi_P \approx 0$, (b) $\pi_P > 0$.

The residue curves for this particular membrane are dependent on the permeate pressure (π_P). (Peters et al. (2006a)) An *arheotrope* (Peters et al. (2006a), Huang et al. (2004)) is a stationary point in the membrane vector field where there is no change in both permeate and retentate compositions with time. A locus of arheotropes was found to exist, as well as migrate from the binary butene/MTBE line ($\pi_P = 0$) through to the pure methanol node (π_P = saturation pressure of methanol). This results in the operating line extending from the methanol node, through $x(0)$, and terminating at the locus of arheotropes.

The operating line, as before, reveals some interesting results. These results may seem somewhat trivial, but the operating line enables one to identify them quickly and easily.

- It is still only ever possible to obtain a pure composition for one component only, namely methanol. That particular result is expected, since the membrane is designed to do such a separation.
- Unlike the non-selective membrane, this particular membrane will allow a sufficient amount of methanol through, yielding a good recovery of it. Depending on the feed composition and the permeate pressure, it may even be possible to recover all the methanol initially present, in a finite period of time!
- If the permeate pressure is such that the feed composition lies in the ineffective separation region (i.e. the grey region in Figure 3.4(b)), then the retentate will become enriched with methanol. This is said to be ineffective since the membrane was not designed to enrich the retentate with methanol, but rather deplete it.

3.3 BATCH MEMBRANE OPERATION: PERMEATION TIME

Suppose it is desired to separate a fluid mixture of components A, B and C in a batch still incorporating a Knudsen membrane (i.e. constant relative permeabilities) until we achieve a specified final purity of $x(f)$. The initial charge of material, $R(0)$, is known, as well as its composition, $x(0)$. When designing such an experiment or, more importantly, when using such apparatus for commercial production of a particular product, it is vital to know the following:

- How long will the separation from $x(0)$ to $x(f)$ take, and
- What final amount of material, $R(f)$, of composition $x(f)$ will be available.

The desired product may be the permeate. In this case, the amount of material accumulated can then further be calculated by mass balance.

Even though the M-RCM only informs one of the changes in the retentate composition, it is possible to extract the required information from it, in conjunction with the relevant permeation model and material balances. Consider, for demonstration purposes, the following example: A mixture of $x(0)$ = [0.7, 0.1] that needs to reach a final purity of $x(f)$ = [0.023, 0.68]. The separation will be done in a batch still using a gas separation membrane with constant relative permeabilities (refer to Section 3.2.2). The residue curve, and corresponding (local) permeate curve are displayed in Figure 3.5(a).

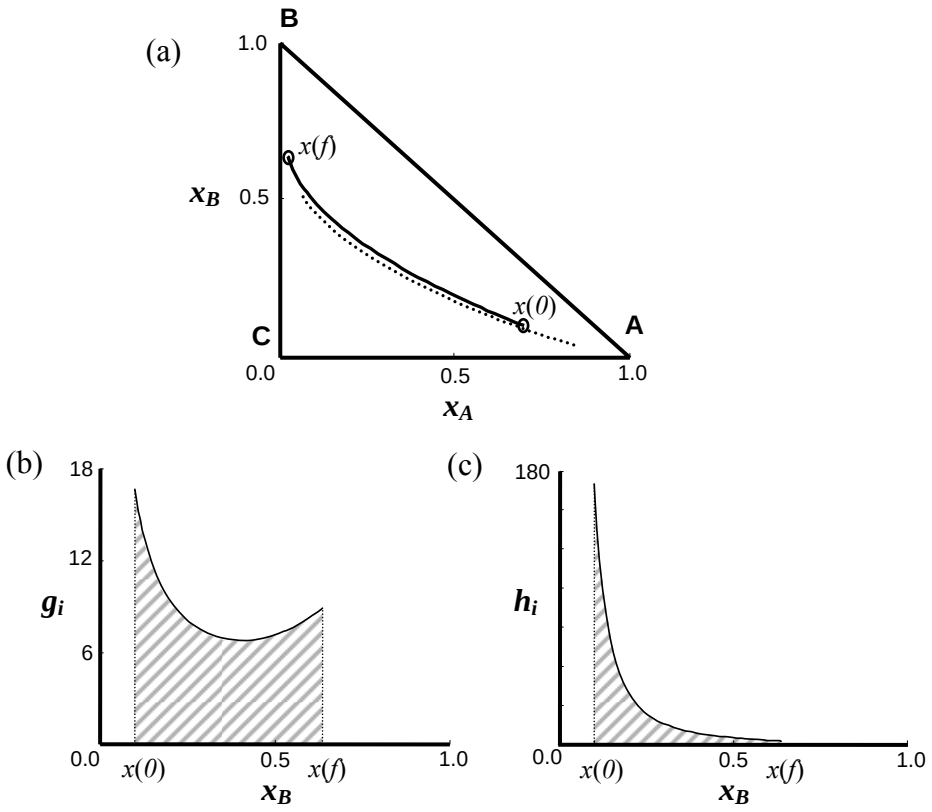

Figure 3.5: (a) Residue (solid) and Permeate (dashed) curves for example.
(b) Inverse of separation vector (g_i) versus x_B.
(c) Graph of h_i versus x_B.

Now, from the residue curve equation (equation 3.1), we see that:

$$\tau = \int_{x_i(0)}^{x_i(f)} \frac{1}{x_i - y_i(x)} \cdot dx_i \tag{3.8}$$

This is the familiar Rayleigh Equation (King (1971)). It is depicting that the area under the graph of $g_i = \frac{1}{x_i - y_i(x)}$ versus x_i between the limits of $x_i(0)$ and $x_i(f)$ would yield the dimensionless time required to achieve the separation. This is graphically displayed in Figure 3.5(b) for component 2. It is worth noting that τ is in fact a function of x, and further τ is the same for all i. This now enables one to quantify the amount of residual fluid remaining in the still since, from equation 3.2:

$$R(f) = R(t) = R(0) \cdot e^{-\tau} \tag{3.9}$$

It is evident that as τ increases, the amount of retentate available reduces since a large τ would correspond to a high-purity separation (i.e. $y_i \rightarrow x_i$). In order to determine the actual time needed for separation, consider the overall mass balance over the still:

$$\frac{dR}{dt} = -\dot{P} \tag{3.10}$$

If one were to assume a constant permeate removal rate then

$$t = \frac{R(0)}{\dot{P}}\left(1 - e^{-\tau}\right) \tag{3.11}$$

However, it is not likely that the permeation rate will remain constant throughout the entire separation, since it is a function of the retentate composition, amongst other

things. Thus, by integrating equation 3.10, differentiating equation 3.8, and using the Knudsen model for permeation with a vacuum on the permeate side, the following equation results (refer to Appendix C for proof):

$$t = R(0)\frac{\delta}{A \cdot P_i' \cdot \pi_R} \cdot \int_{x_i(0)}^{x_i(f)} \left(\frac{e^{-\tau}}{x_i} \cdot \frac{1}{x_i - y_i(x)} \right) \cdot dx_i \qquad (3.12)$$

Feng et al. (1992) arrive at a similar expression. Once again, it can be noticed that by computing the area under the graph of $h_i = \frac{e^{-\tau}}{x_i} \cdot \frac{1}{x_i - y_i(x)}$ versus x_i between $x_i(0)$ and $x_i(f)$ would yield a scaled-time. Figure 3.5(c) illustrates this for component 2 of the earlier-mentioned example. Multiplying by the relevant constants displayed in equation 3.12 would give the real time needed to achieve the required separation. One could calculate t for every component, but the result would remain the same. It is worth noting that the area under the graph of h_i versus x_i (which yields the scaled-time) will not be same for each component. The ratio of the area for component i to that of j will be equal to α_{ij}^{M}.

Furthermore, the permeation time depends on a number of physical parameters. As one increases the membrane area, A, or retentate pressure, π_R, the time needed for permeation will decrease. The time would increase with an increase in membrane thickness since the permeating material now has a longer distance to travel through the membrane.

3.4 CONTINUOUS MEMBRANE OPERATION: NON-REFLUX EQUIPMENT

A single stage non-reflux membrane module is the most common unit used for continuous operation. An example of such a unit is shown in Figure 3.6.

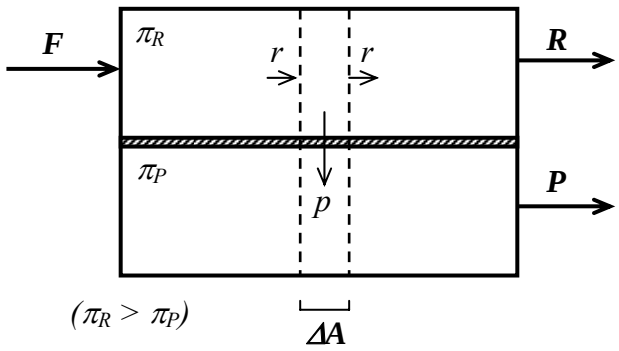

Figure 3.6: Single stage non-reflux continuous membrane operating under a co-current flow regime.

A feed stream enters the unit at an appropriate chosen pressure (π_R) where it comes into contact with the membrane. A permeate pressure (π_P) is maintained on the downstream side of the membrane, resulting in material moving through the membrane. Material permeates in the direction normal to the membrane. The actual shapes of the module and membrane may vary from unit to unit. The unit could be spiral wound, or a plate module, or even consist of hollow fibres. Any shape allows for an effective membrane area (A) for separation to occur.

There are a number of ideal flow patterns that can occur within the membrane module, shown in Figure 3.6. The important ones include complete mixing, cross flow, counter-current flow and co-current flow. The method displayed here is done for co-current flow, but is applicable to all the flow patterns, and any combination thereof.

It is important to note that when talking about the material that permeates, we are only referring to the material resulting from the *local flux* at each point down the length of membrane area. Once that material enters into the bulk permeate stream, it will mix with the already-present material resulting in a mixed composition. This mixed, or accumulated, composition will be discussed later in this section, and also in more detail in a future publication (refer to Chapter 4). *[Note that a superscript of* * *will be used to denote compositions that relate to the local composition (for example, the composition of the permeate as it emerges from the membrane will be denoted as* y^**). Any bulk compositions will be written un-superscripted.]*

3.4.1 MATERIAL BALANCES

Consider the co-current flow regime displayed in Figure 3.6. When operating a membrane module in such a manner, the composition of the retentate changes down the length of the membrane, until it reaches the product composition at end of the module. The compositional change occurs in a plug-flow manner. An overall and component mass balance over the strip of area size ΔA can be written, assuming steady-state:

$$r\big|_A = p \cdot \Delta A + r\big|_{A+\Delta A} \tag{3.13}$$

$$\left(r \cdot x_i\right)\big|_A = \left(p \cdot y_i^*\right) \cdot \Delta A + \left(r \cdot x_i\right)\big|_{A+\Delta A} \tag{3.14}$$

where r is the retentate flow rate [mol/s],

p is the local permeate flux [mol/m^2s],

x_i is the bulk retentate composition,

y_i^* is the local permeate composition, and

A is the effective membrane area [m^2]

Since permeation occurs continually down the length of the membrane, rather than at discrete points, it is obvious that the limit $\Delta A \rightarrow 0$ should be imposed. Combining the resulting two equations, the following is obtained

$$\frac{dx_i}{dA'} = \left(x_i - y_i^*\right) \text{ for } i = 1,\ 2,\ ...,\ c-1 \tag{3.15}$$

where A' is the dimensionless membrane area, defined by

$$A' = \ln\left[F \Big/ R(A)\right], \tag{3.16}$$

with F and $R(A)$ being the total molar retentate flow in the separator at $A = 0$ (i.e. initially) and at area A, respectively. Thus, A' is the natural logarithm of the reciprocal of fraction of retentate that needs to be removed (i.e. permeated) to obtain a desired purity. (*Note*: The format of the proof in Appendix A may be followed.)

Note that equation 3.15 can be applied to membranes of different shapes (tubular, sheet, etc.). For example, in a flat sheet membrane module, $dA' = w \cdot dz'$, where w is the width of the sheet and z is its length. The appropriate relationship can be written for other types of membrane shapes.

Bausa and Marquardt (2000) give a similar proof of this equation for this mode of operation. In their paper, they analyze hybrid distillation-membrane systems and use a similar result to the one shown in equation 3.15 for the modelling of the membrane module. They also provide the relevant energy balance equation, since there is a temperature drop down the length of the membrane. This is especially true in pervaporation systems where the heat of vaporisation is withdrawn from the liquid as it permeates and ultimately vaporises. Due to the scope of this report, the energy balance, although useful, is not necessary here and will thus not be discussed further.

The derivation given here is for a co-current flow pattern, but can be performed for all other common flow regimes. These are left to the reader, and are not shown here, but the result obtained will be as given in equation 3.15.

3.4.2 RELEVANCE OF THE BATCH EXPERIMENT

It can be seen that equation 3.15 is mathematically equivalent to the residue curve equation (equation 3.1). The time variable in the batch operation corresponds to a position (spatial) variable in the continuous operation. Clement et al. (1992) arrive at the same result, referring to it as a "surface area-time duality". Thus, the composition profile of the retentate down the length of the membrane will follow a *residue curve*, as the retentate continually becomes enriched in the least permeable species. The exact residue curve followed depends on the feed composition, since it corresponds to the initial retentate composition. (Refer to the M-RCM shown in Figure 3.1).

This implies, in principle, that a membrane can be analysed for its performance using a simple batch experiment.

3.4.3 LOCAL PERMEATE MIXING WITH THE BULK STREAM

Permeation occurs continually down the length of the membrane. Local permeation involves material permeating at every point through the membrane. As each local permeate leaves the membrane it is mixed with the previously-permeated material. In this case, the composition of the permeate also changes in a plug-flow manner.

The graphical representation, using an M-RCM, for a particular feed to a non-reflux module is as shown for the batch process in Figure 3.3(a). The feed composition to the module is $x(0)$, and the lines represented by (i), (ii) and (iii) retain their original

description. Lines (i) and (iii) are the compositional change of the retentate and bulk permeate respectively.

The material balance across the module from the feed to any point down the length of the membrane can be written. It informs us that the feed composition, as well as the corresponding permeate and retentate compositions at any point, will lie on a straight line in the Mass Balance Triangle (MBT). Additionally, the feed and retentate compositions will also lie on the same residue curve. It is therefore possible to display, graphically, the region of operability for a non-reflux membrane module. The operation leaf is as shown in Figure 3.3(b) for the ideal system, and in Figures 3.4(a) and (b) for the methanol/butene/MTBE system. Furthermore, the results obtained for the batch process are directly applicable to the non-reflux case. These results are listed in Section 3.2.

3.4.4 PERMEATION AREA

An essential design parameter for membrane permeators is the area required for separation. As discussed earlier in this section, the area (or length) variable in the continuous operation corresponds to the time variable in the batch set-up. Thus, equation 3.12 becomes applicable when calculate the real area needed, remembering that t becomes A, and τ becomes A'. More importantly, however, is that previously in the batch experiment the membrane area was constant. In continuous operation it is changing down the length of the unit. Thus, taking this into account, equation 3.12 needs to be altered as such:

$$A = R(0) \cdot \int_{x_i(0)}^{x_i(f)} \left(\frac{e^{-A'}}{J} \cdot \frac{1}{x_i - y_i(x)} \right) \cdot dx_i \qquad (3.17a)$$

$$A = R(0)\frac{\delta}{P_i' \cdot \pi_R} \cdot \int_{x_i(0)}^{x_i(f)} \left(\frac{e^{-A'}}{x_i} \cdot \frac{1}{x_i - y_i(x)} \right) \cdot dx_i \qquad (3.17b)$$

Equation 3.17a is general and applicable for any flux model. Equation 3.17b is the result for Knudsen permeation. The methods described in Section 3.3 can be adjusted appropriately to facilitate the determination of the area.

3.5 CONTINUOUS MEMBRANE OPERATION: REFLUX EQUIPMENT

3.5.1 TOTAL REFLUX

Consider altering the conditions of operation of the non-reflux separator shown in Figure 3.6 as follows: The flow pattern is changed to counter-current, and material is recycled back to the column at either end. This is diagrammatically shown in Figure 3.7(a).

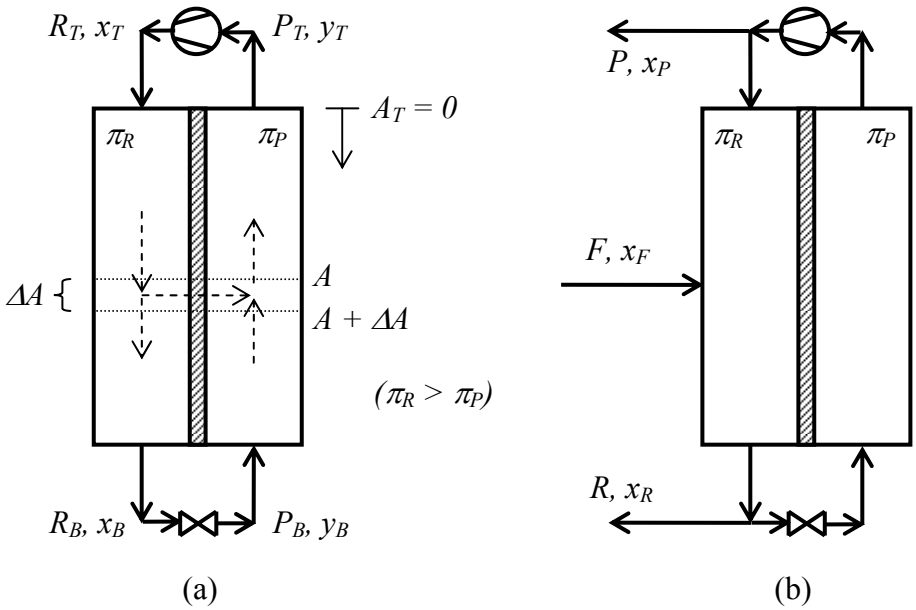

Figure 3.7: Membrane column. (a) Total reflux, (b) Infinite and Finite Reflux.

The unit shown in Figure 3.7(a) is not of any practical use since it has no feed or products. However, the theory and understanding it provides does furnish one with useful insights into both infinite and finite reflux operation.

By writing the material balances over a differential segment of the column, and taking the limit as $\Delta A \rightarrow 0$, it can be shown that the differential equation (DE) in equation 3.15 holds true for the reflux equipment. As before, it is noticed that the same DE results as for the batch process. The dimensionless time variable, τ, in the batch operation (equation 3.1) becomes the dimensionless space (or length) variable in the equation for the continuous reflux process. The path the retentate would trace out would be the appropriate residue curve on the M-RCM (Figure 3.1) that passes through the point x_T.

Permeation is mono-directional, i.e. from retentate phase to permeate phase only. Thus both P and R are continually changing down the length of the column. They will either increase or decrease monotonically, depending on the flow pattern. In the counter-current regime displayed in Figure 3.7(a), both P and R are decreasing in magnitude from the top of the column down.

If the column operates under total reflux conditions, then *all* the material is recycled back to the column. This results in $P = R$ at every point normal to the membrane, remembering that P and R are still decreasing down the column. Furthermore, by using the material balances one can prove that $x_i = y_i$ for all i at any cross-sectional point down the length of the column. These compositions refer to that of the *bulk* in both streams.

The process shown in Figure 3.7(a) is a membrane column, operating under total reflux. The continuous membrane column was first acknowledged by Hwang and Thorman (1980), as discussed in the Introduction. The next section of this chapter

deals with the addition and removal of feed and products to and from the column respectively.

Rautenbach and Albrecht (1989) discuss reflux cascades of membranes, as well as the membrane column. They conclude that the membrane column "can be regarded as a reflux cascade with an infinite number of stages". What is interesting to note is that Rautenbach and Albrecht (1989) undergo a thought process to arrive at the membrane column, while in this chapter it has been shown that the continuous membrane column is equivalent to permeating in a batch still, when operating at total reflux.

3.5.2 INFINITE REFLUX

When operating under the conditions of infinite reflux, there is a feed to the unit, as well as products being drawn off, such as the schematic shown in Figure 3.7(b). However, the magnitudes of the feed and product flows are extremely small compared to the flows that exist within the column. Therefore one can assume that the column approximates the behaviour of a total reflux column. It is then obvious that an infinite reflux membrane unit exhibits the same mathematical and graphical behaviour on the M-RCM as the total reflux separator does.

3.5.2.1 BOW-TIE REGIONS IN IDEAL M-RCM'S

The mass balance over a simple finite or infinite reflux membrane unit dictates the feed, top and bottom products to lie on the same straight line, known as the mass balance line. This line can be determined by the well-known "lever-arm rule". Furthermore, the top and bottom products have to lie on the same residue curve when operating at total or infinite reflux (Fien and Lui (1994)). This result is intuitive from the discussions given in previous sections.

Using these phenomena, it is now possible to identify two important mass balance lines in membrane separations. (i) A *direct split* mass balance line connects the feed composition and the unstable node in a region, indicating a sharp split with the highest permeating component as the pure top product of a membrane. (ii) An *indirect split* mass balance line connects the feed composition and the stable node, indicating a sharp split with the lowest permeating component as the pure bottoms product of a membrane column (or the retentate of the membrane module). Graphical representations of these sharp splits are shown in Figure 3.8.

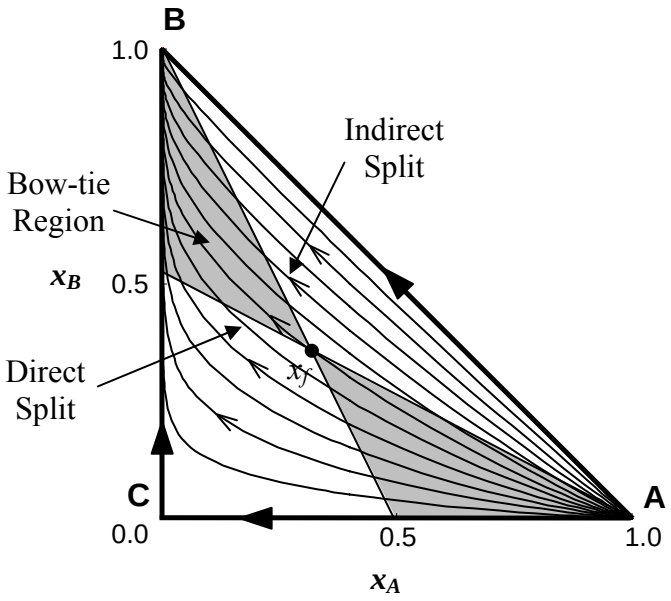

Figure 3.8: Bow-tie region bounded by direct and indirect mass balance lines.

A region of feasible combinations of permeate and retentate products exists for a specified feed composition. In other words, there is a range of material balance lines that make the column feasible. All these material balances are referred to as *non-sharp splits*. The region of non-sharp splits is known as a *bow-tie region*. It is bounded by the direct and indirect split mass balance lines. Obviously, any single residue curve has to pass through both parts of the region in order for feasibility to be

ensured. The reader is referred to Fien and Liu (1994) for further insight into this regard. The bow-tie region for a membrane column is shaded in Figure 3.8.

3.5.2.2 SEQUENCING

In order to separate an ideal 3-component system using a single-feed, two-product continuously operated membrane – that can either be reflux or non-reflux, a minimum of 2 units are necessary to obtain essentially pure components. Note that this discussion will be done from the point of view of reflux separators, but the principle is exactly the same for non-reflux membrane modules. Furthermore, any particular module may consist of several single-stage membranes in a non-reflux cascade in order to achieve the required purity.

Non-Selective Membranes

A non-selective membrane is one which allows all components to pass through, but at different rates. For the M-RCM shown in Figure 3.1, the order of permeability from highest to lowest is A-C-B. There are three possible ways of sequencing units at infinite reflux in order to achieve a separation of all 3 components. The first method requires 2 units, the first of which performs the direct split to produce pure A as shown in Figure 3.9(a), and then the second separates the binary mixture of B and C. Figure 3.9(b) follows a similar sequence, but incorporates the indirect split, resulting in the tops needing to be further purified, as shown. In the last configuration (Figure 3.9(c)), the first membrane follows neither the direct nor indirect split, but rather performs a non-sharp split within the bow-tie region, resulting in both the tops and bottoms products of this column requiring further purification in order to obtain the pure products.

It is worth noting that in each of the 3 cases examined, the membrane material used in each unit is the same - i.e. every membrane has the same relative permeabilities for

each component. Every unit will still be able to achieve the desired separation since the membrane is not selective to any component – each component moves through the membrane at different rates.

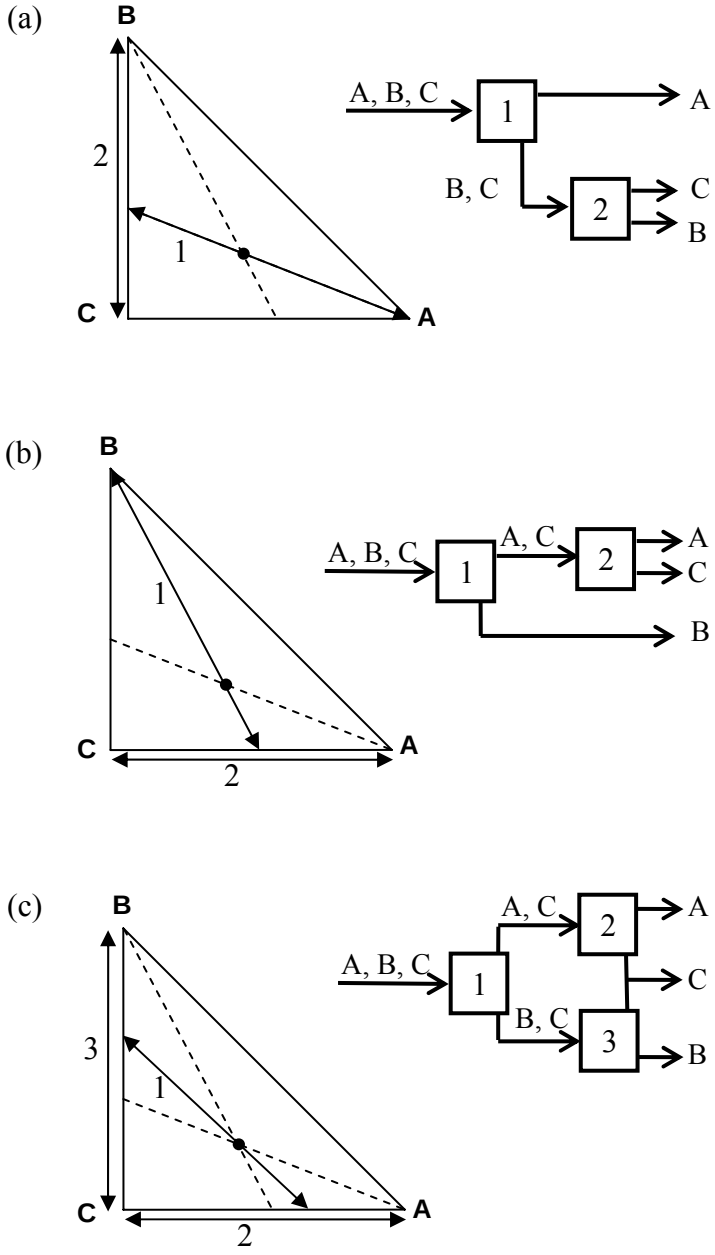

Figure 3.9: Sequencing of membrane columns using (a) direct split, (b) indirect split, and (c) non-sharp split.

Selective Membranes

Since the residue curves in the selective system have essentially no curvature, and are effectively straight lines, the feed, permeate and retentate compositions all lie on same straight line, which happens to be the residue curve passing through the feed point. Thus, for a single unit operating with a vacuum on the permeate side, the permeate product would be a pure methanol stream, while the retentate would be the binary butene/MTBE mixture that the appropriate residue curve ends on. Figure 3.10(a) shows a schematic representation of such a separation.

Due to the nature of the membrane material, it is only possible to define the direct split mass balance. The membrane is selective to methanol permeation, with the butene and MTBE moving through at essentially the same rate. The separation of the MTBE from the butene would not be possible if one uses the same membrane.

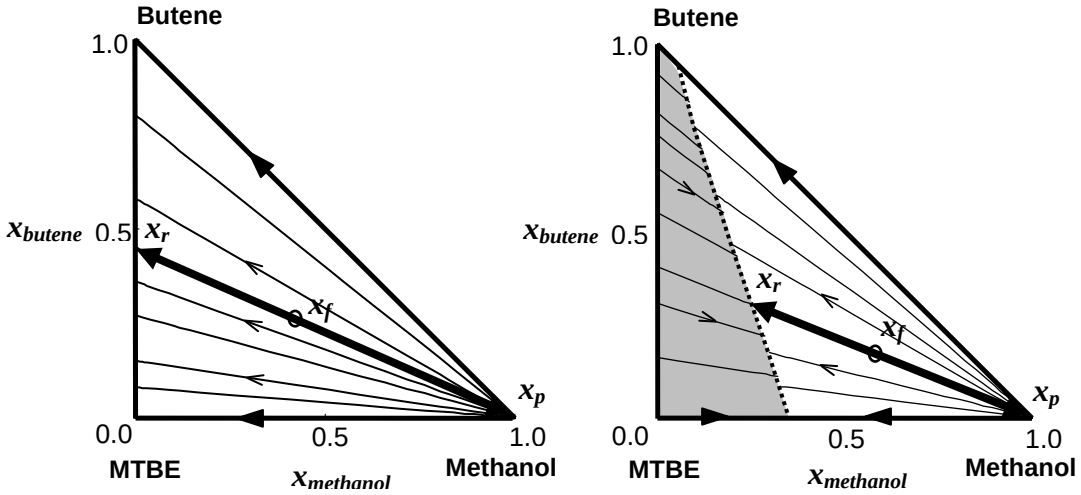

(a) (b)

Figure 3.10: Sequencing of cascades of membrane modules for methanol separation at (a) $\pi_p \approx 0$, and (b) $\pi_p > 0$.

For the case where the permeate pressure is non-zero, a representation of the separation is shown in Figure 3.10(b). In this case, the permeate is still a pure

methanol stream, but the retentate is a mixture still containing methanol, since it is not possible to remove all the methanol from the feed under such operating conditions.

3.5.3 FINITE REFLUX

When operating the column shown in Figure 3.7(b) at finite reflux, the internal flows are no longer equal to each other, as was assumed for the total and infinite reflux cases. This results in a different, more general, DE that describes the retentate composition change with time. However, the DE for such a scenario is neither simple to obtain nor to apply, since the internal flows are themselves changing with position as well. Although it may seem trivial to some extent, these constraints greatly affect the DE and resulting retentate profile. This work has been intriguing and fascinating to the authors, and will form the basis of a future publication (see Chapter 4) where a more detailed understanding and appreciation will be provided.

3.6 HYBRID DISTILLATION-MEMBRANE COLUMNS

With the advent of M-RCM's, a novel approach to designing and synthesizing a hybrid distillation-membrane process has emerged. This section serves to furnish the reader with a brief, yet explanatory, overview of this innovative method. This will be demonstrated through the use of an example.

MTBE is a fuel additive and is the desired product in the traditional Hüls Process (Bausa and Marquardt (2000), Peters et al. (2006b)). An alternative method of separation to that used in the Hüls Process involves the use of membrane technology. The membrane used for the methanol/butene/MTBE system, discussed in Section 3.5.2.2, can not be employed as a stand-alone unit to produce pure MTBE. Using that

particular membrane, it is only possible to obtain a pure methanol stream (refer to Figure 3.10(a) and(b)). As shown by Peters et al. (2006a), each of the curves in the M-RCM ($\pi_P = 0$) terminate when they reach the MTBE/butene binary since it was shown that the flux of each component goes to zero at that point. Thus, pure MTBE or butene can not be obtained from the membrane, unless the curve followed is either the binary MTBE/methanol boundary or the butene/methanol boundary, which is very unlikely. For this reason, the membrane needs to be used in conjunction with either a different membrane (able of removing MTBE from the mixture), or with a distillation column.

The Distillation Residue Curve Map (D-RCM) for the methanol/butene/MTBE system is shown in Figure 3.11. The D-RCM reveals the presence of 2 binary azeotropes, which in turn create a distillation boundary that is difficult to cross.

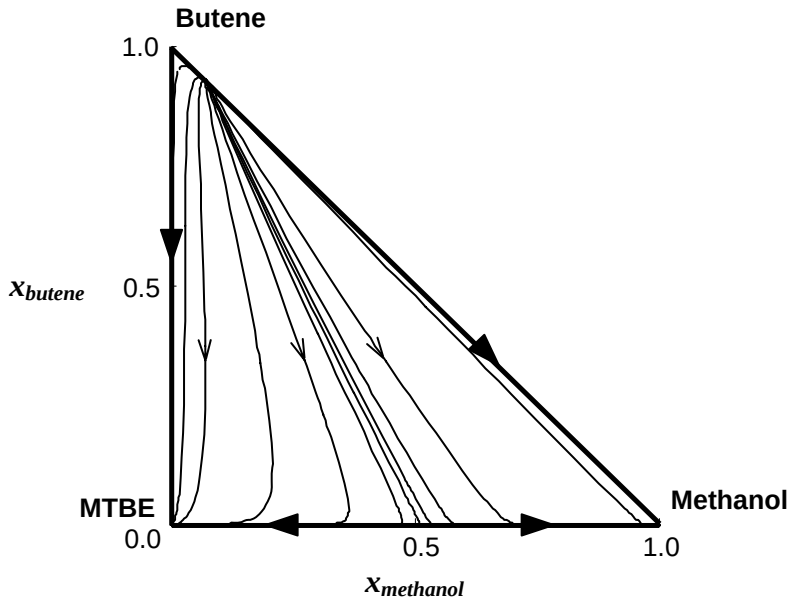

Figure 3.11: D-RCM at P = 6bar.

Analysis of the properties and behaviour of the D-RCM in conjunction with that of the M-RCM equips one with the necessary tools to graphically configure a hybrid

process. To facilitate the construction a hybrid design it is important to sequence the separation units such that each unit operates in the region of the composition space where its separation ability is best suited and most effective.

Numerous hybrid configurations can be investigated, such as membrane placement either upstream or downstream from the column. One could also side-connect the membrane to the column in various ways, thereby creating a recycle with the column. In this chapter, two particular configurations will be examined, so as to display the application the M-RCM has in hybrid processes:

- In the first, an example of how one can *synthesize* a configuration is discussed.
- In the second, a system is chosen and the graphical details of the *design* are given.

3.6.1 SYNTHESIS OF A HYBRID CONFIGURATION

When *synthesizing* a hybrid process, the configuration is not fixed, but is rather depicted by the objectives of the process – i.e. producing the required product streams. For the system at hand, MTBE has the highest boiling point, and would thus traditionally be expected to be the bottoms product of a distillation column, irrespective of membrane placement. A stripping section operation leaf (Castillo et al. (1998)) can thus be generated, as shown in Figure 3.12(a). In much the same manner, a rectifying operating leaf can be plotted using the lowest boiling composition on the D-RCM, namely the methanol/butene binary azeotrope (refer to Figure 3.12(b)). Both operating leaves have been superimposed in Figure 3.12(c).

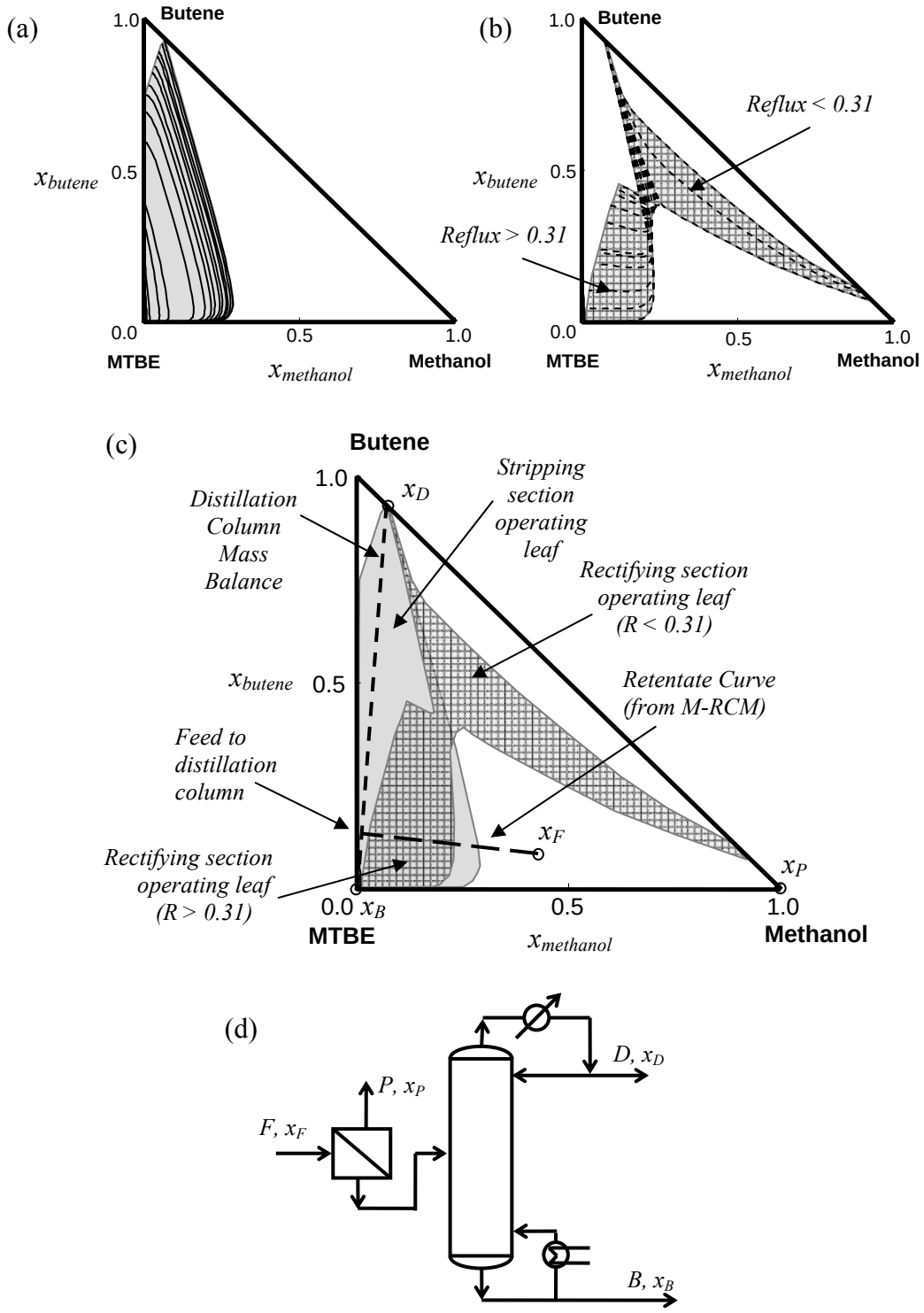

Figure 3.12: (a) Stripping section operation leaf, (b) Rectifying section operating leaf (c) Operating leaves superimposed, and membrane profile for the (d) process configuration. (Reproduced from Peters et al. (2006b))

It can be seen that the rectifying leaf exhibits a bifurcation, resulting in an "open" leaf. This occurs at a reflux of about 0.31. There is, however, an overlap of the two leaves (for reflux values greater than 0.31 in the rectifying section), indicating that a standard single feed, two product column is feasible. For the column to be practical, material balance dictates that the feed composition (to the column) is to lie on the straight line connecting x_D and x_B. The overall feed (to the separation system), however, does not obey this requirement. The composition of the overall feed would probably be located as shown in Figure 3.12(c) (refer to point x_F).

A non-reflux membrane unit can be used prior to the distillation column so as to move the overall feed to a point on the straight line connecting x_D and x_B. The membrane is capable of depleting the feed of most of its methanol, and is thus best suited here. Following the curve on the M-RCM, which passes through the overall feed composition, until it intersects with the distillation column mass balance line, will map out the compositional change of the retentate. Figure 3.12(c) shows this path. Figure 3.12(d) shows the synthesized process configuration.

Notice how the membrane is able to cross the distillation boundary since it is not a VLE-based separation. Once the distillation feed (flowrate and composition) is obtained, the design of the column proceeds using "traditional" methods. The actual choice of reboil/reflux ratio(s) depends on an optimization process, which is out of the scope of this particular report.

3.6.2 DESIGN OF A HYBRID CONFIGURATION

Consider the hybrid configuration shown in Figure 3.13(a). This particular process has been proposed to perform the required separation. Using D- and M-RCM's, the feasibility of this design can be verified. Since such a design would probably entail modifying an existing plant, rather than building a new one, the operating conditions

of the distillation column will be kept at its original design values. For this reason, the pressure in column will be assumed to be 6 bar (Bausa and Marquardt (2000)).

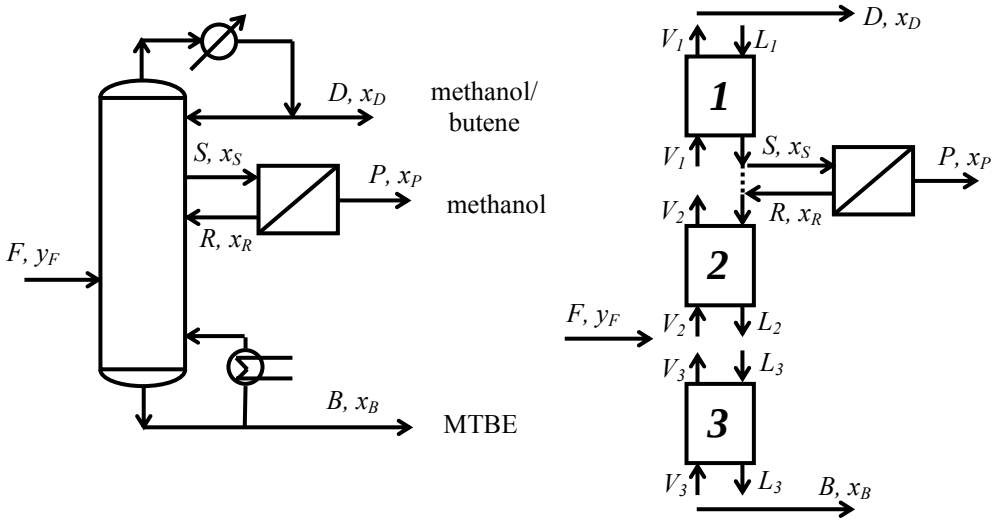

Figure 3.13: (a) A possible hybrid configuration,
(b) The column sections for the hybrid system
(reproduced from Peters et al. (2006b))

The design in Figure 3.13(a) can be divided into *column sections* (*CS*) (Tapp et al. (2004)), as shown in Figure 3.13(b). Each CS (1–3) has its own unique profile described by the Difference Point Equation (DPE) (the constant molar overflow assumption is employed):

$$\frac{dx}{dn} = \left(\frac{1}{R_\Delta} + 1\right)\left(x - y^*\right) + \frac{1}{R_\Delta}\left(X_\Delta - x\right) \tag{3.18}$$

with $$X_\Delta = \frac{V \cdot y_T - L \cdot x_T}{\Delta};\ R_\Delta = \frac{L}{\Delta};\ \text{and}\ \Delta = V - L \neq 0 \tag{3.19a-c}$$

where x is the liquid composition,

n is the number of theoretical stages,

y^* is the vapour in equilibrium with x,

X_Δ is the difference point,

V is the molar vapour flowrate in a CS [mol/s],

L is the molar liquid flowrate in a CS [mol/s],

R_Δ is the reflux ratio,

Δ is the net molar flow in a CS [mol/s]; $\Delta \neq 0$

x_T and y_T are the molar liquid and vapour compositions at the top of a CS

Essentially, the DPE describes how the liquid composition changes down the length of a CS. The profile for each CS depends on the X_Δ- and R_Δ-values for that particular section. With these values set, a Column Profile Map (CPM) can be generated in much the same way as a D- or M-RCM was plotted. A CPM is defined as the "linear transform of the (D-)RCM" (Tapp et al. (2004)).

Holland et al. (2004a) show that any distillation configuration, no matter how complex, can be modelled using CPMs. The example shown here is an extension of the work put forward by Holland et al. (2004a). While they focused on distillation only, we include the addition of a membrane unit connected to column sections.

When designing a hybrid system, such as the one displayed in Figure 3.13, one would like to have available all possible concatenations for a chosen configuration. This would then allow for an easy screening process during optimization.

Regardless of the configuration of the hybrid process, the objective is to meet the separation requirements. By specifying the feed and product compositions, the product flows can be determined for a set feed flowrate. In the arrangement chosen (refer Figure 3.13), one can concatenate the various sections in numerous ways. A "top-down" method is utilized here, but can easily be adapted for other methods, i.e.

"bottom-up". Beginning with the top section (CS 1) the net flow (Δ_1) and difference point ($X_{\Delta 1}$) can be calculated. The reflux ratio ($R_{\Delta 1}$), on contrary, is a choice of the designer – it is the first of 3 degrees of freedom in this design problem. It does, however, have constraints that have to met – these will be discussed later in this section. The liquid (L_1) and vapour (V_1) flows can also be determined. All these values are constant throughout CS 1 under the previously mentioned assumption of constant molar overflow for distillation sections. Performing the necessary material balances around the feed (F), as well as the membrane permeate (P), enables one to define all the process variables for sections 2 and 3 in terms of $R_{\Delta 1}$. The feed is assumed to be all vapour. All these values are summarised in Table 3.1.

Section	$\boldsymbol{\Delta}$	$\boldsymbol{X_{\Delta}}$	$\boldsymbol{R_{\Delta}}$	$\boldsymbol{L}$	$\boldsymbol{V}$
1	D	x_D	$R_{\Delta 1}$	$D \cdot R_{\Delta 1}$	$D \cdot (R_{\Delta 1} + 1)$
2	$P + D$	$\frac{(P \cdot x_P - D \cdot x_D)}{P + D}$	$\frac{(D \cdot R_{\Delta 1} - P)}{P + D}$	$D \cdot R_{\Delta 1} - P$	$D \cdot (R_{\Delta 1} + 1)$
3	$-B$	x_B	$\frac{(D \cdot R_{\Delta 1} - P)}{-B}$	$D \cdot R_{\Delta 1} - P$	$D \cdot (R_{\Delta 1} + 1) - F$

Table 3.1: Design variables in hybrid configuration (refer to Figure 3.13). $R_{\Delta 1}$ is a degree of freedom.

It can be seen that once an $R_{\Delta 1}$-value is set, all the values in Table 3.1 are known. However, setting $R_{\Delta 1}$ alone does not fully specify the entire hybrid system. Another degree of freedom is the amount of material that enters the membrane unit from the end of CS 1. Only liquid is drawn off since a pervaporation membrane is incorporated. The split ratio

$$r = \frac{S}{L_1} \tag{3.20}$$

is defined as the fraction of liquid from the end of Section 1 that reports to membrane module.

Although the range *r*-values have to lie between 0 and 1, the design is only feasible over a smaller, more restricted range. This is to ensure that there is sufficient amount of methanol being drawn of from the end of Section 1. Thus, it can be shown that:

$$r_{\min} = \frac{P}{D \cdot R_{\Delta 1}} \cdot \frac{x_P}{x_S}, \text{ and} \tag{3.21a}$$

$$r_{\max} = 1 \tag{3.21b}$$

where x_S is the composition of the side-draw stream. This is the same as the liquid composition leaving CS 1.

When operating at r_{min}, the amount of methanol that enters the membrane exactly matches the amount being drawn off in the permeate stream (Note: $0 < r_{min} < 1$). Operating at values smaller than r_{min} creates an infeasible retentate composition. r_{max}, on the other hand, allows all the liquid leaving CS 1 to be fed into the membrane module.

Now, x_S is a function of $R_{\Delta 1}$ as well as n_1 (the number of stages in CS 1), amongst others. As $R_{\Delta 1}$ changes, so the profile trajectory for CS 1 is altered. As n_1 changes, so the termination point of CS 1 moves. Thus, it can be seen that r_{min} is not a constant for the system, but does depend on these factors.

Another important composition is that of the liquid entering CS 2:

$$x_{2top} = \frac{D \cdot R_{\Delta 1} \cdot x_S - P \cdot x_P}{D \cdot R_{\Delta 1} - P} \tag{3.22}$$

This is calculated by mixing the retentate stream with remaining liquid from CS 1 that did not go to the membrane. Notice that x_{2top} does not depend on r. This implies that once $R_{\Delta 1}$ and n_1 are set, the location of x_{2top} is fixed. It is obvious that $0 < x_{2top} < 1$, thereby restraining $R_{\Delta 1}$ to set ranges. For this to hold true, it can be shown that:

$$R_{\Delta 1} > \frac{P \cdot x_P}{D \cdot x_S}, \text{ or} \tag{3.23a}$$

$$R_{\Delta 1} < 0 \tag{3.23b}$$

This is diagrammatically represented in Figure 3.14.

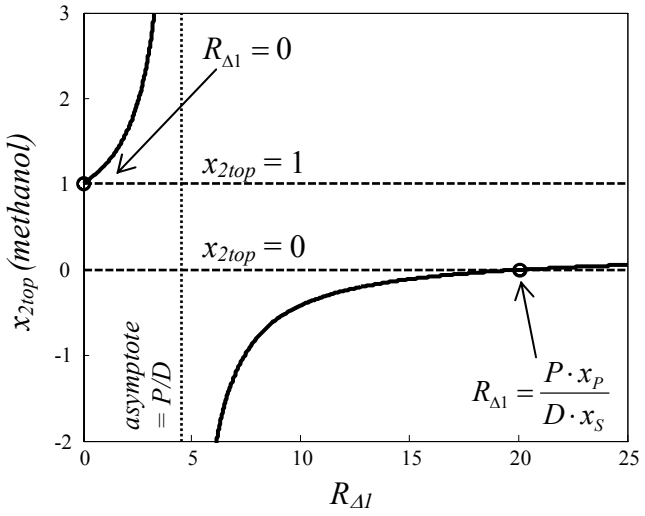

Figure 3.14: Feasibility ranges for $R_{\Delta 1}$ ($0 < x_{2top} < 1$).

Inequality 3.23b is impossible since Section 1 operates in rectifying mode, and $R_{\Delta 1}$ has to be positive by definition (Holland et al. (2004a)). Therefore, $R_{\Delta 1}$ has to adhere to the constraint 3.23a only. This would be the minimum value that $R_{\Delta 1}$ can have,

and would necessitate $x_{2top}(methanol) = 0$. $R_{\Delta 1,min}$ is not set for the system, but does depend on n_1, as discussed previously for r_{min}.

Thus, it can be concluded that this design has 3 degrees of freedom, namely:

- $R_{\Delta 1}$,
- n_1, and
- r

each having to operate within their respective bounds. For demonstration purposes, it will initially be assumed that operation will occur at $r = 0.8$. In order to display the profiles obtainable for this design, $R_{\Delta 1}$- and n_1-values were arbitrarily chosen. Furthermore, for the design to be feasible, it is required that the profiles of each section, including the membrane, intersect in the same order and direction as that of liquid flow in the system. Figure 3.15 shows the column and membrane profiles for operation at $R_{\Delta 1} = 40$ with $n_1 = 5$.

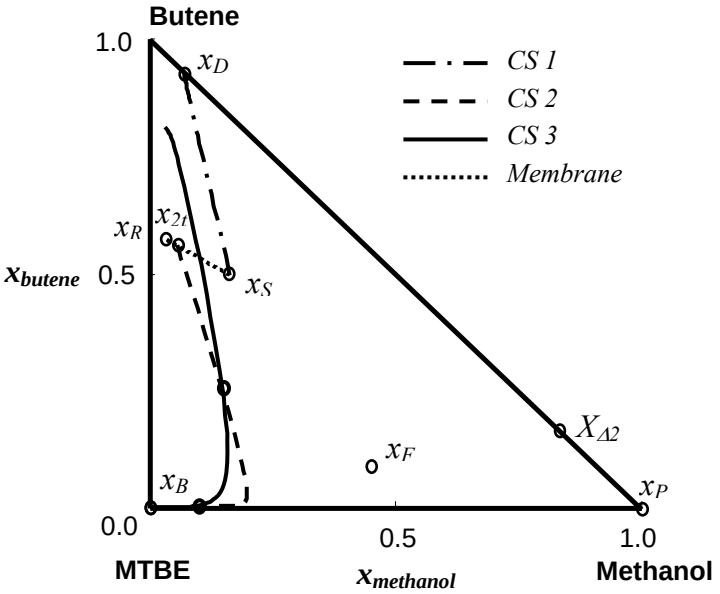

Figure 3.15: Column and membrane profiles for the hybrid design in Figure 3.12 with $R_{\Delta 1} = 40$ and $n_1 = 5$.

Since the feed is a vapour, an intersection of the (liquid) profiles for CS 2 and 3 signifies the end of CS 2 and beginning of CS 3. This is because the composition of the liquid leaving CS 2 will not be altered by the addition of a vapour feed. It is clear in Figure 3.15 that the profiles for CS 2 and 3 intersect twice (at $x_{methanol} = 0.1$ and 0.16). Thus, the termination of CS 2 can occur at either of these points. Figure 3.16(a) and (b) show the possible concatenations of the sections in the hybrid.

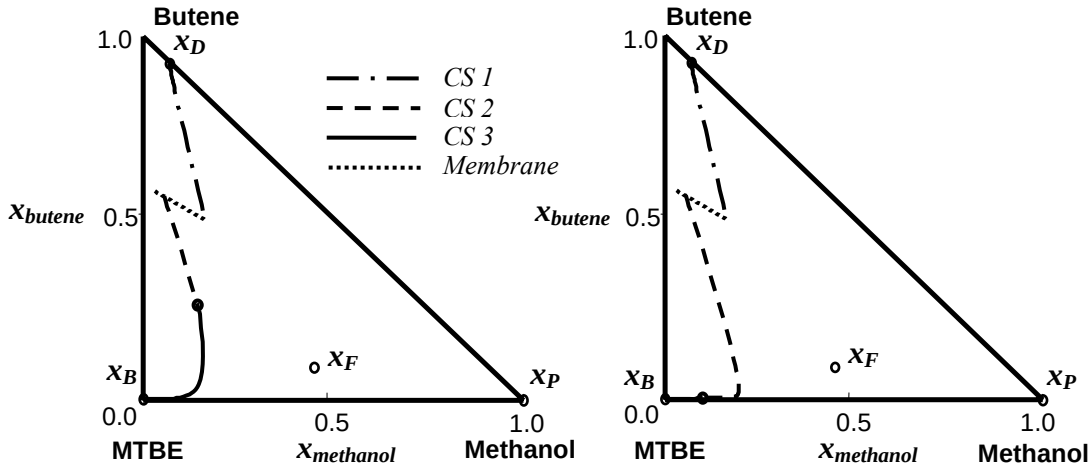

(a) (b)

Figure 3.16: Profile options (a) and (b) for the hybrid design in Figure 3.12 with $R_{\Delta 1} = 40$ and $n_1 = 5$.

To compare these two options one would like to have necessary design parameters easily accessible. With this novel method of design, values such as the number of stages in each CS and the membrane area can be determined with relative ease. This has been done for the 2 options proposed above, and the results tabulated in Table 3.2. The number of stages were calculated from the DPE (equation 3.18), and are theoretical. The membrane area was sought via the methods described in Sections 3.3 and 3.1.4, using the appropriate flux model. (*Note: while it may appear that the membrane area is somewhat large, it is not the aim here to calculate an exact area, but rather to convey an understanding of the simple yet effective methods used.*)

Parameter	***Option (a)***	***Option (b)***
n_1	5	5
n_2	0.6	5.7
n_3	4.8	3.3
A (m^2)	4746.6	4746.6

Table 3.2: Design parameters for the different cases displayed in Figure 3.16.

The diagram in Figure 3.15 shows only one possible profile arrangement for the chosen hybrid design. However, there are numerous ways in which can configure this design based on the degrees of freedom discussed above. A parametric study has been performed that allows for design flexibility. It is therefore possible to generate "*attainable regions*" (*AR*) which integrate the degrees of freedom. *It should, however, be appreciated that the ARs generated here are* ***not*** *the entire AR, but rather a select part of it. The complete AR can be produced, but is detailed and is not done here as it is out of the scope of this report, and will be provided in a later publication.*

For the select ARs, it was assumed that the split ratio, *r*, is set at its minimum value (refer to equation 3.21a). Remember, the split ratio only influences the amount of material that goes to the membrane (and hence the membrane area), but does not affect the location of any of the compositions, except x_R. Thus, 2 types of ARs can be produced: varying $R_{\Delta 1}$ for a set n_1, and vice-versa.

Figure 3.17 shows the AR for a variable $R_{\Delta 1}$ and a set $n_1 = 4$. As discussed previously, $R_{\Delta 1}$ has a minimum value that depends on x_S (refer to equation 3.23a). It can be shown that for this case, $R_{\Delta 1,min} = 41.77$.

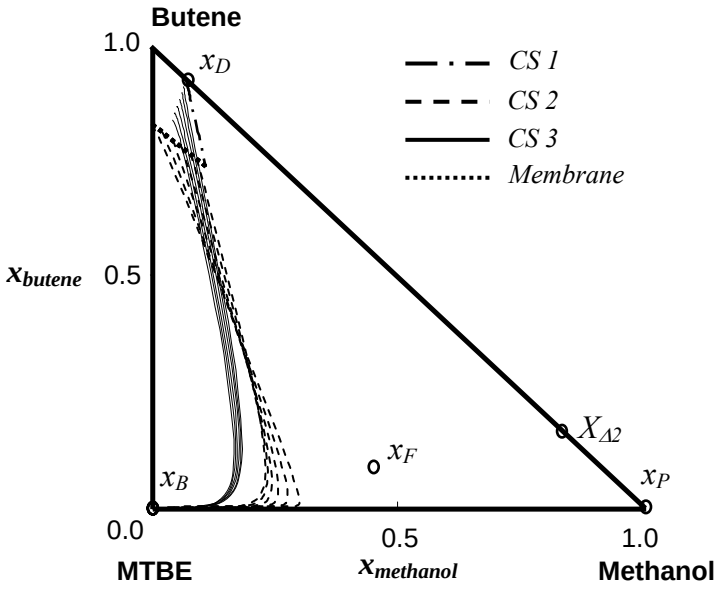

Figure 3.17: Attainable Region for $n_1 = 4$, operating at r_{min}.
Select $R_{\Delta 1}$ -values between 41.77 and 250 have been chosen.

Although not apparent from Figure 3.17, the profile for CS 1 is changing as $R_{\Delta 1}$ changes. The various Section 1 profiles have similar trajectories making it impossible to distinguish on the given scale. Furthermore, there is definite intersection between the profiles for CS 2 and 3 for each $R_{\Delta 1}$. Thus, we can conclude that, for a set n_1, the design is feasible provided that $R_{\Delta 1} \geq R_{\Delta 1,min}$. Similar plots would be obtained for other values of n_1.

Figure 3.18(a), on the other hand, shows the AR for a set value of $R_{\Delta 1} = 70$. The number of stages in CS 1 was varied from 2 to 7 in various increments. A high $R_{\Delta 1}$-value was chosen so as to ensure that it is well above the minimum required for each n_1. For clarity purposes, Figures 3.18(b) and (c) show zoomed in versions of Figure 3.18(a), as indicated by their axes. Of course, for a set $R_{\Delta 1}$, there is a set $R_{\Delta 2}$ and $R_{\Delta 3}$ (refer to Table 3.1). This in turn fixes the profiles for CS 1 and 3, as well as the CPM for Section 2. Hence there is only one possible profile for CS 1 as well as CS 3, as shown. The profile for CS 2 depends on x_{2top}, which changes with each n_1 (or x_S).

But it should be appreciated that all the profiles obtained for CS 2 belong to the same CPM since both $X_{\Delta 2}$ and $R_{\Delta 2}$ are constant.

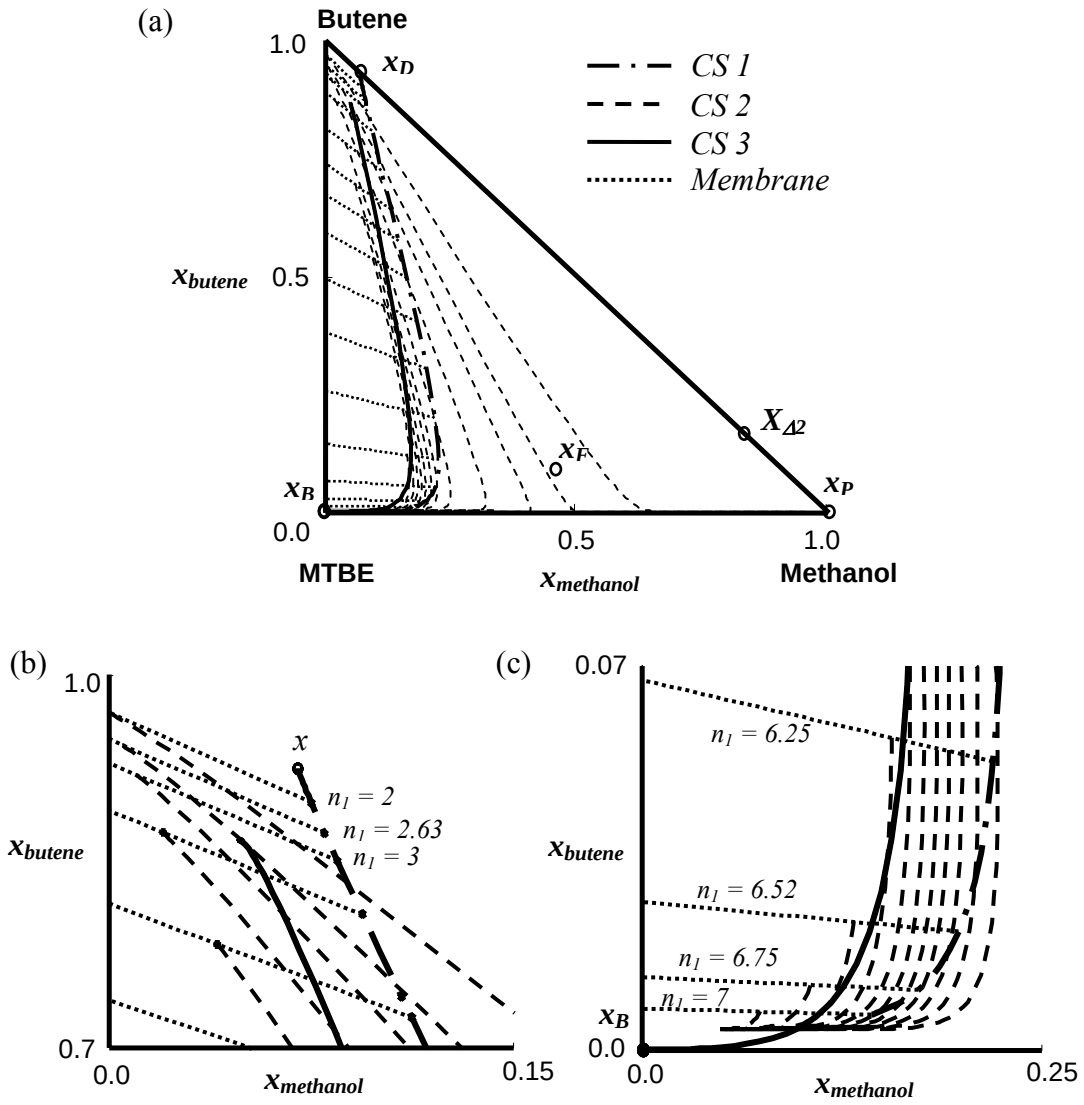

Figure 3.18: (a) Attainable Region for $R_{\Delta 1} = 70$, operating at r_{min}. $2 < n_1 < 7$.
(b) minimum n_1, and (c) maximum n_1 tangent to CS 3 profile.

For each chosen n_1, the membrane profile intersects with that of CS 1, as does CS 2's profile with the membrane profile. However, it can be seen in Figure 3.18(b) that the

profiles for CS 2 and 3 do not intersect for all n_1. For example, when $n_1 = 2$, there is no intersection indicating an infeasible design. It has been determined that the first point of intersection occurs when $n_1 = 2.63$. This is the minimum number of theoretical stages that Section 1 has to have for $R_{\Delta 1} = 70$ in order for a feasible design!

It is further noticed, in Figure 3.18(c), that some profile 2 curves again do not intersect with profile 3 (for $n_1 = 6.75$ and $n_1 = 7$). This means that there are a maximum number of stages that CS 1 can have as well. This maximum occurs at $n_1 = 6.52$, where profile 2 is tangent to profile 3. While it may be thought that adding an excess amount of stages in a column is beneficial, this result is very interesting as it proves that adding too many stages in Section 1 may result in an infeasible design!

Of course the maximum and minimum n_1 values depend on $R_{\Delta 1}$, but can easily be sought for each $R_{\Delta 1}$-value. Similar plots to the one in Figure 3.18(a) can be generated for different $R_{\Delta 3}$-values.

In summation, it has been shown how the M-RCM, in conjunction with the appropriate distillation profiles create a method of design that can be used to quickly evaluate feasible options for a particular design. Using the graphical method not only makes the design process easier to visualize and understand, but it also does provide the designer with useful and necessary design parameters. The operating ranges of the $R_{\Delta 1}$ result, as do the number of stages in each section. Using earlier discussed techniques, the membrane area can also be determined in each scenario.

The method can be adapted accordingly for other process configurations, with the ultimate design chosen by a screening or optimization procedure.

It is agreed that, for this particular hybrid, the role of the membrane residue curve (which is linear) may be small when compared to that of the distillation sections.

However, it is the *method* of analysis that is of importance here – this method can be adapted for any system using whichever membrane best suits the separation.

3.7 CONCLUSION

This chapter serves to furnish the reader with the novel graphical methods developed in analysing and designing membrane permeating systems. RCMs, traditionally believed to be suitable for equilibrium-based processes only, have shown their validity and capability for membrane separations – a kinetic-based process. It has been shown how several common continuous membrane structures are mathematically related to the simple batch experiment. The time variable in the batch is analogous to the spatial variable in continuous operation. This now enables one to extract more valuable information from batch experiments when attempting to scale them up.

It has been demonstrated how the retentate composition in a non-reflux continuous unit will follow the residue curve that passes through the initial (feed) composition. A similar result is arrived at for membrane columns operated under the assumptions of either total or infinite reflux, with the residue curve passing through both the top and bottom composition points. Sequencing columns at infinite reflux has been discussed. Finite reflux, being the more useful mode of operation, is not so straightforward due to the complexities of the situation. Hence, a further publication (refer to Chapter 4) will present detailed discussions on the profiles for finite reflux membrane columns.

The M-RCM, in conjunction with the appropriate flux equations, allows a designer to determine fundamental design parameters such as permeation area (or time) required in a continuous (or batch) process. The details of determining these values have been discussed within the chapter.

A novel approach in synthesizing and designing hybrid distillation-membrane processes emerges: using the M-RCM in conjunction with column profile maps (CPMs) allows one to graphically interpret hybrids in an efficient manner. With the development of M-RCMs, not only is it possible to understand the fundamentals of membrane separations more easily, but it is now possible to design such hybrid systems using a novel graphical technique. Furthermore, by focussing on the membrane in *isolation*, one is not limited to a single hybrid configuration, making the possibilities infinite. By looking at the M-RCM independently from the D-RCM, one can *synthesize* all possible combinations and indeed try to find whether to use one or the other or combinations of both. This method of synthesis has proven to be effective, as discussed with the methanol/butene/MTBE example.

CHAPTER 4:

COLUMN PROFILES FOR MEMBRANE COLUMN SECTIONS

The material in this chapter has been submitted for publication in Industrial and Engineering Chemistry Research. The current reference is: Peters, M.; Kauchali, S.; Hildebrandt, D.; Glasser, D. Column profiles for membrane column sections. *Ind. Eng. Chem. Res.*, **2007**, submitted for publication.

ABSTRACT

A novel graphical method of analysing continuous membrane separation systems has been developed. The method is applicable to all counter- and co-current membrane modules – single-stage, cascades, and membrane columns. All configurations can be broken down into "column sections", no matter how complex the arrangement. Each column section, which resembles a typical single-stage separator, is modelled using the difference point equation. The difference point equation tracks the change in the retentate composition down the length of the column section. For demonstration purposes, a simple constant relative permeability flux model is employed to determine the permeate composition as well as the continually changing retentate flow. All possible operating conditions of a column section are explored. Each condition is a result of the relationships between the flows and compositions at the top of a column section. Using the difference point equation, column profiles for each condition can be plotted. The behaviour of the profiles is discussed both mathematically and graphically. This innovative way of investigating membrane processes provides a unique way of synthesizing and designing them.

4.1 INTRODUCTION

Novel separation methods and techniques have been the focus for engineers in recent decades. While traditional separation procedures have established their industrial value, innovative methods have been emerging in recent years. These fresh approaches have come about in the light of designing more economical and environmentally attractive processes. Membrane-based separation procedures are one of many alternatives proving to be a viable option.

A vast array of different types of membranes, ranging from reverse osmosis to ultra-filtration, has been developed for various applications (Wijmans and Baker (1995), Rautenbach and Albrecht (1989)). An immense amount of research has been completed in permeation modelling (Rautenbach and Albrecht (1985a), Rautenbach and Albrecht (1985b), Marriott et al. (2001), Marriott and Sørensen (2003a)). As will be evident, the nature of the work given in this chapter is *general* and can be applied to any membrane, and its associated flux model. For demonstration purposes, however, only diffusion membranes (i.e. gas separation and pervaporation) will be discussed here. The driving force for separation in diffusion membranes is the difference in partial pressures for each component on either side of the membrane. The work can then further be extended and applied to other membrane types.

Consider some of the unit operations used for continuous membrane separation. A conventional separator, shown in Figure 4.1, consists of a single feed (F) mixture entering a membrane unit. The mixture is separated into 2 product streams – namely, the permeate (P) and retentate (R). Numerous possibilities in flow regimes that have been proposed for such a separator, with the counter-current option being the most efficient (Tsuru and Hwang (1995)). Various external flow arrangements, using a single unit, are also possible, such as recycling the retentate to the feed, or even to the permeate side (not shown).

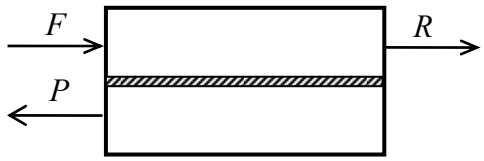

Figure 4.1: Example of a single stage non-reflux continuous membrane unit, operating under a counter-current flow regime.

In some cases, a single unit may not be sufficient: In order to achieve a desired degree of separation, several single-stage modules connected in series, is often advantageous (McCandless (1994)). This is known as cascading. There are numerous configurations that can be employed when cascading, but it can be shown that the simple counter-current recycle cascade is most effective (McCandless (1994)). Such an arrangement of units is what is typically used in solvent (liquid) extraction circuits. Furthermore, the same configuration of interconnected flash stages is equivalent to a distillation column. It was therefore logical that this same analogy be applied for membrane systems: A continuous membrane column, displayed in Figure 4.2, was first identified by Hwang and Thorman (1980).

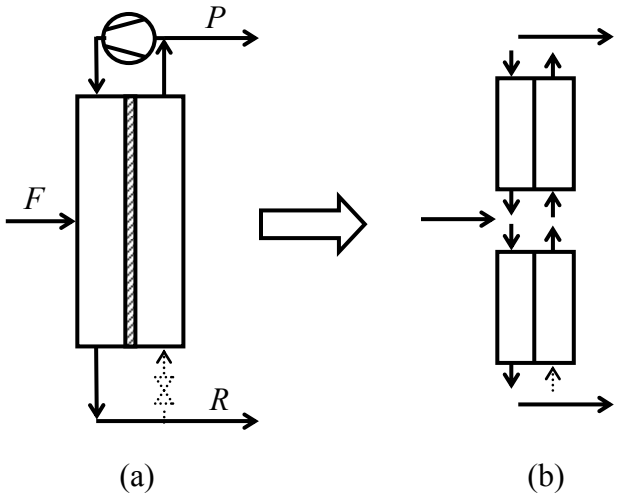

Figure 4.2: (a) A continuous membrane column. (b) Column section breakdown.

The column is filled with hollow-fibre membranes, resembling the design of a shell-tube heat exchanger. A high pressure is maintained on one of side in order to allow permeation through the membrane to the low-pressure side. To allow the recycle streams to flow, a compressor is necessary. It is claimed that complete separation of a binary mixture into pure products is achievable in a finite area (Hwang and Thorman (1980)). The original proposition of a membrane column did not include a retentate recycle, however it has been reported that the inclusion of the recycle has assisted separation in some cases (Tsuru and Hwang (1995)).

Since their inception, membrane columns have been researched somewhat extensively. They were originally designed for gas separations, but Hoover and Hwang (1982) demonstrated how they can be used for pervaporation systems too. A comparison of the membrane column with other design configurations has also been conducted by various authors: Kao et al. (1989) evaluated the performances of the membrane column and two strippers in series, while McCandless (1990) compared the column with counter-current recycle cascades. Vorotyntsev and Drozdov (2001) analyze the ultra-purifying of gases with the use of membrane columns. An optimization technique was proposed by Chang and Hou (2006).

Most publications, however, assume binary mixtures for separation. This assumption is not likely to receive justification in industrial practice. Kothe et al. (1989) studied the separation of ternary gas mixtures using membrane columns, while Blaisdell and Kammermeyer (1973) introduced various models for co- and counter-current gas separation. Agrawal (1996) proposed a procedure to draw membrane cascades for multicomponent gas separation. This was done by using an analogy to distillation. However, there is a lack of a generalized method for the synthesis and design of separation of ternary, and higher order, component mixtures with the use of membrane columns, or any membrane-based process for that matter.

Peters et al. (2006a) began to address this need by introducing Membrane Residue Curve Maps (M-RCMs). Although graphically produced for ternary systems, the ideas and methods are applicable to higher order mixtures. What's more, the theory developed is not restricted to one type of membrane, but is applicable to all types provided the design engineer incorporates the relevant flux model. Applications of these maps to both batch and continuous process were later introduced (Peters et al. (2008)). Amongst being valid for non-reflux equipment, as well as hybrid processes involving membranes, the maps have shown their worth when designing reflux separators, including membrane columns. Peters et al. (2008), however, only looked at total and infinite reflux membrane columns. The aim of this chapter is to furnish the reader with a graphical method of analyzing and visualizing profiles for membrane separators, including the membrane column. With this, one is able to synthesize and design any membrane separation circuit, no matter how complex in its arrangement.

Consider a membrane column, such as the one given in Figure 4.2(a). Analyzing the entire membrane column as a whole, limits one's possibilities to only that particular configuration. This is not useful when it comes to *synthesizing* a separation sequence, especially if it is intended to be optimal. Therefore, a different approach is taken: Any membrane column or cascade can be divided into **column sections (CS)**.

A generalized CS is defined as *a length of column between points of addition and removal of material and/or energy* (Tapp et al. (2004)). This definition is general, and applicable to most, if not all, counter- and co-current applications, such as distillation, absorption and stripping. Although unique in its operation, membrane permeation is no exception to this. Figure 4.2(b) shows an example of a CS breakdown for the membrane column given in Figure 4.2(a). Similar breakdowns can be done for any other arrangement. Analysis of each of the column sections in Figure 4.2(b) reveals that each one resembles a single unit (refer to Figure 4.1). Thus, provided the assumptions of operation are clear and defined, a CS introduces a novel

way of investigating membrane separations. *Note: Although termed "column sections", it does not imply that they are only pertinent for membrane columns, but for any general membrane separator.*

In the section which follows, the theory associated with a CS is discussed. Using material balances, a differential equation has been formulated to describe the change in retentate composition down the length of a CS. This allows one to graphically generate a *column profile*. In Sections 4.3, 4.4 and 4.5 a detailed discussion of all possible modes of operation is given. Column profiles are plotted for each mode, with the behaviour described both physically and mathematically.

4.2 THEORY

4.2.1 MEMBRANE COLUMN SECTIONS

A schematic representation of a membrane CS is shown in Figure 4.3.

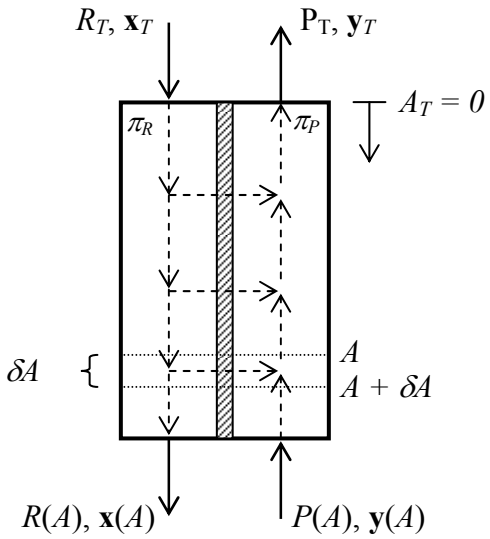

Figure 4.3: A generalized membrane column section.

In Figure 4.3, the following nomenclature applies:

R is the retentate flowrate [mol/s],

P is the permeate flowrate [mol/s],

x is the composition of the retentate phase [-],

y is the composition of the permeate phase [-],

A is the dimensionless membrane area [-]

π_R is the retentate (high) pressure [Pa],

π_P is the retentate (low) pressure [Pa],

$_T$ refers to quantities at the top of the column section.

Throughout the chapter, it is assumed that :

- *All flows and compositions at the top (T) of a column section are known and constant. This assumption can be altered accordingly, if necessary.*
- *The permeate pressure is set sufficiently close to vacuum ($\pi_P \approx 0$), thus permeation will be mono-directional.*
- *Permeation only occurs through the membrane in direction that is perpendicular to the flow of the retentate stream, as indicated in Figure 4.3.*

The actual area of the membrane is not used directly, but is rather embedded within the flux modeling (see later). A dimensionless area is incorporated for locating a position within the column, without being restricted to exact dimensions. However, the dimensionless area is related to real area in much the same way as dimensionless time is related to real time in a batch experiment (Peters et al. (2008)). As a boundary condition, the membrane area is zero at the top of the column. It increases down the length of the column, until the CS is terminated.

4.2.2 THE DIFFERENCE POINT EQUATION

Overall and component material balances can be written (in vector form) around the top of the column and any point down the membrane length (refer to Figure 4.1):

$$P(A) + R_T = P_T + R(A) \tag{4.1}$$

$$P(A)\cdot \mathbf{y}(A) + R_T \cdot \mathbf{x_T} = P_T \cdot \mathbf{y_T} + R(A)\cdot \mathbf{x}(A) \tag{4.2}$$

For purposes of completeness, it should be noted that:

$$\sum_i \mathbf{x}_i = 1 \text{ and } \sum_i \mathbf{y}_i = 1 \tag{4.3}$$

By adding and subtracting the term $\left[R(A+\delta A)\cdot x(A+\delta A)\right]$ to equation 4.2, algebraically manipulating the resulting mass balances, and incorporating an appropriate Taylor series expansion, the Difference Point Equation (DPE) is obtained (refer to Appendix E for the proof):

$$\frac{d\mathbf{x}}{dA} = \left[\frac{\Delta}{R(A)} + 1\right]\left[\mathbf{x} - \mathbf{y}(\mathbf{x})\right] + \frac{\Delta}{R(A)}\left[\mathbf{X}_\Delta - \mathbf{x}\right], \tag{4.4}$$

where Δ and $\mathbf{X}_\Delta$ are defined as:

$$\Delta = P(A) - R(A) \text{ is the net molar flow inside the CS [mol/s], and} \tag{4.5}$$

$$\mathbf{X}_\Delta = \frac{P(A)\cdot \mathbf{y}(A) - R(A)\cdot \mathbf{x}(A)}{\Delta} \text{ is the difference point [-].} \tag{4.6}$$

*The DPE (equation 4.4) mathematically models how the retentate composition (**x**) varies as a function of position (A) in a general membrane CS.*

The DPE was first used by Tapp et al. (2004) for modeling distillation CS. Their assumption of constant molar overflow was valid since material is being transferred in both directions – from vapour to liquid, as well as vice versa. Hence the energy involved in the transfer is such that the assumption is suitable. In a membrane CS, however, the constant molar overflow assumption can not be employed. The following section presents a method for predicting the varying flows.

4.2.3 PERMEATION MODELING

In order to solve the DPE in equation 4.4, it is necessary to understand how **y** is related to **x**. As discussed by Peters et al. (2006a), there are numerous methods of describing this relationship. It was shown, for a gas separation membrane operating at a permeate pressure sufficiently close to vacuum ($\pi_P \approx 0$), that:

$$\frac{y_i}{y_j} = \alpha_{ij}^{M} \frac{x_i}{x_j} \tag{4.7}$$

where α_{ij}^{M} is known as *membrane selectivity*, or the permeability of *i* with respect to *j*:

$$\alpha_{ij}^{M} = \frac{P_i^{'}}{P_j^{'}} \tag{4.8}$$

Using appropriate simplifications, one can rearrange equation 4.7, to obtain:

$$y_i = \frac{\alpha_{ij}^{M} x_i}{\sum_i \alpha_{ij}^{M} x_i} \,. \tag{4.9}$$

It is agreed that the permeabilities of the components may not be constant, but rather depend on a number of factors, such as the retentate and/or permeate composition(s), and that mass transfer through the membrane can be quite complex. However, for demonstration purposes, a simple point of view will be taken. For this reason, *constant relative permeabilities* have been assumed, resulting in what is known as a *Knudsen-membrane* (Huang et al. (2004)).

So as to solve the DPE, it is further required to model how the retentate flow is changing as a function of position, since material is being transferred mono-directionally (from *R* to *P* only). Consider a strip membrane area, as shown in Figure 4.4, where **J** is a vector containing the fluxes of all the components.

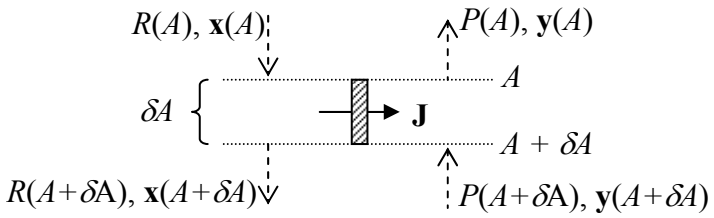

Figure 4.4: Strip of membrane column section.

Expressing the total flux of material that permeates in the area δA [mol/m^{2}s] as:

$$\sum_i \mathbf{J}_i = J\,, \tag{4.10}$$

allows one to write an overall differential material balance over the retentate side:

$$\frac{dR(A)}{dA} = -J\,. \tag{4.11}$$

It can further be shown that:

$$dR(A) = dP(A) \tag{4.12}$$

For a simple gas separation membrane, with constant relative permeabilities (α_{ij}^{M}), the following expression can be derived (refer to equation 4.7):

$$\frac{dR(A)}{dA'} = -\sum_{i} \alpha_{ij}^{M} x_i \tag{4.13}$$

where $A' = A\frac{\pi_R P'_{ref}}{\delta}$ is a normalized form of A, and is dimensionless. Here, δ is the membrane thickness [m].

For any other membrane, manipulation of the appropriate flux model should replace the right hand side of equation 4.13. The subscript *ref* denotes a chosen reference component. *In this chapter, component B is the reference component, and the following relative permeabilities have been assumed throughout:* $\alpha_{AB}^{M} = 3$, $\alpha_{BB}^{M} = 1$, and $\alpha_{BC}^{M} = 1.5$. Thus, the order of permeability (from most to least) is: A-C-B.

Thus, using equation 4.13, in conjunction with equation 4.9, in the DPE, one can solve for, and graphically interpret the retentate profile for a specified column section.

4.2.4 PROPERTIES OF THE DPE

The DPE is derived on a mass balance basis (refer to Section 4.2.1), and is not dependent on the type of membrane used (i.e. diffusion, filtration, reverse-osmosis, etc.). Whilst solving it requires knowledge regarding the membrane flux, the form of the DPE is *general*.

The net flow (Δ) and composition ($\mathbf{X}_\Delta$) are *constant* throughout a CS. This can be easily deduced by overall and component mass balances (equations 4.1 and 4.2):

$$\Delta = P_T - R_T \text{, and} \tag{4.14}$$

$$\mathbf{X}_\Delta = \frac{P_T \cdot \mathbf{y}_\mathbf{T} - R_T \cdot \mathbf{x}_\mathbf{T}}{\Delta}. \tag{4.15}$$

This is a very interesting result: It is saying that there remains a *constant* difference in flows and composition between any two points along a horizontal cross-section in the CS. This occurs despite there being a continuous change in retentate and permeate flows down the length of the column.

The DPE has been derived to model the retentate composition (**x**). An analogous DPE can be sought for the permeate composition (**y**) in much the same manner. Alternatively, **y** can be simply sought from **x** using a material balance over the CS (refer to equation 4.6). What's more, is that the equation is not limited to the counter-current case as discussed, but can be used for other flow regimes (namely, co-current).

A further generality of the DPE is that knowledge of the actual shape and geometry of the membrane within the CS is not necessary. The equation is not restricted, and can be applied to any chosen shape (plate module, hollow fiber, spiral wound, etc.).

It is also worth mentioning that the DPE is not limited to membrane permeation processes, and can be used for any contacting process, as well as any flow regime. Of course, depending on the process, certain constraints will need to be employed, and the DPE adjusted appropriately. Such work is not within the scope of this report, and will not be discussed further here.

In the sections which follow, all possible operating conditions for a CS are detailed. Each condition is a result of the relationships between R_T and P_T, as well as $\mathbf{x_T}$ and $\mathbf{y_T}$.

4.3 COLUMN SECTION PROFILES: OPERATING CONDITION 1

4.3.1 STATEMENT

Let us consider a special case of operation of the membrane CS shown in Figure 4.3 where:

$$P_T = R_T \text{ and } \mathbf{y_T} = \mathbf{x_T} \tag{4.16}$$

This is equivalent to describing a total reflux column, and also sufficiently expresses an infinite reflux column, as discussed by Peters et al. (2008).

4.3.2 MATHEMATICS

The conditions of Case 1 results in:

$$\Delta = 0 \tag{4.17}$$

and thus the DPE (equation 4.4) becomes:

$$\frac{d\mathbf{x}}{dA} = \left[\mathbf{x} - \mathbf{y}(\mathbf{x})\right] \tag{4.18}$$

4.3.3 MEMBRANE RESIDUE CURVE MAP

Equation 4.18 is the Membrane Residue Curve equation as identified by Peters et al. (2006a). Solving this set of equations, in conjunction with the flux model (equation 4.9), for a range of initial conditions ($\mathbf{x}^{o}$) allows one to produce a Membrane Residue Curve Map (M-RCM) as shown in Figure 4.5.

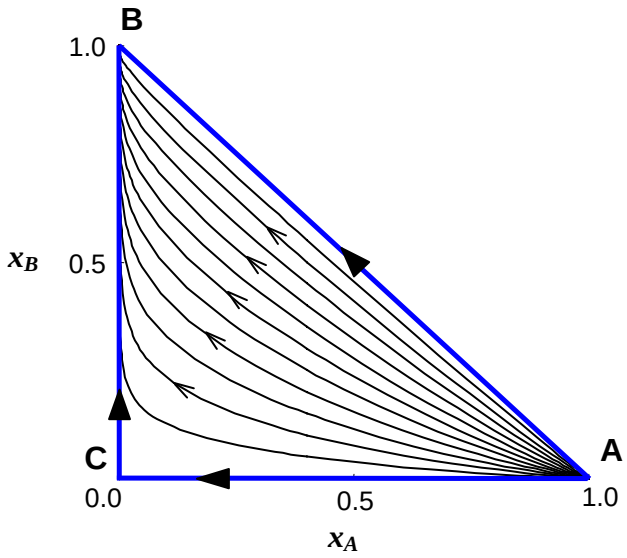

Figure 4.5: Membrane Residue Curve Map (M-RCM) for an ideal A-B-C system with $\alpha_A = 3$, $\alpha_C = 1.5$. (Reproduced from Peters et al. (2006a))

From any given initial condition ($\mathbf{x}^{o}$), integration of equation 4.18 can occur in two directions:

(i) **positive integration** ($A \rightarrow +\infty$) corresponds to determining the retentate composition from the top of the CS to the bottom (i.e. $\mathbf{x}^{\mathbf{o}} = \mathbf{x}_{\mathbf{T}}$), while

(ii) **negative integration** ($A \rightarrow -\infty$) performs the reverse direction, integrating from bottom to top (i.e. $\mathbf{x}^{\mathbf{o}} = \mathbf{x}_{\mathbf{B}}$).

It is customary to indicate the direction of the *positive* integration on such maps (Fien and Lui (1994)), as is done in Figure 4.3.

The Mass Balance Triangle (MBT) or Gibbs Triangle represents the region of physically achievable profiles in ternary systems. One may define this triangular region mathematically as $0 \le x_i \le 1$ for all i. Although describing a real process, the DPE at infinite reflux (or membrane residue curve equation), is merely a mathematical equation. This equation is not bound by any physically relevant initial conditions, and it is possible to evaluate it at initial values of $\mathbf{x}$ outside the MBT. Choosing an $\mathbf{x}^{\mathbf{o}}$ outside of MBT, and integrating in both positive and negative directions, it is possible to populate the entire $x_A - x_B$ space. This is shown in Figure 4.6

The profiles laying outside the MBT may not be physically achievable, but the relevance of this map is very important, and will be discussed in subsequent sections. The nature and location of the stationary points in this map provide insight into the behaviour of the curves.

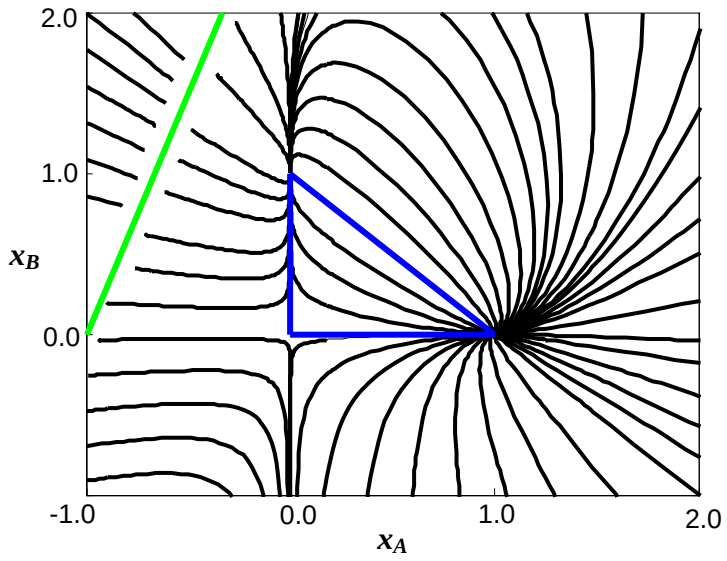

Figure 4.6: Entire M-RCM.
MBT in blue, line of discontinuity in green.

4.3.4 STATIONARY POINTS

In order to locate all the stationary points that exist in the entire space, it is necessary to equate the DPE to zero:

$$\frac{d\mathbf{x}}{dA} = 0, \text{ or } \left[\mathbf{x} = \mathbf{y}(\mathbf{x})\right] \tag{4.19}$$

Solving these equations simultaneously with the flux model given in equation 4.9, it can be shown that only 3 roots exist. Furthermore, the location of these stationary (or pinch) points occurs at each of the 3 pure components.

While one could *graphically* use the direction of movement of curves with respect to a particular node to determine its type (stable, unstable, saddle, etc.), there is a more fundamental and mathematically accepted procedure: Liapounov's first theorem states that the nature of a singular point is topologically similar to the linearized form

of the DPE. The resulting square Jacobian matrix is constant, and not a function of A. Thus, the eigenvalues of the Jacobian, which can be determined, characterizes the type of singularity. The corresponding pair of eigenvectors associated with each point determines the asymptotic direction of the trajectories in the neighborhood of the singular point. Such an analysis on the DPE for Case 1 yields the following:

- pure A is the *unstable node*,
- pure B is the *stable node*, and
- pure C is a *saddle point*.

4.3.5 DISCONTINUITY

The constant relative permeability flux model (equation 4.9) has the inherent property of being undefined when its denominator equals zero. The resulting straight line equation indicates the path of discontinuity. This is graphically depicted in Figure 4.6. The discontinuity arises due to the structure of the flux model, and thus varies according to the model selected. For a chosen membrane (and its associated flux model), the position of the discontinuity will remain fixed. Moreover, the nature of the discontinuity will differ for each model, but any discontinuity will always exist outside the MBT only.

4.4 COLUMN SECTION PROFILES: OPERATING CONDITION 2

4.4.1 STATEMENT

Suppose we still have the CS configuration as depicted in Figure 4.3, with

$$P_T = R_T \text{ but } \mathbf{y_T} \neq \mathbf{x_T} \tag{4.20}$$

4.4.2 MATHEMATICS

Expanding the general DPE (equation 4.4):

$$R(A)\frac{d\mathbf{x}}{dA} = P(A)[\mathbf{x} - \mathbf{y}(\mathbf{x})] + [P_T - R_T]\left[\frac{P_T\mathbf{y_T} - R_T\mathbf{x_T}}{P_T - R_T} - \mathbf{x}\right] \tag{4.21}$$

Multiplying out, and then employing the conditions of the case, it can be shown that:

$$\frac{d\mathbf{x}}{dA} = [\mathbf{x} - \mathbf{y}(\mathbf{x})] + \beta(A)\cdot\boldsymbol{\delta}_\mathbf{T} \tag{4.22}$$

where

$$\beta(A) = \frac{R_T}{R(A)} \tag{4.23}$$

$$\boldsymbol{\delta}_\mathbf{T} = \mathbf{y_T} - \mathbf{x_T} \tag{4.24}$$

$\boldsymbol{\delta}_\mathbf{T}$ is known as the *difference vector* taken at the top of the CS. Furthermore, it can be shown that:

$$\sum_i \boldsymbol{\delta}_{\mathbf{T}i} = 0 \tag{4.25}$$

is a property of $\boldsymbol{\delta}_{\mathbf{T}}$ that needs to be satisfied. Since $\boldsymbol{\delta}_{\mathbf{T}}$ is a difference in two compositions, it follows that certain values (but not all) in the row vector will be of negative sign. It is also worth noting that the entries in $\boldsymbol{\delta}_{\mathbf{T}}$ change value down the length of the column since the flowrates are changing within the column:

$$\boldsymbol{\delta}(A) = \frac{R_T}{R(A)}\boldsymbol{\delta}_{\mathbf{T}} = \beta(A)\cdot\boldsymbol{\delta}_{\mathbf{T}} \tag{4.26}$$

Thus $\boldsymbol{\delta}(A)$ is continually changing. This can be easily proven by material balance around the CS, as well as the conditions of the case.

4.4.3 COLUMN PROFILE

If values of the $\boldsymbol{\delta}_{\mathbf{T}}$ and R_T are arbitrarily chosen (say [*0.1 -0.05*] and *100 mol/s* respectively), then a membrane profile can be generated for a given initial composition. It seems apparent and obvious that this initial condition be the top retentate composition, since this point has been used as a reference. Of course, the corresponding permeate composition is easily determined through $\boldsymbol{\delta}_{\mathbf{T}}$. Using a value of $\mathbf{x}_{\mathbf{T}}$ = [*0.3, 0.3*], and integrating down the length of the column, the profile displayed in Figure 4.7 results.

This type of curve is unique and behaves very differently from those obtained in the M-RCM (Figures 4.5 and 4.6). The behaviour of the profile can be understood by analysis of the DPE for the operating conditions of this case (equation 4.22). Although the curve has no physical meaning once it crosses the AB-boundary, a great deal of useful information can be extracted from the trajectory it follows.

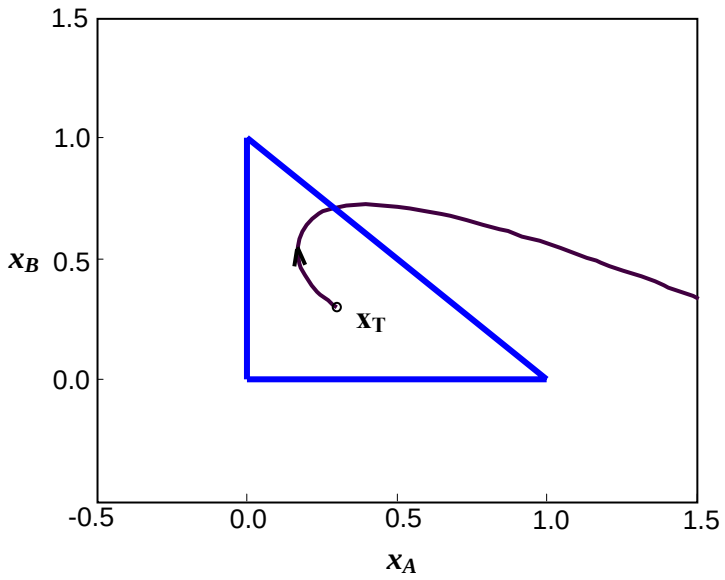

Figure 4.7: Membrane column profile for Case 2. Positive Integration.

$R_T = 100$ *mol/s*, $\boldsymbol{\delta_T} = [0.1, -0.05]$, $\mathbf{x_T} = [0.3, 0.3]$.

4.4.4 ANALYSIS

The DPE for Case 2 is a combination of the separation vector, $\mathbf{s} = \mathbf{x} - \mathbf{y}$, and the difference vector, $\boldsymbol{\delta_T}$. The equation is similar to the one used in Case 1 (equation 4.18), except now that there is an additional vector term that gives rise to new topological features. If this were Case 1, then $\boldsymbol{\delta_T} = 0$. $\beta(A)$ is a scalar multiplier preceding $\boldsymbol{\delta_T}$, and is a ratio of the retentate flow at the column top to that at a point corresponding to A. If the column was operating under the assumption of constant molar overflow, then $\beta(A)$ is unity. However, this assumption is not true for membrane permeation, and $\beta(A)$ has the following values:

At the top of the column:

$$\beta(0) = \frac{R_T}{R_T} = 1 \qquad (4.27a)$$

At any point down the length of the column:

$$\beta(A) = \frac{R_T}{R(A)} > 1 \qquad (4.27b)$$

since the retentate flow is losing material from the column top.

Consider, for a moment, what topological effects would occur if $\beta(A)$ were to remain constant at a value of 1. If this were the case, then the resulting map is shown in Figure 4.8(a).

It is noticed that map obtained has similar topological features to the M-RCM (refer to Figure 4,5). However, it has been shifted, and the nodes are in different positions in Figure 4.8 compared to Figure 4.5. As discussed by Holland et al. (2004b), the three nodes are connected by straight lines due to the collinear nature and direction of the eigenvectors at each node, thus forming a triangle. The blue triangle indicates the MBT, as well as the location of the nodes when $\beta(A) = 0$ (total reflux). The red triangle represents the "transformed" triangle, connecting the 3 nodes appropriately. It can be noticed that previously non-achievable profiles have moved into the physically possible (MBT) space. This shift arises from the addition of $\boldsymbol{\delta_T}$ in the M-RCM equation. The magnitude and direction of $\boldsymbol{\delta_T}$ affects the way in which the map is transformed – this will be discussed later.

If $\beta(A)$ were constant, the column profile would follow the bold curve in Figure 4.8(a), commencing at $\mathbf{x_T} = [0.3, 0.3]$. However, $\beta(A)$ is not a constant value, and is becomes larger down the length of the column. It will only have a value of 1 at the top of column, and at no other point in the column. As soon as $A > 0$, then $\beta(A) > 1$, and $\boldsymbol{\delta_T}$ essentially becomes larger (in absolute value). This implies that the trajectory of the column profile shown in Figure 4.7 will be tangent to the appropriate curve that

passes through the point $\mathbf{x_T}$ on the shifted plot (Figure 4.8(a)) when $\beta(A) = 1$, namely the bold curve in Figure 4.8(a).

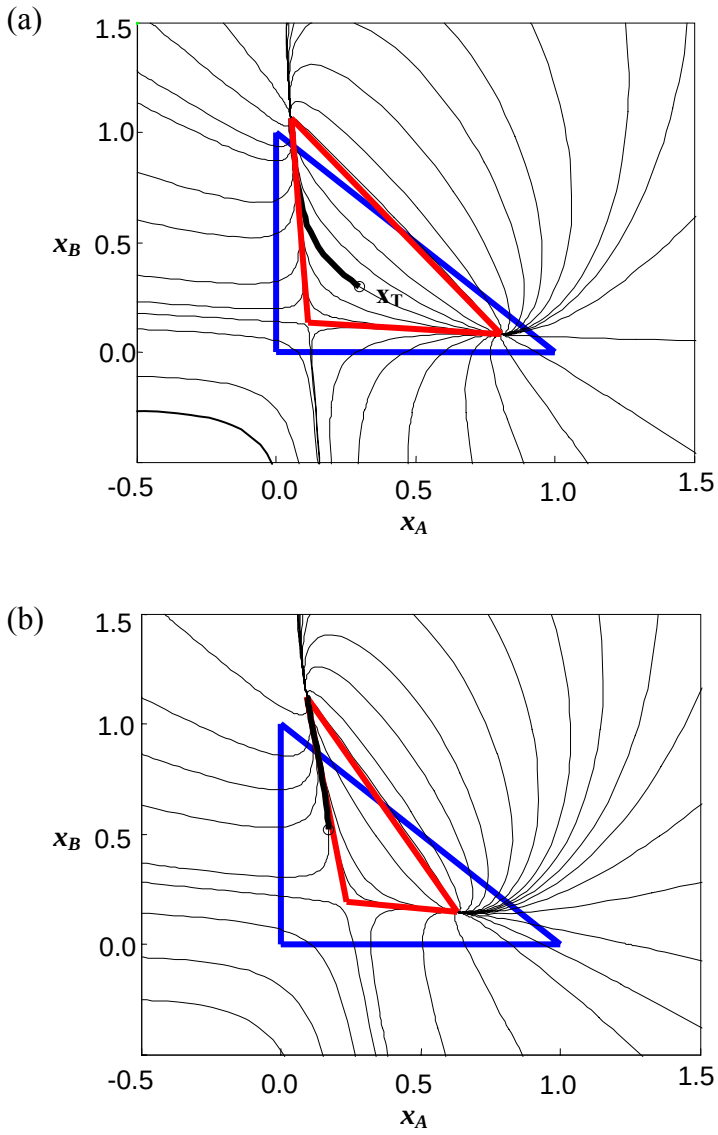

Figure 4.8: Shifted M-RCMs. The blue triangle represents the MBT, the red shows the transformed triangle.

(a) $\beta(A=0) = 1$, (b) $\beta(A) = 1.667$. $\boldsymbol{\delta_T} = [0.1, -0.05]$, $\mathbf{x_T} = [0.3\ 0.3]$.

Actual membrane profile (see Figure 4.4) is tangent to bold profile at the point indicated.

As permeation begins, $\beta(A) > 1$, and the shifted map shown in Figure 4.8(a) will, in fact, shift again! Since $\beta(A)$ is continually changing, the map itself is going to constantly transform. For example at a certain A, it will occur that $\beta(A) = 1.667$. The corresponding map at this value is shown in Figure 4.8(b).

The actual membrane column profile that exists (as shown in Figure 4.7) is not one of the curves shown Figure 4.8(b), but is tangent to the curve that goes through the point when the retentate flow is such that $\beta(A)= 1.667$. This point is easily determined from the data associated with the membrane column profile, and is plotted in Figure 4.8(b). The corresponding curve is shown in bold – it is along the one side of the transformed triangle. It is interesting to note that this particular curve was originally outside the MBT, and has now been shifted in, and forms part of the column profile. Thus, it can be concluded that: *Every point on the membrane column profile is tangent to a curve on a transformed map going through that point. The transformed map corresponds to the appropriate $\beta(A)$–value at that point.* Figure 4.9 shows discrete points on the membrane column profile and the associated tangent curves at the indicated $\beta(A)$-values. Each of the "constant $\beta(A)$" curves is plotted to run to its stable pinch.

It is noticed that, as $\beta(A)$ increases, the membrane column profile tends to maintain a similar direction to the "constant $\beta(A)$" curve for longer. This should be expected since, by analyzing the DPE for this case (equation 4.22), as $\beta(A) \rightarrow \infty$, the difference vector ($\boldsymbol{\delta}_\mathbf{T}$) becomes dominant, suppressing the effect of the separation vector (**s**). Thus, the left-hand side of the differential equation becomes a constant vector (for each $\beta(A)$) which has the direction of $\boldsymbol{\delta}_\mathbf{T}$. This is evident from the profile obtained – as the trajectory proceeds, its ultimate direction becomes that of $\boldsymbol{\delta}_\mathbf{T}$, as shown. Thus, varying the direction of the difference vector will decide the ultimate direction of the membrane column profile, provided $A \rightarrow \infty$.

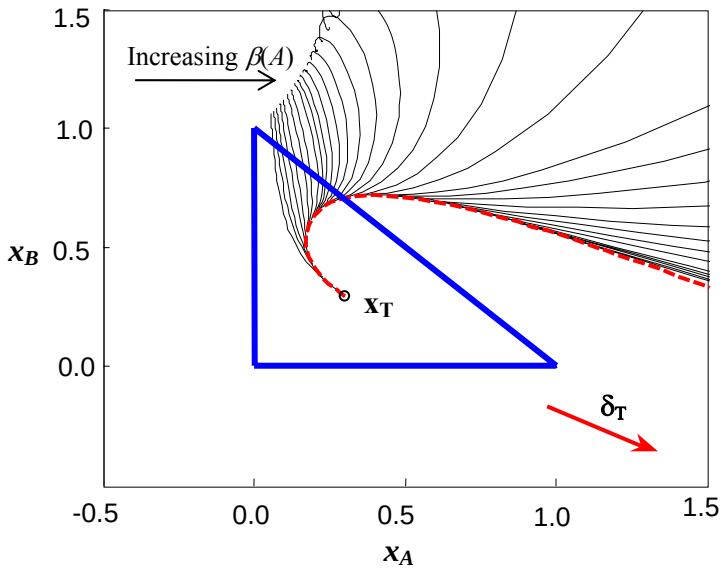

Figure 4.9: Tangency of curves to the column profile.
Each curve corresponds to a different $\beta(A)$-value,
and is allowed to run to its stable pinch point.

4.4.5 PINCH POINT LOCI

It can also be noticed from Figure 4.9 that there is a trend occurring with the pinch points of each "constant $\beta(A)$" curve. Due to the direction of integration, the point where each of these curves pinch would be their stable node. It is not only the stable node that moves, but the unstable and saddle points shift as well. A locus of all these points can be generated for a chosen δ_T. Figure 4.10 shows the pinch point loci for $\delta_T = [0.1, -0.05]$.

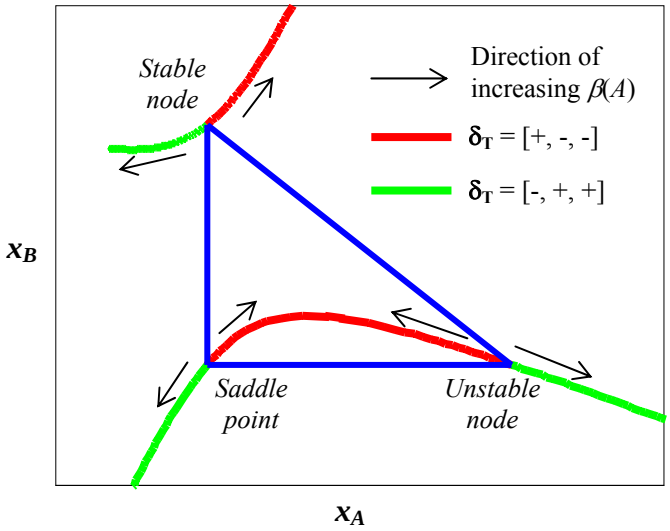

Figure 4.10: Pinch Point Loci for δ_T = [+, –, –].

Since δ_T is the difference vector, behavior of the pinch point loci can be characterized by its direction and magnitude. For a 3 component system, δ_T has 3 entries, each of which can have a possibility of 2 signs (+ or –). This means that there are 8 possible directions that δ_T can have. However, δ_T has the property that all its entries have to sum to zero (equation 4.25). Therefore, the combinations where all entries are positive (or negative) are not valid directions. This leaves 6 directions – 3 unique directions and 3 in opposite direction. By arbitrarily selecting δ_T's in each of the 3 unique directions, and multiplying them by -1 to obtain the other 3 directions, the pinch point loci can be plotted for each direction. This was done in Figure 4.10 for one of the unique directions. Similar plots can be generated for the other 2 unique directions of δ_T but are not given here. (refer to Holland et al. (2004a)).

In Figure 4.10, it occurs that the unstable node approaches the saddle point as $\beta(A)$ increases, depending on the direction of δ_T. When the loci of each node meet, those two particular nodes become complex and the stable node is the only point that exists in the real space.

Although the location of the pinch point curves has no apparent use in the current context of a profile associated with Case 2, there worth will be shown and explained in Cases 3 and 4, as well as in future work and publications on "coupled columns sections" (see Chapter 5).

4.4.6 FURTHER COLUMN PROFILES

When plotting the membrane column profile in Figure 4.7, a randomly chosen $\mathbf{x_T}$ and R_T were chosen. Of course, any positive flowrate for R_T is feasible, as is any point within the MBT is a possible top retentate composition. Figure 4.11(a) displays column profiles for a set $\mathbf{x_T} = [0.3, 0.3]$, varying R_T as indicated. Figure 4.11(b), on the other hand, shows a range of column profiles for select $\mathbf{x_T}$'s at a constant $R_T = 100\ mol/s$.

It can be seen that, irrespective of starting point or flowrate, all curves ultimately end up progressing in the same direction, namely $\boldsymbol{\delta_T} = [0.1, -0.05]$. In Figure 4.11(a), all the curves move off from the same point in the same direction. But the smaller R_T is, the faster $\beta(A)$ becomes larger, resulting in the $\boldsymbol{\delta_T}$ dominating in the DPE sooner. This results in curves with small R_T's progressing in the direction of $\boldsymbol{\delta_T}$ sooner than those with large R_T. What is interesting to note is that, by adjusting $\mathbf{x_T}$ and R_T, it is possible to obtain a profile to runs directly into a pure component. Consider the $R_T = 20\ mol/s$ profile in Figure 4.11(a) that passes through pure A. Interestingly enough, component A is the most permeable component, and is expected to permeate the fastest. However, due to the operating conditions of Case 2, it is evident that can synthesize any membrane column to achieve desired products!

In Figure 4.11(b), the initial direction of each curve is determined by the curve going through the same point on the $\beta(A) = 1$ map (Figure 4.8(a)). This map has been

superimposed on Figure 4.11(b). Curves commencing in the regions outside shifted triangle, but inside the MBT, initially move in a different direction to the profiles that begin within the shifted triangle. This is due to the nature of the profiles in Figure 4.8(a) in that region (they were shifted into the space!).

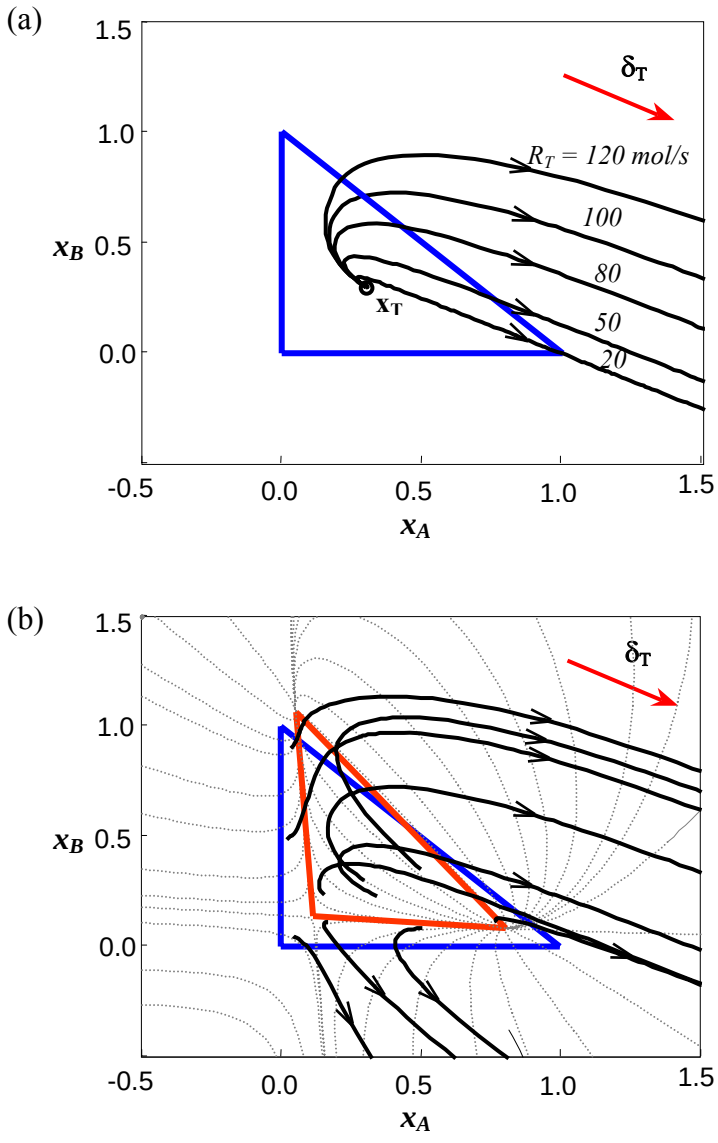

Figure 4.11: Column Profiles for selected values of (a) R_T with $\mathbf{x_T}$ = [*0.3, 0.3*], (b) $\mathbf{x_T}$ with R_T = *100 mol/s*. Figure 4.8(a) has been superimposed.

Residue curves, such as those displayed in Case 1, can not cross by definition and nature of the equations which describe them. However, it is evident from Figure 4.8(b) that membrane column profiles do intersect each other. The reason for this is the varying flowrates within the column section. Every point on a particular profile has associated with it a composition (**x**) as well as a flow (R and/or P) unlike a residue curve which is only related to a composition. If one profile intersects another profile, then they share the same compositional values, but will have different flows. This means that the $\beta(A)$-values for each profile at the point of intersection will be different, and the curves will have different directions at the point. The result is that each curve will map out different paths. No two curves will intersect and move of in the same direction. This is only possible if they both have the same $\beta(A)$-value at that point – and that is only possible if they originate from the same $\mathbf{x_T}$, with the same R_T (i.e. the same curve!).

4.4.7 DIRECTION OF δ_T

It is obvious that the direction of the difference vector, $\boldsymbol{\delta_T}$, influences the trajectory of the profiles for Case 2. As a designer, one could adjust the magnitude and direction of $\boldsymbol{\delta_T}$ in such a way that ensures that the profile obtained achieves the desired products. This is not shown here, but is rather left to the reader.

4.4.8 DIRECTION OF INTEGRATION

When plotting the membrane column profiles, it was assumed that starting the integration from the top of the column down was appropriate. However, the starting point can be anywhere within the CS, and the calculation would include both a positive and a negative integration. If this was the case, then the positive integration would proceed as discussed before, with $\beta(A) \rightarrow \infty$. However the initial $\beta(A)$-value

would not be 1, but rather the $\beta(A)$-value associated with the starting point of integration. The negative integration would start from the same $\beta(A)$-value, and diminish in magnitude. The negative integration would proceed until $\beta(A) = 1$, at which point the integration must terminate since the top of the column has been reached. However, irrespective of integration direction, the curves obtained would be the same.

4.4.9 CROSSING THE MBT BOUNDARY

In the discussions on the column profile thus far, we have allowed the curves to cross the MBT boundary. Of course, this is not physically possible. However it is mathematically possible, and visualizing it has allowed one some valuable insight into the behaviour the profiles. Such information would be unattainable and misinterpreted if one were to look within the bounds of the MBT only.

In reality, each profile would terminate at the boundary it intersects. When this occurs, one component equals zero, meaning that particular species has completely permeated through the membrane. We are then left with a binary mixture. The profile will then continue from the point of intersection with the boundary along the straight line boundary in the direction towards the least permeable component of the two remaining species.

4.5 COLUMN SECTION PROFILES: OPERATING CONDITIONS 3 & 4

4.5.1 STATEMENT

Cases 1 and 2 display the more theoretical operations of a CS, and are unlikely to find any relevance in the commercial, industrial sector. The remaining two possible operating conditions for the CS (Figure 4.3) present situations that are of a far more practical nature. These are:

Case 3:

$$P_T \neq R_T \text{ and } \mathbf{y_T} = \mathbf{x_T} \tag{4.28}$$

Case 4:

$$P_T \neq R_T \text{ but } \mathbf{y_T} \neq \mathbf{x_T} \tag{4.29}$$

Case 3 would represent, for example, the terminating sections (rectifying and stripping) of and entire membrane column configuration. Case 4, alternatively, would be a general CS placed anywhere within the membrane column, or cascade.

4.5.2 MATHEMATICS

Consider the conditions of operation for Case 3. Substituting these into equation 4.15 yields:

$$\mathbf{X_\Delta} = \mathbf{x_T} \tag{4.30}$$

This results in the following DPE for Case 3:

$$\frac{d\mathbf{x}}{dA} = \left[\frac{1}{r_\Delta} + 1\right]\left[\mathbf{x} - \mathbf{y}(\mathbf{x})\right] + \frac{1}{r_\Delta}\left[\mathbf{x_T} - \mathbf{x}\right] \tag{4.31}$$

where

$$r_\Delta = \frac{R(A)}{\Delta} \text{ is known as the (local) reflux ratio.} \tag{4.32}$$

In Case 4, there is no simplification possible, and the DPE is:

$$\frac{d\mathbf{x}}{dA} = \left[\frac{1}{r_\Delta} + 1\right]\left[\mathbf{x} - \mathbf{y}(\mathbf{x})\right] + \frac{1}{r_\Delta}\left[\mathbf{X}_\Delta - \mathbf{x}\right] \tag{4.33}$$

It is noticed that the DPEs describing the scenarios in Cases 3 and 4 (equations 4.31 and 4.33) are mathematically similar to each other. Each comprise of the addition of two vectors, namely: the separation vector, $\mathbf{s} = \mathbf{x} - \mathbf{y}$, and the mixing vector, $\mathbf{m} = \mathbf{X}_\Delta - \mathbf{x}$. The only difference between the two cases is that the difference point ($\mathbf{X}_\Delta$) is equal to the composition of the product being removed in Case 3. So as to avoid repetition, these two cases will be discussed simultaneously, due to the similar nature of their equations.

Now, Δ is pseudo-flowrate, and does not actually exist, except in Case 3 where a product is being withdrawn CS. Since Δ is a difference in 2 flows, it is possible for it to have a positive or even negative sign. Similarly with the entries in $\mathbf{X}_\Delta$, which is the net composition within a CS.

4.5.3 COLUMN PROFILE

The conditions of Case 3 compel all the entries of $\mathbf{X_\Delta} = \mathbf{x_T}$ to have be positive, i.e. to lie within the bounds of the MBT. Case 4, on the other hand, allows $\mathbf{X_\Delta}$ to exist anywhere in the x_A–x_B space, including the MBT. For this reason we will select an $\mathbf{X_\Delta}$ within the MBT, thereby covering columns profiles for both cases concurrently.

Consider the following arbitrary conditions of operation (for Case 4): $\mathbf{X_\Delta}$ =[*0.3, 0.3*], $\mathbf{x_T}$ = [*0.3, 0.2*], Δ = *20 mol/s*, and R_T = *120 mol/s*. (Note: for Case 3, one would have to ensure that $\mathbf{X_\Delta} = \mathbf{x_T}$). Integrating the DPE for Case 4 down the length of the column yields the plot shown in Figure 4.12.

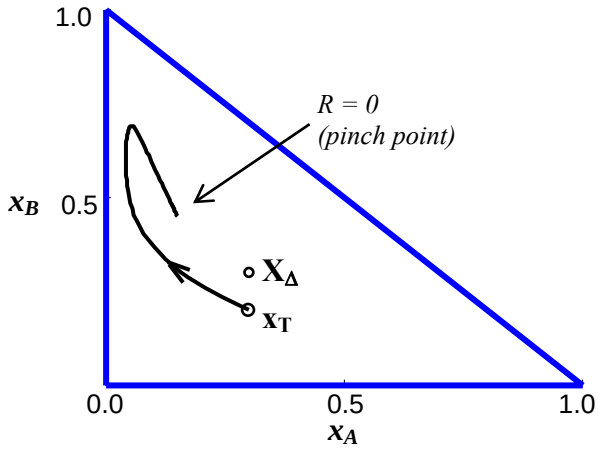

Figure 4.12: Membrane column profile for Cases 3 & 4. Positive Integration.

The curve is terminated when the retentate flow equals zero, as indicated in Figure 4.12. This will be discussed in the section that follows. Furthermore, although not shown here it is possible to determine at what *A* the curve pinches at.

4.5.4 PINCH POINT LOCI

It is important to recognize that every point on the retentate column profile has associated with it two parameters:

- the composition, **x**, and
- the reflux, r_Δ.

Moreover, for a fixed flux model and $\mathbf{X_\Delta}$ (or $\mathbf{x_T}$), each r_Δ has associated with it a set of stationary or pinch point locations. The pinch points are defined by equating the DPE to zero. As r_Δ changes, so do the positions of the pinch points. It is therefore possible to generate a pinch point loci, as shown in Figure 4.13, to visualize the movement of each node.

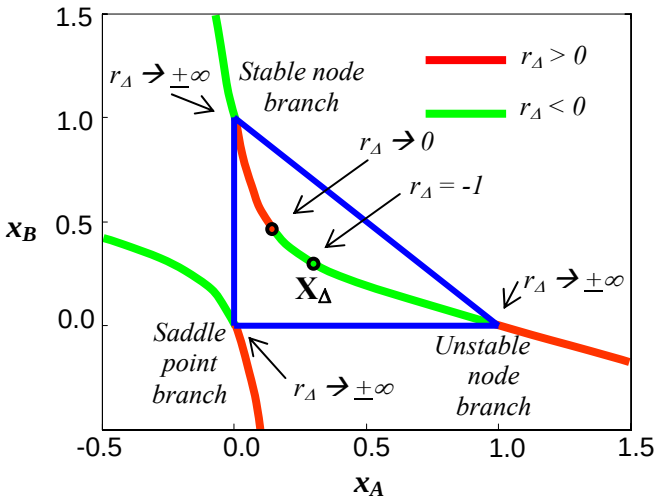

Figure 4.13: Pinch Point Loci for $\mathbf{X_\Delta}$ = [0.3, 0.3].

A property of the pinch point loci, which can be mathematically proven, is that it will always pass through $\mathbf{X_\Delta}$ at $r_\Delta = -1$. This is the case in Figure 4.13.

4.5.5 ANALYSIS OF COLUMN PROFILE

The behaviour of the profile in Figure 4.12 can, once again, be understood by performing a mathematical analysis on the DPE for Cases 3 and 4. As mentioned before, the DPE is a combination of two vectors, **s** and **m**. Each vector is preceded by a scalar, both involving r_{Δ}. Now, r_{Δ} is continually changing: it has its maximum value at the top of the CS, and diminishes to zero as material permeates (refer to equation 4.32). In the example discussed above, the maximum value of r_{Δ} is:

$$r_{\Delta} = \frac{120}{20} = 6 \tag{4.34}$$

The corresponding map, using this value, can be generated, as shown in Figure 4.14.

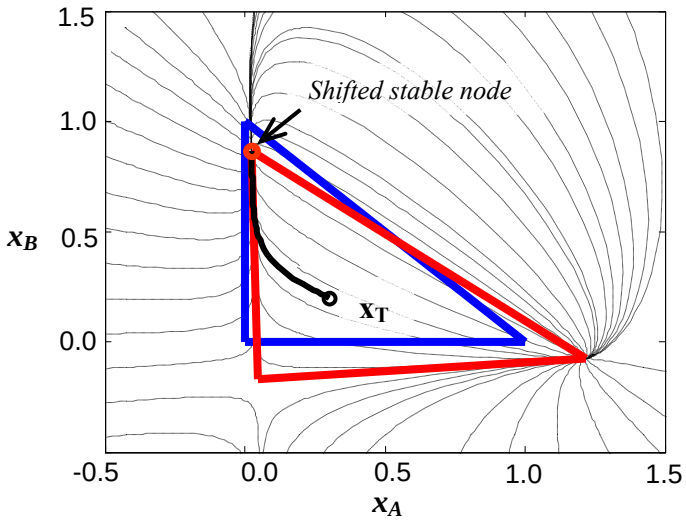

Figure 4.14: Shifted M-RCM. The blue triangle represents the MBT, the red shows the transformed triangle.

$\mathbf{X_\Delta} = [0.3, 0.3]$, $\mathbf{x_T} = [0.3, 0.2]$, $r_{\Delta} = 6$.

Actual membrane profile (see Figure 4.12) is tangent to bold profile at the point indicated

The very first retentate composition, namely $\mathbf{x_T}$, will have the maximum r_Δ-value associated with it. This implies that at the instant permeation begins at the top of the CS, the retentate profile is seeking the stable pinch point that is associated with $r_\Delta = 6$ (refer to Figure 4.13). Since it is seeking this pinch point, the curve will be moving in a direction that is tangent to the profile passing through $\mathbf{x_T}$ and that has a constant r_Δ-value of *6*.

However, a moment later some material has permeated, therefore changing **x** as well as reducing the magnitude of r_Δ. As this happens, the retentate curve is now seeking a different pinch point. Yet again, the column profile is tangent to the "constant r_Δ" profile that passes through **x**, having the same r_Δ. Figure 4.15 shows this tangency effect at arbitrarily chosen discrete points on the column profile.

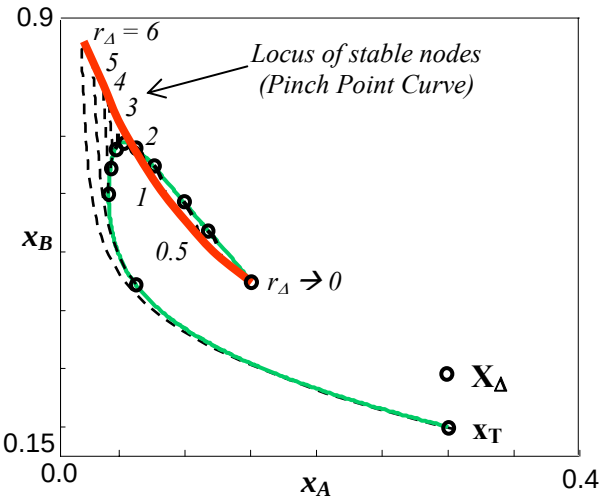

Figure 4.15: Tangency of curves to the column profile.
Each curve corresponds to a different r_Δ-value, and is allowed to run to its stable pinch point.

Analysis of Figure 4.15 gives the understanding necessary to explain the behaviour of the profile. Each point on the profile is seeking its stable node. The stable node itself is continually moving. This implies that the column profile has to adjust itself accordingly so as to move in the appropriate direction in order to seek the mobile

stable node. It will continue to do this until the retentate has run out of material, at which point the profile will terminate.

One can see from Figure 4.15, that profile intersects with the pinch point locus a r_{Δ}-value of about 2. However, it is evident that the profile does not pinch at this point. The reason for this is that there is still material present in the retentate for permeating. Even though there is an intersection between the profile and the locus, this is only instantaneous. A moment later (down the length of membrane), the r_{Δ}-value will decrease, and thus search for another stable node. Therefore, the profile does not terminate if it intersects with the pinch point locus, unless r_{Δ} has gone to zero.

4.5.6 PINCH POINT

By definition of a pinch:

$$\frac{d\mathbf{x}}{dA} = 0, \tag{4.35}$$

Thus, using equations 4.31 or 4.33 at $r_{\Delta} = 0$:

$$\left[\mathbf{x} - \mathbf{y}(\mathbf{x})\right] = -\left[\mathbf{X}_{\Delta} - \mathbf{x}\right] \tag{4.36}$$

Simplifying:

$$\mathbf{y}(\mathbf{x}) = \mathbf{X}_{\Delta} \tag{4.37}$$

This means that when the retentate runs out of material, the very last permeate composition will be that of $\mathbf{X}_{\Delta}$ (or $\mathbf{x}_{\mathbf{T}}$). This result is intuitive, since all the material

has transferred through the membrane. One can simply use the permeation model to determine the composition of the last drop of retentate (refer to equation 4.9). Using the α-values selected and $\mathbf{X_\Delta}$ = [*0.3, 0.3*], the pinch will occur at $\mathbf{x_{pinch}}$ = [*0.15, 0.45*]. This corresponds to the last point on the curve in Figure 4.12. The position of the pinch is fixed for a chosen $\mathbf{X_\Delta}$ and flux model. All curves will terminate at this point, irrespective of $\mathbf{x_T}$ (see next section).

4.5.7 FURTHER COLUMN PROFILES

Arbitrarily chosen values for $\mathbf{x_T}$ and r_Δ were used in order to demonstrate a membrane column profile for Cases 3 and 4. However, any positive flowrate, R_T, is feasible. As is any point within the MBT a possible top retentate composition. Figure 4.16(a) displays column profiles for a fixed $\mathbf{x_T}$ = [*0.3, 0.2*], varying r_Δ as indicated. Figure 4.16(b), on the other hand, shows a range of column profiles for select $\mathbf{x_T}$'s at a constant r_Δ =*6*.

It is noticed in Figure 4.16(a) that increasing the r_Δ at the top of the CS does not alter the termination or pinch point location of each curve. This was discussed previously. The actual path mapped out by the profiles do, however, change. The path followed is a function of stable pinch point locus. The larger r_Δ is at the CS top, the close the curve will begin to approximate an infinite reflux profile. However, as r_Δ reduces substantially, the curve is forced to redirect its path so as to search for the mobile stable node.

The profiles in Figure 4.16(b) exhibit the same properties. Irrespective of their starting point, their trajectories are dictated by the stable node pinch point locus, with all curves ultimately pinch at the same point.

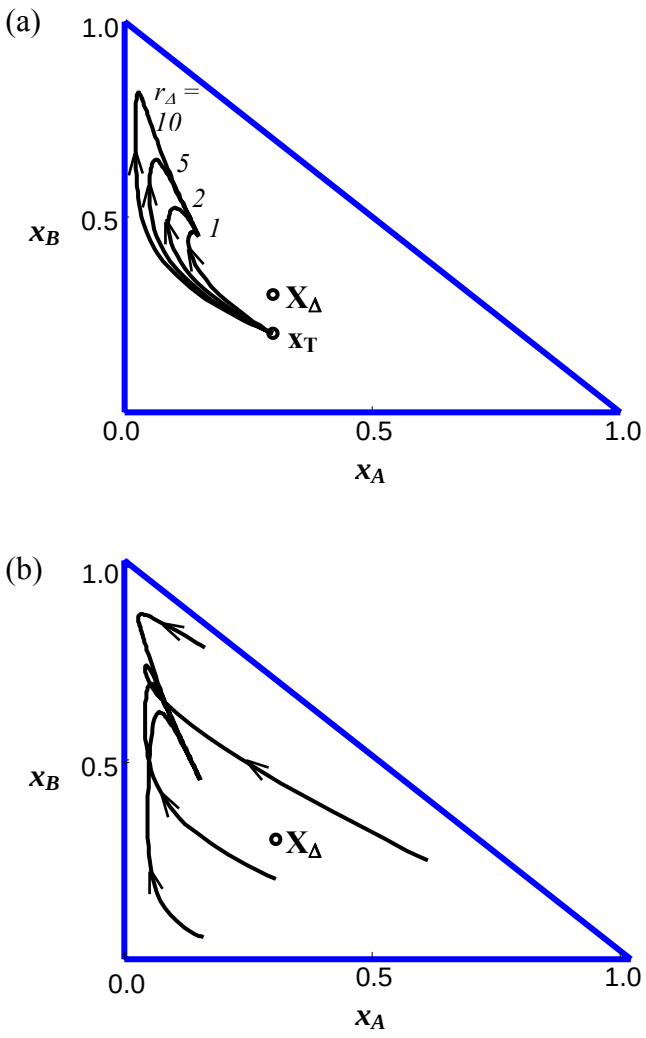

Figure 4.16: Column Profiles for selected values of
(a) r_Δ with $\mathbf{x_T}$ = [*0.3, 0.2*], (b) $\mathbf{x_T}$ with r_Δ = 6.

4.5.8 VARIATIONS IN X_Δ AND r_Δ

By referring to equations 4.15 and 4.32, it can be deduced that r_Δ and $\mathbf{X_\Delta}$ can have negative values.

Consider the possible variations on $\mathbf{X}_{\Delta}$, and their effect on column profiles:

- Analysis and visualization of the pinch point loci associated with each $\mathbf{X}_{\Delta}$ gives insight into the trajectory followed by a profile. This is evident from the above discussions.
- Now, for a 3 component system, $\mathbf{X}_{\Delta}$ has 3 entries, each of which can have a possibility of 2 signs (+ or –). This means that there are 8 possible directions that $\mathbf{X}_{\Delta}$ can have. However, $\mathbf{X}_{\Delta}$ has the property that all its entries have to sum to 1 (since it is a composition). Therefore, the combination where all entries are negative is not valid. Thus 7 possibilities remain.
- Tapp et al. (2004) graphically identified these 7 possibilities as regions within the entire x_A–x_B space. They showed that the pinch point loci for an $\mathbf{X}_{\Delta}$ in each region were different from that in any other region. However, they concluded that the general shape of the pinch point loci for an $\mathbf{X}_{\Delta}$ in a given region was the same, irrespective of where $\mathbf{X}_{\Delta}$ was placed in the region.
- The reader is referred to Tapp et al. (2004) for the graphical representation of these pinch point loci.

r_{Δ} can either be positive or negative, but either way will ultimately tend towards zero as permeation proceeds. A column profile moves in such a way so as to find its associated stable node. However, the stable node pinch point locus has two branches to it, one for each sign of r_{Δ} (refer to Figure 4.13). Thus the sign of r_{Δ} determines which branch the column profile will follow. An example is shown in Figure 4.17, where it can be seen that the profile with r_{Δ} = -6 maps out a path that follows the negative branch of the stable node locus.

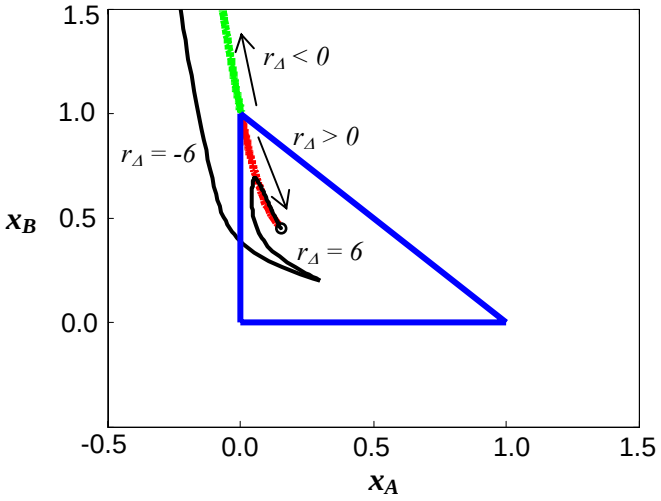

Figure 4.17: Effect of the sign of r_Δ on the trajectory of the profile.
Each profile is influenced by its associated stable pinch point locus.

4.6 APPLICATIONS AND CONCLUSION

A novel graphical method of analysing continuous membrane systems has been developed. It has been shown that any membrane configuration of membrane separators, no matter how complex in its arrangement, can be broken down into column sections. Each CS, which resembles a typical single-stage separator, is modelled using the DPE. The DPE tracks the change in the retentate composition down the length of the CS. For demonstration purposes, a simple constant relative permeability flux model was employed to determine the permeate composition as well as the continually changing retentate flow.

All possible operating conditions of a column section were explored. Each condition is a result of the relationships between the flows and compositions at the top of a column section. Using the DPE, column profiles for each condition were plotted. The behaviour of the profiles was discussed both mathematically and graphically.

The profiles generated provide valuable insight into the operation of all membrane processes, even the simplest single-stage module. Being able to graphically visualize the change in the retentate composition, assists a design engineer in making necessary and informed decisions. Although complex in their behaviour, the nature of the profiles can be understood and explained. With this novel method, one is now able to synthesize and design more informed and creative configurations. Being able to break down any membrane arrangement to its simplest form, allows one to isolate and evaluate the individual building blocks, thereby permitting an optimal design to emerge. This method is also very useful in the design of hybrid systems involving membrane separators. This is the topic of a future publication by the authors (see Chapter 5).

CHAPTER 5:

NOVEL GRAPHICAL DESIGN METHODS FOR COMPLEX MEMBRANE CONFIGURATIONS AND HYBRID PROCESSES

The material in this chapter has been prepared for submission for publication in Industrial and Engineering Chemistry Research.

ABSTRACT

Shortcut methods for the design and synthesis of separation systems are useful, especially in the conceptual stages of a process design. However, current approaches incorporated in these techniques result in them being suitable for traditional designs only, and unable to manage novel or complex configurations. Using column profile trajectories to describe the compositional behaviour of material in both distillation and membrane sections, it will be shown how any configuration, no matter how complex, can be modelled. With this comes an overall deeper understanding of the operation of the chosen system. As an example, a Petlyuk-type arrangement will be considered – firstly incorporating membrane permeation units as the only means of separation, and then secondly linking membrane units with distillation thereby forming a hybrid. The feasibility of each design is discussed, and compositional regions of feasibility are established, where necessary. Although the nature of column profiles may appear to be complicated, this method allows one to quickly and easily understand complex configurations, thus saving time, money and potentially reducing energy consumption.

5.1 INTRODUCTION

Feasible techniques for the synthesis and design of separation processes have long been an objective in the chemical industry. Separation processes are renowned for their high energy consumption, and hence high operating costs. Thus, the need for better methods for the design of separation systems is warranted, especially in the conceptual stages. One firstly needs to be mindful of what methods of separation are available. For fluid mixtures, these include the traditional processes of distillation, absorption as well as solvent extraction, to mention a few. Membrane permeation, although a relatively recent addition to this list, provides a unique method of separation. Any separation circuit may contain numerous units in order to achieve a desired separation – either all of the same operation, or a combination of various methods, thereby forming a hybrid process.

In the distillation field, for instance, several advances have been made to formulate shortcut methods of design (Bausa et al. (1998), Castillo et al. (1998), Pham and Doherty (1990), Fidkowski et al. (1991), Fien and Liu (1994), Zhang and Linninger, (2004), Zhang and Linninger (2006)). Several of these methods have focussed on designing processes that are able to separate multi-component mixtures, as opposed to the simple single-feed-two-product column used for binary separations. As an initial alternative to this, two or more columns can be placed in succession of each other in order to achieve a desired degree of separation of a multi-component mixture. Unfortunately, this method has associated with it high capital and operating costs. The idea of thermally-linked columns, therefore, came about in an attempt to reduce the size of the equipment needed, as well as eliminate some of the condensers and reboilers. While the Petlyuk column is the most popular of these advances, other variations include a main column with a side-rectifier or side-stripper connected to it. Theoretically, these column configurations have the ability to produce the required products. However, their operation is complex, thus resulting in a lack of reliable design methods.

Membrane permeation, although physically and chemically distinct from distillation, has undergone analogous transformations and adaptations to that of distillation. Initially, industrial membrane designs were based on a single, once-through unit, similar to a flash process. Modifications on this stand-alone unit were made to improve its performance, until the idea of cascading was suggested. This then resulted in various forms of cascade arrangements being concatenated over the years, and their efficiencies compared (Kao et al. (1989), McCandless (1994), Vorotyntsev and Drozdov (2001)). With this, and by analogy with the distillation field, a continuous membrane column was later proposed (Hwang and Thorman (1980)). This was revolutionary at the time, and it was claimed that pure products from a binary mixture were achievable. There have been numerous modifications and adjustments to the membrane column (Hoover and Hwang (1982), Hwang and Ghalchi (1982), Kothe et al. (1989)) as well as comparisons of it with other available membrane separators (Kao et al. (1989), McCandless (1990)). Extending these ideas to multi-component systems resulted in having two membrane columns placed in series (Hwang and Ghalchi (1982)), as well as the two-membrane permeator (Kothe et al. (1989)).

Agrawal (1996) suggested various cascade configurations of single-stage membrane units that would mimic some distillation column arrangements, ranging from the conventional column right through to a Petlyuk arrangement. A similar analysis can be done using membrane columns, as opposed to a cascade of membrane units.

While distillation may be the most commonly used method for separation of fluid mixtures, there are instances when it becomes difficult or even impossible to separate some mixtures by distillation alone. Hybrid arrangements provide an alternative solution to this. Numerous shortcut methods of design have been proposed for hybrid processes (Stephan et al. (1995) Pettersen et al. (1996), Hommerich and Rautenbach (1998), Lipnizki (1999), Bausa and Marquardt (2000), Lelkes et al. (2000), Eliceche et al. (2002), Kookos (2003), Daviou et al. (2004), Huang et al. (2004)). However,

most of these methods are either only suitable for a single set configuration, thereby limiting the design procedure, as well as any optimization, or they provide very little insight into the location of feed and side-draw streams, as well as number of stages or membrane are needed.

Even though the above-mentioned arrangements provide attractive ways to separate ternary, or higher order, mixtures with the use of membrane permeation and/or distillation, a reliable method of design does not yet exist. To address this problem, a more creative design approach needs to be employed.

Graphical methods of design have shown their value in several separation systems, including distillation and solvent extraction. In the distillation field, graphical tools such as Distillation Residue Curve Maps (D-RCM's), operation leaves (Castillo et al. (1998)) and, recently, Column Profile Maps (CPM's) (Tapp et al. (2004)) emerged so as to assist design engineers in analysing such systems. Holland et al. (2004a) used the "moving triangle" phenomenon in CPMs to design complex distillation configurations. Membrane Residue Curve Maps (M-RCM's) were proposed by Peters et al. (2006a) with the intention of formulating a graphical technique similar to that for distillation. This was done so as to allow one to be able to evaluate both membrane permeation and distillation from the same viewpoint. Applications of M-RCM's to both batch and continuous processes have been investigated (Peters et al. (2008)). It was shown how a continuous membrane column operated at total (or infinite) reflux was mathematically equivalent to both a single stand-alone unit, as well as batch permeation.

Finite reflux operation has been a previous topic of discussion by Peters et al. (2007). Column Sections (CS), initially identified by Tapp et al. (2004) for distillation systems, were adapted for membrane processes. A generalized CS is defined as a length of column between points of addition and/or removal of material and/or energy (Tapp et al. (2004)). It was shown that any membrane configuration, column or

cascade, can be broken down into CS (Peters et al. (2007)). Differential equations (DEs) were developed to describe the continually changing compositions and flowrates down the length of the CS. Using an appropriate flux model, column profiles for membrane CS were generated.

In this chapter, the ideas and phenomena related to these column profiles are used to both mathematically and graphically analyse complex membrane configurations. As an illustration, a membrane Petlyuk-type arrangement will be considered. Some simplifying assumptions and operating conditions are made, allowing one to evaluate the feasibility of such arrangements. The idea is then ultimately extended to a hybrid arrangement of distillation and membrane permeation. While Peters et al. (2007) introduced membrane column profiles and discussed their topological properties, this chapter will focus on membrane column profiles as a graphical design and analysis tool. It is not the aim of the chapter to completely solve complex membrane and hybrid arrangements, but rather to introduce the idea as to how column profiles can be used to understand and design such processes.

5.2 COLUMN SECTIONS

5.2.1 DEFINITION

As mentioned in the introduction, a CS is defined as a length of column between points of addition and removal of material and/or energy (Tapp et al. (2004)). Although defined for distillation sections, this statement is general and can be applied to any counter- and, in fact, co-current process, including membrane permeation. Figure 5.1 gives a graphical representation of a CS for each of distillation and membrane, including the nomenclature associated with each.

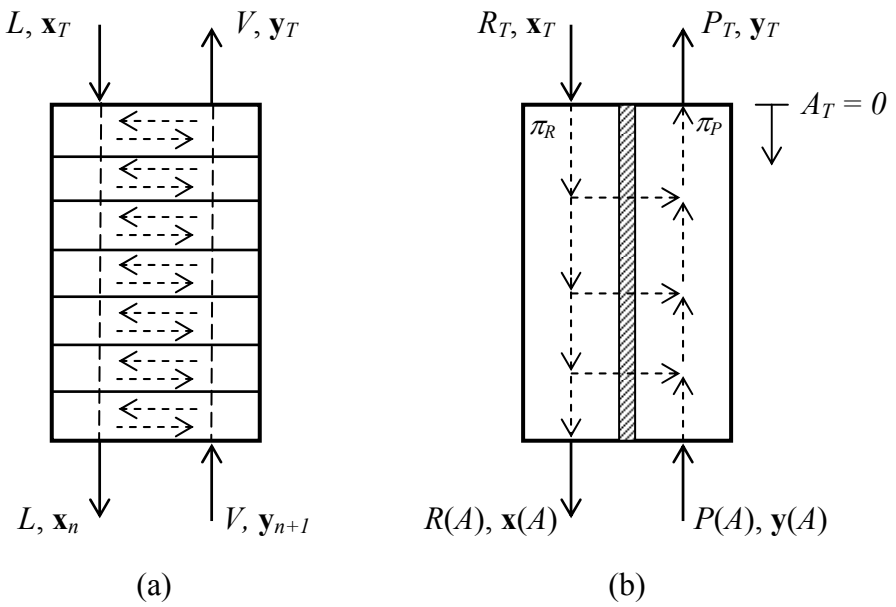

Figure 5.1: Generalized column sections (CS). (a) Distillation, (b) Membrane.

The continual vaporisation and condensation of material is inherent to distillation. This results in the transfer of material from the liquid phase to the vapour, and simultaneously in the reverse direction. Thus, the assumption of *constant molar overflow* is often justified or closely approximated in distillation CSs.

Operation in the membrane CS, on the other hand, relies on the differences in partial pressure on either side of the membrane in order for mass transfer to occur. A diffusion membrane is used throughout this chapter for discussion purposes. It is therefore assumed that the permeate pressure (π_P) is sufficiently close to vacuum. Thus permeation will be mono-directional, and will occur from retentate to permeate, but not in the reverse direction. This results in there being a continual change in the flowrates within in any membrane CS. As drawn in Figure 5.1(b), both the retentate and permeate will have their maximum values at the top of the CS (namely, R_T and P_T).

5.2.2 THE DIFFERENCE POINT EQUATION

The compositional change of material down the length of any general CS is described by the Difference Point Equation (DPE). For a distillation section (Tapp et al. (2004)), the change in the liquid composition (**x**) with respect to position (n) can be described by the following, the written in vector form:

$$\frac{d\mathbf{x}}{dn} = \left[\frac{1}{r_{\Delta D}} + 1\right]\left[\mathbf{x} - \mathbf{y}(\mathbf{x})\right] + \frac{1}{r_{\Delta D}}\left[\mathbf{X}_{\Delta D} - \mathbf{x}\right] \tag{5.1}$$

where Table 5.1 shows the nomenclature that applies.

	Distillation	**Membrane**
Subscript or Superscript	D	M
Column Section reference	DCS	MCS
Downward material flow and composition	Liquid L, **x**	Retentate $R(A)$, **x**
Upward material flow and composition	Vapour V, **y**	Permeate $P(A)$, **y**
Position Variable	Stages n	Area A
Net flow	$\Delta_D = V - L$	$\Delta_M = P(A) - R(A)$
Difference Point	$\mathbf{X}_{\Delta\mathbf{D}} = \frac{V\mathbf{y} - L\mathbf{x}}{\Delta_D}$	$\mathbf{X}_{\Delta\mathbf{M}} = \frac{P(A)\mathbf{y} - R(A)\mathbf{x}}{\Delta_M}$
Reflux Ratio	$r_{\Delta D} = \frac{L}{\Delta_D}$	$r_{\Delta M} = \frac{R(A)}{\Delta_M}$
A subscript of "$_T$" will be used to refer to quantities at the Top of a CS		

Table 5.1: Nomenclature and symbols used in equations 5.1 and 5.2.

For a membrane section (Peters et al. (2007)), the change in the composition of the retentate (**x**) with respect to position (A) is described analogously by:

$$\frac{d\mathbf{x}}{dA} = \left[\frac{1}{r_{\Delta M}} + 1\right]\left[\mathbf{x} - \mathbf{y}(\mathbf{x})\right] + \frac{1}{r_{\Delta M}}\left[\mathbf{X}_{\Delta M} - \mathbf{x}\right] \tag{5.2}$$

Refer to Table 5.1 for a summary of the nomenclature and symbols used. Notice that the form of the equation for each CS is the same, but the nomenclature is different.

Although the DPEs for each section (equations 5.1 and 5.2) share the same mathematical form, there are some subtle, yet important differences. Since each DPE is describing a unique system, the way in which **y**(**x**) is modelled relates to the operation of each process – this is discussed in the next section. As mentioned earlier, the flows of the liquid and vapour streams in the DCS are constant, resulting in fixed values for Δ_D, $\mathbf{X_{\Delta D}}$, and $r_{\Delta D}$. Thus the scalar terms on the right hand side of equation 5.1, which involve $r_{\Delta D}$, remain constant in a DCS. In the MCS, the flows of the retentate and permeate are decreasing in value from the top of MCS down, but it can be shown by material balance that Δ_M and $\mathbf{X_{\Delta M}}$ are constant (refer to Peters et al. (2007)). However, by definition, $r_{\Delta M}$ varies in magnitude, also having its maximum value at the top of the MCS. This has to be accounted for in equation 5.2. This means that the scalar terms in equation 5.2 change with position (A). This is rather subtle but, as will be shown later, causes significant differences in the behaviour of the column profiles for MCS when compared to that of DCS.

5.2.3 VAPOUR-LIQUID EQUILIBRIUM AND PERMEATION FLUX

For demonstration purposes, simple vapour-liquid equilibrium (VLE) and permeation flux models will be used to mathematically describe the vapour and permeate compositions, respectively.

A constant relative volatility VLE model is used for distillation:

$$y_i = \frac{\alpha_{ij}^{D} x_i}{\sum_i \alpha_{ij}^{D} x_i} \tag{5.3}$$

where α_{ij}^{D} is the volatility of component *i* with respect to *j*.

A constant relative permeability flux model for gas separation is incorporated for membrane sections:

$$y_i = \frac{\alpha_{ij}^{M} x_i}{\sum_i \alpha_{ij}^{M} x_i} \tag{5.4}$$

where α_{ij}^{M} is the permeability of component *i* with respect to *j*.

The form of equation 5.4 may be the same as that of equation 5.3, but this occurs as a result of the assumption of a vacuum being maintained on the permeate side in the MCS (refer to Peters et al. (2007)).

Given that the retentate (and permeate) flow is changing, one can show that (Peters et al. (2007)):

$$\frac{dR(A)}{dA'} = -\sum_i \alpha_{ij}^M x_i \tag{5.5}$$

where $A' = A\frac{\pi_R P'_{ref}}{\delta}$ is a scaled dimensionless area.

It can be seen that the retentate flow is a function of position as well as its corresponding composition.

5.2.4 COLUMN PROFILES

With the DPEs (equations 5.1 or 5.2), in conjunction with the corresponding equilibrium or flux models (equation 5.3, or equations 5.4 and 5.5) allows one to graphically interpret the compositional change of the liquid down the length of the DCS, and that of the retentate down the length of the MCS. Vapour and permeate profiles can also be generated. These are determined by material balance through $\mathbf{X_{\Delta D}}$ and $\mathbf{X_{\Delta M}}$ (refer to Table 5.1), respectively.

5.3 COMPLEX MEMBRANE CONFIGURATION DESIGNS: GENERAL

5.3.1 OVERVIEW

In Section 5.3, only configurations containing membrane operation will be considered. There are numerous configurations and cascade options of membrane units and columns. Some are relatively simple in their design and operation, whilst others are more difficult to design. A Petlyuk-type arrangement will used as an example for illustration purposes, but there are various other configurations that can, at some stage, be analysed in a similar way. Although focussing on only a single design here, the reader is urged to understand the relevance of this method to other arrangements.

Note: *Since in this section of the chapter only membrane units are being dealt with, the subscript "M" will be omitted here. It will be used again in the next section when hybrid configurations of membranes and distillation are discussed. Furthermore, throughout this section, the following constant values for the relative permeabilities will be assumed:* $\alpha_{AB}^{M} = 3$, $\alpha_{BB}^{M} = 1$, *and* $\alpha_{BC}^{M} = 1.5$.

5.3.2 PETLYUK MEMBRANE ARRANGEMENT

Any cascade, configuration or arrangement of membrane permeators or columns can be broken down into a number of CSs, no matter how complex in its design. The CSs are simply identified between the points of addition and removal of material and/or energy. For the Petlyuk arrangement in Figure 5.2(a), the CS breakdown is given in Figure 5.2(b).

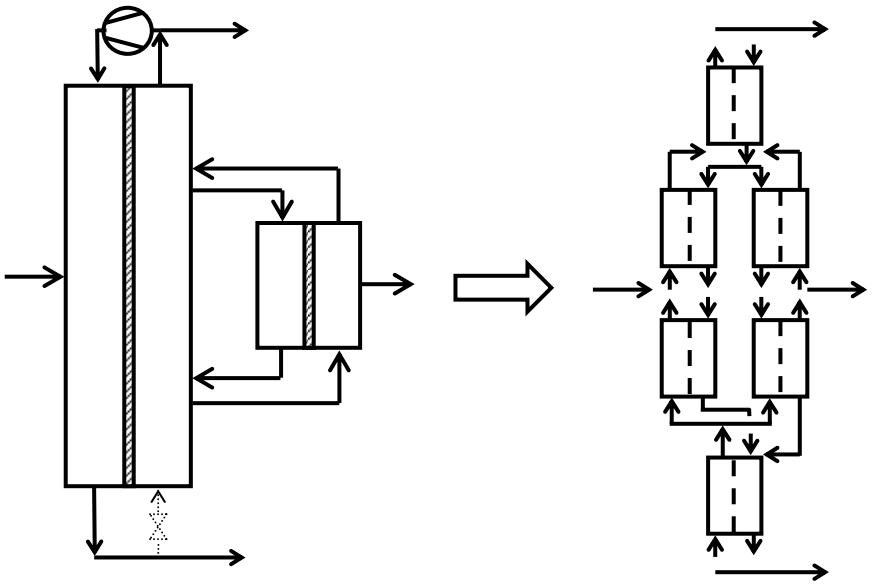

(a) (b)

Figure 5.2: (a) Petlyuk-type arrangement for membranes. (b) Column Section breakdown.

A compressor on the main shell is needed for the recycle of material leaving the top of permeate side back to the retentate side. There is some debate as to whether a similar recycle stream at the bottom of the column is necessary, shown in dotted lines in Figure 5.2(a) (Tsuru and Hwang (1995)). This ultimately is a decision of the designer, and is not of importance in the context of this chapter.

The same retentate and permeate pressures in the main column are assumed for the side fractionator. For this reason, the streams connecting the main shell and the fractionator do not require any equipment for pressure change.

Now, it is assumed that the overall arrangement is operating at infinite reflux. This implies that the addition of feed, or removal of product will have negligible effects on the overall on the flows within each CS. There will still, however, be comparable differences in the flows within each CS. The process in Figure 5.2(b) is then simplified as displayed in Figure 5.3.

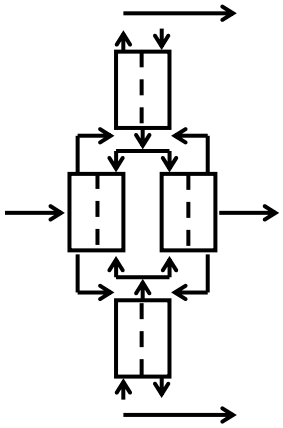

Figure 5.3: Petlyuk arrangement operating at overall infinite reflux.

Because any material entering the top CS in Figure 5.3 must also leave at the same point, this section is performing the same operation as the compressor (see Figure 5.2(a)) mixing material from the middle two sections, and then returning it to these sections at different compositions. The same can be said about the bottom section behaving like a pressure-reducer (valve). This then allows one to further simplify the arrangement, as given in Figure 5.4.

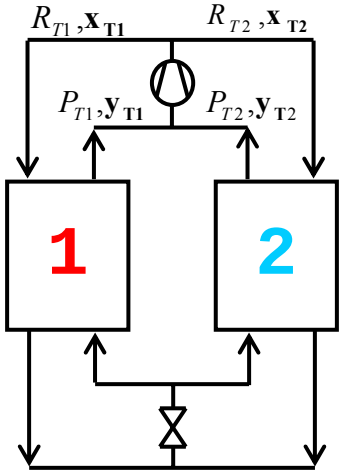

Figure 5.4: Coupled membrane column sections.

Although the top and bottom sections are not present in the simplified diagram (Figure 5.4), the do in fact exist. However, under the assumption of infinite reflux, the DPE for these two sections in Figure 5.3 reduces to the membrane residue curve equation (Peters et al. (2006a), Peters et al. (2007)). This implies that their respective profiles will follow *residue curves*. Thus, the determination and behaviour of the so-called "coupled column" arrangement in Figure 5.4 is of importance for feasibility of the Petlyuk configuration.

5.3.3 MATERIAL BALANCES

Since there is a split in the exit stream of the compressor in Figure 5.4, it should be apparent that:

$$\mathbf{x_{T1}} = \mathbf{x_{T2}} \tag{5.6}$$

It is further assumed that there is an *equal* split in flows, i.e.

$$R_{T1} = R_{T2}\,. \tag{5.7}$$

This assumption is maintained throughout the chapter, but can be relaxed where necessary – this is left to the reader. Overall and component material balances around the compressor can also be written, in vector notation:

$$P_{T1} + P_{T2} = R_{T1} + R_{T2} \tag{5.8}$$

$$P_{T1}\mathbf{y_{T1}} + P_{T2}\mathbf{y_{T2}} = R_{T1}\mathbf{x_{T1}} + R_{T2}\mathbf{x_{T2}} \tag{5.9}$$

There are various modes of operation that can occur within the system shown in Figure 5.4. Each mode is defined by the assumptions regarding the retentate and

permeate flows and/or compositions. In order to limit discussions, however, only 2 scenarios will be examined here. This will be done so as to demonstrate how column profiles can be used to graphically verify the feasibility of complex membrane configurations such as the coupled membrane sections.

It is worth noting, as mentioned before, that if a*ll* top flows are equal **and** *all* top compositions are equal as well, then the result would be that each CS would follow the same membrane residue curve (Peters et al. (2006a)).

5.4 COMPLEX MEMBRANE CONFIGURATION DESIGNS: OPERATING CONDITION 1

5.4.1 STATEMENT

Consider the following *general* operating conditions within CS1:

$$P_{T1} \neq R_{T1} \text{ and } \mathbf{y_{T1}} \neq \mathbf{x_{T1}} \tag{5.10}$$

From the material balances (equations 5.8 and 9), it can be shown the same relationships must apply for CS2. Furthermore, while equations 5.6 and 5.7 still hold true, it is taken that $\mathbf{y_{T1}} \neq \mathbf{y_{T2}}$.

5.4.2 MATHEMATICS

The DPE for membrane sections (equation 5.2) is employed to mathematically and graphically determine the behaviour of the retentate in each CS under these conditions. It is taken that integration commences at the top of the column, where all

variables are assumed to be known. Since there is equality in the top retentate compositions on either side, both column profiles will originate at the same point, namely $\mathbf{x_T}$.

Now, re-arranging the material balance in equation 5.8 and substituting in Δ (refer to Table 5.1):

$$P_{T1} - R_{T1} = -\left(P_{T2} - R_{T2}\right) \Rightarrow \Delta_1 = -\Delta_2 \tag{5.11}$$

It can be noticed that the net flow of material in the one CS is in the reverse direction of that in the other CS. By incorporating equation 5.7, it can be shown that the following relationship between the reflux ratios on either side exists:

$$r_{\Delta 1}\big|_T = -\,r_{\Delta 2}\big|_T \tag{5.12}$$

Similarly, it can be shown that there is equality in the difference points:

$$\mathbf{X_{\Delta 1}} = \mathbf{X_{\Delta 2}} \tag{5.13}$$

Thus, the designer has the freedom of choosing the reflux ratio and difference point for one CS. The same quantities for the other CS are set by mass balance.

As mentioned before, the reflux ratio in any membrane CS will have its maximum absolute value at the top of the CS, and thereafter decrease in magnitude towards zero. Tables 5.2(a) and (b) show how the signs of the permeate and retentate flows change as one moves down the length of the CS, operating with either a positive or negative r_Δ-value respectively. Note: By the definition of r_Δ, and that R has to maintain a positive value, Δ will share the same sign as r_Δ.

Reading Tables 5.2(a) and (b) from left to right allows one to monitor the sign change (if any) in the flows as they would occur during permeation. The flows, like r_{Δ}, also have their maximum value at the top of the CS and decrease as permeation proceeds. Thus, any one of the flows equating to zero signifies the termination of that particular CS. From Table 5.2(a), it can be seen that the CS with r_{Δ} positive will terminate at $r_{\Delta} = 0$ since the retentate has been depleted of material, while Table 5.2(b) indicates that the other CS will end at $r_{\Delta} = -1$ due to the permeate becoming zero. These values will be maintained throughout this section of the chapter as the conditions necessary for termination.

$r_{\Delta} = R/\Delta$	$r_{\Delta} > 1$	$r_{\Delta} = 1$	$0 < r_{\Delta} < 1$	$r_{\Delta} = 0$
$\Delta = P - R$	+	+	+	+
P	+	+	+	+
R	+	+	+	0

Table 5.2(a): Signs of permeate and retentate flows for a CS with a positive r_{Δ}.

$r_{\Delta} = R/\Delta$	$r_{\Delta} < -1$	$r_{\Delta} = -1$	$-1 < r_{\Delta} < 0$	$r_{\Delta} = 0$
$\Delta = P - R$	–	–	–	–
P	+	0	–	–
R	+	+	+	0

Table 5.2(b): Signs of permeate and retentate flows for a CS with a negative r_{Δ}.

While both CS's share the same absolute reflux ratio at the top of the column (refer to equation 5.12), they will not exhibit the same r_{Δ}-value at corresponding lengths down each CS. This is because the rate of change of R with position is a function of **x** (refer to equation 5.5), which is different in either CS. This then implies that one CS will terminate, or pinch, sooner than the other, and different areas are required in each CS in order to allow them both to reach their respective termination r_{Δ}'s.

5.4.3 COLUMN PROFILES

Consider the following arbitrarily chosen values for CS1:

- $r_{\Delta 1}\big|_T = 5 = -r_{\Delta 2}\big|_T$
- $\mathbf{X_{\Delta 1}} = [0.3, 0.3] = \mathbf{X_{\Delta 2}}$
- $\mathbf{x_{T1}} = [0.2, 0.3] = \mathbf{x_{T2}}$
- $R_{T1} = 100\ mol/s = R_{T2}$

It is possible to generate the column profiles for both CS1 and CS2, as shown in Figure 5.5. The solid red curves in Figure 5.5 represent the retentate column profiles for each CS, as indicated, while the dotted curves represent that of the permeate. Both retentate curves originate at $\mathbf{x_T}$, as shown. The starting point of the permeate profiles is determined by material balance across each CS. The profiles for each CS were plotted until their respective termination r_Δ-values were reached.

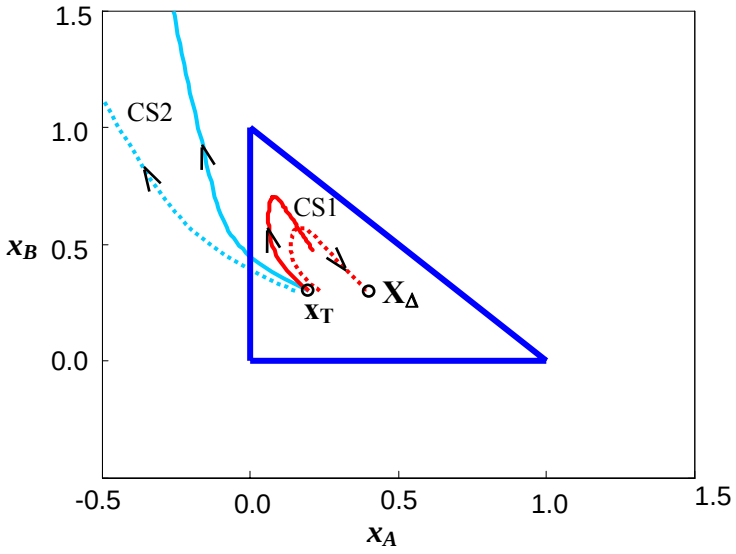

Figure 5.5: Retentate (solid) and permeate (dotted) column profiles for CS 1 (red) and 2 (blue).
$\mathbf{x_T} = [0.2, 0.3]$, $\mathbf{X_\Delta} = [0.3, 0.3]$, $r_{\Delta 1} = 5$, and $r_{\Delta 2} = -5$.

5.4.4 REQUIREMENTS FOR FEASIBILITY

In order for the coupled CS configuration, shown in Figure 5.4, to be feasible, it is necessary for:

- The *retentate profiles* to intersect within the MBT,
- The *permeate profiles* to intersect within the MBT, and
- The *direction of movement* of the profiles to conform to the direction of flow in the coupled CS arrangement.

Now, by the inherent operating conditions, as well as the assumption of commencing integration from the top of each CS, the retentate profiles will always intersect at $\mathbf{x_T}$, irrespective of its location.

The intersecting of the permeate profiles, however, is not guaranteed, but would signify the end of each CS if the arrangement is feasible. It can be seen that the material exiting the pressure-reducer (valve) splits prior to being fed into each CS. This implies that the permeate compositions at the bottom of each CS are the same, thus requiring an intersection of their respective profiles.

Analysis of the profiles obtained in Figure 5.5 reveals that no such intersection exists for the operating values selected. This indicates an infeasible configuration for the chosen conditions.

The next question that arises is what operating conditions and values are necessary in order to obtain feasibility. One could, for example, randomly select $\mathbf{x_T}$-values (while keeping the other conditions constant), and check for any intersections in the permeate profiles that may occur. However, this will prove to be somewhat laborious, thus a more comprehensive analysis has been performed.

To begin with, it is essential to have an understanding of the mathematical and graphical behaviour of any given single column profile. Peters et al. (2007) have previously examined, in detail, the nature of column profiles for membrane column sections. A brief discussion, highlighting the essential points, is given here, but the reader is referred to Peters et al. (2007) for further insight.

5.4.5 Analysis and Behaviour of Column Profiles

Consider a retentate column profile, beginning at a given $\mathbf{x_T}$, with a fixed flux model and $\mathbf{X_\Delta}$. According to the DPE (equation 5.2), every point on the profile has related to it a composition ($\mathbf{x}$) as well as a flow in the form of reflux (r_Δ). Analysis of Table 5.1 reveals that r_Δ will have its maximum value at the top of the CS, and then diminishes towards zero as permeation proceeds since the retentate is losing material.

Pinch Point Curves

Now, the DPE describing this profile is said to pinch when the right-hand side is equated to zero. From this, it can be deduced that every value of r_Δ has associated with it a set of unique stationary points in the composition space. It can further be shown that, for a "constant α" flux model, a maximum of three stationary points exist for any r_Δ (Holland et al. (2004b)). The movement of the stable, unstable and saddle point nodes as a function of r_Δ are graphically shown in Figure 5.6(a). The stable node is located at pure B at infinite reflux, and moves away from this point in either direction as r_Δ diminishes in size. The direction of movement is related to the sign of r_Δ, as shown.

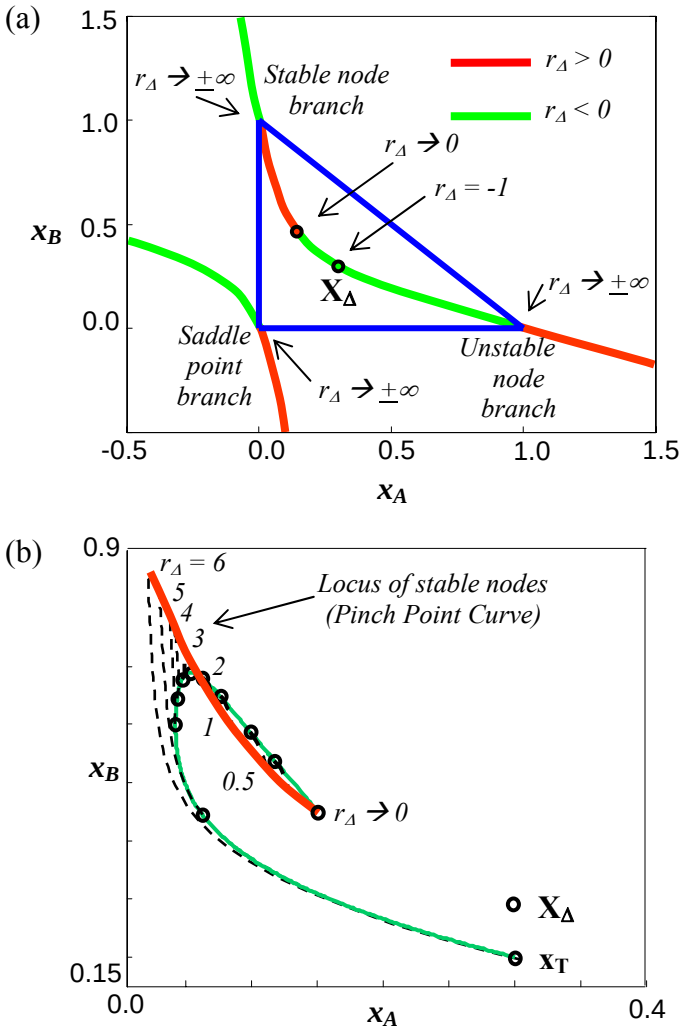

Figure 5.6: (a) Pinch point loci for $\mathbf{X_\Delta} = [0.3, 0.3]$.
(b) Tangency of curves to a column profile commencing at $\mathbf{x_T} = [0.3, 0.2]$. Each curve corresponds to a different r_Δ-value, and is allowed to run to its stable pinch point.
(reproduced from Peters et al. (2007))

The actual column profile does not ever terminate at (and, in fact, may not even reach) any of these stationary points, except for point where $r_\Delta = 0$. This is because of the perpetual change in r_Δ. However, the profile's direction of movement is dictated by the position and movement of the stable nodes: Every point along the column profile has a unique r_Δ-value associated with it. Furthermore, at each point there exists a "constant r_Δ" curve that is tangent to the profile. Each of these

"constant r_Δ" curves run to their respective stable nodes. But the location of the stable node is related to the value of r_Δ on the profile. This value is continually changing, resulting in the stable node continually moving. Thus, the column profile is seeking a "mobile" stable node! Figure 5.6(b) graphically describes this phenomenon. The green curve is any arbitrarily chosen column profile. The red curve is the stable node pinch point loci for $r_\Delta > 0$. The dotted curves represent discrete "constant r_Δ" curves for the values indicated.

Profile Pinch Point

A general property of any retentate column profile is that it will only ever terminate when $r_\Delta = 0$, regardless of the location of $\mathbf{x_T}$, as is evident in Figure 5.6(b). This is obvious since it implies that the retentate flow has run out of material. Furthermore, by equating the DPE to zero, and evaluating the resulting equation at $r_\Delta = 0$, it can be shown that:

$$\mathbf{y}\left(\mathbf{x}\big|_{r_\Delta \to 0}\right) = \mathbf{X_\Delta} \tag{5.14}$$

This indicates that the corresponding permeate profile will always terminate at $\mathbf{X_\Delta}$. The result is intuitive, yet quite interesting too – the termination point of all permeate profiles are known as soon as $\mathbf{X_\Delta}$ is set, prior to plotting the profiles themselves! What's more, is that the location of the retentate pinch can be calculated using equation 5.14 and the flux model (equation 5.4), and is thus also known before any profiles are generated.

Location of a Profile to its Pinch Point Loci

Notice that, in Figure 5.6(b), as r_Δ decreases in magnitude, the column profile approximates the pinch point curve. This arises since the profile is seeking a mobile stable node. The profile is initially moving a direction to find this node, and eventually does reach it at some point (at $r_\Delta \approx 2$ in Figure 5.6(b)), crossing the pinch

point loci. However, it does not terminate there since the retentate still has material available for permeation, thereby causing the profile to proceed further. But now the mobile stable node has moved past the curve, and the profile has to re-adjust its direction in order to continue searching for it. By this stage, the profile is already within a close proximity to the pinch point curve, and thus continues to follow it closely until the retentate is depleted of material.

Now, it has further been observed that all column profiles will, as $r_{\Delta} \to 0$, ultimately orientate themselves in such way they always end up on the same side of their corresponding branch of the pinch point curve. This is irrespective of the position of $\mathbf{x_T}$ relative to the pinch point loci. Consider Figure 5.6(b) as an example: the column profile is found to approximate the pinch point loci, lying above it. This is found to be the case for all profiles with a positive r_{Δ}. The same phenomenon occurs on the negative r_{Δ} stable node branch. A reason for this occurrence is due to the behaviour and direction of the eigenvectors associated with a profile; bearing in mind that one eigenvector will always dominate. Of course, the location of a profile relative to its loci is dependant on both α^M-values as well as $\mathbf{X_{\Delta}}$. In the example discussed, the positive r_{Δ} profile always lies above the positive branch of the stable node pinch point curve, while the other CS profile ends up on the left hand side of the negative branch.

Permeate Profile behaviour

In describing the behaviour of the retentate column profile, the pinch point loci incorporated was that relating to the retentate. Of course, the corresponding permeate pinch point loci can be generated by material balance. This would be useful when analyzing the permeate profiles. This is not done here, as the results obtained previously are directly applicable to both retentate and permeate profiles.

Negative Reflux Ratios

Furthermore, the discussion given above was done by considering a retentate profile with $r_{\Delta} > 0$. Again, similar conclusions are arrived it for profiles with $r_{\Delta} < 0$. The only difference is that these profiles will follow the negative branch of the pinch point loci (refer to Figure 5.6(a)). However, the nature of the profiles and the pinch point loci are somewhat more complicated now:

- The pinch point loci for $r_{\Delta} > 0$ has a well-defined path (for the $\mathbf{X}_{\Delta}$-value chosen) such that all stable nodes with $r_{\Delta} > 0$ exist on the indicated curve shown in Figure 5.6(a). This is not true when is speaking about the pinch point loci for $r_{\Delta} < 0$. This curve appears to head off to a very large value of x_B. But, as $r_{\Delta} \rightarrow -1$ there can only be a single node – This can be mathematically proven from the DPE. This means that, if the pinch point loci are continuous, which they appear to be, then there must be a way in which this $r_{\Delta} < 0$ curve moves towards large x_B-values, yet arrives back at a known location within the MBT when $r_{\Delta} = -1$. This now suddenly introduces rather complicated topological phenomena. However, it is not felt necessary to explore its details and the effect it has on column profiles, since one is able to do so sufficiently without it. But it is worth being aware as to what does graphically occur.

- A discontinuity arises due to the nature of the flux model being a rational function (equation 5.4). It can be found by equating the denominator to zero. In this case, it is a straight line. The discontinuity will always lie outside the MBT. No column profiles are defined or exist on the discontinuity. Thus, if a column profile enters it, it can move past the discontinuity. Now, the only profiles that will approach the discontinuity will be those having $r_{\Delta} < 0$. But not all profiles tend towards it, but rather depend on their location and r_{Δ}-

value in the vicinity of the discontinuity. If a profile does approach the discontinuity, then it will terminate before r_{Δ} is allowed to reach zero.

5.4.6 FEASIBLE COUPLED COLUMNS

It is with this understanding of the nature of the profiles that one can now answer the initial question of what operating conditions are necessary to yield a feasible coupled CS arrangement:

Retentate Profiles and the Pinch Point Curve

It has been established that the direction of movement of a column profile is directly influenced by the stable node pinch point curve: A profile will move so as to seek its stable node, as $r_{\Delta} \to 0$. However, the sign of r_{Δ} determines which branch of the stable pinch point curve the profile will follow. Due to material balance, the reflux in one CS will always be positive, while the other will maintain a negative value. This inherently means that the two respective retentate profiles will seek stable nodes that exist on the opposite branches of the pinch point loci. These branches always move in the opposite direction to each other for all $\mathbf{X_{\Delta}}$ (refer to Figure 5.6(a), and Tapp et al. (2004) for all other pinch point loci with different $\mathbf{X_{\Delta}}$ locations). Thus, the two retentate profiles will begin at the same point, namely $\mathbf{x_T}$, and then diverge, not necessarily intersecting again.

Furthermore, since the profiles ultimately end up on a particular side of the pinch point loci (refer to Section 5.4.5), it should become graphically and geometrically apparent that the pinch point loci then becomes a so-called boundary for the region of possible $\mathbf{x_T}$-values. In some instances, a profile may intersect with the pinch point loci, while in others it will either never intersect, or cross the pinch point loci twice. This all depends on the location $\mathbf{x_T}$ with respect to the side of the pinch point loci that the profile ultimately ends up on. If a retentate profile intersects with the pinch point

loci, then it is guaranteed that its corresponding permeate curve (for the same CS) will itself intersect with the retentate curve. In order to explain and understand this statement, consider the permeate curves.

Permeate Profiles and the Pinch Point Curve

The permeate profiles were plotted by calculating the permeate composition that satisfies the material balance. Re-arranging the expression for $\mathbf{X_\Delta}$ in Table 5.1, one can express the permeate composition, for any CS, as a function of its r_Δ and $\mathbf{x}$:

$$\mathbf{y}(\mathbf{x}) = \frac{r_\Delta}{1+r_\Delta}\mathbf{x} + \frac{1}{1+r_\Delta}\mathbf{X_\Delta} \tag{5.15}$$

By employing the familiar "lever-arm" rule, the following conclusions regarding the position of a permeate curve with respect to the value of r_Δ are arrived at:

- Profiles with a positive r_Δ:
  - For $r_\Delta > 0$, the permeate composition will lie in between $\mathbf{x}$ and $\mathbf{X_\Delta}$, on the straight line connecting them.
  - At $r_\Delta = 0$, $\mathbf{y} = \mathbf{X_\Delta}$, as discussed before (see equation 5.14).
- Profiles with a negative r_Δ:
  - For $r_\Delta < -1$, $\mathbf{x}$ will lie between $\mathbf{y}$ and $\mathbf{X_\Delta}$.
  - At $r_\Delta = -1$, $\mathbf{y}$ is undefined. This is due to the permeate having no more material (refer to Table 5.2(b)).

These can all be graphically interpreted as displayed in Figure 5.7.

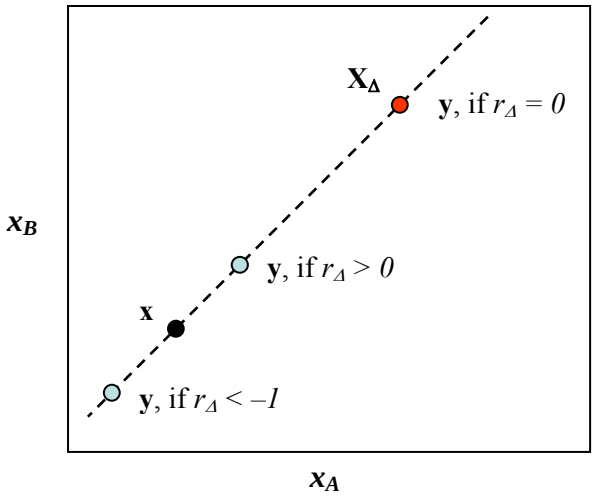

Figure 5.7: Effect of the sign of r_Δ on the location of **y** with respect to **x** and $\mathbf{X}_\Delta$.

Figure 5.7 shows that the location of the permeate profiles are on opposite sides of the retentate profiles. In order for the coupled column arrangement to be feasible, it is required that the permeate profiles intersect. How is this possible, especially when the two retentate profiles themselves move in (general) opposite directions? Consider, once again the pinch point loci:

The determination of the nodes on the pinch point locus is done by equating the right hand side of the DPE (equation 5.2) to zero:

$$\frac{d\mathbf{x}}{dA} = 0 = \left[\frac{1}{r_\Delta} + 1\right]\left[\mathbf{x} - \mathbf{y}(\mathbf{x})\right] + \frac{1}{r_\Delta}\left[\mathbf{X}_\Delta - \mathbf{x}\right] \tag{5.16}$$

Re-arranging equation 5.16 for **y**(**x**) yields the exact same expression arrived at in equation 5.15. However, in this instance, the expression is not describing the permeate profile. It is rather depicting the pinch location of **y**(**x**) for any r_Δ. Now, it is agreed that the pinch point curve always passes through $\mathbf{X}_\Delta$, irrespective of its position. Also, the location of **y**(**x**) relative to **x** is determined by the position of $\mathbf{X}_\Delta$. Thus, when a retentate profile intersects with the pinch point loci, the straight line

connecting $\mathbf{X_\Delta}$, $\mathbf{x}$ and $\mathbf{y(x)}$ is in fact, tangent to the retentate profile on the pinch point curve. This is due to the DPE being equated to zero (equation 5.15). Thus, in order to obey the geometry of the situation, the location of $\mathbf{y(x)}$ has to change relative to the loci and $\mathbf{X_\Delta}$. This thereby ensures that, when a retentate profile intersects with the pinch point curve, the permeate profile will intersect with the retentate profile for a given CS.

Figures 5.8 serves as an example of this. The retentate and permeate profiles are shown by solid and dotted lines respectively. For clarity purposes, the pinch point loci are represented by crosses. The mass balance lines, described by equation 5.15, are the dashed lines shown. These have been drawn in at the top of the CS, and then again when the profile passes through the pinch point loci. Notice the tangency, as well as the resulting retentate and permeate intersection.

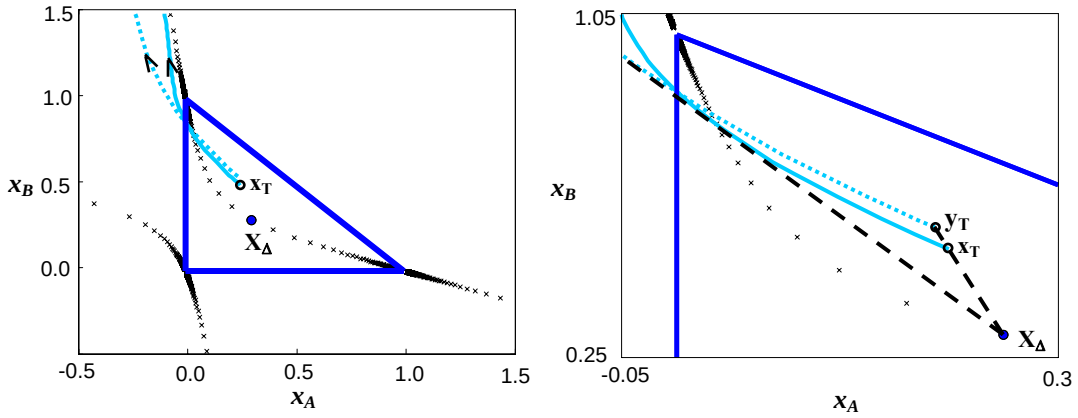

Figure 5.8: (a) Example of retentate profile (solid) passing through the pinch point loci (crosses), resulting in the permeate curve (dotted) intersecting with the retentate.
(b) Zoomed in version of (a), showing the mass balance lines (dashed).

Region of feasible top compositions

With the understanding that a retentate profile crossing the pinch point loci results in the permeate profile intersecting the retentate, the following can be said: An $\mathbf{x_T}$-

location that causes *both* retentate profiles for each CS to each cross the pinch point loci at least once may result in a feasible coupled column arrangement. This condition is necessary. However, as will be discussed further, it is not sufficient to ensure feasibility. For the $\mathbf{X_\Delta}$-value chosen, the region of possible $\mathbf{x_T}$ locations is shown in Figure 5.9, remembering that $\mathbf{x_T}$ must lie within the bounds of the MBT. It can be seen that the in the example used initially (see Figure 5.5), the $\mathbf{x_T}$-value was not in this region, thereby creating an infeasible arrangement.

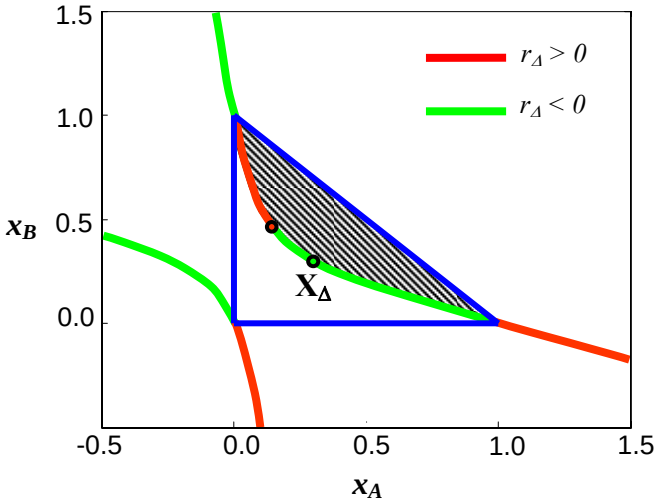

Figure 5.9: Region of $\mathbf{x_T}$-locations for feasibility with $\mathbf{X_\Delta} = [0.3, 0.3]$ in the membrane coupled column sections.

Feasible Regions using other $\mathbf{X_\Delta}$ *directions*

In the entire $x_A - x_B$ space, there are in fact 7 possible regions that $\mathbf{X_\Delta}$ can exist (Tapp et al. (2004)). These were identified according the direction of $\mathbf{X_\Delta}$, which is dictated by the signs of the 3 entries vector. Up to now, the determination of a feasible $\mathbf{x_T}$ region has been discussed in detail for one of the 7 directions of XD – that is $\mathbf{X_\Delta}$ located within the MBT. Applying the same ideas and mathematical understanding of the profiles and pinch point loci to the 6 remaining directions of $\mathbf{X_\Delta}$, feasible $\mathbf{x_T}$ regions were sought, if they existed within the MBT. It was found that only 2 other

locations of $\mathbf{X_\Delta}$ yielded profiles for each CS that resulted in them both crossing the pinch point loci, thereby creating a feasible region. Examples of these are shown in Figure 5.10(a) and (b). It was observed that only $\mathbf{X_\Delta}$ directions that yielded stable node pinch point loci that moved through the MBT, such as those shown in Figures 5.6(a) and 5.10(a) and (b), resulted in feasible $\mathbf{x_T}$ regions.

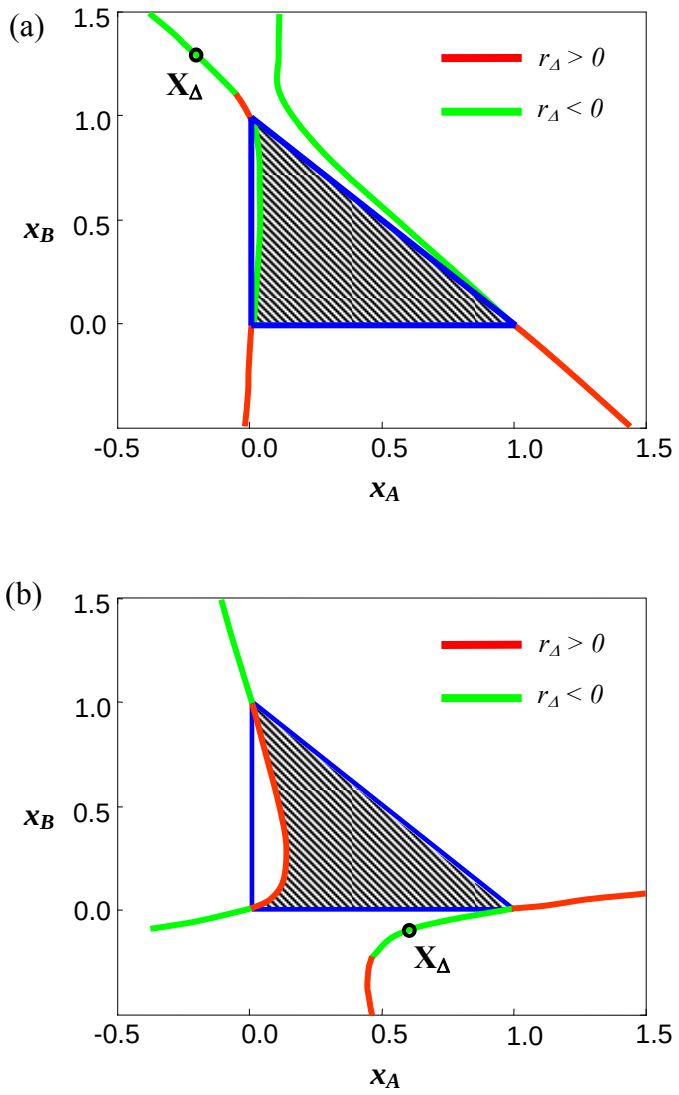

Figure 5.10: Feasible $\mathbf{x_T}$ regions for (a) $\mathbf{X_\Delta}$ = [–,+,–] and (b) $\mathbf{X_\Delta}$ = [+,–,+].

Minimum Reflux Ratio

Thus far, for a given $\mathbf{X_\Delta}$, it has been discussed in detail how to obtain a region of $\mathbf{x_T}$ that may ultimately result in a feasible arrangement. However, consider the diagrams shown in Figures 5.11(a) – (c). An $\mathbf{x_T}$ value, within the feasible region was arbitrarily chosen, and the starting magnitude of the reflux was increased, as indicated.

It can evidently be seen from the diagrams in Figure 5.11 that, for a given $\mathbf{x_T}$, there is required minimum initial (top) reflux in order for feasibility to exist. If the reflux is too low, as is the case in Figure 5.11(a), then no permeate intersection will occur despite being in the correct region. As the top reflux increases, so the permeate curves approach each other. This happens since, as the reflux increases, the profiles for both CS's initially follow a path very similar to an infinite reflux profile, or residue curve (refer to Peters et al. (2006a)). There is some reflux that will eventually allow the permeate curves to tangentially meet at a point, as displayed in Figure 5.11(b) thereby creating a feasible arrangement. This is the minimum reflux needed for feasibility.

At any initial reflux ratios above this minimum, the permeate curves intersect twice, as is shown in Figure 5.11(c). This indicates that multiple steady states are possible within the system. However, the degree of separation can be controlled by the amount of membrane area available in each CS for permeation. The two intersection points require different membrane areas in each CS. From the direction of movement of the profiles, it can be determined that the second intersection point requires a larger membrane area in CS 1, but a smaller area in CS 2.

The minimum reflux value can be determined by incorporating the tangency relationship between the two permeate curves. However, since the behaviour of the profiles is quite complex, a basic search algorithm was employed. For the value of $\mathbf{x_T}$ = [*0.45, 0.4*], it was found that the minimum reflux was 16.037. However, it goes without say that each $\mathbf{x_T}$ point has associated with it a different minimum reflux.

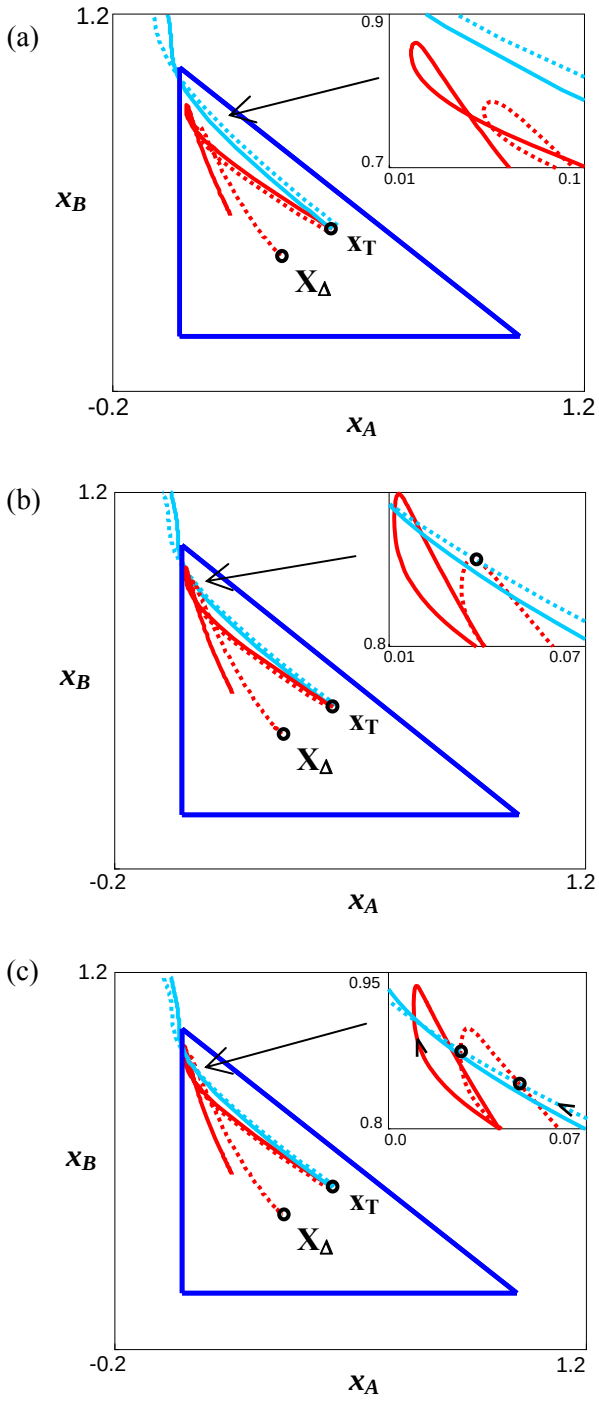

Figure 5.11: Retentate (solid) and permeate (dotted) profiles for CS 1 (red) and CS 2 (blue), commencing at $\mathbf{x_T} = [0.45, 0.4]$, with $\mathbf{X_\Delta} = [0.3, 0.3]$ operating at (a) $r_{\Delta 1}\big|_T = 10 = -r_{\Delta 2}\big|_T$, (b) $r_{\Delta 1}\big|_T = 16.037 = -r_{\Delta 2}\big|_T$, and (c) $r_{\Delta 1}\big|_T = 20 = -r_{\Delta 2}\big|_T$.

What is important to recognize though, is that although one is able to define a feasible region of $\mathbf{x_T}$ locations using $\mathbf{X_\Delta}$ and the pinch point loci, one also has to ensure that operation occurs above the minimum top reflux for chosen starting composition.

Once the correct region is located (if it exists) according to the $\mathbf{X_\Delta}$, and the minimum top reflux for $\mathbf{x_T}$ is determined, the profiles for the coupled column sections can be generated. In order to complete the design, one would need to plot the profiles for the top an bottom CS's (refer to Figure 5.3). These two CS's operate on residue curves (Peters et al. (2006a), Peters et al. (2008)) because all the permeate fed to the compressor must return as retentate (and vice versa for the valve). Thus, one can easily generate these residue curves at the top and bottom compositions of the coupled CS arrangement, thereby completing the design. These profiles would run into the unstable and stable pure component nodes.

5.5 COMPLEX MEMBRANE CONFIGURATION DESIGNS: OPERATING CONDITION 2

5.5.1 STATEMENT

Consider now the following more *specific* operating conditions within CS1:

$$\mathbf{y_{T1}} \neq \mathbf{x_{T1}} \text{ but } P_{T1} = R_{T1} \tag{5.17}$$

From the material balances over the compressor (equations 5.8 and 5.9), it can be shown that similar relationships hold true for CS2. Furthermore, it is taken that: $\mathbf{y_{T1}} \neq \mathbf{y_{T2}}$.

5.5.2 MATHEMATICS

By appropriately expanding the DPE for each CS (1 or 2):

$$\frac{d\mathbf{x}}{dA} = \frac{P(A)}{R(A)}\left[\mathbf{x} - \mathbf{y}(\mathbf{x})\right] + \frac{\left[P_T - R_T\right]}{R(A)}\left[\frac{P_T \mathbf{y}_\mathbf{T} - R_T \mathbf{x}_\mathbf{T}}{P_T - R_T} - \mathbf{x}\right] \tag{518}$$

Multiplying out, and then employing the conditions set in equation 5.17, it can be shown that the equation collapses to:

$$\frac{d\mathbf{x}}{dA} = \left[\mathbf{x} - \mathbf{y}(\mathbf{x})\right] + \beta(A) \cdot \boldsymbol{\delta}_\mathbf{T} \tag{5.19}$$

where

$$\beta(A) = \frac{R_T}{R(A)} \tag{5.20}$$

$$\boldsymbol{\delta}_\mathbf{T} = \mathbf{y}_\mathbf{T} - \mathbf{x}_\mathbf{T} \tag{5.21}$$

$\boldsymbol{\delta}_\mathbf{T}$ is known as the *difference vector* taken at the top of the CS. Since $\boldsymbol{\delta}_\mathbf{T}$ is a difference in two compositions, it follows that certain values (but not all) in the row vector will be of negative sign. Furthermore, by definition, the entries in $\boldsymbol{\delta}_\mathbf{T}$ must sum zero. $\beta(A)$ is a scalar multiplier preceding $\boldsymbol{\delta}_\mathbf{T}$, and is a ratio of the retentate flow at the column top to that at a point corresponding to A. $\beta(A) = 1$ at the top of each CS, while anywhere else in a CS, $\beta(A) > 1$, increasing down the length of a CS.

Each CS is modelled using equation 5.19. Solving this equation graphically yields the respective column profiles for each CS. As with Operating Condition 1 (see Section 5.4), it is taken that integration commences at the top of the column. Since

there is equality in the top retentate compositions on either side, both column profiles will originate at the same point, namely $\mathbf{x_T}$.

From equations 5.9 and 5.17:

$$\mathbf{y}_{T1} - \mathbf{x}_{T1} = -\left(\mathbf{y}_{T2} - \mathbf{x}_{T2}\right) \tag{5.22}$$

It follows that:

$$\boldsymbol{\delta}_{T1} = -\boldsymbol{\delta}_{T2} \tag{5.23}$$

Thus, the designer has the freedom of choosing the direction of the difference vector for one CS. However, that for the other CS is set by mass balance.

5.5.3 COLUMN PROFILES

Consider the following arbitrarily chosen values for CS1:

- $\boldsymbol{\delta}_{T1} = [0.04, -0.08] = -\boldsymbol{\delta}_{T2}$
- $\mathbf{x}_{T1} = [0.3, 0.3] = \mathbf{x}_{T2}$
- $R_{T1} = 100\ mol/s = R_{T2}$

It is possible to generate the column profiles for both CS1 and CS2, as shown in Figure 5.12.

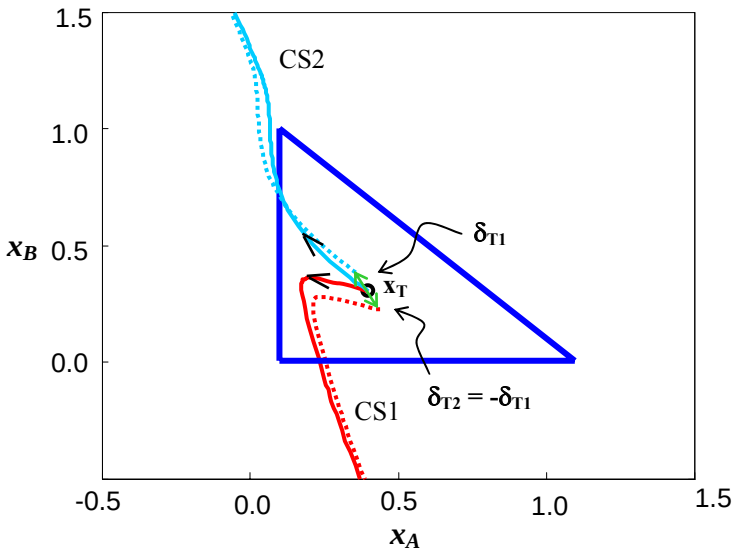

Figure 5.12: Retentate (solid) and permeate (dotted) column profiles for CS 1 (red) and CS 2 (blue).

$\mathbf{x_T} = [0.3, 0.3]$, $R_{T1} = 100\ mol/s = R_{T2}$, $\boldsymbol{\delta_{T1}} = [0.04, -0.08] = -\boldsymbol{\delta_{T2}}$ are represented in green.

5.5.4 FEASIBILITY

As before, the same feasibility requirements are necessary here (refer to Section 5.4.4). These include the intersections of both the retentate profiles within the MBT, as well as that for permeate profiles. This is not the case in Figure 5.12, thereby making the arrangement infeasible. In order to establish whether this result is specific to the conditions chosen, or is general, one needs to consider the retentate profiles and the DPE which describes them (namely, equation 5.19).

A behavioural analysis of the individual profiles for each CS can be performed in much the same manner as was done for those in Operating Condition 1 (see Section 5.4.5), but it is not necessary to explain this as the results are intuitive. The details have been detailed by Peters et al. (2007), and the reader is referred this for further insight.

The right-hand side of the DPE for this case (equation 5.19) is the summation of two vectors, namely the separation vector ($\mathbf{s} = \mathbf{x} - \mathbf{y}$) and the difference vector ($\boldsymbol{\delta}_\mathbf{T}$). Unlike the DPE used for Operating Condition 1 (equation 5.2) where both vectors were preceded by scalar quantities, only the difference vector in equation 5.19 is preceded a the scalar quantity. This scalar is $\beta(A)$, and is defined by equation 5.20. Now, $\beta(A)$ begins at a value of 1 at the top of a CS, and then increases in magnitude down its length. As $\beta(A)$ becomes sufficiently large, it results in $\boldsymbol{\delta}_\mathbf{T}$ becoming the dominant vector in the DPE. This causes the effect of the separation vector to become negligible, and the retentate profile to ultimately move in the direction of $\boldsymbol{\delta}_\mathbf{T}$. Now, each CS has a $\boldsymbol{\delta}_\mathbf{T}$ that is opposite of the other (see equation 5.23). This implies that, although, the profiles for each CS begin at the same point, $\mathbf{x}_\mathbf{T}$, they will eventually move off from each other, going in opposite directions, dictated by their respective $\boldsymbol{\delta}_\mathbf{T}$'s.

The permeate profiles for each CS, on the other hand will always differ from that of the retentate by $\beta(A)\cdot\boldsymbol{\delta}_\mathbf{T}$. This is a result of the mass balance constraint, and can be proven accordingly. This simply means that while the permeate profile for one CS will be "ahead" of its corresponding retentate profile, the other permeate profile would be "behind" its retentate profile. Figure 5.12 serves an example of this. Furthermore, the permeate profile, although off-set from the retentate profile, will ultimately the follow the same direction as the retentate profile, namely $\boldsymbol{\delta}_\mathbf{T}$. Now, since the off-set of the permeate profile, as well as the ultimate direction of movement of the retentate and permeate profiles, are dictated by $\boldsymbol{\delta}_\mathbf{T}$, it appears that the position of the permeate profiles for each CS will be such that they may never intersect (refer to Figure 5.12). But is this a general result for all $\mathbf{x}_\mathbf{T}$ locations and $\boldsymbol{\delta}_\mathbf{T}$ directions?

For feasibility, it is required that the permeate profiles must intersect. As it is agreed that the permeate profiles lay on opposite sides of their respective retentate profiles,

the only way that permeate profiles will meet is if they themselves cross their corresponding retentate profiles. This is not the case in Figure 5.12 – the profiles for CS 2 intersect, but those for CS 1 do not.

Now, consider the work displayed by Holland et al. (2004) where they performed a related analysis for a coupled distillation system. Physically a very different process from membrane permeation however mathematically similar, as has been shown. The only difference, mathematically speaking, is that in membrane permeation there is the added complexity of varying (decreasing) flow down the length of the CS, whilst in distillation it is valid to assume it constant. In other words, when describing a distillation system, $\beta(A)$ would be held at a constant value of 1. For this value it was shown that regions of feasibility do, in fact, exist (Holland et al. (2004)), but can not be sought for all directions of $\boldsymbol{\delta}_{\mathbf{T}}$. However, the direction used in Figure 5.12 does result in a region of feasibility. Consider Figure 5.14(a) – the same arbitrarily chosen values are employed, except the retentate and permeate flows are fixed. The profiles are allowed to run to their respective pinch points. All the necessary conditions for feasibility are met, as shown.

This leads on to question whether or not this result is unique for the constant molar flow assumption only. Figure 5.13(b) shows the resulting profiles for varying flow when commencing with a relatively large R_T-value of *1000 mol/s*. The required permeate intersection(s) occurs, in the correct direction, implying a feasible configuration is possible. Also, when comparing Figure 5.12 with Figure 5.13(b), it can be deduced that there is some minimum R_T-value for feasibility. This minimum value would correspond to a single intersection between the permeate profiles, and can be sought as described in Section 5.4.6. As before, this minimum flow depends on the location of $\mathbf{x}_{\mathbf{T}}$.

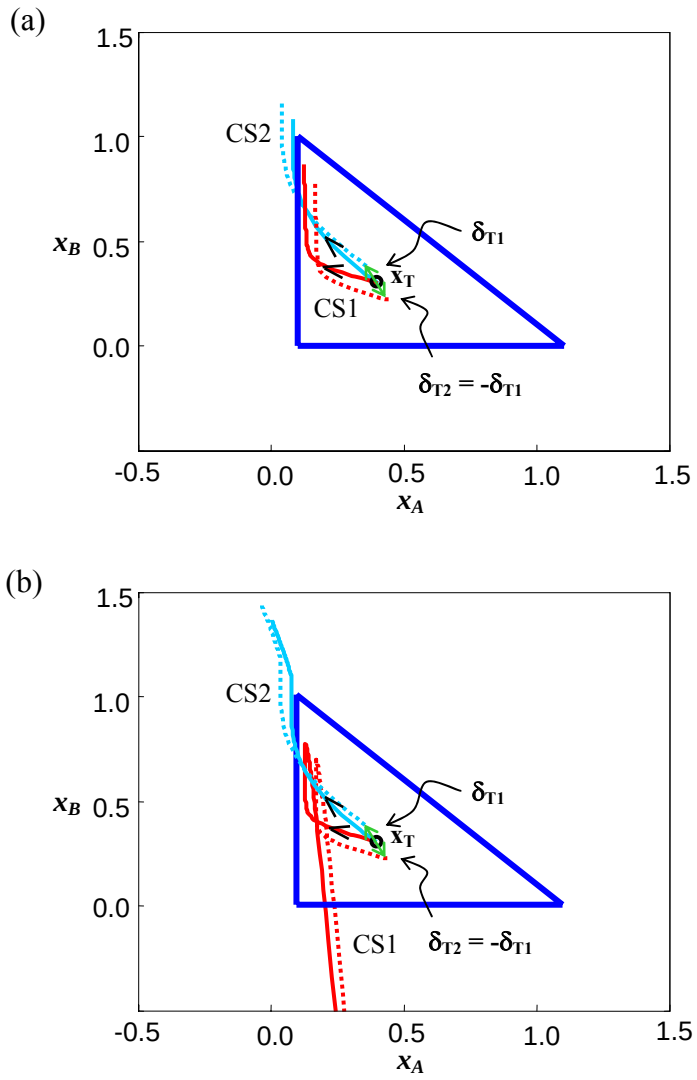

Figure 5.13: Retentate (solid) and permeate (dotted) column profiles for CS 1 (red) and CS 2 (blue).

$\mathbf{x_T} = [0.3, 0.3]$, $\boldsymbol{\delta_{T1}} = [0.04, -0.08] = -\boldsymbol{\delta_{T2}}$ are represented in green.

(a) Fixed flowrates (i.e. $\beta(A) = 1$), (b) Varying flowrates with $R_{T1} = 100\ mol/s = R_{T2}$.

Using a relatively large R_T-value results in $\beta(A)$ decreasing at a slower rate when compared to commencing with a smaller R_T-value. Thus the difference vector does not dominate as rapidly, thereby allowing to separation vector to influence the trajectory of the profiles. The profiles then initially mimic the "constant $\beta(A) = 1$" profiles to a certain extent (refer to Figure 5.13), until some point when the relative

sizes of the two vectors swops over, causing the profiles to move in the direction dictated by $\boldsymbol{\delta_T}$. This change over occurs within the vicinity of the pinch point curve (not shown). As discussed prior to this (see Section 5.4.6), the crossing of the pinch point curve is what allows for intersection between the retentate and permeate profiles. This can be deduced mathematically from the equation describing each permeate curve, as well as the pinch equation.

It can therefore be concluded that the same regions identified by Holland et al. (2004) for a given $\boldsymbol{\delta_T}$ apply for membrane systems with varying flow. There is, of course, the additional requirement that operation occurs above the minimum R_T-value for the chosen $\mathbf{x_T}$-location.

It is worth noting that the slowing down the rate at which $\beta(A)$ decreases in magnitude can be done by simply increasing R_T, as discussed. There is another way that one can slow its rate by keeping R_T at a fixed, or similar value. Altering the physical conditions of each CS, such as the operating pressures, membrane thickness, etc, results in a more gradual decrease in the retentate flow, and hence $\beta(A)$. This result can easily be deduced from equation 5.5.

5.6 COMPARISON WITH COMPLEX DISTILLATION SYSTEMS

Research by Holland et al. (2004) used column profiles and the idea of "moving triangles" to model the behaviour of complex distillation systems. This idea has now been extended to membrane systems. However, the results obtained for the distillation process are very different to the conclusions reached in the preceding sections regarding membrane systems. For example, Holland et al. (2004) show that for the distillation-equivalent of Operating Condition 1 (involving the difference vector, $\mathbf{X_\Delta}$) different regions of feasibility exist for each process. The reason for this,

and other differences, lies with the DPE that is used to describe each type of CS. Both DPE's involve the addition of two vectors (refer to equations 5.1 and 5.2 for Operating Condition 1, and equation 5.19 for Operating Condition 2), both of which are preceded by the same scalar quantities. However, the scalar values in the DPE for the DCS are *fixed* for any given section, while for a MCS it has to vary due to ever-changing flows. This results in the nodes for a DCS being stationary (and hence the idea of a "moved triangle"), but mobile for MCS. With this, and the effect of material loss, very different and unique column profile behaviour occurs within membrane sections. The column profiles in a DCS move towards a single, fixed stable node. In the MCS, the node is continually moving, and the profile has to adjust its direction so as to seek this node. It becomes apparent then that the required directions of movement and profile intersections are very different in each scenario, resulting in unique conclusions for each process regarding feasibility.

Needless to say that, if one could employ the "constant molar overflow" assumption within a MCS, the results obtained would then mimic that obtained for distillation. This, however, is only possible in extreme cases, when the membrane is selective a component in the retentate that has a very dilute concentration.

Due to these interesting differences that arise, the next section explores and introduces the design options of creating hybrids from distillation and membrane processes.

5.7 HYBRID DISTILLATION-MEMBRANE DESIGN

5.7.1 OVERVIEW

In the previous sections (see sections 5.4 and 5.5) an example of a complex configuration of membrane units was suggested. Through material balance constraints, as well as the behavioural properties of the retentate and permeate profiles, it was revealed how regions of feasible configurations could be sought.

One could now address the same arrangement of units, but alter the operation occurring in some of them, thereby creating a hybrid process. As a case study, a membrane module thermally-linked to a distillation column will be analysed. Distillation is equilibrium-based, while membrane permeation is rate-based, and combining the two into a hybrid should allow for each one to operate in the compositional space where it is best-suited. The arrangement of the units is as shown in Figure 5.2(a), except the main shell is no longer a membrane column, but rather distillation. Since no specifications about the number of stages, membrane area, or feed/side-draw locations have been made, the arrangement can be considered to be a super-structure. In other words, there are a number of possible variations of the configuration. Some of these variations that stem from this arrangement are shown in Figure 5.14.

There are a number of other possible variations not shown. Thus, by analysing the hybrid design proposed in Figure 5.2(a) does not limit one to a set design, but rather encompasses a wide range of configuration options. Of course, in initial conceptual design stages, what is required to discern is whether an arrangement of equipment is feasible or not.

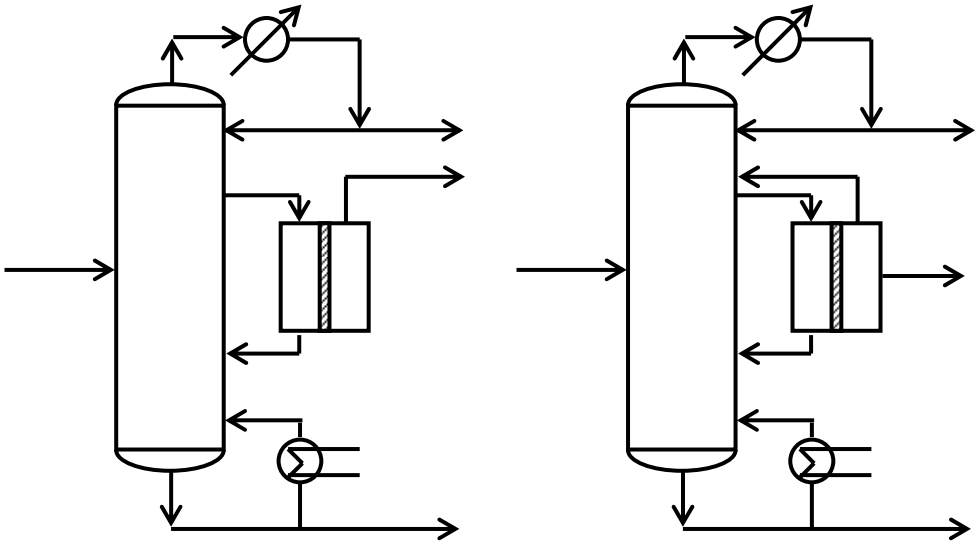

Figure 5.14: Possible variations of a membrane module thermally linked to a distillation column.

In the same way as before, a CS breakdown can be performed (refer to Figure 5.2(b)). Using the same assumptions of infinite reflux as a starting point, the same coupled sections arrangement can be arrived at. However, it is now a membrane section coupled with a distillation section, as shown in Figure 5.15. It is taken that the retentate side of the membrane operates at a pressure that matches that of the distillation column.

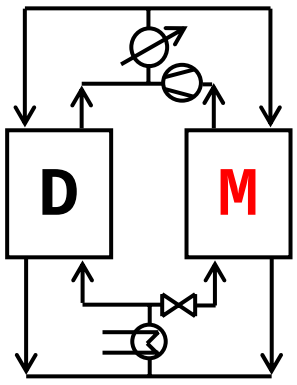

Figure 5.15: Coupled distillation and membrane column sections.

Verifying the feasibility of this simplified form of a hybrid combination would begin to give insight and answers about the operation and possibilities of the entire design.

5.7.2 MATERIAL BALANCES

Re-arranging the material balance around the compressor/condenser in Figure 5.15:

$$P_T - R_T = -(V - L) \Rightarrow \Delta_M = -\Delta_D \tag{5.24}$$

This leads on to the following relationship between the reflux ratios at the top of each CS:

$$r_{\Delta M}\big|_T = -r_{\Delta D} \tag{5.25}$$

The reflux ratio in the MCS decreases down its length, while the reflux ratio in the DCS remains constant.

By component material balance, it can be shown that there is equality in the difference points:

$$\mathbf{X}_{\Delta M} = \mathbf{X}_{\Delta D} \tag{5.26}$$

Thus, the designer has the freedom of choosing the reflux ratio and difference point for one CS. The same quantities for the other CS are set by mass balance.

The following operating conditions will be assumed:

- $r_{\Delta M}\big|_T = 5 = -r_{\Delta D}$
- $\mathbf{X_{\Delta M}} = [0.3, 0.3] = \mathbf{X_{\Delta D}}$
- $\alpha_{AB}^{D} = 3$, $\alpha_{BB}^{D} = 1$ and $\alpha_{CB}^{D} = 1.5$
- $\alpha_{AB}^{M} = 3$, $\alpha_{BB}^{M} = 1.5$ and $\alpha_{CB}^{M} = 1$

The respective α-values used for distillation and membrane permeation are different – it is assumed that one would use a membrane that has different separation capabilities to that of the distillation. Note that $r_{\Delta M} > 0$, while $r_{\Delta D} < 0$. Since $\mathbf{X_{\Delta M}}$ and $\mathbf{X_{\Delta D}}$ are equal by mass balance, they will both be referred to as $\mathbf{X_{\Delta}}$ for simplicity purposes!

5.7.3 FEASIBILITY

Requirements

For a feasible coupled column section arrangement, it is required that the retentate profile intersects with the liquid profile, as well as the permeate profile intersecting with the vapour profile. Furthermore, the direction of movement of the profiles, and the order of intersection must be in accordance with the flow arrangement in the coupled CS configuration.

Now, it is already known that the liquid and retentate profiles will always intersect (at $\mathbf{x_T}$). Thus, all possible intersections between the vapour and permeate profiles need to be sought after for a feasible arrangement.

Permeate Profiles

Initially, consider any general *permeate profile*: Irrespective of the location of its starting point, its termination point is fixed at $\mathbf{X_\Delta}$, and occurs as $r_{\Delta M} \rightarrow 0$ (refer to equation 5.14). This can be confirmed by the arbitrarily plotted profiles in Figure 5.16. Also, no matter the location of $\mathbf{x_T}$, both the retentate and permeate profiles will move in a direction so as to seek their respective "mobile" stable nodes as $r_{\Delta M} \rightarrow 0$. This was discussed in Section 5.4.5, as well as by Peters et al. (2007). It has been previously demonstrated that, at some point, the retentate profile would very closely follow its stable node pinch point locus. The same can be said about the permeate profile mapping out a path that mimics its respective pinch point locus. This is demonstrated in Figure 5.16. (Note that the permeate pinch point locus differs from that of the retentate by material balance, and is calculated accordingly.) Since it is assumed that $r_{\Delta M} > 0$ for the MCS, the location and movement of the *positive branch* of permeate stable node pinch point locus is of interest.

Remembering that it is required to find where the vapour profile intersects with the permeate profile, one can now rather search for the vapour profiles that intersect with the permeate pinch point locus. This is valid since all permeate profiles eventually follow the pinch point locus. It may be argued that the actual permeate profile only follows the pinch point locus for a short while. However, as one varies the magnitude of R_T (and hence P_T) the profile follows the pinch point locus for longer (Peters et al. (2007)). Also, as will be revealed later, the location of $\mathbf{x_T}$'s that results in feasibility, as well as the relative position of the vapour and permeate to each other, is such that an intersection with the permeate pinch point locus is guaranteed.

While it is agreed that the permeate profile does not match the pinch point locus exactly, it is very close proximity to the locus. Thus, using the pinch point locus is justified, especially for conceptual stages of synthesis and design, where accuracy is not of great importance.

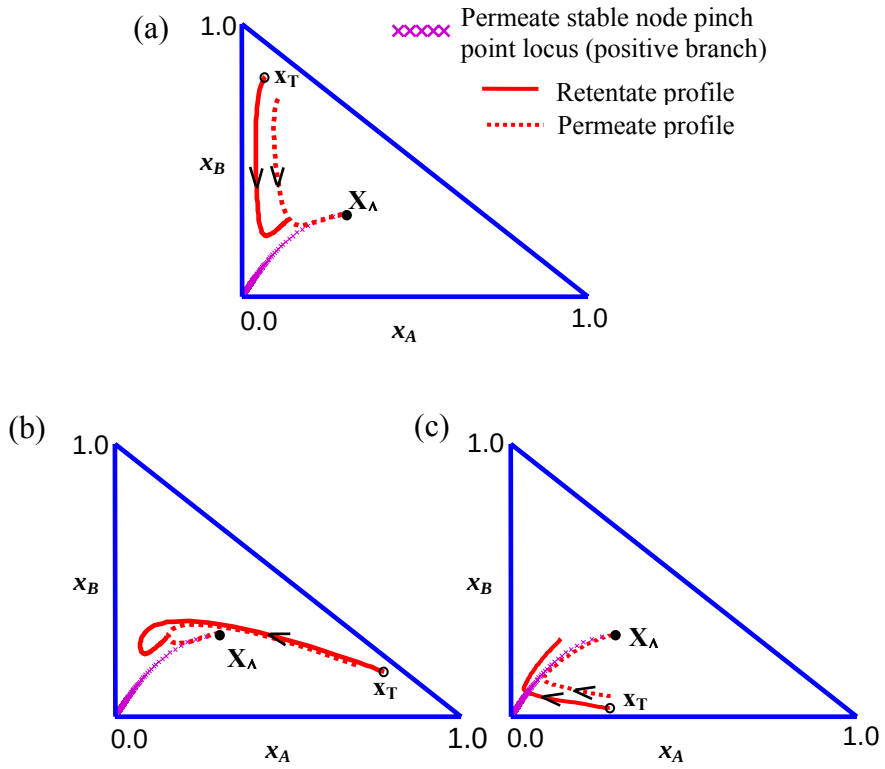

Figure 5.16: (a) – (c) Commencing the retentate profiles at various $\mathbf{x_T}$-values. The corresponding permeate profile eventually always approximates its pinch point curve.

The location of **y** *relative to* **x**

For both the DCS and the MCS, the respective vapour and permeate curves are determined by material balance, as described by equation 5.15. When using this equation for the DCS, the $r_{\Delta D}$ is held constant, while for the MCS, $r_{\Delta M}$ varies, as previously discussed.

It has been assumed that for the MCS, $r_{\Delta M} > 0$. This implies that each **y** has to lie between $\mathbf{X_\Delta}$ and the corresponding **x** co-ordinate. For the DCS, on the other hand, $r_{\Delta D} < 0$ signifying that **x** now lies between $\mathbf{X_\Delta}$ and **y**, on the straight line that connects them. Thus, the position of the permeate with respect to the retentate is on the opposite side of the vapour compared to the liquid.

Previously, when discussing the coupled membrane sections (refer to Section 5.4.6), the same phenomenon of opposite relative positions of **y** with respect to **x** occurred. It was this fact that lead to an overall infeasibility in the coupled membrane sections. However, one can not immediately say that this is the case now with a membrane section coupled to a distillation section. Previously, the profiles of both membrane sections were moving in the direction of the stable node pinch point locus – one followed the negative branch, the other the positive. This caused them to diverge. In the current scenario, on the other hand, only the one set of profiles follows the pinch point curve. The distillation profiles, alternatively, seek a single fixed node since $r_{\Delta D}$ is constant. This may very well lead on to the necessary intersections needed for feasibility.

Vapour Profiles

Up to now, it has been established what the position of the vapour profile relative to the liquid profile is. Furthermore, it is now agreed that if a vapour profile intersects the permeate stable node pinch point locus, then a feasible configuration is obtained. Of course, the location of $\mathbf{x_T}$ ultimately determines if this will occur. It therefore needs to be established what region of $\mathbf{x_T}$, within the MBT, yields feasibility.

Consider 2 arbitrarily chosen starting conditions for the liquid profiles, as shown in Figure 5.17. Their corresponding vapour profiles are plotted as well.

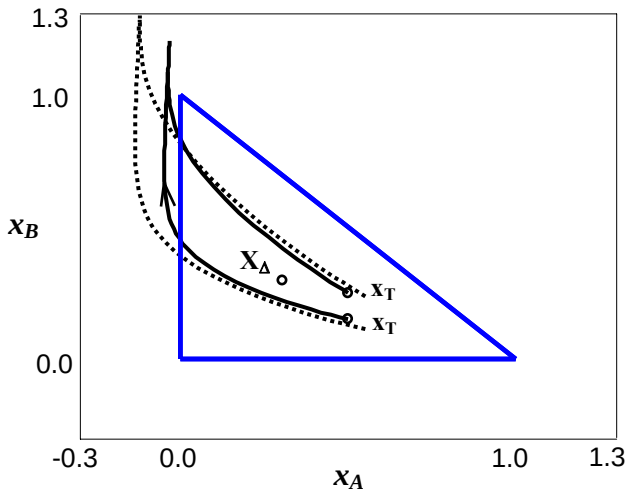

Figure 5.17: Some liquid profiles (solid), and their corresponding vapour profiles (dashed) relative to $\mathbf{X_\Delta}$.

It can be seen from Figure 5.17 that in one case the vapour profile lies below the liquid profile, while in another it lies above. This arises since the position of the vapour curve relative to its liquid curve is determined by $\mathbf{X_\Delta}$. Out of the two profiles shown, only the one with the vapour positioned below the liquid is useful since it would pass through the permeate stable node pinch point locus. However, this is not the only profile that would exhibit such and intersection, but rather there are numerous profiles that would satisfy this condition. Since their dependency on $\mathbf{X_\Delta}$ is significant, all these profiles would exist in a defined region, rather than being randomly positioned. Of course, this region would have to exist within the MBT.

Since the relevant vapour curves are required to pass through the permeate stable node pinch point locus, they would have to commence at a point before the locus, such that their direction of movement ensures an intersection with the locus. In this case, all profiles to the right of the locus move in the appropriate direction. Thus, the permeate stable node pinch point locus forms a boundary of the feasible region.

Liquid Pinch Point Locus

It is evident from Figure 5.17 that the relative position of the vapour changes from below to above the liquid profile as $\mathbf{x_T}$ is altered. This means that at some starting point between these two extremes, the vapour curve, although commencing behind the liquid, would appear to follow the same trajectory as the liquid. It is worth noting that this overlap between the profiles would only occur up until some point when the two curves would diverge from each other, heading off to their respective pinch points. Now, in order to obtain this overlap between the profiles, the initial **y**-value not only must lie on the straight line connecting $\mathbf{X_\Delta}$ and **x** produced, but the line should also be tangent at **x**. This coincides with the definition of a pinch point for the liquid – by equating the DPE to zero:

$$\left(1 + r_{\Delta D}\right)\left(\mathbf{x} - \mathbf{y}\left(\mathbf{x}\right)\right) = -\left(\mathbf{X}_\Delta - \mathbf{x}\right) \tag{5.27}$$

Equation 5.27 is saying that the points **x**, **y** and $\mathbf{X_\Delta}$ are collinear, and the straight line connecting them is tangent to the profile commencing at **x**. In other words, if a point on the liquid pinch point curve is used as $\mathbf{x_T}$, then the two profiles would overlap. This would be the case for all points on the liquid pinch point locus. Thus, the liquid pinch point locus forms another boundary of the feasible region! For the α^D-values assumed, and the $\mathbf{X_\Delta}$-value chosen, the liquid pinch point curve is plotted in Figure 5.18. Only the part of the curve within the MBT is shown, since this is the only section that is of importance here.

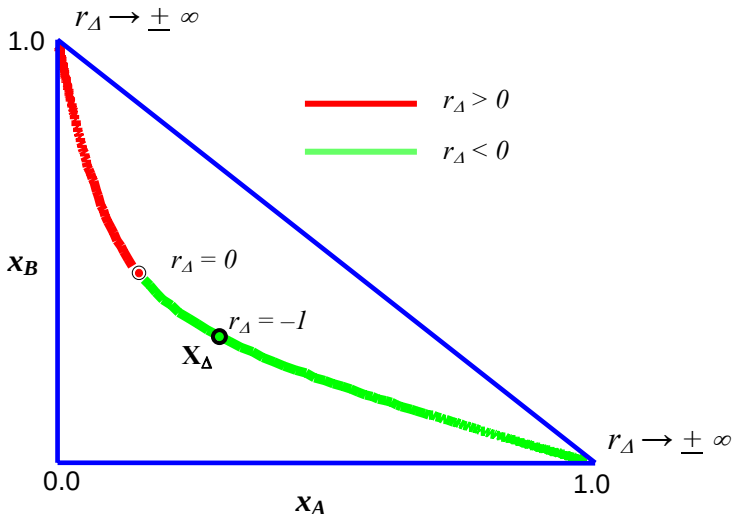

Figure 5.18: Liquid pinch point locus within the MBT.

Superimposing the permeate stable node pinch point curve on Figure 5.18, and remembering that all $\mathbf{x_T}$-values to the right of it allow for a feasible intersection, the region can be initially defined, as shown in Figure 5.19. It is worth noting that both these pinch point loci pass through and share the same $\mathbf{X_\Delta}$.

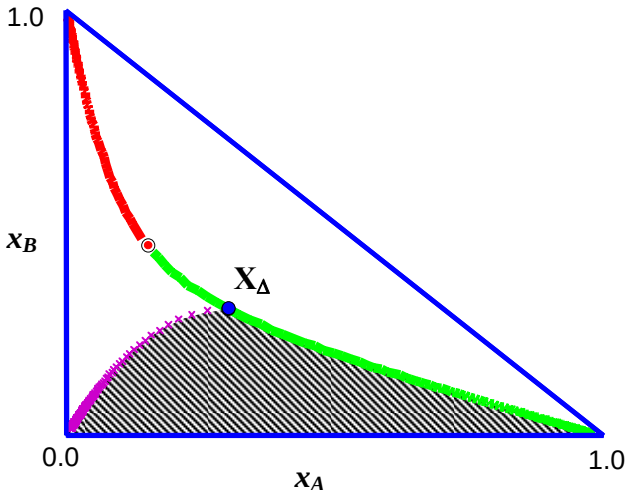

Figure 5.19: The permeate (purple) and liquid (green) pinch point loci defining an initial region of feasibility.

It can be seen that the only part of the liquid pinch point locus that is now relevant to the situation is the negative branch of the unstable node. This is somewhat expected since $r_{\Delta D} < 0$, and the profiles are required to move away from the unstable node towards the stable, intersecting with the permeate pinch point locus on the way.

Shifted Distillation Triangle

All the liquid profiles for the DCS exist on a single map known as a Column Profile Map (CPM). A similar map can be generated for the vapour profiles. Note that no such maps can be produced for the membrane (retentate and permeate) profiles since there are too many variables making it impossible to show all profiles in a single map.

Tapp et al. (2004) defined a CPM as linear transform of the Residue Curve Map (RCM). In other words, the profiles in the RCM have, graphically speaking, been shifted and possibly rotated slightly in order to produce the CPM. In doing so, the three nodes move as well from the pure component locations. Holland et al. (2004b) discuss the direction of the eigenvectors at each of the shifted nodes is such that one can connect the nodes with straight lines, thus forming a triangle. This is known as the "shifted" or "moved" triangle, from the original MBT. The CPM using the assumed values chosen for the DCS discussed above is plotted in Figure 5.20.

Now, the permeate profiles will always move towards $\mathbf{X}_{\Delta}$ and terminate there. Thus, it should be obvious that only liquid (and hence vapour) profiles within the shifted triangle will result in a feasible arrangement. This is due to their direction of movement.

Thus, the feasible region obtained in Figure 5.19 is further reduced in spatial size. Figure 5.21 shows the complete region.

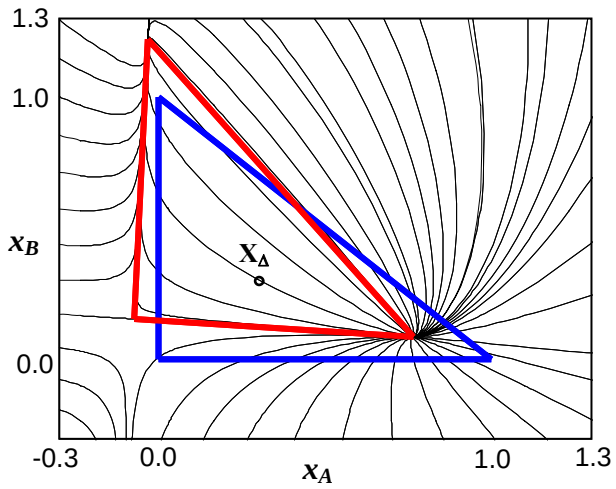

Figure 5.20: CPM for the DCS at $r_{\Delta D} = -5$ and $\mathbf{X}_\Delta = [0.3, 0.3]$.
MBT in blue, shifted triangle in red.

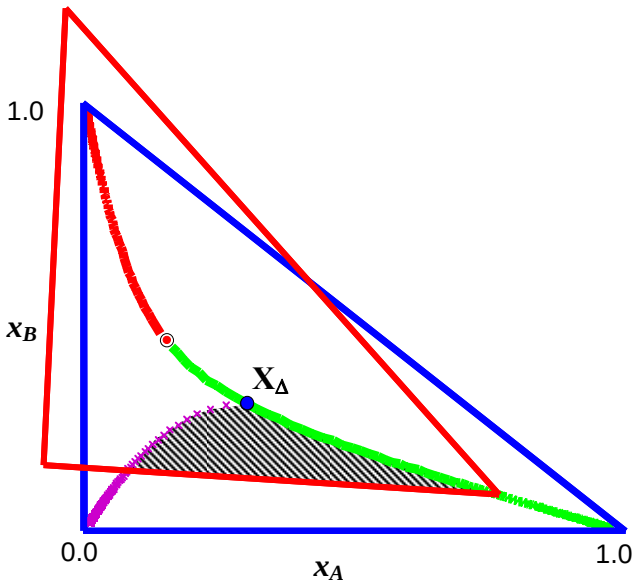

Figure 5.21: Region of possible $\mathbf{x}_T$ locations, for the operating conditions chosen, that would result in a feasible arrangement

This region shows all possible $\mathbf{x}_T$-values that will result in the coupled distillation and membrane sections being feasible, for the operating conditions assumed.

Column Profiles

Figure 5.22(a) shows the profiles obtained for an arbitrarily chosen $\mathbf{x_T}$-value within the region.

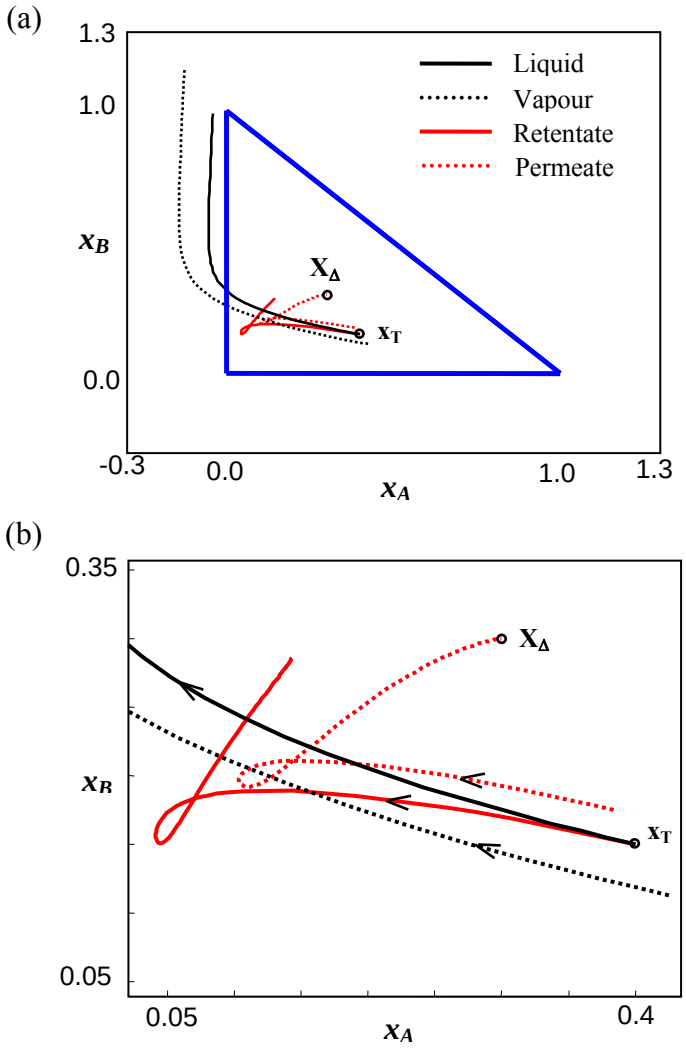

Figure 5.22: (a) Column profiles for the membrane and distillation sections with $\mathbf{x_T}$ in the feasible region.
(b) Zoomed in version of (a).

Figure 5.22(b) is a zoomed version of Figure 5.22(a). It can be seen that the vapour and permeate profiles intersect twice. This indicates that multiple steady states in

hybrid processes is very possible and needs to be taken into account, especially for control purposes.

Starting at any point outside this region would result in an infeasible configuration.

As with the coupled membrane scenario, to complete the design, one would generate the residue curves for the top and bottom sections (Figure 5.3) commencing at the appropriate compositions, and terminating at the pure components.

Regions of Feasibility: General

Although this region was generated for a specific set of operating conditions, the theory can be extended to any chosen values of $\mathbf{X}_{\Delta}$, α_D, α_M, and $r_{\Delta D}$ (or $r_{\Delta M}$). No matter what the conditions are, the region, if it exists, can be found by enclosing the area formed between:

- the positive branch of the pinch point locus for stable node of the *permeate*,
- the negative branch of the pinch point locus for the unstable node of the *liquid*, and
- the region within the moved triangle.

Of course, the region has to lie within the bounds of MBT.

One could also increase the size of the region by varying the size of the reflux ratios at the top of each CS. The larger $r_{\Delta D}$ is, the closer the nodes of the shifted triangle lie towards those of the MBT. This would then allow for a larger feasible region. However, there is a trade-off that the higher the reflux, the bigger the equipment and operating costs. This would have to be considered in an optimization technique incorporating a cost function.

The true power of using column profiles for both membrane and distillation design is that it provides important graphical insight into the behaviour of the proposed configuration. Other techniques rely on trial and error and some are based on rules of thumb. This does not improve the designers understanding of the process.

5.8 CONCLUSION

The use of column profiles for both membrane and distillation systems is a very powerful shortcut design technique. Any membrane arrangement, or hybrid configuration, no matter how complex, can be modelled using the CS approach. The resulting profiles allow an understanding of the behaviour of the operation of each CS. One does not need to blindly design a complex system by using trial-and-error methods. Although the method shown in this chapter is useful for conceptual stages of a design, it does provide a very good initialization point in rigorous simulation packages when more accurate and detailed results are needed. Ultimately, because there is a deeper understanding of the operation of the system, and also because the technique is relatively quick, the designer is able to make insightful decisions early on, hence saving money and time.

It should be appreciated that this work is not applicable to membrane permeation and distillation only, but can easily be adapted for *any* separation method. With both constant and non-constant flow assumptions have been tackled here, this then equips one to use the methods displayed for the separation procedure of their choice. Of course, details of equilibrium/flux model, flow assumptions and directions, etc. need to be decided upon. But the method and results arrived at here would still apply.

CHAPTER 6:

RELIABLE METHODOLOGY FOR FINDING ALL STATIONARY POINTS IN MULTICOMPONENT NONIDEAL MIXTURES

The material presented in this Chapter was done together with Dr. Libin Zhang (University of Illinois at Chicago) and has been prepared for publication. I was involved in the preliminary fundamentals, but he is responsible for the Newton-Raphson method and Bifurcation Detection which constitute a major portion of the work. He wrote the paper, with Prof. A. Linninger and myself as a co-authors. He agreed for me to place it in my thesis.

Although different in nature from the previous chapters, this work is relevant in this thesis since it begins to address the need for finding reliable methods for calculating stationary points and pinch point loci. As was shown in Chapters 4 and 5, the knowledge of these is important. This chapter is written from a distillation point of view, but its relevance should be evident from the prior chapters.

ABSTRACT

The determination of the existence and composition of fixed points is important from both theoretical and practical standpoints in the analysis of column behavior and in the synthesis and design of separation systems. A novel format of continuous methods has been developed so that one can locate all fixed points starting from the pure components and azeotropes for multicomponent mixtures. Interval methods for

validating the results are further presented. The interval method has an advantage that enables one to verify the nonexistence of the stationary points if none are present. The technique displayed is general and can be applied using any thermodynamic models. However, the continuous method has to carefully construct the proper homotopy function. The classification and order of the fixed points also are given by calculating the eigenvalue and the entropy at the fixed point. The special continuous method is presented to compute all fixed points.

6.1 INTRODUCTION

Distillation columns are the most common operational unit in chemical processes, and always accounts for a large portion of the capital costs and energy consumption. Hence, the development of systematic approaches for synthesizing optimal separation sequences is of practical importance. Some researchers proposed rigorous mathematical programs for synthesizing the separative distillation network (Viswanathan and Grossmann (1993), Bauer and Stichlmair (1998), Smith and Pantelides (1995), Lang and Biegler (2002)). One of the current practical approaches is to determine the feasibility and minimum reflux in sharp separations based on topological concepts (Levy et al. (1985), Julka and Doherty (1990, 1993), Bausa et al. (1998), Watzdorf et al. (1999), Doherty and Malone (2001)). Zhang and Linninger (2004, 2006) presented a stochastic approach to synthesize a separation network with their novel temperature collocation method. Tapp et al. (2004) introduced the idea of a generalized column section, and defined it as a length of column terminated at either end by the addition and/or removal of material and/or energy. The difference point equation (DPE) was incorporated as a tool to mathematically describe the liquid composition profile down the length of a column section. Using this, Column Profile Maps (CPM) were generated, and were classified as a simple graphical transformation of the well-known Residue Curve Map (RCM). The location of the fixed points can be identified by this column profile maps. Holland et al. (2004b) also classified each of the stationary points obtained by an appropriate eigenvalue-analysis.

A key element in the aforementioned design procedures is determining the location of *all* the fixed points of the distillation map (Julka and Doherty (1990)). However, most conventional nonlinear solvers (e.g. Newton-Raphson and trust region approaches), are iteration methods which can only solve the system of equations locally (Lucia and Fang, (2003)). In order to use the local method to compute

multiple roots of a given system of nonlinear algebraic equations, a priori knowledge of initial conditions close to the solution is necessary.

Several methods have been proposed to solve pinch equations in literature (Julka and Doherty (1993), Fidkowski et al. (1991, 1993)). Homotopy continuation methods find roots of systems of nonlinear equations by tracking the homotopy path from one or multiple starting points (Watson et al. (1987), Knapp and Doherty (1994)). Given a known point on or near a homotopy path, a path tracking algorithm follows the path by determining new points near the path. Most of the path tracking algorithms are based on a predictor-corrector procedure, and use step size control algorithms based on the convergence pattern of the corrector (Allgower (1981)) or the curvature of the path currently being traced (den Heijer and Rheinboldt (1981)). Homotopy continuation methods have been successfully applied to find the azeotropes for the different mixtures. Fidkowski et al. (1991) and Bausa et al. (1998) briefly discussed how to obtain the pinch points by use of the continuation method with constructing different homotopy functions. However, their methods still need the previous knowledge about the azeotropic points of the mixture, which is another challenge to the nonlinear solvers. In this chapter, we will present a new homotopy formulation able to find all fixed points from pure components.

Outline: The difference point equation for any general distillation column section and related pinch equations are introduced in section two. Section three briefly describes the predict-correction tracking path continuation method. A novel homotopy continuation function is further presented to identify the fixed points with pervious knowledge about azeotrope points. Pinch points for the ideal, non-ideal and azeotropic mixtures for validating the new continuation function will be discussed in section four. A tangent pinch point for acetaldehyde, methanol and water mixture also is given to further approve the reliability of the homotopy-continuation method in this section. The paper closes with conclusion and future research direction.

6.2 THE FORMULATION OF THE FIXED POINTS IN A DISTILLATION COLUMN

The difference point equation (DPE) was developed as a mathematical description of the liquid composition profile throughout any general distillation column section (Tapp, et al. (2004)). A column section is defined as a length of column terminated on either end by the addition and/or removal of material and/or energy. The DPE is:

$$\frac{dx_i}{dn} = \left(1 + \frac{1}{r_\Delta}\right)\left(x_i - y_i\right) + \frac{1}{r_\Delta}\left(X_{\Delta i} - x_i\right) \text{ for } i = 1\ldots c-1 \qquad (6.1)$$

where $R_\Delta = \frac{L}{\Delta}$, $X_{\Delta i} = \frac{Vy_i - Lx_i}{\Delta}$ and $\Delta = V - L \ \left(\Delta \neq 0\right)$.

x_i is the liquid composition for component i,

y_i is the vapor composition for component i,

n is the number of stages,

r_Δ is the reflux ratio,

$X_{\Delta i}$ is the difference point,

c is the number of components,

L is the liquid flowrate,

V is the vapor flowrate,

Δ is the net flow.

6.3 DEFINITION OF A PINCH POINT

The pinch point can be defined when the liquid and vapor phase in column section approach equilibrium and the driving forces for mass transfer between two phases are diminished. Based on this definition, the stationary points (SPs) of the DPE can be obtained by applying the following equation:

$$\frac{dx_i}{dn} = 0 \tag{6.2}$$

The pinch conditions of the DPE evaluated at the nodes for a c component system can be written as:

$$f_i = \left(R_\Delta + 1\right)\left(x_i - y_i\right) + \left(X_{\Delta i} - x_i\right) = 0 \text{ for } i = 1\ldots c-1 \tag{6.3}$$

$$y_i = x_i K_i \text{ for } i = 1\ldots c \tag{6.4}$$

The vapor composition is a function of that of the liquid, and is determined with an appropriate vapor liquid equilibrium (VLE) model. Furthermore, the compositions have to sum to unity:

$$\sum x_i K_i - 1 = 0 \tag{6.5}$$

For the very simple case of a constant α or ideal model, the SPs can be easily sought by an analytical technique or a very basic numerical calculation. An example is shown for an ideal model in Figure 6.1 with X_Δ = [*0.95, 0.049*] and r_Δ = *4*. A column profile, commencing at X_Δ and terminating at the stable pinch point (γ), is displayed. Each SP has associated with it a temperature, as indicated in Figure 6.1(a). The residual errors of equations 6.3 and 6.5 as a function of temperature are given in Figure 6.1(b).

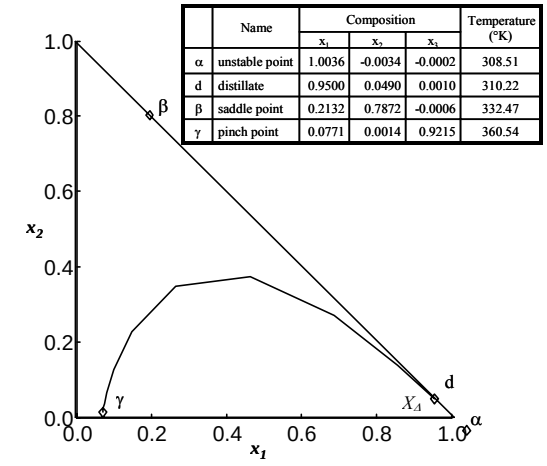

	Name	Composition			Temperature (°K)
		x_1	x_2	x_3	
α	unstable point	1.0036	-0.0034	-0.0002	308.51
d	distillate	0.9500	0.0490	0.0010	310.22
β	saddle point	0.2132	0.7872	-0.0006	332.47
γ	pinch point	0.0771	0.0014	0.9215	360.54

(a)

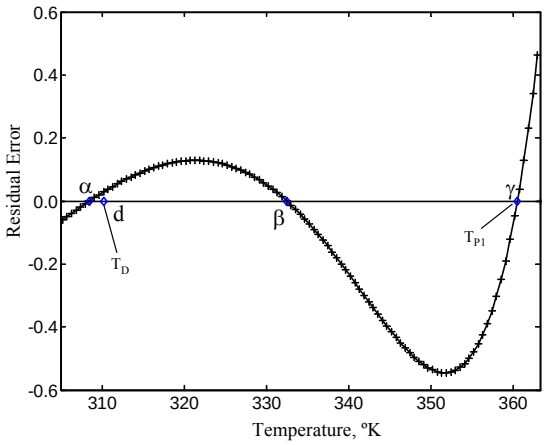

(b)

Figure 6.1: Fixed points in a ternary mixture and residual errors of equations 6.3 and 6.5.

However, as the thermodynamic models become more complex, so does the determination of the location of the SPs.

What we have developed is a method that can be used to locate the compositional position of the SPs for a set X_Δ and r_Δ. In this paper, two methods, namely (*i*) homotopy continuation and (*ii*) interval analysis, are applied to find all the fixed points in DPE profiles. The two different methods will be examined by different case studies will be applied.

Brief introductions about Newton's interval analysis and homotopy continuous methods are given in the next section.

6.4 INTERVAL ANALYSIS AND HOMOTOPY CONTINUOUS METHOD

An interval Newton/generalized bisection (IN/GB) technique and homotopy method are presented to find all fixed points in composition space in the subsections.

6.4.1 INTERVAL ANALYSIS

Recently, it has been shown that interval-Newton approach can be applied to reliably solve numerous nonlinear equations found in chemical engineering (Stadtherr et al. (1995), Stradi, et al. (2001)). The interval Newton/generalized bisection (IN/GB) algorithm used has been summarized (Kearfott (1996)). Properly implemented, this technique provides the power to find, with mathematical and computational certainty, enclosures of all solutions of a system of nonlinear equations, provided only that initial upper and lower bounds are available for all variables. This is made possible through the use of the existence and uniqueness test provided by the interval Newton method. Our implementation of the IN/GB method for the fixed point problem is based on appropriately modified FORTRAN-90 routines from the packages INTLIB (Kearfott (1996)).

6.4.2 HOMOTOPY CONTINUOUS METHOD

A homotopy is defined by a continuous function $H(x, t)$ such that $H(x, 0) = g(x)$ and $H(x, 1) = f(x)$, where t is the homotopy parameter, and $g(x)$ is a continuous and

smooth function such that a solution to $g(x) = 0$, x_0 is known. The linear homotopy function is defined as following:

$$H(x,t) = tf(x) + (1-t)g(x) = 0 \tag{6.6}$$

This function is usually defined for $t \in [0, 1]$, and then it is called a convex homotopy, which means that H is a convex combination of f and g. For convex homotopies, each curve satisfying equation 6.1 and connecting $t = 0$ $(x = x_0)$ and $t = 1$ $(x = x^*)$ is called a homotopy path. If we deal with the entire set of curves of a homotopy system $h(x, t) = 0$ regardless of the value of t, then H is called a global homotopy. Homotopy continuation methods find a solution to $f(x) = 0$ by tracking the path from $t = 0$ $[g(x) = 0; x=x_0]$ to $t = 1$ $[f(x) = 0; x=x^*]$, if such a path exists. In the chapter, the easiest way is to let the homotopy function starting from pure component using an ideal VLE model. In order to implement the approach, the following novel homotopy function is proposed:

$$H(x,t) = (1+R_\Delta)\left(x_i - \left((1-t) + t\frac{\gamma_i}{\phi_i}\right)\frac{p_i}{P}x_i\right) + t\left(X_{\Delta i} - x_i\right) = 0 \tag{6.7}$$

Equation 6.7 becomes equation 6.8 when $t = 0$:

$$H(x,0) = x - \frac{p^s}{P}x = 0 \tag{6.8}$$

This is the residue curve equation with ideal VLE properties, as shown in Figure 6.2(a). With an increase in t, the VLE properties and operating conditions will gradually increase.

When $t = 1$, equation 6.9 will be identified with the pinch equations, equations 6.3:

$$H(x,1) = (1+R_{\Delta})\left(x_i - \frac{\gamma_i}{\phi_i}\frac{p_i}{P}x_i\right) + (X_{\Delta i} - x_i) = 0 \qquad (6.9)$$

Finally the solutions of homotopy function will be the solutions of pinch equations, as is given in Figure 6.2(b) (refer to Figure 6.1(a)).

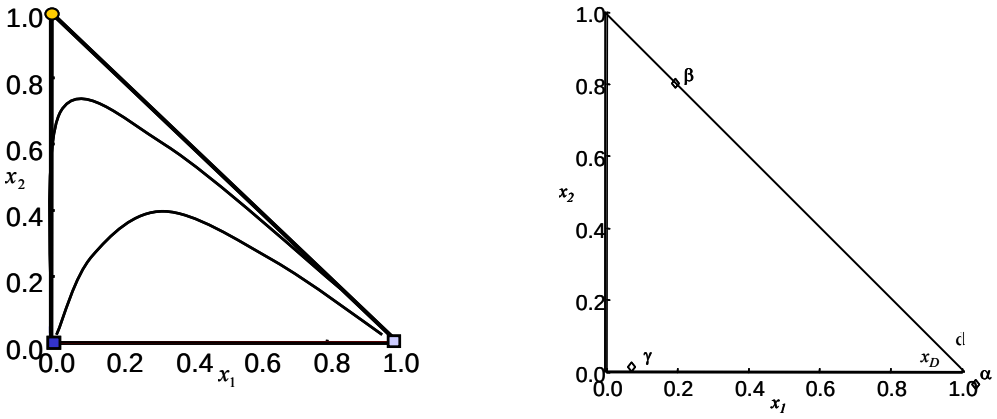

(a) $t = 0$ (b) $t = 1$

Figure 6.2: The homotopy continuation function. The simple function is the residue map equations with ideal mixture. (a) Its solution is the pure component (A,B,C) at $t = 0$. (b) Final solution is the pinch point when $t = 1$.

The following section will explain the detailed steps to realize the homotopy method.

6.4.2.1 PREDICTOR STEP – EULER'S METHOD

The Euler predictor is defined as the unit tangent vector multiplied the step size, i.e., the first order predictor. The unit tangent vectors $du/ds = [dx/ds,\ dt/ds]^T$ at $s = s_k$ satisfy

$$\begin{bmatrix} \dfrac{\partial H(x,t)}{\partial x} & \dfrac{\partial H(x,t)}{\partial t} \\ \dfrac{dx}{ds} & \dfrac{dt}{ds} \end{bmatrix} \begin{bmatrix} \dfrac{dx}{ds} \\ \dfrac{dt}{ds} \end{bmatrix} = \begin{bmatrix} 0 \\ 1 \end{bmatrix} \tag{6.10}$$

Furthermore, to keep the path tracking direction consistent, the unit tangent vectors for $\boldsymbol{k > 1}$ must satisfy the following condition:

$$\frac{du}{ds}(s_{k-1})\frac{du}{ds}(s_k) > 0 \tag{6.11}$$

If the norm of the tangent vector is left to later adjustment, the bottom row of the matrix in equation 6.10 can be replaced by a known row vector to make the system linear. The formula to be used for $k > 1$ is as follows:

$$\begin{bmatrix} \dfrac{\partial H(x,t)}{\partial x} & \dfrac{\partial H(x,t)}{\partial t} \\ \dfrac{dx}{ds}(s_{k-1}) & \dfrac{dt}{ds}(s_{k-1}) \end{bmatrix} \begin{bmatrix} \dfrac{dx}{ds} \\ \dfrac{dt}{ds} \end{bmatrix} = \begin{bmatrix} 0 \\ 1 \end{bmatrix} \tag{6.12}$$

If $(du/ds)^T(du/ds) \neq 0$, equation 6.8 gives a tangent vector v^k. The unit tangent vector is obtained by

$$\frac{du}{ds}(s_k) = \frac{v^k}{\|v^k\|} \tag{6.13}$$

The next point near the homotopy path (predicted point) is

$$u^{k+1} = u^k + \frac{du}{ds}(s_k)\Delta s_k \tag{6.14}$$

6.4.2.2 CORRECTOR ITERATION – NEWTON-RAPHSON METHOD

A more accurate point near the homotopy path can be obtained by Newton's method, which is locally convergent. If the predicted point is sufficiently close to the curve, the corrector iteration is guaranteed to converge to a point on the exact curve (den Heijer and Rheinboldt (1981)). Note that if u^k is sufficiently close to the homotopy path, equation 6.14 with a sufficiently small Δs_k gives u_0^{k+1} which is sufficiently close to the homotopy path.

A point after *i* iterations of the corrector process is represented by u_i^{k+1}. The Newton corrector, Δu_i^{k+1}, is obtained by solving the following system of equations:

$$\begin{bmatrix} \dfrac{\partial h(x_i,t_i)}{\partial x} & \dfrac{\partial h(x_i,t_i)}{\partial t} \\ \dfrac{dx}{ds} & \dfrac{dt}{ds} \end{bmatrix} \begin{bmatrix} \Delta x_i \\ \Delta t_i \end{bmatrix} = \begin{bmatrix} -h(x_i,t_i) \\ 0 \end{bmatrix} \tag{6.15}$$

A corrected point is obtained by applying the full step as follows:

$$u_{i+1}^{k+1} = u_i^{k+1} + \Delta u_i^{k+1} \tag{6.16}$$

This corrector process is repeated until the convergence condition is satisfied.

6.4.2.3 BRANCH SWITCHING AND BIFURCATION DETECTION

A rigorous mathematical definition of a bifurcation requires the concept of topological equivalence of phase portraits. For simplicity, however, one can think of a bifurcation as a point on a solution curve at which two or more solution branches

intersect. As noted, the Implicit Function Theorem implies that a unique solution branch passes through any regular point, therefore a bifurcation can only occur at solutions which do not satisfy the full rank condition. That is, a necessary condition for bifurcation at the solution:

$$rank\left[h_x(x,t), h_t(x,t)\right] < n \tag{6.17}$$

Basis vectors for the null space $N\left(h_x(x,t)\right) = span\left(\phi_1, \cdots \phi_m\right)$ and its transpose $N\left(h_x^T(x,t)\right) = span\left(\psi_1, \cdots \psi_m\right)$ can be used to determine if bifurcation occurs at a singular point. Furthermore, the basis vectors of the null space and its transpose are used to calculate direction vectors of the branches which appear. A rank deficiency of a simple singular point is exactly 1. The singular point is a simple bifurcation point which only two solution branches intersect if $h_t(x,t) \in N\left(h_x(x,t)\right)$, otherwise it is a limit point or turning point if $h_t(x,t) \notin N\left(h_x(x,t)\right)$.

In the singular point, vectors ϕ, span the null space of $h_x(x,t)$, and a vector, ψ, that spans the null space of its transpose. Bifurcation direction at a simple singular point can be computed by solving the so–called *algebraic bifurcation equation* (ABE) in equation 6.18:

$$c_{11}\alpha_1^2 + 2c_{12}\alpha_1\alpha_0 + c_{22}\alpha_0^2 = 0 \tag{6.18}$$

where $c_{11} = \psi_1 h_{xx}\phi_1\phi_1$,

$c_{12} = \psi_1\left(h_{xx}\phi_0 + h_{xt}\right)\phi_1$, and

$c_{22} = \psi_1\left(h_{xx}\phi_0\phi_0 + 2h_{xt}\phi_0 + h_{tt}\right)$

Keller (1987) shows that if a simple singular point is a bifurcation, then there are two branches and the direction vectors can be calculated by:

$$\begin{bmatrix} \frac{dx}{ds} \\ \frac{dt}{ds} \end{bmatrix} = \alpha_1 \phi_1 + \alpha_0 \phi_2 \tag{6.19}$$

The continuation method traces the curve in steps, however, and it is therefore likely that, in practice, the method will "skip over" bifurcations. In order to find the bifurcation point, a continuation method must include a procedure for detection of singular points. The bisection method is applied to locate the singular point after the determinant of the Jacobian of the augmented system changes sign.

6.5 RESULTS AND DISCUSSION

In this section, the ideal, nonideal and azeotropic mixtures are employed to demonstrate the homotopy continuous method and interval analysis. The tangent pinch in nonideal mixture also is identified by homotopy method further to show the robustness of the two approaches.

6.5.1 IDEAL MIXTURE

Figure 6.3 illustrates that the distillate, d ($X_\Delta = X_D$) and stable pinch points γ span all possible rectifying profiles for a given specification. Rectifying composition profiles start at the distillate and terminate in the stationary stable pinch point. For high purity separations, the profiles approach a saddle point dividing the composition profile into two branches reachable only after traversing an infinite number of equilibrium trays. Each pinch point is also associated with a specific bubble point temperature as

illustrated in Figure 6.3. The bifurcation trajectories of the ideal mixture show that the homotopy approach successfully reached all solutions from pure products without any difficulties.

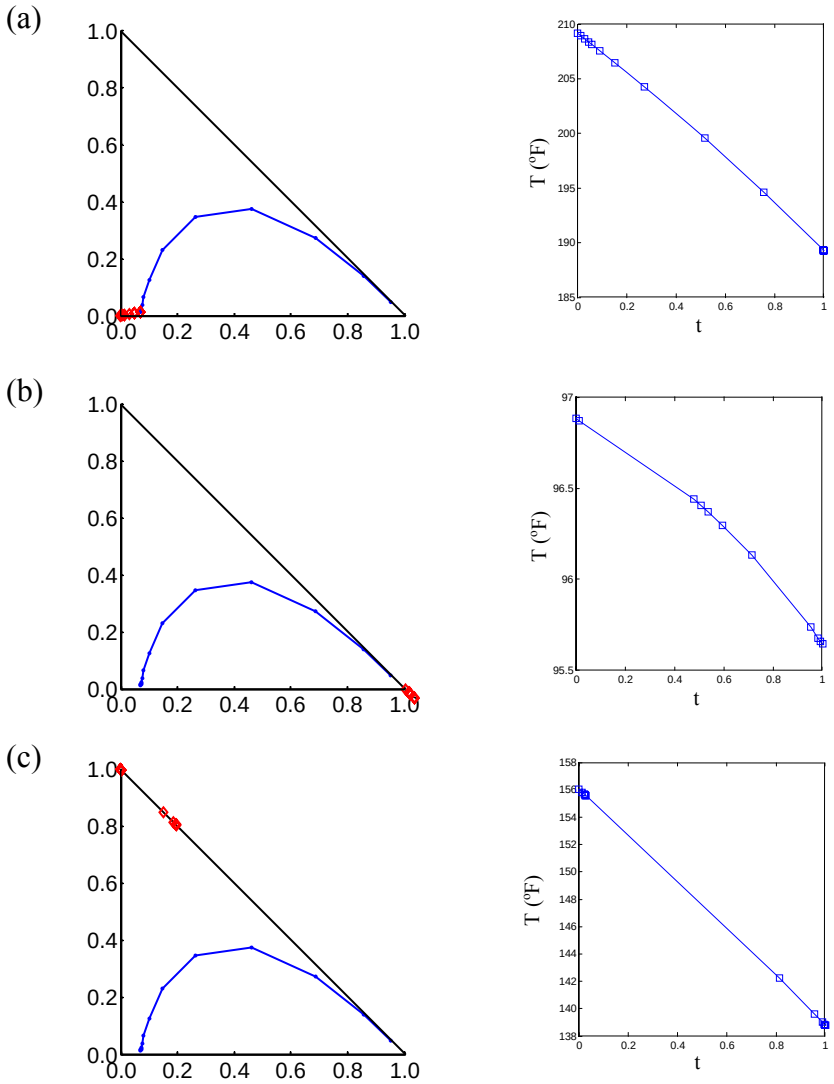

Figure 6.3: Solution branch on the composition triangle and bifurcation diagram for the fixed points for the ideal mixture

(a) Stable pinch point, (b) Unstable Pinch point, (c) Saddle point

6.5.2 NONIDEAL MIXTURES WITH AZEOTROPE

We consider a mixture of acetone/chloroform/benzene. This mixture exhibits a high boiling binary azeotrope. For a given feed, reflux ratio and product compositions, this system shows the three stationary points, the unstable point, α, a saddle point, β, and a stable pinch point, γ. Having known all the solutions of the pinch equations, the problem of identifying the stationary nodes arises. Figure 6.4(a) reports all the fixed points of rectifying section with mixture acetone/chloroform/benzene by homotopy continuation method. The bifurcation diagram as shown in Figure 6.4(b) provides evolution trajectories of three solutions starting from pure component.

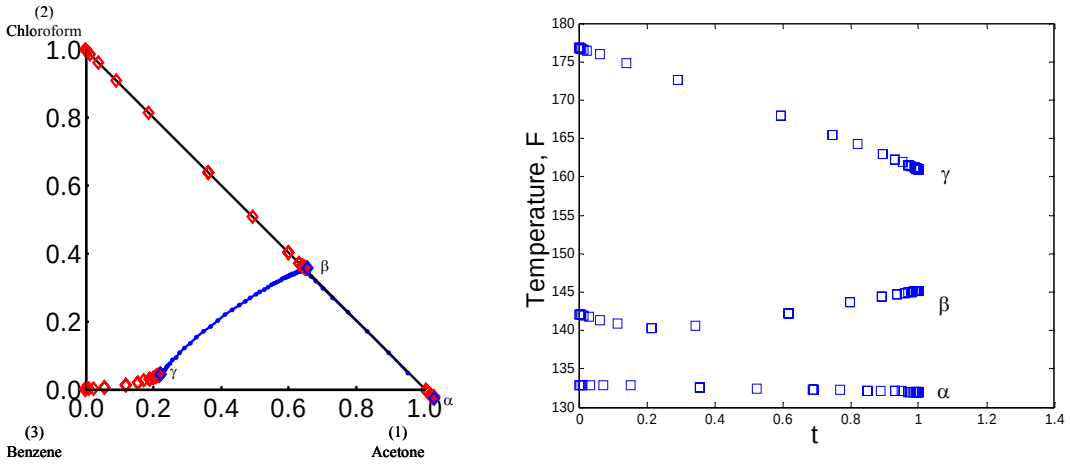

(a) (b)

Figure 6.4: Solution branch on the composition triangle (a) and bifurcation diagram (b) for the fixed points for the azeotropic mixture (Acetone, Chloroform and Benzene).
(α) Unstable Point, (β) Saddle Point, (γ) Pinch Point.

Another nonideal mixture of acetone/chloroform/methanol further demonstrates the robustness of the proposed method with obtaining successfully all solution from pure components as depicted in Figure 6.5(a). The closest unstable node, α, was solved by homotopy method and verified by interval method as documented in Figure 6.5(b). The detailed bifurcation trajectory of pinch point, γ, shows that T starts to decrease

when t = 0.33, then increase thereafter, finally reaching the solution. The proposed method solves successfully the problem without failure at the turn point as shown in Figure 6.5(c).

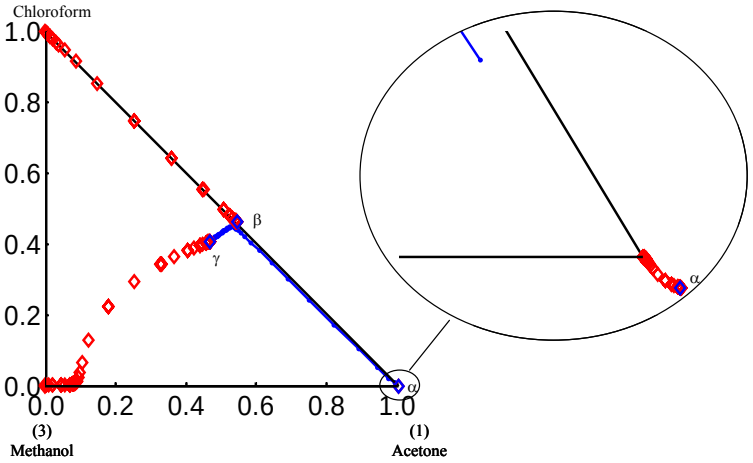

(a)

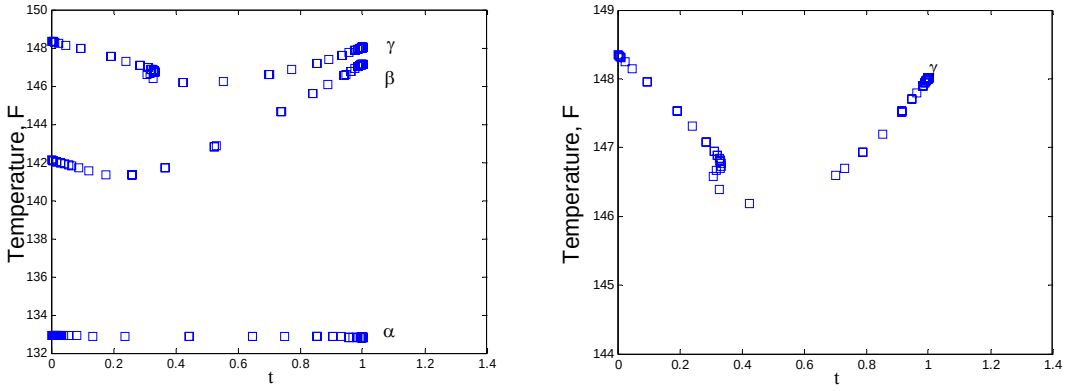

(b) (c)

Figure 6.5: Solution branch on the composition triangle (a), bifurcation diagram (b) for all fixed points and (c) trajectory of pinch branch γ for the azeotropic mixture (Acetone, Chloroform and Methanol). (α) Unstable Point, (β) Saddle Point, (γ) Pinch Point.

6.5.3 NONIDEAL MIXTURES WITH TANGENT PINCH POINT

Tangent pinches can occur in non-ideal mixtures. In a separation problem exhibiting tangent pinches, the composition profiles possess additional stationary nodes, i.e. the tangent pinch node. The existence of the tangent pinch can be detected by bifurcation analysis. In a separation controlled by tangent pinch, the composition profile terminates at the tangent pinch point as shown in Figure 6.6(a). However, when the reflux ratio increases slightly, the composition profile will extend to a pinch point as depicted in Figure 6.6(b). Novel homotopy function accurately renders the tangent pinch point. Tangent point branch bifurcated from the saddle branch can be obtained with bifurcation at $t = 0.27$ as depicted in Figure 6.6(c).

6.6 CONCLUSION

In this chapter, a novel formulation of a homotopy function for reliably locating fixed points in multicomponent mixtures is proposed. We applied the technique here to identify successfully all stationary points of nonideal mixtures which have very strong nonlinear behaviors. The novel homotopy function helps us find all solutions from pure component. The identification of tangent pinch point suggested the robustness of the proposed approach. The interval method has been employed to validate the solutions from homotopy continuation method.

	Feed	Distillation	Bottoms
1 Acetaldehyde	0.3000	0.5030	$1.00 \bullet 10^{-10}$
2 Methanol	0.3000	0.4960	0.1030
3 Water	0.4000	0.0010	0.9897

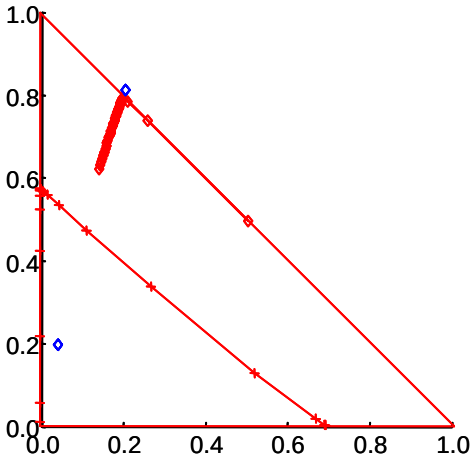

(a) $r_{\Delta} = 0.60$

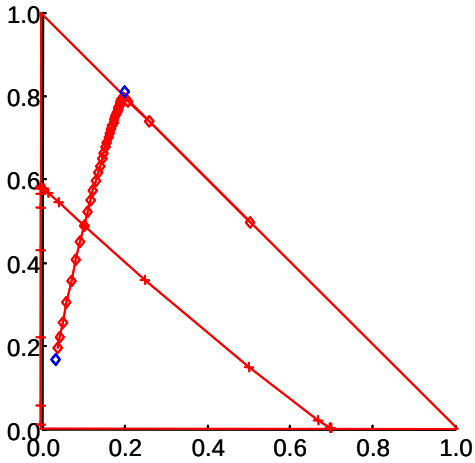

(b) $r_{\Delta} = 0.65$

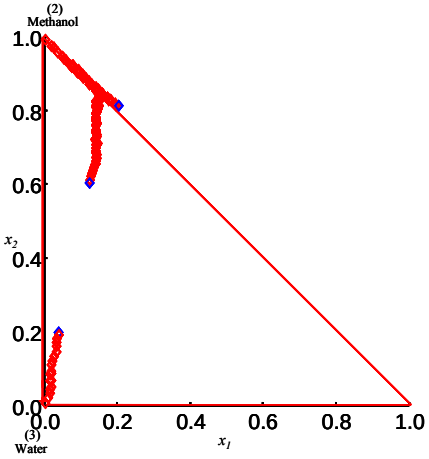

Figure 6.6: Composition profiles showing the presence of tangent pinch and solution branch successfully identified tangent pinch for a nonideal mixture (Acetaldhyde, Methonal and Water) by homotopy continuation method.

CHAPTER 7:

CONCLUDING REMARKS

Thesis Results

The work contained in this thesis has, by introducing an innovative method, contributed to analysing, designing and synthesising membrane separation processes. It is believed that an extremely useful and versatile technique has been developed. The method is not restricted to a single type of membrane, but, with the appropriate flux equations, can easily be adapted for any membrane. The choice and accuracy of the flux equations is a choice of the designer, and was not the focus of the thesis. But once decided upon, the ideas displayed in the thesis can be employed for design purposes.

Although the M-RCM was developed for a batch membrane process, it has been revealed how it is directly applicable to a wide range of continuous processes. A number of important results emerged from this, each being contributing to the separations field in their own right:

- The M-RCM can be used to explain and understand the behaviour of the conventional industrial membrane permeators.
- The same applies for total and infinite reflux membrane columns. While these are not practical applications, the theoretical results they yield are useful when explaining finite reflux arrangements.
- The profiles in the M-RCM allow one to graphically visualise the change in the retentate in either a batch still or continuous unit.
- Furthermore, the M-RCM also provides some necessary design parameters such as what time (or area) is needed to achieve a desired separation in a batch (or continuous) process.

Complex membrane columns and cascade arrangements have been researched (eg. Hwang and Ghalchi (1982), Kothe et al. (1989)), but a shortcut method for design and synthesis for these was lacking. In this thesis, it has been shown how, with the identification of a membrane column section, a novel design tool is developed. Any arrangement, no matter how complex, can be broken down into column sections. These are the basic building blocks that make up any arrangement. An understanding of the behaviour of each column sections allows one to synthesize and concatenate sections into a configuration that achieves the desired result. The compositional change of the retentate in any column section has been mathematically modelled using the difference point equation. All possible flow cases within a column section were identified, and their corresponding profiles investigated. Some of the important results are listed:

- The DPE for a column section operating at total reflux reduces to the M-RCM equation, as expected.
- The behaviour of a column profile, operating at finite conditions, is influenced by the movement of the stable node pinch point locus.
- A profile will continue to exist until it either the retentate or permeate runs out of material. When this occurs, the profile pinches, and the column section terminates, normally in a finite area.

Using these results, thermally-linked membrane columns were examined. It was found that such an arrangement is feasible, provided that the top composition was within a region bounded by the MBT and the appropriate pinch point curve. Furthermore, there exists a minimum reflux for each composition in that region. Operation would have to occur at or above the minimum reflux.

One of the most important and exciting results of the work in the thesis was the research completed thus far on hybrid processes. By analysing membrane permeation from the same mathematical viewpoint as distillation, combinations of the two

processes can be performed with ease. Also, since graphical techniques were developed for membrane systems as individual processes, any configuration and design of distillation and membrane units is possible. Analyzing them simultaneously (such as was done by Huang et al. (2004)) has a shortcoming in that it limits one to a single design. However, by decoupling the two unit operations from each other allows for all possible configurations to emerge – that is, *synthesize* rather than design. This was evident from the results obtained for the methanol/butene/MTBE system – an attainable region for the process was determined.

The technique then took on a new approach by collectively treating a hybrid arrangement as a thermally coupled arrangement between distillation and membrane units. With the use of column sections, general rules for classifying regions of feasible arrangements were developed.

Recommendations and Future Work

It should be appreciated that the work presented is not applicable to membrane permeation and distillation only, but can easily be adapted for *any* separation method. With both constant and non-constant flow assumptions have been tackled here, this then equips one to use the methods displayed for the separation procedure of their choice. Of course, details of equilibrium/flux model, flow assumptions and directions, etc. need to be decided upon. But the method and results arrived at here would still apply. This could be the basis of further research in the separations field.

Experimental validation of the profiles in the M-RCM is another possibility that could be explored. This could then be extended to formulating a batch- or continuous-scale experiment to mimic the finite reflux membrane column section.

Further theoretical and experimental work can be investigated with regard to hybrid designs, and the use of column profiles to design such processes.

REFERENCES

Agrawal, R. Membrane Cascade Schemes for Multicomponent Gas Separation. *Ind. Eng. Chem. Res.*, **1996**, *35*, 3607–3617.

Allgower, E.L. A survey of homotopy methods for smooth mappings. In: *E.L. Allgower, K. Glashoff and H.-O. Peitgen, Editors, Lecture Notes in Mathematics No. 878, Numerical Solution of Nonlinear Equations*, Springer-Verlag: New York, 1981, pp. 1–29.

Barbosa, D.; Doherty, M. F. The influence of Equilibrium Chemical Reactions on Vapor-Liquid Phase Diagrams. *Chem. Eng. Sci.* **1988**, *43*, 529–540.

Bauer, M. H.; Stichlmair, J. Design and economic optimization of azeotropic distillation processes using mixed-integer nonlinear programming. *Comp. Chem. Eng.*, **1998**, *22*, 1271–1286.

Bausa, J.; Marquardt, W. Shortcut Design Methods for Hybrid Membrane/Distillation Process for the Separation of Nonideal Multicomponent Mixtures. *Ind. Eng. Chem. Res.* **2000**, *39*, 1658–1672.

Bausa, J.; Watzdorf, R. V.; Marquardt, W. Shortcut Methods for Nonideal Multicomponent Distillation: 1. Simple Columns. *AIChE J.*, **1998**, *44* (*10*), 2181–2198, 1998.

Blaisdell, C. T.; Kammermeyer, K. Counter-current and co-current gas separation. *Chem. Eng. Sci.*, **1973**, *28*, 1249–1255.

Castillo, F. J. L.; Thong, D. Y. -C.; Towler, G. P. Homogeneous Azeotropic Distillation. 1. Design procedure for single-feed columns at nontotal reflux. *Ind. Eng. Chem. Res.*, **1998**, *37*, 987–997.

Chang, H.; Hou, W. Optimization of membrane gas permeation systems using genetic algorithm. *Chem. Eng. Sci.*, **2006**, *61*, 5355–5368.

Clement, R.; Bendjama, Z.; Nguyen, Q. T.; Néel, J. Extraction of organics from aqueous solutions by Pervaporation. A novel method for membrane characterization and process design in ethyl acetate separation. *J. Membr. Sci.*, **1992**, *66*, 193–203.

Daviou, M. C.; Hoch, P. M.; Eliceche, A. Design of membrane modules used in hybrid distillation/pervaporation systems. *Ind. Eng. Chem. Res.*, **2004**, *43*, 3403–3412.

den Heijerm C.; Rheinboldt, W. C. On steplength algorithms for a class of continuation methods. *SIAM J. Numer. Anal.* **1981,** *18*, pp. 925–948.

Doherty, M. F. Malone, M. F. *Conceptual Design of Distillation Systems*, McGraw-Hill: New York, 2001.

Eliceche, A. M.; Davio, M. C.; Hoch, P. M.; Uribe, I. O. Optimisation of azeotropic distillation columns combined with pervaporation membranes. *Comput. Chem. Eng.*, **2002**, *26*, 563–573.

Feng, X.; Huang, R. Y. M. Separation of isopropanol from water by Pervaporation using silicone-based membranes. *J. Membr. Sci.*, **1992**, *74*, 171–181.

Fidkowski, Z. T.; Malone, M. F.; Doherty, M. F. Nonideal multicomponent distillation: Use of bifurcation theory for design. *AIChE J.*, **1991**, *37* (12), 1761–1779.

Fidkowski, Z. T.; Doherty, M. F.; Malone, M. F. Feasibility of Separations for Distillation of Non-ideal Ternary Mixtures. *AIChE J.*, **1993**, *39* (*8*), 1303–1321.

Fien, G. A. F.; Liu, Y. A. Heuristic Synthesis and Shortcut Design of Separation Processes Using Residue Curve Maps: A Review. *Ind. Eng. Chem. Res.* **1994**, *33*, 2505–2522.

Holland, S. T.; Tapp, M.; Hildebrandt, D.; Glasser, D.; Hausberger, B. Novel separation system design using "moving triangles". *Comput. Chem. Eng*, **2004a**, *29*, 181–189.

Holland, S. T.; Tapp, M.; Hildebrandt, D.; Glasser, D. Column profile maps. 2. Singular points and phase diagram behaviour in ideal and non-ideal systems. *Ind. Eng. Chem. Res.*, **2004b**, *43*, 3590–3603.

Hommerich, U.; Rautenbach, R. Design and optimization of a combined pervaporation/distillation process for the production of MTBE. *J. Mem. Sci.*, **1998**, *146*, 53–64.

Hoover, K. C.; Hwang, S. T. Pervaporation by continuous membrane column. *J. Mem. Sci.*, **1982**, *10*, 253–271 .

Huang, Y., Sundmacher, K., Qi, Z. & Schlunder, E. Residue curve maps of reactive membrane separation. *Chem. Eng. Sci.* **2004**, 59, 2863–2879.

Hwang, S. T.; Ghalchi, S. Methane Separation by a continuous membrane column. *J. Mem. Sci.*, **1982**, *11*, 187–198.

Hwang, S.; Thorman, J. M. The Continuous Membrane Column. *AIChE J.*, **1980**, *26* (4), 558–566.

Julka, V.; Doherty, M. F. Geometric Behavior and Minimum Flows for Nonideal Multicomponent Distillation. *Chem. Eng. Sci.*, **1990**, *45* (*7*), 1801–1822.

Julka, V.; Doherty, M. F. Geometric Nonlinear Analysis of Multicomponent nonideal Distillation: A Simple Computer-Aided Design Procedure. *Chem. Eng. Sci.*, **1993**, *48* (*8*), 1367–1391.

Kao, Y. K.; Qiu, M. M; Hwang, S. T. Critical evaluations of two membrane gas permeators designs: Continuous membrane column and two strippers in series. *Ind. Eng. Chem. Res.*, **1989**, *28*, 1514–1520.

Kearfott, R. B. Rigorous Global Search: Continuous Problems. Kluwer Academic Publishers: Dordrecht, Netherlands, 1996.

Keller, H. B. Lectures on Numerical Methods in Bifurcation Problems. Springer-Verlag: Heidelberg, Germany, 1987.

King, C. J. *Separation Processes*, McGraw-Hill: New York,1971.

Kiva, V. N.; Hilmen, E. K.; Skogestad, S. Azeotropic phase equilibrium diagrams: a survey. *Chem. Eng. Sci.* **2003**, *58*, 1903–1953.

Knapp, J. P.; Doherty, M. F. Minimum Entrainer Flows for Extractive Distillation: A Bifurcation Theoretic Approach. *AIChE J.*, **1994**, *40* (*2*), 243–268.

Kookos, I. Optimal design of membrane/distillation column hybrid processes. *Ind. Ng. Chem. Res.*, **2003**, *42*, 1731–1738.

Kothe, K. D.; Chen, S.; Kao, Y. K.; Hwang, S. T. A study of the separation behaviour of different membrane columns with respect to ternary gas mixtures. *J. Mem. Sci.*, **1989**, *46*, 261–281.

Lang Y.; Biegler L.T.; Distributed stream method for tray optimization. *AIChE J.*, **2002**, *48*, 582–595.

Lelkes, Z.; Szitkai, Z.; Rev, E.; Fonyo, Z. Rigorous MINLP model for ethanol dehydration system. *Comput. Chem. Eng*, **2000**, *24*, 1331–1336.

Levy, S.; Van Dongen, D.; Doherty, M. F. Design and Synthesis of Homogenous Azeotropic Distillations. 2. Minimum Reflux Calculations for Nonideal and Azeotropic Columns. *Ind. Eng. Chem. Fundam.*, **1985,** *24* (*4*), 463–474.

Lipnizki, F.; Field, R. W.; Ten, P. K. Pervaporation-based hybrid process: a review of process design, applications and economics. *J. Mem. Sci.*, **1999**, *153*, 183–210.

Lu, Y.; Zhang, L.; Chen, H.; Qian, Z; Gao, C. Hybrid process of distillation side-connected with pervaporation for separation of Methanol/MTBE/C_4 mixture. *Desalination*, **2002**, *149*, 81–87.

Lucia A.; Fang Y. Multivariable terrain methods. *AIChE J.*, **2003**, *49*, 2553.

Marriot, J. I.; Sørensen, E.; Bogle, I. D. L. Detailed mathematical modelling of membrane modules. *Comput. Chem. Eng.*, **2001**, *25*, 693–700.

Marriott, J.; Sørensen, E. A general approach to modelling membrane modules. *Chem. Eng. Sci.*, **2003a**, *58*, 4975–4990.

Marriott, J.; Sørensen, E. The optimal design of membrane systems. *Chem. Eng. Sci.*, **2003b**, *58*, 4991–5004.

Matson, S. L.; Lopez, J.; Quinn, J. A. Separation of gases with synthetic membranes. *Chem. Eng. Sci.*, **1983**, *38* (4), 503–524.

McCandless, F. P. Comparison of counter-current recycle cascades with continuous membrane columns for gas separation. *Ind. Eng. Chem. Res.*, **1990**, *29*, 2167–2170.

McCandless, F. P. A comparison of membrane cascades, some one-compressor recycle permeators, and distillation. *J. Mem. Sci.*, **1994**, *89*, 51–72.

Peters, M.; Kauchali, S.; Hildebrandt, D.; Glasser, D. Derivation and Properties of Membrane Residue Curve Maps, *Ind. Eng. Chem. Res.*, **2006a**, *45*, 9080–9087.

Peters, M.; Kauchali, S.; Hildebrandt, D.; Glasser, D. Separation of methanol/butene/MTBE using hybrid distillation-membrane processes. In *Distillation & Absorption 2006*, **2006b** IChemE, *Symposium Series 152*. Sorensen, E. (Ed.), 152–161.

Peters, M.; Kauchali, S.; Hildebrandt, D.; Glasser, D. Application of Membrane Residue Curve Maps to Batch and Continuous Processes. *Ind. Eng. Chem. Res.*, **2008**, accepted for publication.

Peters, M.; Kauchali, S.; Hildebrandt, D.; Glasser, D. Column profiles for membrane column sections. *Ind. Eng. Chem. Res.*, **2007**, submitted for publication.

Pettersen, T.; Argo, A.; Noble, R. D.; Koval, C. A. Design of combined membrane and distillation processes. *Sep. Tech.*, **1996**, *6*, 175–187.

Pham, H. N.; Doherty, M. F. Design and synthesis of heterogeneous azeotropic distillations – III. Column sequences. *Chem. Eng. Sci.*, **1990**, *45* (7), 1845–1854.

Pressly, T. G.; Ng, K. M. A Break-Even Analysis of Distillation-Membrane Hybrids. *AIChE J.*, **1998**, *44* (1), 93–105.

Qiao, X.; Chung, T.; Guo, W. F.; Matsuura, T.; Teoh, M. M. Dehyration of isopropanol and its comparison with dehydration of butanol isomers from thermodynamic and molecular aspects. *J. Membr. Sci.*, **2005**, *252*, 37–49.

Rautenbach, R,; Albrecht, R. The Separation Potential of Pervaporation. Part 1. Discussion of Transport equations and comparison with Reverse Osmosis. *J. Membr. Sci.*, **1985a**, *25*, 1–23.

Rautenbach, R.; Albrecht, R. The Separation Potential of Pervaporation. Part 1. Proceess Design and Economics. *J. Membr. Sci.*, **1985b**, *25*, 25–54.

Rautenbach, R.; Albrecht, R. *Membrane Processes*, John Wiley: New York, 1989

Serafimov, L. A. General principles of the course of unidistribution lines in vapour-liquid equilibrium diagrams of ternary mixtures. *Physical-chemical foundations of rectification, collection of papers by Moscow Lomonosov Institute of Fine Chemical Technology*; MITChT: Moscow, 1970; pp. 20–30.

Smith E. M.; Pantelides C. C. Design of reaction/separation networks using detailed models. *Comp. Chem. Eng.*, **1995**, *19*, S83–S88.

Sommer, S.; Melin, T.; Design and Optimization of Hybrid Separation Processes for the Dehydration of 2-Propanol and Other Organics. *Ind. Eng. Chem. Res.*, **2004**, *43*, 5248–5259.

Stadther, M. A.; Schnepper, C.A.; Brennecke, J. F. Robust phase stability analysis using interval methods. *AIChE Symp. Ser.*, **1995**, *91* (*304*), 356.

Stepahn, W.; Noble, D. R.; Koval, C. A. Design methodology for a membrane/distillation column hybrid process. *J. Membr. Sci.***, 1995**, *99*, 259–272.

Stoica-Guzun, A.; Abulescu, C.; Juncu, G. H.; Floarea, O. Extraction of urea with liquid surfactant membranes in a batch system. *Chem. Eng. Sci.*, **1996**, *51*, 4745 – 4747.

Stradi, B. A.; Brennecke, J. F.; Kohn, J. P.; Stadtherr, M. A. Reliable computation of mixture critical points. *AIChE J.*, **2001**, *47*, 212–221.

Tapp, M.; Holland, S. T.; Hildebrandt, D.; Glasser, D. Column Profile Maps. 1. Derivation and Interpretation. *Ind. Eng. Chem. Res.*, **2004**, *43*, 364–374.

Tessendorf, S.; Gani, R.; Michelsen, M. L. Modeling, simulation and optimization of membrane-based gas separation systems. *Chem. Eng. Sci.*, **1999**, *54*, 943–955.

Tsuru, T; Hwang, S. T. Permeators and continuous membrane columns with retentate recycle. *J. Mem. Sci.*, **1995**, *98*, 57–67.

Van Hoof, V.; Van den Abeele, L.; Bukenhoudt, A.; Dotremont, C.; Leysen, R. Economic comparison between azeotropic distillation and different hybrid systems combining distillation with pervaporation for the dehydration of isopropanol. *Sep. Purif. Technol.*, **2004**, *37* (1), 33–49.

Verhoef, A.; Degreve, J.; Huybrechs, B.; van Veen, H.; Pex, P.; Van der Bruggen, B. Simulation of a hybrid pervaporation-distillation process. *Comput. Chem. Eng.*, **2007**, doi: 10.1016/j.compchemeng.2007.04.014.

Viswanathan J,; Grossmann I. E. Optimal feed locations and number of trays for distillation columns with multiple feeds. *Ind. Chem. Eng. Res.*, **1993**; *32*, 2942–1949.

Vorotyntsev, V. M.; Drozdov, P. N. Ultrapurification of gases in a continuous membrane column cascade. *Sep. Purif. Techol.*, **2001**, *22-23*, 367–376.

Watson, L. T.; Billups, S. C.; Morgan, A. P. ALGORITHM 652: HOMPACK: A Suite of Codes for Globally Convergent Homotopy Algorithm, *ACM TOMS*, **1987**, *13*, 281.

Watzdorf, R. V.; Bausa, J.; Marquardt, W. Shortcut Methods for Nonideal Multicomponent Distillation: 2. Complex Columns. *AIChE J.*, **1999**, *45* (*8*), 1615–1628.

Wijmans, J. G.; Baker, R. W. The solution-diffusion model: a review. *J. Membr. Sci.*, **1995**, *107*, 1–21.

Yoshisato, R. A.; Hwang, S. Computer Simulation of a Continuous Membrane Column. *J. Membr. Sci.*, **1984**, *107*, 1–21.

Zhang, L.; Linninger A. A. Temperature Collocation Algorithm for Fast and Robust Distillation Design. *Ind. Eng. Chem Res.*, **2004**, *43*, 3163–3182.

Zhang, L.; Linninger, A. A. Towards computer-aided separation synthesis. *AIChE J.*, **2006**, *52* (4), 1392–1409.

APPENDIX A: DERIVATION OF THE RESIDUE CURVE EQUATION

Refer to Figure 2.1. It is known that, from equation 2.1:

$$\dot{P} = -\frac{d}{dt}(R), \tag{A.1}$$

and that, from equation 2.2:

$$0 = \dot{P} \cdot y_i + \frac{d}{dt}(R \cdot x_i) = \dot{P} \cdot y_i + R \cdot \frac{d}{dt}(x_i) + x_i \cdot \frac{d}{dt}(R). \tag{A.2}$$

Substituting equation A.1 into A.2:

$$0 = y_i \cdot \left(-\frac{d}{dt}(R) \right) + R \cdot \frac{d}{dt}(x_i) + x_i \cdot \frac{d}{dt}(R). \tag{A.3}$$

Rearranging:

$$\frac{R\dfrac{d}{dt}(x_i)}{-\dfrac{d}{dt}(R)} = (x - y) \tag{A.4}$$

Cancelling:

$$-R\frac{d}{dR}(x_i) = (x - y) \tag{A.5}$$

Now, it can be shown that:

$$\frac{d}{dR}\left(\ln\left(\frac{k}{R}\right)\right) = -\frac{1}{R}, \tag{A.6}$$

where k is a constant. Hence:

$$d\ln\left(\frac{k}{R}\right) = -\frac{dR}{R}. \tag{A.7}$$

Let:

$$d\tau = -\frac{dR}{R}. \tag{A.8}$$

Thus:

$$\frac{d}{d\tau}(x_i) = (x_i - y_i) \tag{A.9}$$

This is the residue curve equation. Further manipulation is needed in order to define τ.

By rearranging equation A.1 and substituting into equation A.8:

$$d\tau = \frac{P}{R}dt. \tag{A.10}$$

Or:

$$\tau = \frac{P}{R} t \,. \tag{A.11}$$

Thus, at $t = 0$, $\tau = 0$, and $R = R(0)$, hence:

$$\ln\left(\frac{k}{R(0)}\right) = 0 \tag{A.12}$$

Or:

$$k = R(0) \,. \tag{A.13}$$

Thus:

$$d\tau = d\ln\left(\frac{R(0)}{R(t)}\right) \tag{A.14}$$

Or:

$$\tau = \ln\left(\frac{R(0)}{R(t)}\right) \tag{A.15}$$

APPENDIX B: FLUX MODEL FOR METHANOL/BUTENE/MTBE

PERVAP 1137 (Sulzer ChemTech ®) has the following empirical formulae for calculating the flux of each component through the membrane (1 = methanol, 2 = butene, 3 = MTBE) (Bausa and Marquardt (2000)):

$$J_1 = k_1\left(\gamma_1 x_1 + \frac{\pi_P}{p_1^0}\right)\left(\gamma_1 p_1^0 x_1 - \pi_P\right) \tag{B.1}$$

$$J_2 = k_2\gamma_2 p_2^0 x_2 J_1 \tag{B.2}$$

$$J_3 = k_3\gamma_3 p_3^0 x_3 J_1 \tag{B.3}$$

where k_i is the transfer parameter value for component i (see below for the values)

γ_i is the activity coefficient for component i,

p_i^0 is the saturation pressure of component i.

1 = Methanol, 2 = Pentane, 3 = MTBE. Pentene is used since there was a lack of experimental data for i-Butene, and also since it is chemically similar to 1-Butene. The parameter values, with appropriate units, are:

$$k_1 = 4.000\times10^{-5}\,\frac{kmol}{s\cdot m^2\cdot bar}, \tag{B.4}$$

$$k_2 = 1.375\times10^{-4}\,/\,bar\text{, and} \tag{B.5}$$

$$k_3 = 3.250\times10^{-4}\,/\,bar \tag{B.6}$$

APPENDIX C: PROOF OF EQUATION FOR DETERMINING PERMEATION TIME IN A BATCH PROCESS

The material balance over the batch still is (refer Figures 2.1 and 3.2, and equation 2.1):

$$\frac{dR}{dt} = -\dot{P} \tag{C.1}$$

Thus

$$t = -\int_{R(0)}^{R(t)} \frac{1}{\dot{P}} \cdot dR \tag{C.2}$$

The permeate removal rate is not a constant, and depends on the flux of material through the membrane:

$$J = \sum_{i=1}^{c} J_i = \frac{\dot{P}}{A} \sum_{i=1}^{c} y_i = \frac{\dot{P}}{A} \tag{C.3}$$

Thus

$$\dot{P} = JA \tag{C.4}$$

Resulting in

$$t = -\frac{1}{A} \int_{R(0)}^{R(t)} \frac{1}{J} \cdot dR \tag{C.5}$$

for a constant area (batch). Since J is a function of x, need to change dR to dx_i. The residue curve equation is:

$$\frac{d}{d\tau}(x_i) = (x_i - y_i) \tag{C.6}$$

Resulting in

$$d\tau = \frac{dx_i}{x_i - y_i(x)} \tag{C.7}$$

Or

$$\tau = \int_{x_i(0)}^{x_i(f)} \frac{1}{x_i - y_i(x)} \cdot dx_i \tag{C.8}$$

We see that τ is a function of x. Also, from the definition of τ:

$$\tau = \ln\left[R(0) \Big/ R(t) \right] \tag{C.9}$$

Thus

$$R(t) = R(0) \cdot e^{-\tau} \tag{C.10}$$

And

$$d\tau = -\frac{1}{R} dR \tag{C.11}$$

Which means that:

$$dR = -\frac{R(0)\cdot e^{-\tau}}{x_i - y_i(x)}\cdot dx_i \tag{C.12}$$

So

$$t = \frac{R(0)}{A}\int_{x_i(0)}^{x_i(t)} \frac{e^{-\tau}}{x_i - y_i(x)}\cdot\frac{1}{J}\cdot dx_i \tag{C.13}$$

Using the flux of component *i* rather than the total flux:

$$t = \frac{R(0)}{A}\int_{x_i(0)}^{x_i(t)} \frac{y_i(x)\cdot e^{-\tau}}{x_i - y_i(x)}\cdot\frac{1}{J_i}\cdot dx_i \tag{C.14}$$

For gas permeation using constant relative permeabilities (Knudsen membrane) and maintaining a vacuum on the permeate side (refer to equation B.15):

$$t = R(0)\frac{\delta}{A\cdot P_i'\cdot\pi_R}\cdot\int_{x_i(0)}^{x_i(f)} \frac{y_i(x)}{x_i}\frac{1}{x_i - y_i(x)}e^{-\tau}\cdot dx_i \tag{C.15}$$

APPENDIX D: DISTILLATION & ABSORPTION 2006

The material given here was presented at the Distillation & Absorption 2006 Conference in London, UK. This is a scanned version from the Symposium Series for the conference. The reference is Peters et al. (2006b):

> Peters, M.; Kauchali, S.; Hildebrandt, D.; Glasser, D. Separation of methanol/butene/MTBE using hybrid distillation-membrane processes. In *Distillation & Absorption 2006*, **2006b** IChemE, *Symposium Series 152*. Sorensen, E. (Ed.), 152–161.

This work formed the basis for the work presented in Chapter 3, Section 3.6

SYMPOSIUM SERIES NO. 152 © 2006 IChemE

SEPARATION OF METHANOL/BUTENE/MTBE USING HYBRID DISTILLATION-MEMBRANE PROCESSES

Mark.Peters, Shehzaad Kauchali, Diane Hildebrandt, David Glasser
Centre of Materials and Process Synthesis, School of Chemical and Metallurgical Engineering, University of the Witwatersrand, Private Bag 3, WITS 2050, Johannesburg, South Africa;
E-mails: mpeters@prme.wits.ac.za; shehzaad.kauchali@comps.wits.ac.za; dihil@comps.wits.ac.za; david.glasser@comps.wits.ac.za

Distillation Residue Curve Maps (D-RCM's) have proven to be an extremely useful graphical tool in the design and operation of both batch and continuous distillation processes. Recently submitted work by the authors has investigated the applications of Residue Curve Maps for membrane permeation systems. Such maps are referred to as M-RCM's. This paper aims to develop a graphical tool to provide insight in sequencing combinations of unit processes in complex systems. As an example, the separation of a methanol/butene/MTBE system is investigated. MTBE is the desired product, and hence needs to be efficiently recovered from a reactor product. Difficulty arises when separating such a mixture with traditional distillation processes, because of the binary azeotropes that exist between methanol and MTBE, as well as methanol and butene. A membrane is suited for such a separation since it is not limited by relative volatility constraints. Using available data for the permeation rates of the components through a chosen membrane, the M-RCM was plotted. The M-RCM, along with column profile maps, facilitated a graphical method to select a combination of profiles to obtain the desired product(s). The method displayed can be applied to the design, as well as extended to the synthesis of hybrid processes. Maintaining an appropriate permeate pressure, it was found that crossing the distillation boundary is possible!

KEYWORDS: distillation, membranes, residue curve maps, separation, graphical, hybrid, design

INTRODUCTION AND LITERATURE REVIEW

Methyl tertiary-Butyl Ether (MTBE) is a fuel additive. Its demand has increased due to an environmental drive to phase-out lead-compound emissions in fuels. MTBE is produced industrially by the reaction between methanol and *i*-butene. *i*-Butene arises from a cracking plant, and arrives at the reactor as part of a C4 hydrocarbon stream. For simplicity, it is assumed that the C4 stream contains only *i*-butene and 1-butene. The reaction is equilibrium limited, and in order to obtain high conversions of *i*-butene, methanol is fed in excess (Rehfinger and Hoffmann, 1990). It can further be assumed that the ratio of methanol to *i*-butene is such that all the *i*-butene is converted. The reactor product, therefore, consists of recently formed MTBE, unconverted methanol as well as 1-butene.

© 2006 IChemE

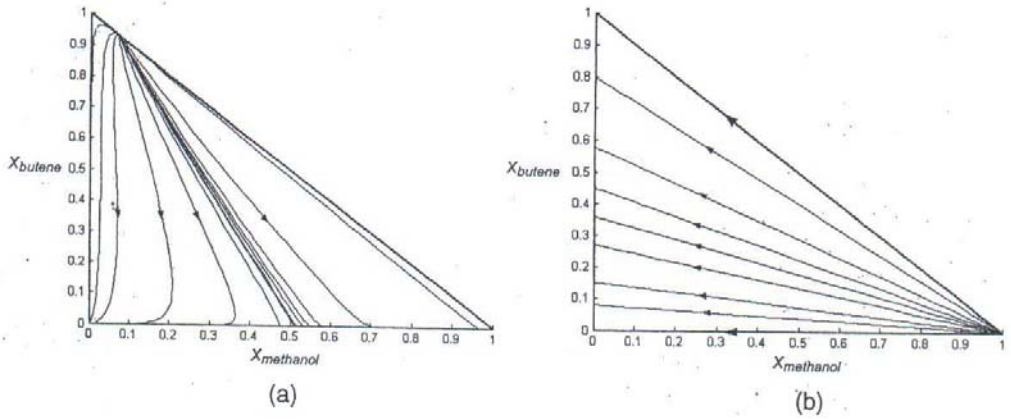

Figure 1. (a) D-RCM at P = 6bar. (b) M-RCM for a vacuum permeate pressure

The reactor product needs to be efficiently separated. Figure 1(a) shows the Distillation Residue Curve Map (D-RCM) for the system. In the traditional Hüls process (Bausa and Marquardt, 2000), a two-column sequence is used. The first column operates at a pressure of 6bar. The distillate composition is nearly that of the butene/methanol azeotrope. This stream is sent back to the cracking plant from where the C4 stream originated. The bottoms is sent to the second column where pure MTBE is produced, as well as an azeotropic mixture of methanol and MTBE. To avoid too much MTBE reporting to the azeotropic mixture, the pressure in the second column is increased to about 12bar. The MTBE is the required product, while the methanol (containing MTBE) is recycled back to the reactor.

In an attempt to recover more of the MTBE that is produced in the reactor, a membrane could be used to facilitate the separation. Various membranes have been developed for such a separation (Bangxiao et al., 2001; Bausa and Marquardt, 2000; Hommerich and Rautenbach, 1998; Lu et al., 2002).

This paper focuses on the use of a distillation-membrane hybrid as an alternative to the Hüls process. Such an alternative is not something new, but has been researched before (Bausa and Marquardt, 2000; Hommerich and Rautenbach, 1998; Lu et al., 2002). What we propose in this paper is simply a novel graphical method of designing such systems. Lu et al. (2002) manage to design a hybrid process using rigorous mathematical calculations, but their method does not enable them to examine other configurations. Hommerich and Rautenbach (1998) examine the feasibility of various process configurations. They design each of these using ASPEN PLUS® with a FORTRAN subroutine for the membrane unit. Their optimization techniques however are somewhat trial-and-error. Bausa and Marquardt (2000) utilize shortcut methods for design of both the distillation and membrane units. This enables them to design the hybrid process graphically. However, the reflux and/or reboil ratios, as well as the number of theoretical trays

 © 2006 IChemE

needed are not so easily accessible. They do furnish the reader with a method to obtain the minimum membrane area required.

In order to formulate a graphical technique for designing hybrid systems, Membrane Residue Curve Maps (M-RCM's) were developed Peters et al. (2006). These maps were developed in much the same manner as D-RCM's. The resulting equations, in fact, were shown to be identical to those used in plotting a D-RCM. Using appropriate flux equations to model the permeate phase as a function of the retentate composition, one is able to plot such a map. The plot shows the compositional change of the retentate as permeation proceeds. PERVAP 1137 is a membrane manufactured by Sulzer Chemtech® that is selective to methanol permeation. Bausa and Marquardt (2000) give flux model data for this particular membrane. Using this data, the M-RCM was plotted, as shown in Figure 1(b).

The membrane can not be used as a stand alone unit to produce the required products, since it is possible to only obtain a pure methanol stream (refer to Figure 1(b)). Hence needs to be used in conjunction with a distillation column. Unlike distillation, the membrane is not dependant on relative volatilities, and hence the distillation boundary can be crossed. Furthermore, the functioning of the membrane is highly dependant on the permeate pressure Peters et al. (2006), and needs to be taken into consideration. It has previously been shown how the map changes with various permeate pressures. For the hybrid design described here, it will be assumed that the permeate pressure is sufficiently close to vacuum.

DESIGN REQUIREMENTS

The required products from the hybrid separation are:

- An essentially pure MTBE stream,
- A pure methanol stream, which will be recycled back to the reactor, and
- A butene-rich stream, which will be returned back to the plant from which it originated.

Table 1 shows the compositions of the feed and product streams.

Table 1. Steam composition

Stream	Composition [methanol, butene, MTBE]
Feed (F)	[0.45, 0.09, 0.46]
Distillate (D)	[0.07, 0.925, 0.005]
Permeate (P)	[1, 0, 0]
Bottoms (B)	[0.001, 10^{-7}, 0.998999]

SYMPOSIUM SERIES NO. 152
© 2006 IChemE

HYBRID DESIGNS

There are many configurations for hybrid systems that can be explored: placing the membrane upstream from the column, or placing it downstream. One could also side-connect the membrane to the column in various ways. In this paper, we will now look at two particular configurations. In the first, an example of how one can *synthesize* a configuration is discussed. In the second, a system is chosen and the details of the method of *design* are given.

MEMBRANE UPSTREAM OF COLUMN

On the D-RCM (refer to Figure 1(a)), MTBE has the highest boiling point, and would thus, traditionally, be expected to be the bottoms product of distillation column, irrespective of membrane placement. Using this, one could generate the operating leaf (Castillo et al. (1998)) for the required MTBE product composition. Similarly, the methanol/butene azeotrope is the lowest boiling point on the D-RCM, and would more than likely be the distillate. The operating leaves for both the rectifying and stripping sections have been superimposed and are shown in Figure 2(a).

One can see that a bifurcation occurs within the rectifying leaf, resulting in an "open" leaf. This occurs at a reflux of about 0.31. Furthermore, and more importantly, there is a definite overlap of the two leaves, indicating that a standard single feed, two

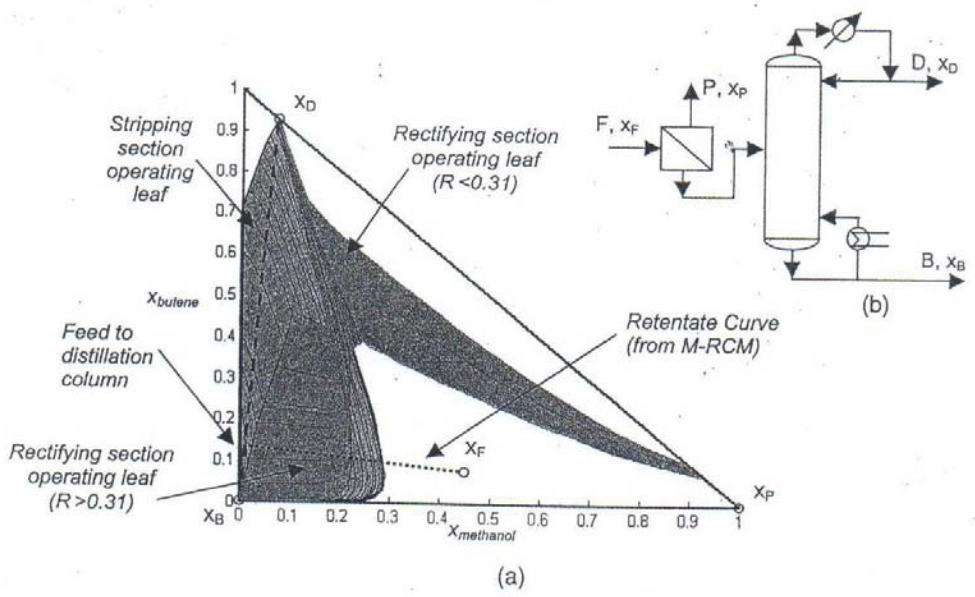

Figure 2. (a) Operating leaves for distillate and bottoms products, and membrane profile for the (b) process configuration

 © 2006 IChemE

product column is feasible. A further requirement for such a column to be practical is that the feed composition (to the column) has to lie on the straight line connecting x_D and x_B, by material balance. The overall feed (from the reactor), however, does not obey this requirement (refer to Figure 2(a)).

A membrane can be used before the column in order to move the overall feed to a point on the straight line connecting x_D and x_B. The membrane will deplete the feed of most of its methanol. The M-RCM shows the exact path the retentate will follow from feed composition to the desired composition of the distillation feed, as shown in Figure 2(a). Figure 2(b) shows the synthesized process configuration.

Once the distillation feed is obtained, the design of the column proceeds using "traditional" methods. The actual choice of reboil/reflux ratio(s) depends on an optimization process, which is out of the scope of this particular report, but will be discussed in a future publication.

MEMBRANE SIDE-CONNECTED TO THE COLUMN

The configuration discussed in Section 3.1 above was synthesized, rather than designed. In this option, a particular chosen sequence of units is designed.

Consider the hybrid configuration shown in Figure 3(a).

The MTBE, having the highest boiling point, will report to the bottom of the column. At 6bar, the highest concentration of butene obtainable, without losing too much MTBE would be the binary methanol/butene azeotrope (refer to Figure 1(a)). The azeotrope has the lowest boiling point on the map, and will be removed at the top of the column. The methanol will be a product of the membrane.

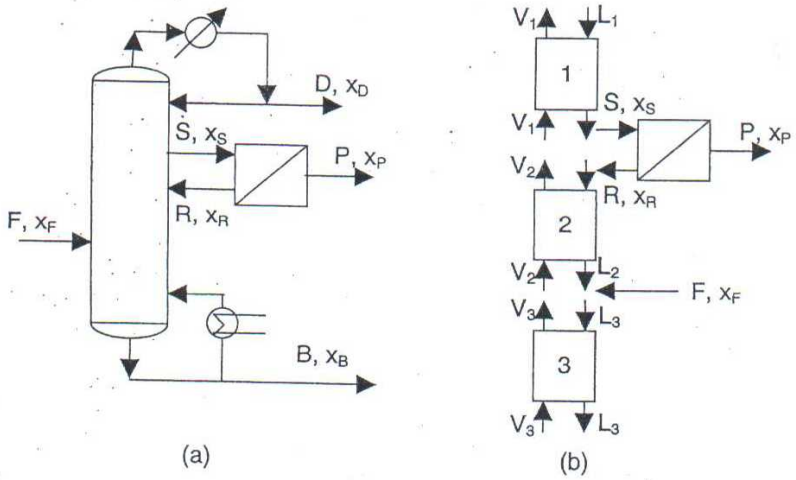

Figure 3. (a) A possible hybrid configuration, (b) the column sections for the hybrid system

 © 2006 IChemE

This process shown in Figure 3(a) can be broken up into the column sections (Tapp et al., 2004), as shown in Figure 3(b). Each column section (1–3) has its own unique profile. The difference point equation (DPE) describing a column profile is (the constant molar overflow assumption is employed):

$$\frac{dx}{dn} = \left(\frac{1}{R_\Delta} + 1\right)(x - y^*) + \frac{1}{R_\Delta}(X_\Delta - x) \tag{1}$$

with

$$X_\Delta = \frac{V \cdot y_T - L \cdot x_T}{\Delta}; \quad R_\Delta = \frac{L}{\Delta} \text{ and } \Delta = V - L \tag{2}$$

where x is the liquid composition
n is the number of theoretical stages
y^* is the vapour in equilibrium with x
X_Δ is the difference point
V is the molar vapour flowrate in a column section [mol/s]
L is the molar liquid flowrate in a column section [mol/s]
R_Δ is the reflux ratio
Δ is the net molar flow in a section [mol/s]
x_T and y_T are the molar liquid and vapour compositions at the top of a column section

The profile for each of the sections depends on the X_Δ- and R_Δ-values for that particular section. It is worth noting that should the constant molar assumption be relaxed, equation (1) still holds true since it is merely a differential material balance across a column section. One can prove this result, but it is not given here since it is out of the scope of this report. Holland et al. (2004) show that any distillation configuration, no matter how complex, can be modeled using column profile maps (CPM). The method described below is an extension of the work put forward by Holland et al. (2004). While Holland et al. (2004) focused on distillation only, we include the addition of a membrane unit linked to column sections.

Method of design

- On the map(s), locate feed point
- Identify and plot compositions of product streams
- Perform overall and component material balance across the *entire* system:

$$F = D + P + B \quad \text{and} \quad Fx_F = Dx_D + Px_P + Bx_B \tag{3}$$

This will allow one to establish the product flowrates for a specified feed.

The method will follow a "bottom-up" calculation, commencing with section 3, and ending at section 1.

 © 2006 IChemE

Section 3:

- In section 3, material is being removed at the end of the section:

$$\Delta_3 = V_3 - L_3 = -B \tag{4}$$

meaning that the net flow of material in section 3 is downward.
- Plot the column profile for section 3 using x_B and various $R_{\Delta 3}$-values. The stripping section operating leaf shown in Figure 2(a) shows various profiles for this section.
- An appropriate $R_{\Delta 3}$-value must be chosen, remembering that it is negative in sign. Figure 4(a) shows the section profile at a selected $R_{\Delta 3}$-value.

Section 2:

- Calculate $X_{\Delta 2}$ using the material balances around the feed point:

$$F = \Delta_2 + B \quad \text{and} \quad Fx_F = \Delta_2 X_{\Delta 2} + Bx_B \tag{5}$$

This implies that x_F must lie on the straight line between $X_{\Delta 2}$ and x_B.
- Calculate $R_{\Delta 2}$ by mass balance across the feed, assuming the feed is all liquid.
- Produce an entire CPM using $X_{\Delta 2}$ and $R_{\Delta 2}$ – use this map to select candidate profiles, when necessary (see later). This map is shown in Figure 4(a).

Section 1:

- The mass balance around the membrane side-draw and return is:

$$\Delta_2 = D + P \quad \text{and} \quad \Delta_2 X_{\Delta 2} = Dx_D + Px_P \tag{6}$$

implying that $x_{\Delta 2}$ must lie on the straight line between x_D and x_P.

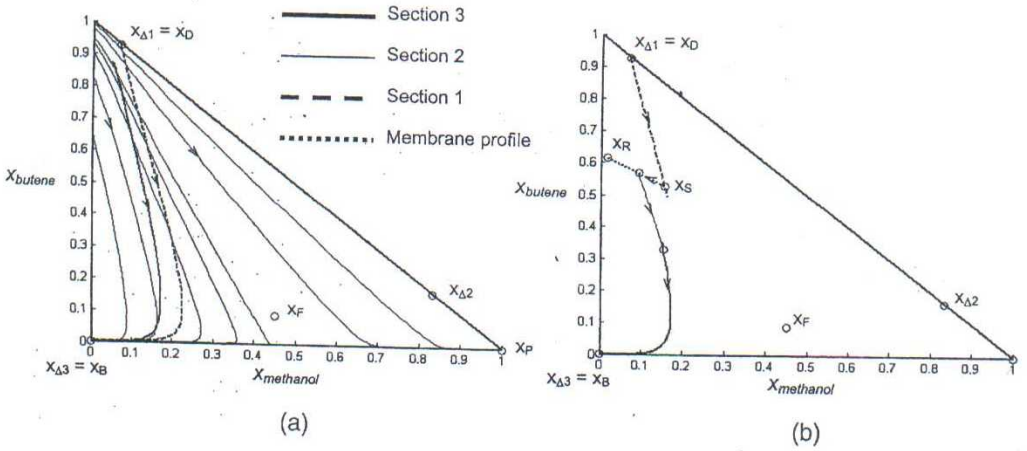

Figure 4. Profile maps for the various column sections (refer to Figure 3(b)) and the membrane unit

 © 2006 IChemE

- Determine $R_{\Delta 1}$ using equation (6)
- $X_{\Delta 1}$ is fixed – it is the distillate composition, x_D.
- Plot column profile for section 1, as shown in Figure 4(a)

Putting it all together...

- Now, starting at the distillate composition, follow the profile for section 1. It is the designers choice where to end this section. But it should be remembered that numerous stages are needed for a profile to "go around the corner" as a profile approaches a saddle node. It is therefore assumed that section 1 should be terminated well before any corners!
- Using section 1's exit liquid composition as the feed to membrane, perform the mass balance to ensure that the retentate composition lies within the MBT. If this is not the case, then one needs to re-set the value for $R_{\Delta 3}$.
- Also remember that not all the liquid leaving section 1 is fed to the membrane, and that the retentate is then mixed with the remaining liquid to give the liquid entering the top of section 2.
- Follow the profile for section 2, ensuring that it intersects with section 3 at composition within the MBT. If this is not the case, then the designer needs to re-evaluate the termination point of section 1.
- It is necessary to note the *direction* of the profiles. The configuration is not feasible if the directions of each of profiles do not match the order of the sections.

Using the above method, a design was arranged. Figure 4(b) shows where the profiles for each section commence and terminate. It is worth noting that this design is, by no means, necessarily the optimal design for the chosen hybrid configuration.

CLOSING REMARKS

In this article, it has been shown that using both D- and M-RCM's it is possible to graphically interpret hybrid distillation/membrane processes. It has been revealed how one can synthesize a configuration for a particular separation, as well as design a given arrangement. The methods, while being trial-and error, utilize a graphical technique making this method novel: With the use of column profiles, it is possible to retrieve data such as the reflux/reboil ratio as well as the theoretical number of stages needed in each section. Furthermore, using the M-RCM, it is possible to obtain the required membrane area to achieve the necessary separation. This approach of designing hybrid systems can be extended to many configurations, which can ultimately be screened by an optimization technique. It should be obvious that the sequencing of the separation units in a hybrid process is such that each unit operates in the region of the composition space where its separation ability is best suited and most effective.

This article only highlights two possible configurations, and does not by any means attempt to optimally design each. Additionally, an overall optimum design is not sought, since it is out the scope this particular article. Future publications from the authors will give detailed methods of optimization techniques that can be employed.

 © 2006 IChemE

NOMENCLATURE

SYMBOLS

B	Bottoms [mol/s]
D	Distillate [mol/s]
Δ	Net molar flow in a section [mol/s]
F	Feed [mol/s]
L	Molar liquid flowrate in a column section [mol/s]
n	Number of stages [−]
P	Permeate [mol/s]
R	Retentate [mol/s]
R_Δ	Reflux ratio [−]
S	Side-draw [mol/s]
V	Molar vapour flowrate in a column section [mol/s]
x	Liquid composition [−]
x_T	Molar liquid composition at the top of a column section [−]
X_Δ	Difference point [−]
y^*	Vapour in equilibrium with x [−]
y_T	Molar vapour composition at the top of a column section [−]

ABBREVIATIONS

CPM	Column Profile Map
DPE	Difference Point Equation
D-RCM	Distillation Residue Curve Map
MBT	Mass Balance Triangle
M-RCM	Membrane Residue Curve Map
MTBE	Methyl tertiary Butyl Ether

REFERENCES

Bangxiao, C., Lu, Y., Hailin, Y. & Congjie, G. (2001). Effect of separating layer in pervaporation composite membrane for MTBE/MeOH separation. *Journal of Membrane Science*, 194, 151–156.

Bausa, J. & Marquardt, W. (2000). Shortcut Design Methods for Hybrid Membrane/Distillation Process for the Separation of Nonideal Multicomponent Mixtures. *Industrial and Engineering Chemistry Research*, 39, 1658–1672.

Castillo, F. J. L., Thong, D. Y. -C. & Towler, G. P. (1998). Homogeneous Azeotropic Distillation. 1. Design procedure for single-feed columns at nontotal reflux. *Industrial and Engineering Chemistry Research*, 37, 987–997.

Holland, S. T., Tapp, M., Hildebrandt, D., Glasser, D. & Hausberger, B. (2004). Novel separation system design using "moving triangles". *Computers and Chemical Engineering*, 29, 181–189.

 © 2006 IChemE

Hömmerich, U. & Rautenbach, R. (1998). Design and optimization of combined pervaporation/distillation processes for the production of MTBE. *Journal of Membrane Science*, 146, 53–64.

Lu, Y., Zhang, L., Chen, H., Qian, Z. & Gao, C. (2002). Hybrid process of distillation side-connected with pervaporation for separation of Methanol/MTBE/C_4 mixture. *Desalination*, 149, 81–87.

Peters, M., Kauchali, S., Hildebrandt, D. & Glasser, D. (Article submitted for publication). Membrane Residue Curve Maps: I. Derivation and Properties. *Submitted to Industrial and Engineering Chemistry Research.*

Rehfinger, A. & Hoffmann, U. (1990). Kinetics of Methyl tertiary Butyl Ether liquid phase synthesis catalyzed by ion exchange resin – I. Intrinsic rate expression in liquid phase activities. *Chemical Engineering Science*, 45 (6), 1605–1617.

Tapp, M., Holland, S. T., Hildebrandt, D. & Glasser, D. (2004). Column Profile Maps. 1. Derivation and Interpretation. *Industrial Engineering and Chemistry Research*, 43, 364–374.

APPENDIX E: PROOF OF THE DIFFERENCE POINT EQUATION (WITH VARYING FLOW AND COMPOSITION)

A generalized column section (distillation or membrane), shown in Figure E.1, is defined as *a length of column between points of addition and removal of material and/or energy* (Tapp et al. (2004)). The constant molar overflow assumption is not employed here.

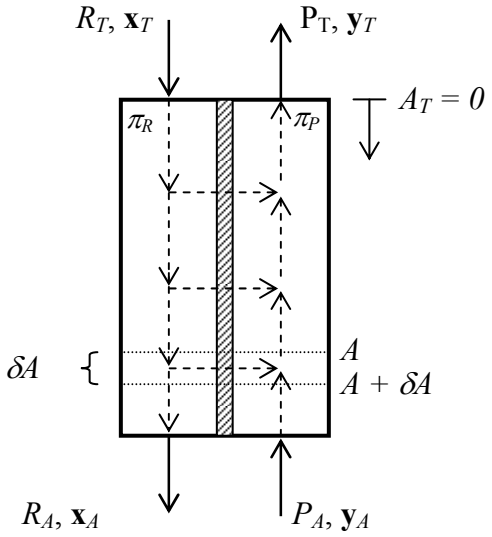

Figure E.1: A generalized membrane column section.

The subscript "*T*" denotes a quantity at the top of the CS, while "*A*" denotes a quantity at any cross-sectional area down the length of the column.

Consider the following overall and component material balances written around the top of the column and any point down the membrane length:

$$P_A + R_T = P_T + R_A \tag{E.1}$$

$$P_A y_A + R_T x_T = P_T y_T + R_A x_A \tag{E.2}$$

Adding and subtracting $R_{A+\delta A}x_{A+\delta A}$ to equation E.2, and re-arranging:

$$P_T y_T - R_T x_T = P_A y_A - R_A x_A + R_{A+\delta A}x_{A+\delta A} - R_{A+\delta A}x_{A+\delta A} \quad \text{(E.3)}$$

Now, defining

$$\delta R = R_{A+\delta A} - R_A, \text{ and} \quad \text{(E.4)}$$

$$\delta x = x_{A+\delta A} - x_A \quad \text{(E.5)}$$

Rearranging equations E.4 and E.5 and substituting into E.3:

$$P_T y_T - R_T x_T = P_A y_A - \left(R_{A+\delta A} - \delta R\right)\left(x_{A+\delta A} - \delta x\right) + R_{A+\delta A}x_{A+\delta A} - R_{A+\delta A}x_{A+\delta A} \quad \text{(E.6)}$$

Multiplying out:

$$P_T y_T - R_T x_T = P_A y_A - R_{A+\delta A}x_{A+\delta A} + R_{A+\delta A}\delta x + \delta R x_{A+\delta A} - \delta R\delta x + R_{A+\delta A}x_{A+\delta A} - R_{A+\delta A}x_{A+\delta A} \quad \text{(E.7)}$$

Canceling, and assuming the product $\delta R\delta x$ is small:

$$P_T y_T - R_T x_T = P_A y_A + R_{A+\delta A}\delta x + \delta R x_{A+\delta A} - R_{A+\delta A}x_{A+\delta A} \quad \text{(E.8)}$$

Substituting equation E.4:

$$P_T y_T - R_T x_T = P_A y_A + R_{A+\delta A}\delta x + \left(R_{A+\delta A} - R_A\right)x_{A+\delta A} - R_{A+\delta A}x_{A+\delta A} \quad \text{(E.9)}$$

and canceling

$$P_T y_T - R_T x_T = P_A y_A + R_{A+\delta A}\delta x - R_A x_{A+\delta A} \tag{E.10}$$

Substituting equation E.5:

$$P_T y_T - R_T x_T = P_A y_A + R_{A+\delta A}\left(x_{A+\delta A} - x_A\right) - R_A x_{A+\delta A} \tag{E.11}$$

Substituting in overall mass balance (equation (1)):

$$P_T y_T - R_T x_T = P_A y_A + R_{A+\delta A}\left(x_{A+\delta A} - x_A\right) - \left(P_A + R_T - P_T\right)x_{A+\delta A} \tag{E.12}$$

Rearranging:

$$P_T y_T - R_T x_T = -P_A\left(x_{A+\delta A} - y_A\right) + R_{A+\delta A}\left(x_{A+\delta A} - x_A\right) + \left(P_T - R_T\right)x_{A+\delta A} \tag{E.13}$$

By defining:

$$\Delta = P_A - R_A \tag{E.14}$$

as the net molar flow inside the column section [mol/s], and

$$X_\Delta = \frac{P_{Am} y_{Am} - R_{Am} x_{Am}}{\Delta} \tag{E.15}$$

as the difference point [-], we see that, by overall mass balance (equation E.1):

$$P_T - R_T = \Delta \tag{E.16}$$

and component mass balance (equation E.5):

$$P_T y_T - R_T x_T = \Delta X_\Delta \tag{E.17}$$

Thus, equation E.13 becomes:

$$\Delta X_\Delta = -P_A\left(x_{A+\delta A} - y_A\right) + R_{A+\delta A}\left(x_{A+\delta A} - x_A\right) + \Delta x_{A+\delta A} \tag{E.18}$$

Rearranging:

$$R_{A+\delta A}\left(x_{A+\delta A} - x_A\right) = P_A\left(x_{A+\delta A} - y_A\right) + \Delta\left(X_\Delta - x_{A+\delta A}\right) \tag{E.19}$$

Now, using a first order Taylor Series expansion on x_A:

$$x_A = x_{A+\delta A} - \left.\frac{dx}{dh}\right|_{h=A+\delta A} \cdot \Delta h \tag{E.20}$$

where Δh is assumed to be unity for a theoretical dimensionless area step. Thus the Taylor expansion becomes:

$$x_A = x_{A+\delta A} - \frac{dx_{A+\delta A}}{d\left(A+\delta A\right)} \tag{E.21}$$

Substituting equation E.21 into E.19:

$$R_{A+\delta A}\left(x_{A+\delta A} - \left(x_{A+\delta A} - \frac{dx_{A+\delta A}}{d\left(A+\delta A\right)}\right)\right) = P_A\left(x_{A+\delta A} - y_A\right) + \Delta\left(X_\Delta - x_{A+\delta A}\right)$$

(E.22)

Canceling, and taking the limit as $\delta A \to 0$:

$$R(A)\frac{dx_i}{dA} = P(A)\left[x_i - y_i(x)\right] + \Delta\left[X_{\Delta_i} - x_i\right], \text{ for } i = 1...c-1 \qquad \text{(E.23)}$$

It is worth noting the following:

- Both R and P are functions of area, i.e. position, as are x_i and y_i. However, y_i itself is a function of all the x_i's, as the equation depicts.
- Δ and X_Δ are constants for a given column section (refer to equations (16) and (17)), and
- The x and y in the equation are in "equilibrium" with each other – that is, they are both leaving streams from the same horizontal position on either side of the membrane. y_i can be modeled as a function of x_i using the appropriate flux equation. (Note: A subtle, yet very important understanding exists within these equations: Although the same flux equation is used to model the change in retentate flow, the y_i and x_i are leaving streams in the above equation, while in the later equation it will be noticed that they are passing streams).